frontiers | Research Topics

# Advances in the diagnosis and genomic research of surveillance-response activities in emerging, re-emerging, and unidentified infectious diseases

**Edited by**
Jun Feng, Tianmu Chen, Hui Chen, Xinyu Feng and Kun Yin

**Published in**
Frontiers in Public Health
Frontiers in Medicine

ISSN 1664-8714
ISBN 978-2-8325-2633-0
DOI 10.3389/978-2-8325-2633-0

## About Frontiers

Frontiers is more than just an open access publisher of scholarly articles: it is a pioneering approach to the world of academia, radically improving the way scholarly research is managed. The grand vision of Frontiers is a world where all people have an equal opportunity to seek, share and generate knowledge. Frontiers provides immediate and permanent online open access to all its publications, but this alone is not enough to realize our grand goals.

## Frontiers journal series

The Frontiers journal series is a multi-tier and interdisciplinary set of open-access, online journals, promising a paradigm shift from the current review, selection and dissemination processes in academic publishing. All Frontiers journals are driven by researchers for researchers; therefore, they constitute a service to the scholarly community. At the same time, the *Frontiers journal series* operates on a revolutionary invention, the tiered publishing system, initially addressing specific communities of scholars, and gradually climbing up to broader public understanding, thus serving the interests of the lay society, too.

## Dedication to quality

Each Frontiers article is a landmark of the highest quality, thanks to genuinely collaborative interactions between authors and review editors, who include some of the world's best academicians. Research must be certified by peers before entering a stream of knowledge that may eventually reach the public - and shape society; therefore, Frontiers only applies the most rigorous and unbiased reviews. Frontiers revolutionizes research publishing by freely delivering the most outstanding research, evaluated with no bias from both the academic and social point of view. By applying the most advanced information technologies, Frontiers is catapulting scholarly publishing into a new generation.

## What are Frontiers Research Topics?

Frontiers Research Topics are very popular trademarks of the *Frontiers journals series*: they are collections of at least ten articles, all centered on a particular subject. With their unique mix of varied contributions from Original Research to Review Articles, Frontiers Research Topics unify the most influential researchers, the latest key findings and historical advances in a hot research area.

Find out more on how to host your own Frontiers Research Topic or contribute to one as an author by contacting the Frontiers editorial office: frontiersin.org/about/contact

# Advances in the diagnosis and genomic research of surveillance-response activities in emerging, re-emerging, and unidentified infectious diseases

**Topic editors**

Jun Feng — Shanghai Municipal Center for Disease Control and Prevention (SCDC), China

Tianmu Chen — Xiamen University, China

Hui Chen — Brigham and Women's Hospital, Harvard Medical School, United States

Xinyu Feng — Chinese Center For Disease Control and Prevention, China

Kun Yin — Shanghai Jiao Tong University, China

**Citation**

Feng, J., Chen, T., Chen, H., Feng, X., Yin, K., eds. (2023). *Advances in the diagnosis and genomic research of surveillance-response activities in emerging, re-emerging, and unidentified infectious diseases*. Lausanne: Frontiers Media SA. doi: 10.3389/978-2-8325-2633-0

# Table of contents

frontiers | Frontiers in Public Health

TYPE Editorial
PUBLISHED 23 May 2023
DOI 10.3389/fpubh.2023.1182918



OPEN ACCESS

EDITED AND REVIEWED BY
Marc Jean Struelens,
Université libre de Bruxelles, Belgium

*CORRESPONDENCE
Kun Yin
✉ kunyin@sjtu.edu.cn
Xinyu Feng
✉ fengxinyu2013@163.com

RECEIVED 09 March 2023
ACCEPTED 12 May 2023
PUBLISHED 23 May 2023

CITATION
Wang C, Feng X, Feng J, Chen H, Chen T and Yin K (2023) Editorial: Advances in the diagnosis and genomic research of surveillance-response activities in emerging, re-emerging, and unidentified infectious diseases.
*Front. Public Health* 11:1182918.
doi: 10.3389/fpubh.2023.1182918



# Editorial: Advances in the diagnosis and genomic research of surveillance-response activities in emerging, re-emerging, and unidentified infectious diseases

Chenxi Wang[1,2], Xinyu Feng[1,3,4,5,6,7]*, Jun Feng[8], Hui Chen[9], Tianmu Chen[10] and Kun Yin[1,2]*

[1]School of Global Health, Chinese Center for Tropical Diseases Research, Shanghai Jiao Tong University School of Medicine, Shanghai, China, [2]One Health Center, Shanghai Jiao Tong University-The University of Edinburgh, Shanghai, China, [3]National Institute of Parasitic Diseases, Chinese Center for Disease Control and Prevention (Chinese Center for Tropical Diseases Research), Shanghai, China, [4]NHC Key Laboratory of Parasite and Vector Biology, Shanghai, China, [5]World Health Organization Collaborating Centre for Tropical Diseases, Shanghai, China, [6]National Center for International Research on Tropical Diseases, Shanghai, China, [7]Department of Biology, College of Life Sciences, Inner Mongolia University, Hohhot, China, [8]Shanghai Municipal Center for Diseases Control and Prevention, Shanghai, China, [9]Brigham and Women's Hospital, Harvard Medical School, Cambridge, MA, United States, [10]State Key Laboratory of Molecular Vaccinology and Molecular Diagnostics, School of Public Health, Xiamen University, Xiamen, Fujian, China

KEYWORDS

**surveillance, infectious diseases, diagnosis, genomic research, public health**

Editorial on the Research Topic
Advances in the diagnosis and genomic research of surveillance-response activities in emerging, re-emerging, and unidentified infectious diseases

Six pandemics of public health emergencies were announced as a global concern, causing numerous deaths and economic losses in this century (1). Strikingly, more than 3.5 million people died from COVID-19 in 2021, exceeding the combined number of deaths resulting from HIV, malaria, and tuberculosis in 2020 (2). The delayed diagnosis and inadequate surveillance of infectious diseases may indirectly lead to ineffective responses, making it harder to control the development of pandemics. Despite advances in health science, infectious diseases, including emerging, re-emerging, and unidentified infectious diseases, remain a major threat to human beings, particularly in low-resource settings.

Recent studies has been made in understanding infectious diseases transmission and dynamics (3). However, there are still gaps between diagnostic capacity and dynamic surveillance of infectious diseases. Nowadays, researchers have made significant efforts to optimize surveillance performance to emerging, reemerging, and unidentified infectious diseases, including diagnosis and genomic research (4, 5). However, increasing efforts are highly required to develop a more effective surveillance technique to continuously monitor, early warning and predict infectious diseases.

Therefore, we focused on the advances in the diagnosis and genomic research of surveillance-response activities in emerging, re-emerging, and unidentified infectious diseases in this Research Topic, which will contribute to infectious disease prediction and the effective decision making. Eleven papers were published worldwide, including opinion articles, original research, and case reports.

## Apply metagenomics and molecular methods to combat infectious diseases

Currently, metagenomic surveillance provides an opportunity to improve the detection and prevention of pathogens by conducting epidemiological investigations (Zhang T. et al.), limiting clonal transmission of bacteria (Chen et al.), and ensuring the effectiveness of interventions (Zeng et al.). Padilla-Blanco et al. described a new variant of SARS-CoV-19 that emerged in Sicily in late 2020. It showed that continuous monitoring of SARS-CoV-2 varirants is helpful in understanding virus evolution and provides timely information on sudden pathogen emergence, especially in times and places where epidemic virus pedigree is seldom explored. More importantly, monitoring viral variants by molecular biology technology can play an significant role in developing appropriate rapid detection tools and predicting potential vaccine escapes in emerging variants. For example, Feng et al. reported a case of *Parvimonas micra* pneumonia in a patient without obvious underlying disease and distal site of infection, expanding the etiology of pneumonia. It demonstrated that metagenomic sequencing allows rapid screening for rare pathogens, especially when regular strategy is ineffective. In addition, Tian et al. continuously monitored the changes in pathogenic bacteria by sequencing and drug sensitivity tests in a case of intracranial infection caused by multidrug-resistant *Acinetobacter baumannii*. As a complication of a series of invasive operations, the infection may seriously affect the prognosis of patients, in which it is necessary to monitor the pathogens in the patients' blood.

## Data-based approaches to combat infectious disease

Rapid advances in Big Data and machine learning provide opportunities to collect and deeply utilize epidemiological data for combating infectious diseases (6–9). Hand-foot-and-mouth disease (HFMD) is a common infectious disease in children caused by a variety of enteroviruses. Yang et al. explored the interaction between multiple viruses and the regular patterns of HFMD in different regions using the susceptibility-exposure-infection-asymptomatic-rehabilitation (SEIAR) model. HFMD is a common infectious disease in children caused by a variety of enteroviruses. The results showed that the incidence of HFMD increased with temperature risk, and the interaction of different pathogens strongly depended on geographic locations. Compared with the transmission of only one major subtype, there was a dilution effect when multiple subtypes of pathogens were transmitted simultaneously. Andagalu et al. conducted a cohort study to evaluate the efficacy of two antimalarial drugs, artemether-lumefantrine (AL) and artesunate-mefloquine (ASAQ), while developing predictive models of treatment outcomes based on immune profile data. Using machine learning to assess humoral immunity to malaria to predict the effectiveness of treatment, the researchers found that ASAQ was more effective. The investigators applied computational methods for the first time to show that serologic immune profiles differentially affect treatment outcomes based on artemisinin-based combination therapies (ACTs), providing an integrated approach to data integration, machine learning, and modeling.

## Promote the diagnosis and response to infectious diseases

Some rapid testing techniques, which have the advantage of rapid, low-cost, and user-friendly, are suitable for epidemiologic studies and show the potential as high-throughput screening tools. A recent study evaluated the rapid detection of anti-Trypanosoma cruzi antibodies, providing recommendations balanced between sensitivity and operability for large-scale investigations (Iturra et al.). In addition, based on previous research, two opinion articles provided some optimization suggestions for antigen detection of SARS-CoV-2 (Zhang J. et al.), and discussed the methods to treat or alleviate the symptoms of infectious diseases (Aydemir and Ulusu).

To effectively address the challenges from infectious disease outbreaks and public health emergencies, we need to strengthen surveillance on unexplained infectious diseases, improve the sensitivity and accuracy of diagnostic assessment, and enhance the capacity for *in situ* analysis and treatment. We expect that further studies on infectious diseases will lead to more cost-benefit programs that improve wellbeing and sustainability in diverse socio-ecological settings and ultimately throughout the world.

Thank all authors who contributed to this research theme, and we invite readers to explore the excellent articles in this compilation.

## Author contributions

KY contributed to the original idea and conceived the paper. CW wrote the initial draft of the paper. The final version was reviewed by XF, JF, TC, and HC. All authors contributed to the article and approved the submitted version.

## Funding

This work was supported by the Natural Science Foundation of Shanghai (22ZR1436200) and the National Natural Science Foundation of China (22104090).

## Conflict of interest

The authors declare that the research was conducted in the absence of any commercial or financial relationships that could be construed as a potential conflict of interest.

## Publisher's note

All claims expressed in this article are solely those of the authors and do not necessarily represent those of their affiliated

organizations, or those of the publisher, the editors and the reviewers. Any product that may be evaluated in this article, or claim that may be made by its manufacturer, is not guaranteed or endorsed by the publisher.

## References

1. Wilder-Smith A, Osman S. Public health emergencies of international concern: a historic overview. *J Travel Med*. (2020) 27:taaa227. doi: 10.1093/jtm/taaa227

2. World Health Organization. *WHO Director-General's Opening Remarks at the Media Briefing on COVID-19*. (2021). Available online at: https://www.who.int/director-general/speeches/detail/who-director-general-s-opening-remarks-at-the-media-briefing-on-covid-19 (accessed December 22, 2021).

3. Chala B, Hamde F. Emerging and re-emerging vector-borne infectious diseases and the challenges for control: a review. *Front Public Health*. (2021) 9:715759. doi: 10.3389/fpubh.2021.715759

4. Robishaw JD, Alter SM, Solano JJ, Shih RD, DeMets DL, Maki DG, et al. Genomic surveillance to combat COVID-19: challenges and opportunities. *Lancet Microbe*. (2021) 2:e481–4. doi: 10.1016/S2666-5247(21)00121-X

5. Xie Y, Li H, Chen F, Udayakumar S, Arora K, Chen H, et al. Clustered regularly interspaced short palindromic repeats-based microfluidic system in infectious diseases diagnosis: current status, challenges, and perspectives. *Adv Sci*. (2022) 9:e2204172. doi: 10.1002/advs.202204172

6. Dolley S. Big data's role in precision public health. *Front Public Health*. (2018) 6:68. doi: 10.3389/fpubh.2018.00068

7. Simonsen L, Gog JR, Olson D, Viboud C. Infectious disease surveillance in the big data era: towards faster and locally relevant systems. *J Infect Dis*. (2016) 214:S380–5. doi: 10.1093/infdis/jiw376

8. Peiffer-Smadja N, Rawson TM, Ahmad R, Buchard A, Georgiou P, Lescure FX, et al. Corrigendum to 'machine learning for clinical decision support in infectious diseases: a narrative review of current applications' clinical microbiology and infection (2020) 584-595. *Clin Microbiol Infect*. (2020) 26:1118. doi: 10.1016/j.cmi.2019.09.009

9. Agany DDM, Pietri JE, Gnimpieba EZ. Assessment of vector-host-pathogen relationships using data mining and machine learning. *Comput Struct Biotechnol J*. (2020) 18:1704–21. doi: 10.1016/j.csbj.2020.06.031

frontiers | Frontiers in Public Health

TYPE Original Research
PUBLISHED 06 September 2022
DOI 10.3389/fpubh.2022.1007130



OPEN ACCESS

EDITED BY
Kun Yin,
Shanghai Jiao Tong University, China

REVIEWED BY
Aiqin Liu,
Harbin Medical University, China
Dongfang Li,
Huazhong Agricultural University, China
Haiju Dong,
Henan Agricultural University, China

*CORRESPONDENCE
Wei Zhao
hayidazhaowei@163.com
Chuanlong Zhu
zhuchuanlong@jsph.org.cn
Gang Lu
luganghn@163.com

†These authors have contributed equally to this work

SPECIALTY SECTION
This article was submitted to Infectious Diseases – Surveillance, Prevention and Treatment, a section of the journal Frontiers in Public Health

RECEIVED 30 July 2022
ACCEPTED 18 August 2022
PUBLISHED 06 September 2022

CITATION
Zhang T, Ren G, Zhou H, Qiang Y, Li J, Zhang Y, Li T, Zhou Y, Wang Y, Lai X, Lei S, Tan F, Liu R, Li W, He J, Zhao W, Zhu C and Lu G (2022) Molecular prevalence and genetic diversity analysis of *Enterocytozoon bieneusi* in humans in Hainan Province, China: High diversity and unique endemic genetic characteristics. *Front. Public Health* 10:1007130. doi: 10.3389/fpubh.2022.1007130



# Molecular prevalence and genetic diversity analysis of *Enterocytozoon bieneusi* in humans in Hainan Province, China: High diversity and unique endemic genetic characteristics

Tiemin Zhang[1†], Guangxu Ren[2,3,4†], Huanhuan Zhou[2,3,4†], Yu Qiang[2,3,4], Jiaqi Li[2,3,4], Yun Zhang[2,3,4], Tingting Li[2,3,4], Yunfei Zhou[2,3,4], Yuan Wang[2,3,4], Xiuyi Lai[2,3,4], Shen Lei[2,3,4], Feng Tan[5], Rui Liu[6], Wenting Li[6], Jing He[6], Wei Zhao[5*], Chuanlong Zhu[6*] and Gang Lu[2,3,4,6*]

[1]Department of General Surgery, The Second Affiliated Hospital of Hainan Medical University, Haikou, China, [2]Key Laboratory of Tropical Translational Medicine of Ministry of Education, Hainan Medical University, Haikou, China, [3]Hainan Medical University-The University of Hong Kong Joint Laboratory of Tropical Infectious Diseases, Hainan Medical University, Haikou, China, [4]Department of Pathogenic Biology, Hainan Medical University, Haikou, China, [5]Department of Parasitology, Wenzhou Medical University, Wenzhou, China, [6]Department of Tropical Diseases, The Second Affiliated Hospital of Hainan Medical University, Haikou, China

*Enterocytozoon bieneusi* is a zoonotic pathogen commonly found in humans and animals all over the world. Here, we investigated the occurrence and genotype constitute of *E. bieneusi* among the individuals from Haikou city of Hainan, China. A total of 1,264 fecal samples of humans were collected, including 628 samples from patients with diarrhea (325 adults and 303 children) and 636 samples from the asymptomatic population (383 college students and 253 kindergarten children). *E. bieneusi* was detected using nested polymerase chain reaction (PCR) amplification of the internal transcribed spacer (ITS) region. A phylogenetic tree was constructed using a neighbor-joining tree construction method. The overall prevalence of *E. bieneusi* was 3.7% (47/1,264), while it was 5.6% in the patients with diarrhea (5.8% in adults and 5.3% in children) and 1.9% in the asymptomatic population (2.9% in college students and 0.4% in kindergarten children). The prevalence of *E. bieneusi* in humans with diarrhea was significantly higher than that in the asymptomatic population ($\chi^2 = 36.9$; $P < 0.05$). A total of 28 genotypes were identified, including ten known genotypes: CHG2 ($n = 3$), CHG3 ($n = 5$), CHG5 ($n = 10$), CM21 ($n = 1$), EbpA ($n = 1$), EbpC ($n = 1$), PigEBITS4 ($n = 1$), PigEBITS7 ($n = 1$), SHR1 ($n = 4$), Type IV ($n = 2$), and 18 novel genotypes (HNH-1 to HNH-18; one each). All these genotypes were categorized into three groups, including group 1 ($n = 6$), group 2 ($n = 14$), and group 13 ($n = 8$). This was the first study on the identification of *E. bieneusi* among humans in Hainan, China. The correlation between *E. bieneusi* infection and diarrhea was observed.

The high diversity and distinctive distribution of *E. bieneusi* genotypes found in this study reflected the unique epidemic genetic characteristics of *E. bieneusi* in humans living in Hainan.

KEYWORDS

***Enterocytozoon bieneusi*, genotype, human, zoonotic, Hainan**

# Introduction

Phylum Microsporidia is recognized as a group of opportunistic infectious agents worldwide and comprises more than 1,500 species, belonging to 160 genera (1, 2). They are intracellular pathogens, infecting the members of every phylum of the animal kingdom (2). The identification of Microsporidia species in water sources led to their inclusion in the Category B list of biodefense pathogens by the National Institutes of Health (NIH) and microbial contaminant candidates list of concern for waterborne transmission by the Environmental Protection Agency (EPA) (2). To date, a total of 17 species, belonging to the nine genera of Microsporidia, have been identified as opportunistic human pathogens (2). Among them, *Enterocytozoon bieneusi* is the most frequently identified species, which was first found in an AIDS patient in France in 1985 (3). *E. bieneusi*, as an opportunistic pathogen infecting the alimentary tract of hosts, causes a wide spectrum of clinical symptoms in humans, ranging from asymptomatic or self-limiting symptoms in immunocompetent individuals to severe and life-threatening symptoms in the immunocompromised person (4). Humans can acquire *E. bieneusi* infection through several transmission routes, including direct contact with the infected persons (anthroponotic transmission) or animals (zoonotic transmission) and the ingestion of contaminated water or food (4).

*E. bieneusi* is a complex species, having multiple genotypes and diverse host ranges and pathogenicity (4). Many molecular epidemiologic studies have determined the distribution of *E. bieneusi* genotypes in different hosts and have inferred the possible routes of transmission and source of infections (1). To date, more than 685 genotypes of *E. bieneusi* have been identified using PCR analysis of the internal transcribed spacer (ITS) region of the rRNA gene of *E. bieneusi* (1). Among these, at least 33 genotypes have been found in both humans and animals, supporting the presumption of their zoonotic potential (4, 5). On the other hand, all the identified genotypes can be grouped into thirteen different clades, which are named groups 1–13 based on their phylogenetic analysis (6). Groups 1 and 2 are the two largest groups, accounting for 94% of the total genotypes, and are called zoonotic groups (4). These two groups contain almost all the genotypes detected in humans and also contain a vast majority of genotypes from various animal hosts; some genotypes are detected both in humans and animals (4). In contrast, the genotypes, belonging to the remaining 11 groups, are found mostly in the specific hosts and wastewater (4, 7). Understanding the source of *E. bieneusi* infection to cut off its route of transmission is important in adequately controlling its infection in humans due to the lack of effective vaccines and drugs.

Hainan, the only tropical island province in China, has a unique geographical landform, ecological environment, living customs, and culture of Li nationality. It has a wide variety of wild animals and arthropods, thereby having a high incidence of tropical infectious diseases. *E. bieneusi* was primarily detected in the farmed and wild animals in Hainan with a reported prevalence of over 10% (5, 6, 8–10). These data showed that *E. bieneusi* has been widely distributed in Hainan, China. However, the prevalence of this pathogen, causing human infections, has not been reported yet. Therefore, the present study aimed to determine the prevalence and genotypes of *E. bieneusi* among humans in Hainan, China by sequencing and analyzing the ITS region of the rRNA gene. This study also assessed the possible transmission patterns and infection sources of this pathogen by homology and phylogenetic analyses. The results might contribute to developing the control strategies of *E. bieneusi* in Hainan Province, China.

# Materials and methods

## Ethics approval and consent to participate

Approvals for these studies were obtained from the Ethics Committees of Hainan Medical University. Written informed consent was signed by each of adult participants and guardians of minors under 17 years of age after the purposes and procedures of the study were explained to them.

## Specimens

From July 2018 to December 2019, a total of 1,264 fecal samples were collected from Hainan Province of China. Among

TABLE 1 Prevalence and distribution of *E. bieneusi* genotypes in humans in Hainan Province of China.

| Clinical symptoms | No. positive/No. examined (%) | Known genotype (*n*) | Novel genotype (*n*) |
|---|---|---|---|
| **Diarrhea** | | | |
| Adults | 19/325 (5.8) | CHG5 (4), CHG3 (3), CHG2 (1), EbpA (1), SHR1 (1), Type-IV (1), PigEBITS4 (1), CM21 (1) | HNH-1 to 6 (1 each) |
| Children | 16/303 (5.3) | SHR1 (3), CHG5 (2), CHG2 (2), CHG3 (2), EbpC (1), Type-IV (1) | HNH-7 to 11 (1 each) |
| Subtotal | 35/628 (5.6) | CHG5 (6), CHG3 (5), SHR1 (4), CHG2 (3), Type-IV (2), EbpA, PigEBITS4, CM21, EbpC (1 each) | HNH-1 to 11 (1 each) |
| **Non-Diarrhea** | | | |
| Adults | 11/383 (2.9) | CHG5 (4), PigEBITS7 (1) | HNH-12 to 17 (1 each) |
| Children | 1/253 (0.4) | / | HNH-18 (1) |
| Subtotal | 12/636 (1.9) | CHG5 (4), PigEBITS7 (1) | HNH-12 to 18 (1 each) |
| Total | 47/1,264 (3.7) | CHG5 (10), CHG3 (5), SHR1 (4), CHG2 (3), Type-IV (2), EbpC, EbpA, PigEBITS7, PigEBITS4, CM21 (1 each) | HNH 1 to 18 (1 each) |

them, 628 were from patients with diarrhea in the Second Affiliated Hospital of Hainan Medical University, comprising 325 adults and 303 minors. 636 were from asymptomatic people, including 383 college students from Hainan Medical University and 253 children from Shan'gao kindergarten (Table 1). Only one fecal sample per participant was included in the present study. The samples (formed stool: 20 g; watery stool: 30 mL) were placed in a plastic fecal collection box, with collection date, stool characteristics (liquid stool or formed stool) and patient identity (age and gender) being recorded. The collected samples were immediately stored at 4°C and sent to our laboratory for parasite testing within 24 h. The doctors communicated and provided consulting services, a voluntarily participated in the survey and signed a written informed consent form. All the participants did not undergo the antiparasitic treatment.

## DNA extraction

Genomic DNA was extracted from ~200 mg of each fecal sample using a QIAamp DNA Stool Mini Kit (QIAgen, Hilden, Germany), following the manufacturer's instructions. In order to obtain a high yield of DNA, the lysis temperature was increased to 95°C according to the manufacturer's suggestions. The extracted DNA samples were eluted in 200 μl of AE buffer and stored at −20°C in a freezer prior to PCR analysis.

## PCR amplification

The presence of *E. bieneusi*-positive DNA was detected using nested PCR amplification of a 410 bp nucleotide fragment of the rRNA gene including 243 bp of the ITS region. The primers and PCR conditions have been previously described (11). TaKaRa Taq DNA Polymerase (TaKaRa Bio Inc., Tokyo, Japan) was used in all the PCR reactions. A negative control without DNA and a positive control with DNA of the *E. bieneusi* BEB6 genotype from goat were included in all the PCR tests. All the secondary PCR products were run on a 1.5% agarose gel and visualized by staining the gel with Goldenview.

## Nucleotide sequencing and analysis

All the secondary PCR products of the expected size were directly sequenced with the same set of primers, which was used for the secondary PCR by Life Technologies (Guangzhou, China), using a Big Dye1 Terminator v3.1 cycle sequencing kit (Applied Biosystems, Carlsbad, CA, USA). The obtained nucleotide sequences were aligned with each other and compared to the reference sequences downloaded from GenBank using the Basic Local Alignment Search Tool (BLAST) (http://www.ncbi.nlm.nih.gov/BLAST/) and ClustalX 1.83 (http://www.clustal.org/) in order to determine the genotypes. According to the established nomenclature system, the nucleotide sequences of the ITS region identical to known genotypes were given the first published name; the

TABLE 2 Homology analysis of the novel genotypes of *E. bieneusi* identified in this study.

| Genetic group | Genotype (accession no)[a] | Genotype (accession no)[b] | Nucleotide (site) |
|---|---|---|---|
| Group 1 | HNH-14 (MT193640) | EbpC (MH024028) | Insertions T (52); G (53) |
| Group 2 | HNH-1 (MT193627) | CHG3 (KP262362) | C → T (232) |
| | HNH-4 (MT193630) | | A → G (164) |
| | HNH-10 (MT193636) | | A → G (108) and T → A (182) |
| | HNH-13 (MT193639) | | T → C (99) |
| | HNH-17 (MT193643) | | T → C (79) |
| | HNH-18 (MT193644) | | C → T (153) |
| | HNH-6 (MT193632) | CHG2 (KP262366) | G → A (82) |
| | HNH-9 (MT193635) | | T → A (172) |
| | HNH-11 (MT193637) | CHG5 (KP262365) | G → T (210) |
| | HNH-16 (MT193642) | | C → T (232) |
| Group 13 | HNH-2 (MT193628) | SHR1 (MN523336) | T → A (52) |
| | HNH-3 (MT193629) | | T → C (111) |
| | HNH-5 (MT193631) | | A → G(101) |
| | HNH-7 (MT193633) | | T → C (213) |
| | HNH-8 (MT193634) | | T → C (99) |
| | HNH-12 (MT193638) | | A → G (71); T → C (105) |
| | HNH-15 (MT193641) | | Deletion A (143) |

[a]Accession nos. of the novel ITS genotypes obtained in this study.
[b]Accession nos. of the known genotypes having the largest homology with the novel ones obtained in this study.

nucleotide sequences with single nucleotide substitutions, deletions, or insertions as compared to the known ITS genotypes were considered novel genotypes (12). Meanwhile, the novel genotypes were confirmed by sequencing another two separate PCR products of the same preparations.

## Phylogenetic analysis

In order to better assess the genetic diversity of *E. bieneusi* genotypes in the present study and to determine the genetic correlations of novel genotypes to the known ones, a neighboring-joining phylogenetic tree was constructed using Mega X software (http://www.megasoftware.net/). The phylogenetic tree was based on the evolutionary distances calculated using a Kimura 2-parameter model and analyzed using bootstrap analysis with 1,000 replicates for reliability.

## Statistical analyses

Chi-square analysis was performed to assess the correlations of the prevalence of *E. bieneusi* by group: between diarrheal patients and asymptomatic populations and between adult group and minor group using SPSS (Statistical Package for the Social Sciences) version 17.0. The difference was considered statistically significant when the $P < 0.05$.

## Nucleotide sequence accession numbers

The nucleotide sequences of novel genotypes of *E. bieneusi* obtained in the present study were deposited in the GenBank database under accession numbers: MT193627 to MT193644.

# Results

## Prevalence of *E. bieneusi*

*E. bieneusi* was detected in 3.7% (47/1,264) of the feces samples (Table 1). The *E. bieneusi* prevalence was significantly higher in patients with diarrhea (5.6%) than that in the asymptomatic populations (1.9%) ($\chi^2 = 36.9$; $P < 0.05$). Different prevalences of *E. bieneusi* were observed between adults and minors: 5.8 and 5.3% in diarrheal patients and 2.9 and 0.4% in asymptomatic populations. However, by $\chi^2$-test, significant difference in prevalence was only observed in college students and kindergarten children ($\chi^2 = 5.6$; $P = 0.02$).

## Characterization and distribution of *E. bieneusi* genotypes

The sequence analysis of 47 *E. bieneusi* isolates obtained in this study identified a total of 28 genotypes, including ten known genotypes (CHG2, CHG3, CHG5, CM21, EbpA,

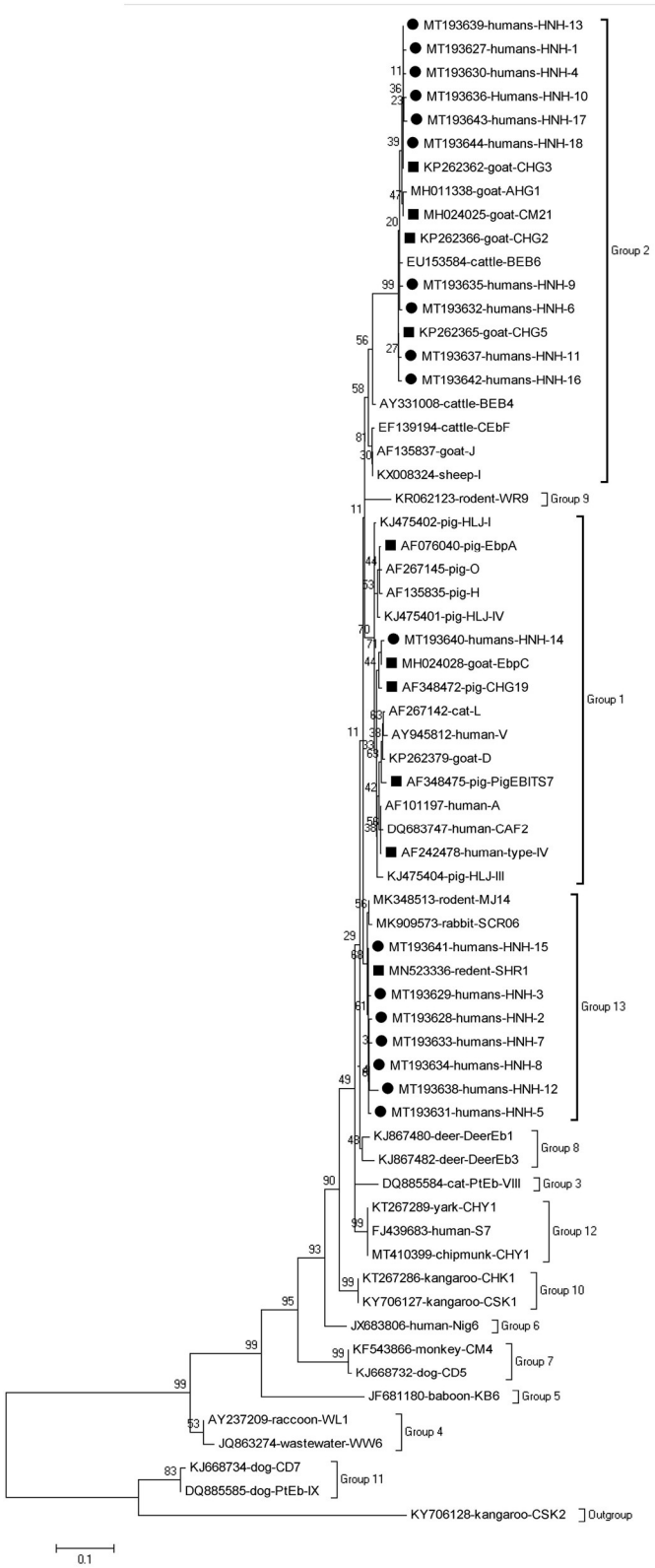


FIGURE 1
Phylogenetic relationship of the genotypes of *E. bieneusi* in humans. The tree was constructed by a neighboring-joining phylogenetic analysis of ITS sequences using the Kimura-2-parameter model and with 1,000 replicates. Each sequence is identified by its accession number, host origin, and genotype designation. The square and circle filled in black indicate known and novel genotypes, respectively.

EbpC, PigEBITS4, PigEBITS7, SHR1, and Type IV) and 18 novel genotypes (HNH-1 to HNH-18). Among them, CHG5 accounted for the largest proportion (21.3%, 10/47), followed by CHG3 (10.6%, 5/47), SHR1 (8.5%, 4/47), CHG2 (6.4%, 3/47), Type IV (4.3%, 2/47), and the remaining 23 genotypes (each 2.1%, 1/47). Genotype distribution of *E. bieneusi* in different groups could be seen in Table 1. Genotype CHG5 was the most widely distributed in humans in the investigated areas, which was detected in both the diarrhea patients and the asymptomatic populations. Meanwhile, result of the homology analysis of the novel genotypes of *E. bieneusi* showing in Table 2.

## Phylogenetic analysis

The phylogenetic analysis of the ITS region of *E. bieneusi* divided the genotypes, which were identified in humans in this study, into three groups. Five known genotypes (EbpA, EbpC, PigEBITS4, PigEBITS7 and Type IV) and one novel genotype (HNH-14) were categorized into group 1. Four known genotypes (CM21, CHG5, CHG3, and CHG2) and ten novel genotypes (HNH-1, HNH-4, HNH-6, HNH-9 to HNH-11, HNH-13, and HNH-16 to HNH-18) were categorized into group 2. The remaining one known genotype (SHR1) and seven novel genotypes (HNH-2, HNH-3, HNH-5, HNH-7, HNH-8, HNH-12, and HNH-15) were categorized into group 13 (Figure 1).

# Discussion

Since its first report on humans in China in 2011, a total of 14 epidemiological studies on the prevalence of *E. bieneusi* have been performed in ten provinces/municipalities of China, including Xinjiang, Yunnan, Shanghai, Henan, Heilongjiang, Jilin, Chongqing, Shandong, Guangxi, and Hubei Provinces (13–16). The highest prevalence was 22.5% in Changchun (17) and the lowest prevalence was 0.2% in Wuhan (18). The overall prevalence was 6.4, 8.1, and 3.6% among diarrhea patients, HIV patients, and healthy individuals in China, respectively (15). In the present study, a total of 3.7% (47/1,264) of the human fecal samples from Hainan province were tested positive for *E. bieneusi* using PCR and sequencing analysis of the ITS gene region. Overall, this prevalence was lower than the average prevalence, especially among the kindergarten children with diarrhea, among whom, the prevalence was only 5.3%, which was not higher than that in the adults. Previous studies have shown that the prevalence of *E. bieneusi* was high up to 78% in children in Uganda (19). About 22.5% of diarrhea infection in children was caused by *E. bieneusi* in northeast China (17), which might be due to the regional differences because, in Hainan, the kindergarten children are less exposed to animals due to the fewer pets in the families.

In the present study, the prevalence of *E. bieneusi* in diarrhea patients (5.6%) was significantly higher than that in the asymptomatic population (1.9%) ($\chi^2 = 36.9$; $P < 0.05$). In China, two previous studies revealed significantly higher prevalence of *E. bieneusi* in children with diarrhea than in children without diarrhea: 4.9% (11/223) vs. 3.7% (13/350) in Shanghai (20); 25.0% (1/4) vs. 7.2% (18/251) in Heilongjiang (21). Besides, researchers from other study also reported that children with diseases or diarrhea were more susceptible to *E. bieneusi* infection (22). Therefore, *E. bieneusi* infection might be an important factor causing diarrhea. Therefore, it is necessary to monitor the infection of *E. bieneusi* among patients with diarrhea especially in the immunocompromised populations in order to avoid patient death due to misdiagnosis.

Among the known genotypes identified in this study, the genotypes Type-IV, EbpC, EbpA, and PigEBITS7 have been previously reported in humans and animals in several provinces of China and other countries (4). The remaining six known genotypes (CHG2, CHG3, CHG5, CM21, PigEBITS4, and SHR1) and 18 novel genotypes (HNH-1 to HNH-18) were reported for the first time in humans. This not only enriched the *E. bieneusi* genotypes, which can infect humans, and expanded the host range of these genotypes but also suggested that the ruminant-specific genotypes (CHG2, CHG3, and CHG5) could also infect humans. Therefore, the zoonotic risk of these genotypes should also be reevaluated. Actually, the 10 known genotypes (CHG2, CHG3, CHG5, CM21, EbpA, EbpC, PigEBITS4, PigEBITS7, SHR1, and Type IV) were all identified in a large number of farm animals in Hainan province (5, 6, 8–10). Therefore, it was speculated that these genotypes, infecting humans in this region, might have come from animals.

In this study, the 18 novel genotypes identified belonged to three groups: genotype HNH-14 in group 1; genotypes HNH-1, HNH-4, HNH-6, HNH-9 toHNH-11, HNH-13, and HNH-16 to HNH-18 in group 2; genotypes HNH-2, HNH-3, HNH-5, HNH-7, HNH-8, HNH-12, and HNH-15 in group 13. Prior to this study, a total of 66 genotypes have been identified in humans, among which, 48, 12, 2, and 4 genotypes belong to Groups 1, 2, 5, and 6, respectively (1, 4). The genotypes identified in humans, belonging to Group 1, might have zoonotic potential due to their close relation to a wide range of hosts and the lack of geographic segregation among humans (4). The identification of the previously considered ruminant-adapted group 2 genotypes (notably BEB4, BEB6, CHN3, I, and J) in the humans, residing in the Czech Republic and China, indicated a possibility of zoonotic transmission for these genotypes (4, 17, 23). The genotypes in groups 5, 6 had a relatively narrow host range and robust geographic specificity because the genotypes, such as Nig3, Nig4, Nig6, and Nig7, have been identified in humans only in Africa (24, 25). The fact of 50% (14/28) and 28.6% (8/28) of the genotypes of groups 2 and 13, respectively, revealed unique epidemic genetic characteristics of *E. bieneusi* in humans living in Hainan, China.

In conclusion, this was the first study on the identification of *E. bieneusi* in humans in Hainan, China. The prevalence of *E. bieneusi* was 3.7% (47/1,264). The prevalence of *E. bieneusi* in humans with diarrhea was significantly higher than that in the asymptomatic population. The high diversity and distinctive distribution of *E. bieneusi* genotypes found in this study reflected the unique epidemic genetic characteristics of *E. bieneusi* in humans living in Hainan.

## Data availability statement

The datasets presented in this study can be found in online repositories. The names of the repository/repositories and accession number(s) can be found in the article/supplementary material.

## Ethics statement

Approval for these studies were obtained from the Ethics Committee of Hainan Medical University. Written informed consent was signed by each participant (for the 17-year-old participants, the consent forms were obtained from their parents or guardian) after they or their parents or guardian were informed of the purposes and procedures of the study.

## Author contributions

WZ, GL, and CZ contributed to the study conceive and design. TZ, RL, WL, JH, and CZ contributed to acquisition of clinical sample. GR, HZ, YQ, JL, YZha, TL, YZho, YW, XL, and SL performed experiments. TZ, GR, HZ, and WZ contributed to acquisition of clinical data. GR and WZ contributed to statistical analysis. WZ contributed to writing the manuscript. GL obtained funding. FT and CZ provided administrative, technical support, and constructive discussion. All authors approved of the final version to be published and agree to be accountable for all aspects of the manuscript.

## Funding

This work was supported by the National Natural Science Foundation of China (82060375 and 81760378), Research Project of Hainan Academician Innovation Platform (YSPTZX202004), Major Science and Technology Program of Hainan Province (ZDKJ202003), Hainan Talent Development Project (SRC200003), Open Foundation of Key Laboratory of Tropical Translational Medicine of Ministry of Education, Hainan Medical University (2020TTM004), and Hainan Province Clinical Medical Center.

## Conflict of interest

The authors declare that the research was conducted in the absence of any commercial or financial relationships that could be construed as a potential conflict of interest.

## Publisher's note

All claims expressed in this article are solely those of the authors and do not necessarily represent those of their affiliated organizations, or those of the publisher, the editors and the reviewers. Any product that may be evaluated in this article, or claim that may be made by its manufacturer, is not guaranteed or endorsed by the publisher.

## References

1. Ruan Y, Xu X, He Q, Li L, Guo J, Bao J, et al. The largest meta-analysis on the global prevalence of microsporidia in mammals, avian and water provides insights into the epidemic features of these ubiquitous pathogens. *Parasite Vectors.* (2021) 14:186. doi: 10.1186/s13071-021-04700-x

2. Wei J, Fei Z, Pan G, Weiss LM, Zhou Z. Current therapy and therapeutic targets for microsporidiosis. *Front Microbiol.* (2022) 13:835390. doi: 10.3389/fmicb.2022.835390

3. Desportes I, Le Charpentier Y, Galian A, Bernard F, Cochand-Priollet B, Lavergne A, et al. Occurrence of a new microsporidan: *Enterocytozoon bieneusi* n.g., n. sp., in the enterocytes of a human patient with AIDS. *J Protozool.* (1985) 32:250–4. doi: 10.1111/j.1550-7408.1985.tb03046.x

4. Li W, Feng Y, Santin M. Host specificity of enterocytozoon bieneusi and public health implications. *Trends Parasitol.* (2019) 35:436–51. doi: 10.1016/j.pt.2019.04.004

5. Zhou HH, Zheng XL, Ma TM, Qi M, Zhou JG, Liu HJ, et al. Molecular detection of Enterocytozoon bieneusi in farm-raised pigs in Hainan Province, China: infection rates, genotype distributions, zoonotic potential. *Parasite.* (2020) 27:12. doi: 10.1051/parasite/2020009

6. Zhao W, Zhou H, Yang L, Ma T, Zhou J, Liu H, et al. Prevalence, genetic diversity and implications for public health of *Enterocytozoon bieneusi* in various rodents from Hainan Province, China. *Parasite Vectors.* (2020) 13:438. doi: 10.1186/s13071-020-04314-9.

7. Guo Y, Alderisio KA, Yang W, Cama V, Feng Y, Xiao L. Host specificity and source of *Enterocytozoon bieneusi* genotypes in a drinking source watershed. *Appl Environ Microbiol.* (2014) 80:218–25. doi: 10.1128/AEM.02997-13.

8. Zhao W, Ren GX, Qiang Y, Li J, Pu J, Zhang Y, et al. Molecular-Based detection of *Enterocytozoon bieneusi* in farmed masked palm civets (*Paguma larvata*) in Hainan, China: A high-prevalence, specificity, and zoonotic potential of ITS genotypes. *Front Vet Sci.* (2021) 8:714249. doi: 10.3389/fvets.2021.714249

9. Zhou HH, Zheng XL, Ma TM, Qi M, Cao ZX, Chao Z, et al. Genotype identification and phylogenetic analysis of *Enterocytozoon bieneusi* in farmed black goats (Capra hircus) from China's Hainan Province. *Parasite.* (2019) 26:62. doi: 10.1051/parasite/2019064.

10. Zheng XL, Zhou HH, Ren G, Ma TM, Cao ZX, Wei LM, et al. Genotyping and zoonotic potential of *Enterocytozoon bieneusi* in cattle farmed in Hainan Province, the southernmost region of China. *Parasite.* (2020) 27:65. doi: 10.1051/parasite/2020065

11. Mirjalali H, Mirhendi H, Meamar AR, Mohebali M, Askari Z, Mirsamadi ES, et al. Genotyping and molecular analysis of *Enterocytozoon bieneusi* isolated from immunocompromised patients in Iran. *Infect Genet Evol.* (2015) 36:244–249. doi: 10.1016/j.meegid.2015.09.022

12. Santín M, Fayer R. Enterocytozoon bieneusi genotype nomenclature based on the internal transcribed spacer sequence: a consensus. *J Eukaryot Microbiol.* (2009) 56:34–8. doi: 10.1111/j.1550-7408.2008.00380.x

13. Zang M, Li J, Tang C, Ding S, Huang W, Qin Q, et al. Prevalence and phylogenetic analysis of microsporidium *Enterocytozoon bieneusi* in diarrheal patients. *Pathogens.* (2021) 10:128. doi: 10.3390/pathogens10020128

14. Qi M, Yu F, Zhao A, Zhang Y, Wei Z, Li D, et al. Unusual dominant genotype NIA1 of *Enterocytozoon bieneusi* in children in Southern Xinjiang, China. *PLoS Negl Trop Dis.* (2020) 14:e0008293. doi: 10.1371/journal.pntd.0008293

15. Gong B, Yang Y, Liu X, Cao J, Xu M, Xu N, et al. First survey of *Enterocytozoon bieneusi* and dominant genotype Peru6 among ethnic minority groups in southwestern China's Yunnan Province and assessment of risk factors. *PLoS Negl Trop Dis.* (2019) 13:e0007356. doi: 10.1371/journal.pntd.0007356

16. Li J, Ren Y, Chen H, Huang W, Feng X, Hu W. Risk evaluation of pathogenic intestinal protozoa infection among laboratory macaques, animal facility workers, and nearby villagers from one health perspective. *Front Vet Sci.* (2021) 8:696568. doi: 10.3389/fvets.2021.696568

17. Zhang X, Wang Z, Su Y, Liang X, Sun X, Peng S, et al. Identification and genotyping of *Enterocytozoon bieneusi* in China. *J Clin Microbiol.* (2011) 49:2006–8. doi: 10.1128/JCM.00372-11

18. Wang T, Fan Y, Koehler AV, Ma G, Li T, Hu M, et al. First survey of cryptosporidium, giardia and enterocytozoon in diarrhoeic children from Wuhan, China. *Infect Genet Evol.* (2017) 51:127–31. doi: 10.1016/j.meegid.2017.03.006

19. Tumwine JK, Kekitiinwa A, Bakeera-Kitaka S, Ndeezi G, Downing R, Feng X, et al. Cryptosporidiosis and microsporidiosis in ugandan children with persistent diarrhea with and without concurrent infection with the human immunodeficiency virus. *Am J Trop Med Hyg.* (2005) 73:921–5. doi: 10.4269/ajtmh.2005.73.921

20. Liu H, Shen Y, Yin J, Yuan Z, Jiang Y, Xu Y, et al. Prevalence and genetic characterization of cryptosporidium, enterocytozoon, giardia and cyclospora in diarrheal outpatients in China. *BMC Infect Dis.* (2014) 14:25. doi: 10.1186/1471-2334-14-25

21. Yang J, Song M, Wan Q, Li Y, Lu Y, Jiang Y, et al. Enterocytozoon bieneusi genotypes in children in Northeast China and assessment of risk of zoonotic transmission. *J Clin Microbiol.* (2014) 52:4363–4367. doi: 10.1128/JCM.02295-14

22. Yu F, Li D, Chang Y, Wu Y, Guo Z, Jia L, et al. Molecular characterization of three intestinal protozoans in hospitalized children with different disease backgrounds in Zhengzhou, central China. *Parasite Vectors.* (2019) 12:543. doi: 10.1186/s13071-019-3800-5

23. Wang L, Zhang H, Zhao X, Zhang L, Zhang G, Guo M, et al. Zoonotic cryptosporidium species and *Enterocytozoon bieneusi* genotypes in HIV-positive patients on antiretroviral therapy. *J Clin Microbiol.* (2013) 51:557–63. doi: 10.1128/JCM.02758-12

24. Akinbo FO, Okaka CE, Omoregie R, Dearen T, Leon ET, Xiao L. Molecular epidemiologic characterization of *Enterocytozoon bieneusi* in HIV-infected persons in Benin City, Nigeria. *Am J Trop Med Hyg.* (2012) 86:441–5. doi: 10.4269/ajtmh.2012.11-0548

25. Akinbo FO, Okaka CE, Omoregie R, Adamu H, Xiao L. Unusual *Enterocytozoon bieneusi* genotypes and *Cryptosporidium hominis* subtypes in HIV-infected patients on highly active antiretroviral therapy. *Am J Trop Med Hyg.* (2013) 89:157–61. doi: 10.4269/ajtmh.12-0635

frontiers | Frontiers in Public Health

TYPE Original Research
PUBLISHED 13 September 2022
DOI 10.3389/fpubh.2022.988317



OPEN ACCESS

EDITED BY
Jun Feng,
Shanghai Municipal Center for Disease Control and Prevention (SCDC), China

REVIEWED BY
Xiang-Dang Du,
Henan Agricultural University, China
Jian Sun,
South China Agricultural University, China

*CORRESPONDENCE
Yunyi Zhang
yyzhang@cdc.zj.cn
Min Yue
myue@zju.edu.cn

†These authors have contributed equally to this work

SPECIALTY SECTION
This article was submitted to Infectious Diseases – Surveillance, Prevention and Treatment, a section of the journal Frontiers in Public Health

RECEIVED 07 July 2022
ACCEPTED 17 August 2022
PUBLISHED 13 September 2022

CITATION
Chen J, Ed-Dra A, Zhou H, Wu B, Zhang Y and Yue M (2022) Antimicrobial resistance and genomic investigation of non-typhoidal *Salmonella* isolated from outpatients in Shaoxing city, China. *Front. Public Health* 10:988317. doi: 10.3389/fpubh.2022.988317



# Antimicrobial resistance and genomic investigation of non-typhoidal *Salmonella* isolated from outpatients in Shaoxing city, China

Jiancai Chen[1†], Abdelaziz Ed-Dra[2†], Haiyang Zhou[3†], Beibei Wu[1], Yunyi Zhang[1*] and Min Yue[2,3,4,5*]

[1]Zhejiang Provincial Center for Disease Control and Prevention, Hangzhou, China, [2]Hainan Institute of Zhejiang University, Sanya, China, [3]Department of Veterinary Medicine, Institute of Preventive Veterinary Sciences, Zhejiang University College of Animal Sciences, Hangzhou, China, [4]Zhejiang Provincial Key Laboratory of Preventive Veterinary Medicine, Hangzhou, China, [5]State Key Laboratory for Diagnosis and Treatment of Infectious Diseases, National Clinical Research Center for Infectious Diseases, National Medical Center for Infectious Diseases, The First Affiliated Hospital, College of Medicine, Zhejiang University, Hangzhou, China

Human non-typhoidal salmonellosis is among the leading cause of morbidity and mortality worldwide, resulting in huge economic losses and threatening the public health systems. To date, epidemiological characteristics of non-typhoidal *Salmonella* (NTS) implicated in human salmonellosis in China are still obscure. Herein, we investigate the antimicrobial resistance and genomic features of NTS isolated from outpatients in Shaoxing city in 2020. Eighty-seven *Salmonella* isolates were recovered and tested against 28 different antimicrobial agents, representing 12 categories. The results showed high resistance to cefazolin (86.21%), streptomycin (81.61%), ampicillin (77.01%), ampicillin-sulbactam (74.71%), doxycycline (72.41%), tetracycline (71.26%), and levofloxacin (70.11%). Moreover, 83.91% of isolates were resistant to ≥3 categories, which were considered multi-drug resistant (MDR). Whole-genome sequencing (WGS) combined with bioinformatic analysis was used to predict serovars, MLST types, plasmid replicons, antimicrobial resistance genes, and virulence genes, in addition to the construction of phylogenomic to determine the epidemiological relatedness between isolates. Fifteen serovars and 16 STs were identified, with the dominance of *S.* I 4, [5], 12:i:– ST34 (25.29%), *S.* Enteritidis ST11 (22.99%), and *S.* Typhimurium ST19. Additionally, 50 resistance genes representing ten categories were detected with a high prevalence of *aac(6')-Iaa* (100%), $bla_{TEM-1B}$ (65.52%), and *tet(A)* (52.87%), encoding resistance to aminoglycosides, $\beta$-lactams, and tetracyclines, respectively; in addition to chromosomic mutations affecting *gyrA* gene. Moreover, we showed the detection of 18 different plasmids with the dominance of IncFIB(S) and IncFII(S) (39.08%). Interestingly, all isolates harbor the typical virulence genes implicated in the virulence mechanisms of *Salmonella*, while one isolate of *S.* Jangwani contains the *cdtB* gene encoding typhoid toxin production. Furthermore, the phylogenomic analysis showed that all isolates of the same serovar are very close to each other and clustered

together in the same clade. Together, we showed a high incidence of MDR among the studied isolates which is alarming for public health services and is a major threat to the currently available treatments to deal with human salmonellosis; hence, efforts should be gathered to further introduce WGS in routinely monitoring of AMR *Salmonella* in the medical field in order to enhance the effectiveness of surveillance systems and to limit the spread of MDR clones.

KEYWORDS

**non-typhoidal *Salmonella*, whole genome sequencing, antimicrobial resistance, virulence, gastroenteritis, public health, salmonellosis**

## Introduction

Gastroenteritis is a common disease in both developing and developed countries and is considered a significant economic burden leading to high financial loss for worldwide health care systems. Most gastroenteritis cases are self-limited in immunocompetent patients. At the same time, it can persist for a long time with severe symptoms and diarrhea in immunocompromised patients, including young children and the elderly. According to recent data, over 1.7 billion global cases of diarrheal disease are reported annually, leading to about 2.2 million deaths (1). In China, infectious diarrhea, excluding cholera, dysentery, and enteric fever, caused more than one million cases annually from 2014 to 2019, which the National Notifiable Diseases Reporting System classified as Category C infectious disease (2). Bacteria take second place among the agents causing gastroenteritis after viruses (3).

Non-typhoidal *Salmonella* (NTS) are among the most common etiological agents causing acute gastroenteritis worldwide. It is estimated that *Salmonella* species were responsible for about 180 million (9%) of the diarrheal diseases that occur globally each year, leading to 298,000 deaths, representing 41% of all diarrheal disease-associated deaths (4, 5). In China, the incidence of non-typhoidal salmonellosis was estimated at 626.5 cases per 100,000 persons (6). *Salmonella* is a Gram-negative, rod-shaped, non-spore-forming, and facultatively anaerobic bacterium, belonging to the Enterobacteriaceae family. To date, more than 2,600 *Salmonella* serovars have been described (7), where only some of them were reported to cause human salmonellosis (8–17). The digestive tract of vertebrates is considered the main reservoir of *Salmonella* species, and animal farms are the primary source for the development and dissemination (6, 18–22). *Salmonella* might contaminate animal carcasses during transport, slaughtering, and then transmitted to humans *via* the farm-to-fork route (23–30), causing severe infections and threatening public health systems.

Antibiotics have been widely used to treat salmonellosis in the veterinary or medical fields. However, since the 1950s, resistance to the usual antimicrobial agents has appeared and increased until rising the threatened limits. Currently, the third-generation cephalosporins and quinolones are used as the last line of defense to treat salmonellosis in both adult and young patients, while polymyxins are used to treat the cases of multidrug resistance Enterobacteriaceae (31, 32). However, recent investigations have reported the resistance of *Salmonella* isolates recovered from animal farms, food chain processes, foods, and humans to different antibiotics, including the third-generation cephalosporins, quinolones, polymyxins, aminoglycosides, and others (18, 31, 33), with the usual detection of superbug isolates which further complicates the epidemiological situation and is considered a serious threat to public health by limiting choices for therapeutic treatment of patients (34).

In this regard, the earlier detection and accurate diagnosis of multidrug-resistant (MDR) isolate based on high throughput surveillance are the key solutions to limit the spread and dissemination of harmful superbug clones. Today the advance in high throughput sequencing encourages the use of WGS on a large scale for the epidemiological investigation to monitor MDR pathogens (23, 35). Additionally, the ongoing decreases in sequencing costs and the increase of online platforms available for analyzing, sharing, and comparing genomic data, enormously helped the harmonization use of WGS in different areas (36–38). In China, several cases of human salmonellosis were recorded each year, however, the in-depth analysis of the implicated *Salmonella* isolates is still obscure. To proof of concept, this study aims to use WGS as a cost-effective method to provide genomic features, including MLST patterns, antimicrobial resistance and virulence genes, plasmid replicons, and genetic diversity of *Salmonella* isolates recovered from outpatients in Shaoxing city, Zhejiang province, China.

# Materials and methods

## Sample collection and *Salmonella* identification

A total of 87 *Salmonella* isolates were collected from outpatients in different counties (Zhuji, Shengzhou, Xinchang, Keqiao, Shangyu, and Yuecheng) of Shaoxing city, Zhejiang province, China (Supplementary Table S1). During the year 2020, diarrheal samples were collected from outpatients having gastroenteritis. *Salmonella* isolates were isolated, identified, and characterized according to the previously described methods (11, 12, 14, 16). Briefly, a 10 mL buffered peptone water was used for the pre-enrichment of human fecal samples (Oxoid, United Kingdom), then 0.1 mL of the pre-enriched samples were added to 10 mL of Rappaport Vassiliadis broth (Oxoid, United Kingdom) and incubated at 42°C for 24 h. After incubation, the samples were streaked onto Xylose Lysine Desoxycholate (XLD) (Oxoid, United Kingdom) and incubated at 37°C for 18–24 h. The suspected colonies of *Salmonella* on XLD were round, transparent red or pink with or without typical black centers. The suspected colonies were confirmed using matrix-assisted laser desorption ionization-time of flight mass spectrometry (MALDI-TOF MS) and polymerase chain reaction (PCR) to amplify the *invA* gene using specific primers as described previously (5, 16, 39). Furthermore, The PCR-confirmed *Salmonella* isolates were serotyped by slide agglutination method to define O and H antigens using commercial antisera (SSI Diagnostica, Hillerød, Denmark) according to White–Kauffmann–Le Minor scheme (40).

## Antimicrobial susceptibility testing

The antimicrobial susceptibility of the studied *Salmonella* isolates was evaluated toward a panel of 28 different antimicrobial agents belonging to 12 categories by using the broth dilution method. The tested antimicrobial agents were as follow: Penicillins (Ampicillin, AMP), β-lactam combination agents (Amoxicillin-clavulanic acid, AMC; Ampicillin-sulbactam, SAM), Aminoglycosides (Amikacin, AMK; Gentamicin, GEN; Kanamycin, KAN; Streptomycin, STR), Tetracyclines (Tetracycline, TET; Minocycline, MIN; Doxycycline, DOX); Phenicols (Chloramphenicol, CHL), Folate pathway inhibitors (Trimethoprim-sulfamethoxazole, SXT; Sulfafurazole, SIZ); Cephems (Cefazolin, CFZ; Cefoxitin, FOX; Cefotaxime, CTX; Ceftazidime, CAZ; Cefepime, FEP); Carbapenems (Imipenem, IPM; Meropenem, MEM); Quinolones (Nalidixic acid, NAL; Ciprofloxacin, CIP; levofloxacin, LVX; Gemifloxacin, GEM); Macrolides (Azithromycin, AZM); Lipopeptides (Colistin, CST; Polymyxin B, PMB); Monobactams (Aztreonam, ATM) (Table 1). The interpretation of results was performed according to the recommendation of the Clinical Laboratory Standard Institute guidelines (CLSI), and the European Committee for Antimicrobial Susceptibility Testing (EUCAST) (41, 42), and the isolates presented intermediate resistance were considered resistant for the ease of analysis. However, isolates that are non-susceptible to at least one antimicrobial agent in three or more than three antimicrobial categories were considered multidrug-resistant (MDR) (43). *Escherichia coli* ATCC 25922 was used as a control strain.

## Genomic DNA extraction and sequencing

The genomic DNA of all the studied isolates were extracted using TIANamp bacteria DNA kit (Tiangen Biotech, China) according to the manufacturer's instructions, from overnight cultures in Luria–Bertani (LB) broth incubated at 37 °C. The obtained genomic DNA was quantified using a Qubit 2.0 fluorometer (Invitrogen, USA) and then sequenced by using Illumina NovaSeq 6000 platform as previously described (14, 20, 35).

## Bioinformatic analysis

The obtained raw reads were checked for sequencing quality using FastQC and trimmed using Trimmomatic (44), in which the low-quality sequences and joint sequences were removed. The clean data were then assembled using SPAdes 4.0.1 (45) with "careful" correction option to reduce the number of mismatches in the final assembly and annotated by using the Rapid Annotation Subsystem Technology (RAST) server (https://rast.nmpdr.org/) and Prokka v.1.14 (46). The assembled contigs were then used to predict plasmid replicons and antimicrobial-resistance genes using PlasmidFinder 2.1 (https://cge.cbs.dtu.dk/services/PlasmidFinder/) and ResFinder 3.2 tools (https://cge.cbs.dtu.dk/services/ResFinder/), respectively, with a similarity cut-off of 90%. The prediction of serovar and sequence type were performed using SeqSero 1.2 (https://cge.food.dtu.dk/services/SeqSero/) and MLST 2.0 (https://cge.food.dtu.dk/services/MLST/) available on the Center for Genomic Epidemiology (CGE) platform. The genomic mutations affecting the quinolone resistance-determining region (QRDR) were detected by using Staramr software against PointFinder v1.9 (https://github.com/phac-nml/staramr). Additionally, virulence genes were predicted using the virulence factors database (VFDB) (47). All bioinformatic analyses were conducted on our in-house Galaxy platform as previously described (20). On the other hand, the association between antimicrobial resistance genes and the corresponding plasmid replicons has been investigated according to the method described previously (18).

TABLE 1 Antimicrobial susceptibility percentage of *Salmonella* ($n = 87$) isolated from outpatients.

| Antimicrobial agent | Code | Concentration range (μg/ mL) | Breakpoint interpretive criteria (μg/mL)* | | | Results in percentage (%) | |
|---|---|---|---|---|---|---|---|
| | | | S | I | R | S | R** |
| **Aminoglycosides** | | | | | | | |
| Amikacin | AMK | 0.5–128 | ≤16 | 32 | ≥64 | 87 (100%) | 0 (0%) |
| Gentamicin | GEN | 0.12–128 | ≤4 | 8 | ≥16 | 77 (88.51%) | 10 (11.49%) |
| Kanamycin | KAN | 0.5–128 | ≤16 | 32 | ≥64 | 82 (94.25%) | 5 (5.75%) |
| Streptomycin[a] | STR | 0.5–128 | ≤8 | 16 | ≥32 | 16 (18.39%) | 71 (81.61%) |
| **β-lactam combination agents** | | | | | | | |
| Amoxicillin-clavulanic acid | AMC | 0.25/0.12–128/64 | ≤8/4 | 16/8 | ≥ 32/16 | 65 (74.71%) | 22 (25.29%) |
| Ampicillin-sulbactam | SAM | 0.25/0.12–128/64 | ≤8/4 | 16/8 | ≥ 32/16 | 22 (25.29%) | 65 (74.71%) |
| **Tetracyclines** | | | | | | | |
| Tetracycline | TET | 0.12–128 | ≤4 | 8 | ≥16 | 25 (28.74%) | 62 (71.26%) |
| Minocycline | MIN | 0.12–128 | ≤4 | 8 | ≥16 | 40 (45.98%) | 47 (54.02%) |
| Doxycycline | DOX | 0.12–128 | ≤4 | 8 | ≥16 | 24 (27.59%) | 63 (72.41%) |
| **Folate pathway inhibitors** | | | | | | | |
| Trimethoprim-sulfamethoxazole | SXT | 0.25/4.75–32/608 | ≤2/38 | – | ≥4/76 | 63 (72.41%) | 24 (27.59%) |
| Sulfafurazole[b] | SIZ | 16–512 | ≤256 | – | ≥512 | 32 (36.78%) | 55 (63.22%) |
| **Cephems** | | | | | | | |
| Cefazolin | CFZ | 0.032–64 | ≤2 | 4 | ≥8 | 12 (13.79%) | 75 (86.21%) |
| Cefoxitin | FOX | 0.5–128 | ≤8 | 16 | ≥32 | 87 (100%) | 0 (0%) |
| Cefotaxime | CTX | 0.032–64 | ≤1 | 2 | ≥4 | 78 (89.66%) | 9 (10.34%) |
| Ceftazidime | CAZ | 0.032–64 | ≤4 | 8 | ≥16 | 81 (93.10%) | 6 (6.90%) |
| Cefepime | FEP | 0.032–64 | ≤2 | – | ≥16 | 85 (97.70%) | 2 (2.30%) |
| **Carbapenems** | | | | | | | |
| Imipenem | IPM | 0.12–64 | ≤1 | 2 | ≥4 | 86 (98.85%) | 1 (1.15%) |
| Meropenem | MEM | 0.12–64 | ≤1 | 2 | ≥4 | 86 (98.85%) | 1 (1.15%) |
| **Quinolones** | | | | | | | |
| Nalidixic acid | NAL | 0.5–128 | ≤16 | – | ≥32 | 51 (58.62%) | 36 (41.38%) |
| Ciprofloxacin | CIP | 0.004–16 | ≤0.06 | 0.12∼0.5 | ≥1 | 28 (32.18%) | 59 (67.82%) |
| Levofloxacin | LVX | 0.004–16 | ≤0.12 | 0.25∼1 | ≥2 | 26 (29.89%) | 61 (70.11%) |
| Gemifloxacin | GEM | 0.004–16 | ≤0.25 | 0.5 | ≥1 | 72 (82.76%) | 15 (17.24%) |
| **Macrolides** | | | | | | | |
| Azithromycin | AZM | 0.5–128 | ≤16 | – | ≥32 | 81 (93.10%) | 6 (6.90%) |
| **Lipopeptides** | | | | | | | |
| Colistin | CST | 0.12–32 | ≤2 | – | ≥4 | 67 (77.01%) | 20 (22.99%) |
| Polymyxin B | PMB | 0.12–32 | ≤2 | – | ≥4 | 73 (83.91%) | 14 (16.09%) |
| **Monobactams** | | | | | | | |
| Aztreonam | ATM | 0.25–64 | ≤4 | 8 | ≥16 | 79 (90.80%) | 8 (9.20%) |
| **Penicillins** | | | | | | | |
| Ampicillin | AMP | 0.5–64 | ≤8 | 16 | ≥32 | 20 (22.99%) | 67 (77.01%) |
| **Phenicols** | | | | | | | |
| Chloramphenicol | CHL | 0.5–128 | ≤8 | 16 | ≥32 | 59 (67.82%) | 28 (32.18%) |

*S, susceptible; I, intermediate resistance; R, resistant.
**Intermediate results were merged with resistant results.
[a]For streptomycin, we used the same MIC breakpoints as for netilmicin.
[b]For Sulfafurazole, we used the same MIC breakpoints as for sulfonamides.

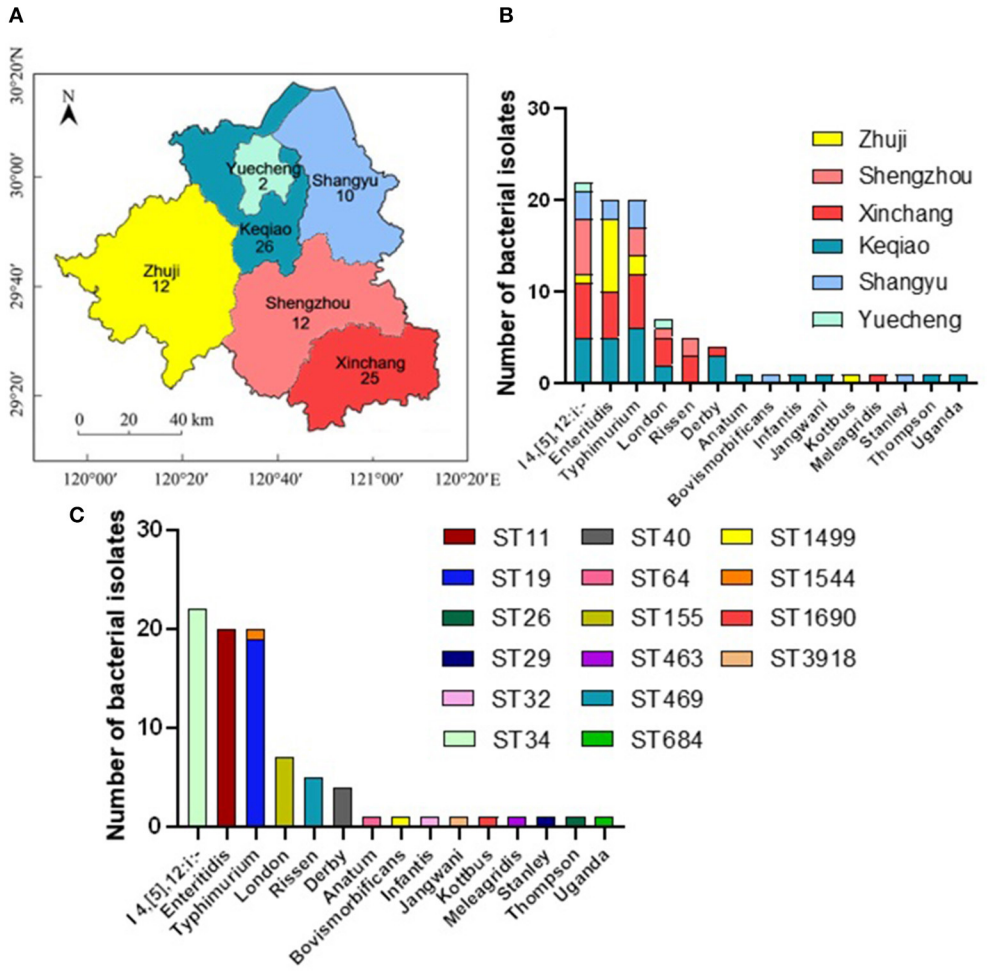


FIGURE 1
The distribution of different serovars among six counties in Shaoxing city, Zhejiang province, China. **(A)** The geographical distribution of the *Salmonella* isolates in Shaoxing with six counties which were examined in current investigations. N.B., The number indicates the numbers of isolates collected from individual county. **(B)** The distribution of fifteen serovars of *Salmonella* isolates. The dominant serovars are *S.* I 4, [5], 12:i:-, *S.* Enteritidis, and *S.* Typhimurium. **(C)** The prevalence of individual serovar with their sequence type (ST) detected in this study.

## Phylogenomic analysis

The core single-nucleotide polymorphism (SNP) of all the studied *Salmonella* strains was analyzed using Snippy v4.4.4 against the reference strain *S.* Typhimurium SL 1344. The phylogenetic tree was constructed using IQ-TREE v.1.6.12 with TVM + F + ASC model and 1,000 bootstraps, as previously described (13, 22). Moreover, the whole-genome multilocus sequence typing (wgMLST) was used to conduct wgMLST phylogenomic tree by using cano-wgMLST_Bac Compare software as described recently (20, 48), with default parameters and *S.* Typhimurium strain SL 1344 as reference strain.

# Results

## Distribution of *Salmonella* serovars

In this study, 87 *Salmonella* isolates have been isolated and identified, including 26 from Keqiao county (29.88%), 25 from Xinchang (28.74%), 12 from Zhuji (13.79%), 12 from Shengzhou (13.79%), ten from Shangyu (11.49%), and two from Yuecheng (2.30%) (Figure 1A). These isolates have been shared between male (44/87; 50.57%) and female (49.43%) patients (Supplementary Table S1). The serotyping method has identified 15 different serovars with the dominance of the monophasic variant I 4, [5], 12:i:– (22/87; 25.29%), followed by Enteritidis

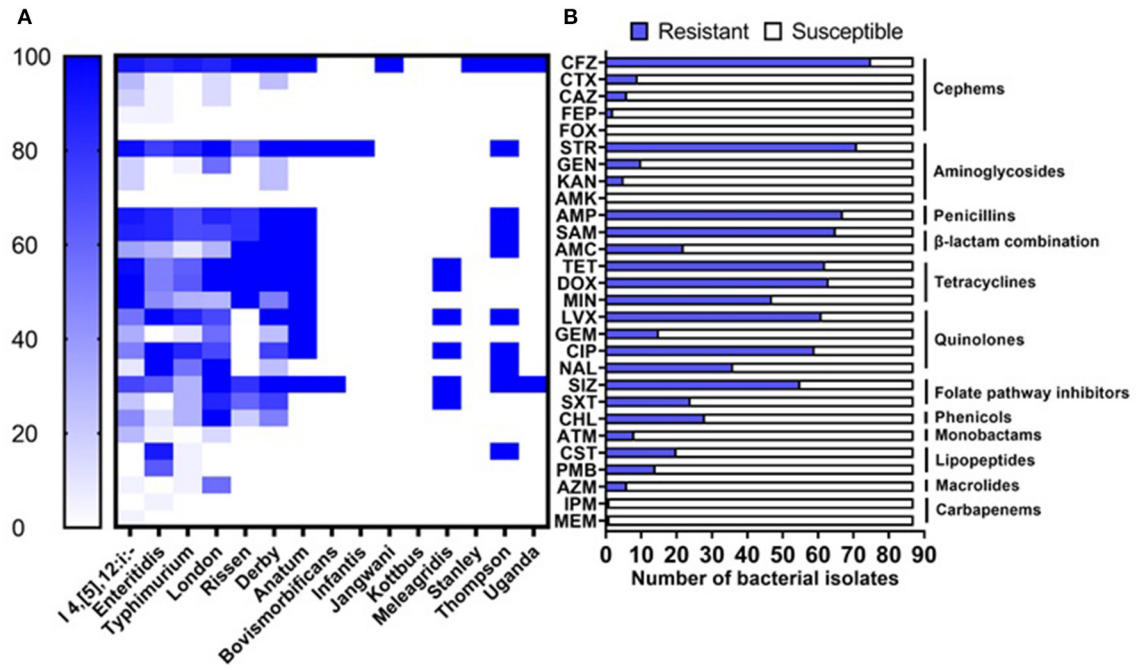


FIGURE 2
Antimicrobial resistance of *Salmonella* isolates. **(A)** Resistance of isolates grouped by serovars to the tested antimicrobial agents. **(B)** Prevalence of resistance against 28 antimicrobial agents belonging to 12 categories.

(20/87; 22.99%), and Typhimurium (Figure 1B). Additionally, allelic profiles analysis showed the identification of 16 sequence types (STs) with the dominance of ST34 (22/87; 25.29%), ST11 (20/87; 22.99%), and ST19 (19/87; 21.84%) (Figure 1C). All serovars presented one ST, except *S.* Typhimurium, which was divided into ST19 ($n = 19$) and ST1544 ($n = 1$).

## Phenotypic antimicrobial resistance

Phenotypic antimicrobial susceptibility of the 87 isolates has been evaluated toward 28 antimicrobial agents representing 12 different categories by broth dilution method according to CLSI and EUCAST recommendations. The highest resistance was observed against cefazolin (75/87; 86.21%), streptomycin (71/87; 81.61%), ampicillin (67/87; 77.01%), the combination of ampicillin-sulbactam (65/87; 74.71%), doxycycline (63/87; 72.41%), tetracycline (62/87; 71.26%), and levofloxacin (61/87; 70.11%), while all isolates were susceptible to cefoxitin and amikacin (Table 1, Figure 2B). Based on serovars distribution, our results showed that the abundant serovars (>3 isolates), especially the monophasic variant I 4, [5], 12:i:–, Enteritidis, Typhimurium, London, and Derby, present high resistance to multiple antimicrobial agents (Figure 2A). Additionally, we detected 57 different antimicrobial resistance patterns, in which 85/87 (97.70%) of isolates presented resistance to at least one category, 73/87 (83.91%) given resistance to three or more than three categories which were considered MDR. In contrast, 67/87 (77.01) isolates were resistant to five or more antimicrobial categories (Supplementary Table S2).

## Genotypic antimicrobial resistance

In order to understand the genetic arsenal behind the acquisition of antimicrobial resistance. The whole genome sequences of all isolates ($n = 87$) were screened for the detection of antimicrobial determinants encoding resistance to different antimicrobial categories, in addition to genomic mutations in the quinolone resistance-determining region (QRDR) affecting the DNA gyrase and DNA topoisomerase IV genes. The results showed the detection of 50 determinants encoding resistance to 11 different antimicrobial categories, in addition to four different mutations on the gene *gyrA* encoding resistance to quinolone (Supplementary Table S1). The most prevalent antimicrobial determinants were *aac (6')-Iaa_1* (100%), *aph (6)-Id_1* (52.87%), and *aph (3")-Ib_5* (50.57%) encoding resistance to aminoglycosides, $bla_{\text{TEM}-1B\_1}$ (65.52%) encoding resistance to β-lactams, and *tet (A)_6* (52.87%) encoding resistance to tetracyclines (Supplementary Table S1). The monophasic variant of *S.*

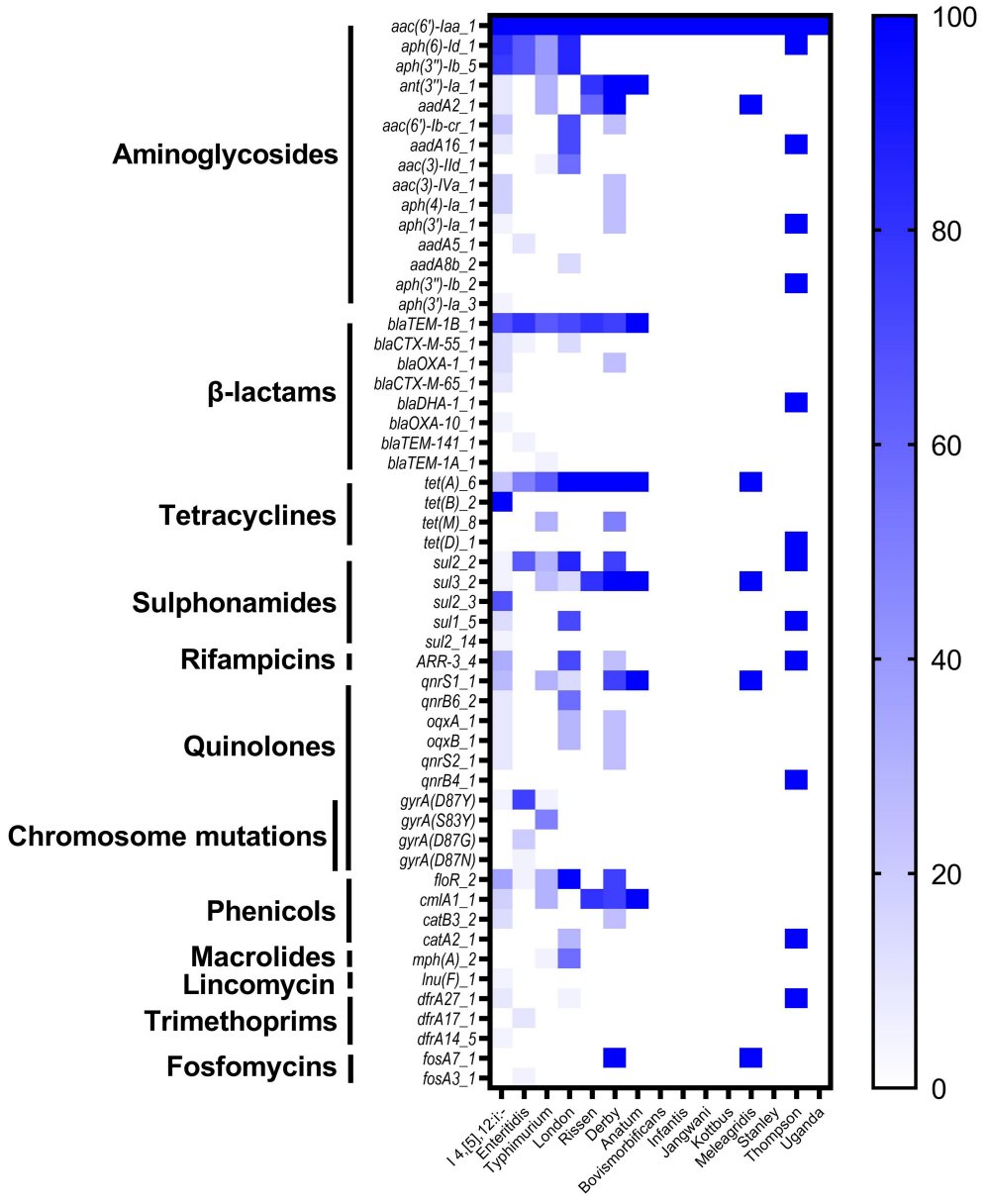


FIGURE 3
The heatmap of antimicrobial resistance genes (ARGs) and chromosomic mutations in the studied *Salmonella* isolates.

Typhimurium I 4, [5], 12:i:– harbors more diversified resistance genes (36 genes) followed by serovars London and Derby (22 genes for each one), while serovars Typhimurium and Enteritidis harbor 18 and 15 resistance genes, respectively (Figure 3). Additionally, genomic mutations conferring resistance to quinolones were only detected in serovars I 4, [5], 12:i:–, Enteritidis, and Typhimurium, where single and double mutations in the gene *gyrA* were observed (Figure 3).

## Virulence genes prediction

To provide accurate data about the virulence of studied isolates, we conducted an in-depth analysis to predict virulence genes implicated in the virulence and pathogenicity mechanism of *Salmonella* based on WGS, and the results were presented in Figure 4 and Supplementary Table S1. We detected 117 different virulence genes and the number of genes per isolate varies between 92 and 112. In addition to the

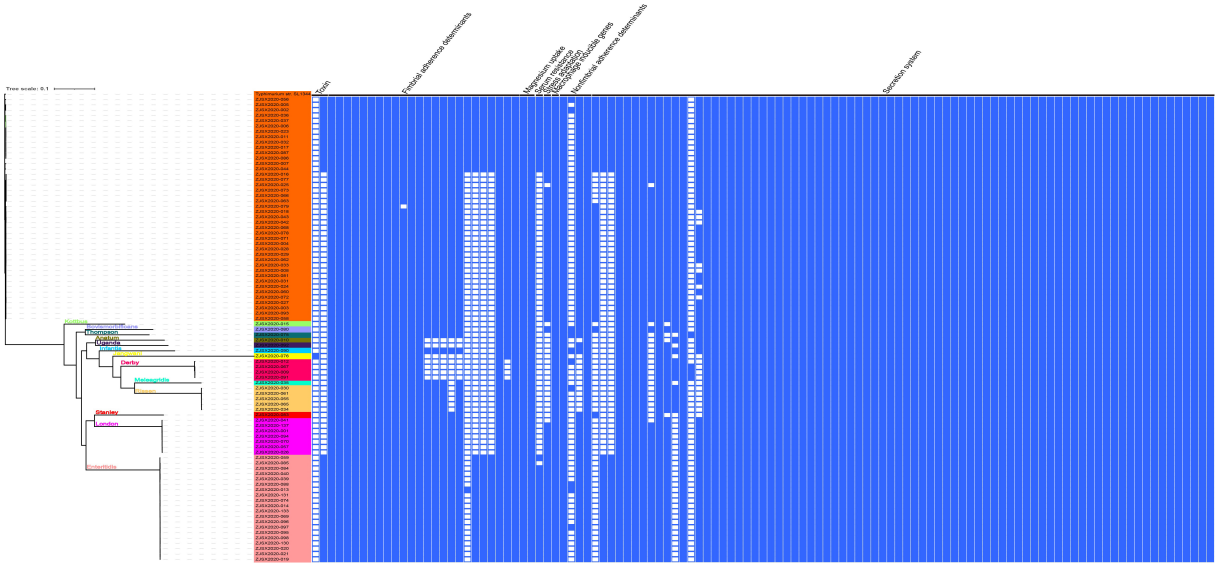


FIGURE 4
The combinatorial graph of the wgMLST phylogenomic evolutionary tree and virulence genes in the studied *Salmonella* isolates. The presence of virulence gene was marked with blue color while the absence was marked with white color. The tree was rooted by using *S.* Typhimurium SL 1344.

typical virulence genes carried on *Salmonella* pathogenicity islands (SPIs), we detected *cdtB* gene encoding typhoid toxin production in one isolate of *S.* Jangwani. The *spv* locus that clustered genes implicated in the virulence system of non-typhoid *Salmonella*, the *pef* locus clustered genes encoding fimbriae, and *rck* gene encoding serum resistance, were only detected in *Salmonella* serovars Typhimurium and Enteritidis. Furthermore, *sodCI* gene encoding for stress adaptation was detected in the monophasic variant I 4, [5], 12:i:–, *S.* Typhimurium, *S.* Enteritidis, *S.* London, and *S.* Bovismorbificans. While the gene *grvA* encoding for anti-virulence was detected in serovars London, Typhimurium, and Bovismorbificans.

## Plasmid replicons

The distribution of plasmid replicons among the studied *Salmonella* isolates was performed by screening the whole genome sequences in the PlasmidFinder tool. In this study, 18 different plasmids were detected where the plasmids IncFIB (S)_1 and IncFII (S)_1 were the most prevalent (34/87; 39.08% for each one), followed by IncX1_4 (13/87; 14.94%), and IncHI2A_1, IncHI2_1 and IncFIB(K)_1_Kpn3 (6/87; 6.90% for each one) (Supplementary Table S1). Additionally, we reported that the monophasic variant I 4, [5], 12:i:– harbors more diversified plasmids ($n = 9$) compared with other serovars, followed by Enteritidis ($n = 5$); However, isolates belonging to serovars Rissen, Bovismorbificans, Infantis, Jangwani, Stanley, and Uganda didn't harbor any plasmid (Figure 5).

## Association of plasmids and antimicrobial resistance genes

The association between plasmid replicons and antimicrobial resistance genes has been investigated and the results are presented in Supplementary Table S3. We demonstrated that the plasmid type IncX1 was the main carrier of antimicrobial resistance, carrying multiple resistance genes like *sul2*, *aph (3")-Ib*, *aph (6)-Id*, *tet (A)* encoding resistance to sulphonamides, aminoglycosides, and tetracyclines, respectively. However, the plasmid types IncFII(S) and IncFIB(S) were the leading carriers of the gene $bla_{\mathrm{TEM-1B}}$ encoding resistance to $\beta$-lactam. Notably, the co-occurrence between plasmid replicons and antimicrobial resistance genes was mainly observed in serovar Enteritidis.

## Phylogenomic analysis

The sequenced and assembled genomes have been first checked for quality assessment and results were presented in Supplementary Table S4. The results showed that the number of contigs (≥300 bp) varies between 30 and 117 contigs while the average genomes size of draft assemblies was 4,920,864 bp and the average $N_{50}$ was 320,121 bp. Moreover, to determine

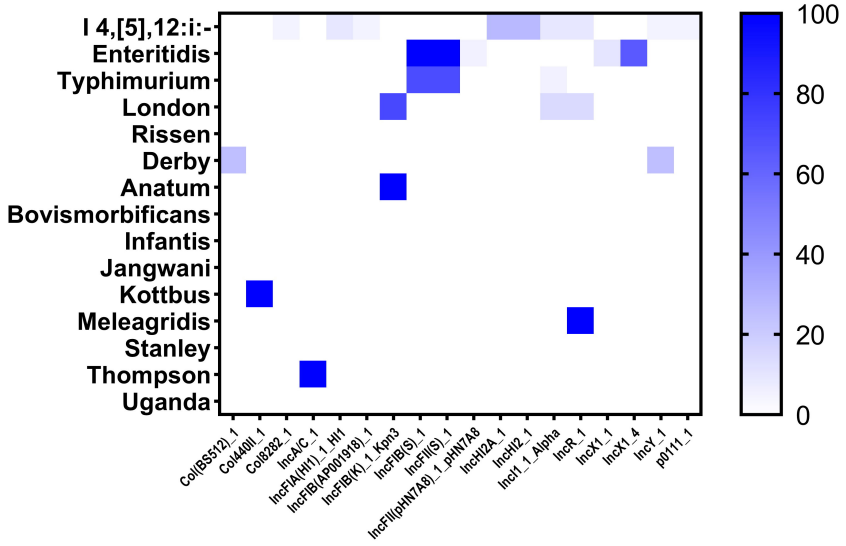


FIGURE 5
The heatmap of plasmids distribution in different *Salmonella* isolates. The strength of the colors corresponds to the numerical value of the prevalence of the plasmids. Dark blue color indicates high prevalence and white color for gene absence.

the epidemiological relatedness between the studied *Salmonella* isolates, we conducted a phylogenomic analysis based on core single-nucleotide polymorphism (SNP) and whole-genome multilocus sequence typing (wgMLST) (Figure 4, 6). The results showed that isolates belonging to the same serovar are very close to each other and clustered together in the same clade. A substantial similarity has been seen between isolates of the monophasic variant I 4, [5], 12:i: and Typhimurium, which were grouped in the same clade. Moreover, isolates of serovars Enteritidis, London, and Stanley have been grouped in the same clade indicating a high association between them. Furthermore, the association between phylogenomic tree and distribution of virulence factors showed few differences in the patterns of virulence factor cassettes between different serovars (Figure 4).

## Discussion

Non-typhoidal salmonellosis is a common disease caused by the bacteria *Salmonella*, leading to a huge economic burden, which threatens healthcare systems worldwide (49–51). *Salmonella* originated from animal reservoirs are transmitted to humans *via* the food chain causing gastroenteritis and sometimes invasive infections. Generally, the consumption of food or water contaminated with NTS is the leading cause of human salmonellosis. In this study, we presented the epidemiological characteristics of NTS isolates recovered from outpatients in Shaoxing city based on WGS combined with accurate bioinformatics tools and in-depth phenotypic methods, these results may provide the scientific background about the MDR *Salmonella* circulated in Chinese hospitals and may help health service authorities to implement effective programs to limit the spread and dissemination of MDR clones in medical field.

In this study, 87 *Salmonella* isolates were identified, these isolates belonged to 15 different serovars and 16 STs. The dominant serovar was the monophasic variant I 4, [5], 12:i:– ST34, followed by *S.* Enteritidis ST11, and *S.* Typhimurium ST19. These serovars are currently considered the most common serovars implicated in human salmonellosis (52, 53). Since the mid-1990s, the implication of the monophasic variant I 4, [5], 12:i:– in human salmonellosis has significantly increased, which is currently classified among the most five predominant serovars in NTS infections (52, 54). However, *S.* Enteritidis is well known as a worldwide foodborne pathogen and is widely linked to the consumption of egg-derived products (55, 56). In China, *S.* Typhimurium is considered the most common serovar causing NTS infections. Ke et al. reported that *S.* Typhimurium was the most predominant serovar (62.6%) among isolates recovered from children between 2012 and 2019 in a tertiary hospital in Ningbo, Zhejiang, China (57). Similarly, Wu et al. showed the dominance of *S.* Typhimurium (79.2%) among isolates recovered from children with NTS infections between 2009 and 2018 in Chongqing, China (58). Another Chinese study carried out in the Conghua district of Guangzhou, between June and October 2020 isolated *S.* Typhimurium as the most common serovar in hospitalized patients (59). Moreover, in Vietnam *S.* Typhimurium dominated NTS isolates (41.8%) from

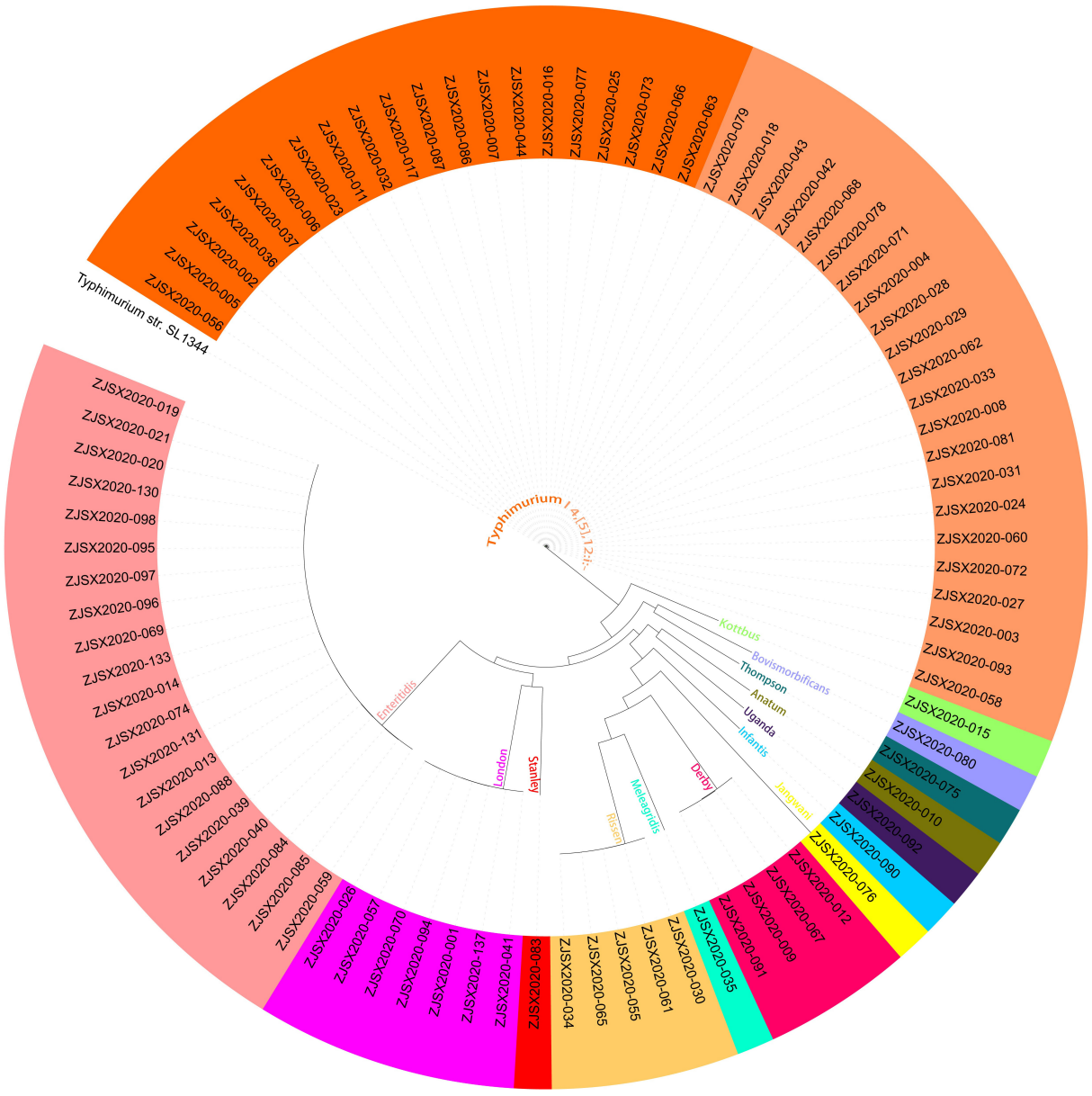


FIGURE 6
The core genome SNP-based phylogenomic tree by maximum likelihood (TVM+F+ASC) of 87 *Salmonella* isolates. The tree was rooted by using S. Typhimurium SL 1344.

hospitalized children in Ho Chi Minh city, Vietnam (60). In Thailand, Sinwat et al. reported *S.* Typhimurium as the major serovar for diarrhoeal patients (61). The wide spread of *S.* Typhimurium among patients in Southeast Asian countries could be due to the common source of contamination, especially with the high trading exchange between these countries.

In order to provide accurate epidemiological information about the current antimicrobial susceptibility situation of clinical NTS, all the isolated strains were tested against a panel of 28 different antimicrobial agents belonging to 12 categories. The common resistance was observed against cefazolin (1st generation of cephalosporin), streptomycin (aminoglycoside), ampicillin (penecillins), the combination of ampicillin-sulbactam, doxycycline and tetracycline (tetracyclines), and levofloxacin (quinolones). The high resistance to these categories has becoming frequently observed in *Salmonella* isolates recovered from food, human, and animal samples (6, 19, 25, 26, 58, 62). Moreover, we reported a high incidence of MDR among isolates (83.91%) which was higher than that found in *Salmonella* recovered from hospitalized patients in the

Conghua district of Guangzhou, China (47.06%) (59), and from children with NTS infections in Chongqing, China (13.7%) (58). Indeed, the extensive and continued use of antibiotics in medical and veterinary fields has led to the development of MDR strains which threaten public health by limiting the effectiveness of available antimicrobials for therapeutic usage. Hence, infections with these MDR isolates may lead to therapeutic failure, especially with the limit in alternative antibiotics able to treat these cases.

The screening of antimicrobial resistance genes was performed based on WGS and results showed the detection of 50 genes encoding resistance to 11 categories in addition to 4 mutations affecting the gene *gyrA*. All isolates (100%) were positive for the genes *aac (6')-Iaa* encoding resistance to aminoglycosides, while 65.52% contain $bla_{\mathrm{TEM-1B}}$ encoding resistance to β-lactams and 52.87% contain *tet (A)* gene encoding resistance to tetracyclines. Generally, resistance to aminoglycosides is associated with enzymatic modification by using certain enzymes, including aminoglycoside phosphotransferases, aminoglycoside acetyltransferases, and aminoglycoside adenyltransferases encoded by the genes *aphA*, *aacC*, and *aadA*, respectively (63, 64). Resistance to $\beta$-lactams is mediated by *bla* genes encoding enzymes ($\beta$-lactamases) capable of hydrolyzing the $\beta$-lactam ring of $\beta$-lactam antibiotics. In this study, we detected *bla* genes in predominant serovars, including the monophasic variant I 4, [5], 12:i:–, Enteritidis, Typhimurium, in addition to serovars London, Rissen, Derby, Anatum, and Thompson. Thus, it has been reported that different types of $bla_{\mathrm{TEM}}$ are mostly linked with ampicillin-resistant *Salmonella* serovars (65), which may explain the high incidence of ampicillin resistance. We also detected the *tet* genes encoding resistance to tetracyclines, in addition to different genes encoding resistance to chloramphenicol. Resistance to tetracyclines and chloramphenicol is often associated with efflux pumps mechanisms encoded by *tet* and *floR* genes, respectively; yet, resistance to chloramphenicol may also be associated with modification of the antibiotic target by chloramphenicol acetyltransferases encoded by *cat* genes (66). Moreover, the genes *sul1-3,* mediating resistance to sulphonamides, have been detected in all predominant serovars, while genes *dfrA* encoding resistance to trimethoprim were only detected in the monophasic variant I 4, [5], 12:i:–, Enteritidis, London, and Thompson. Furthermore, the genes *qnr* encoding decreased susceptibility to quinolones were detected in the monophasic variant I 4, [5], 12:i:–, Typhimurium, London, Derby, Anatum, Meleagridis, and Thompson. The resistance to quinolones could be due to the acquisition of resistance genes carried on mobile plasmids as well as the presence of chromosomic mutations affecting *gyr* and *par* genes (18, 67).

The virulome analysis of the studied isolates showed the detection of the typical genes implicated in the virulence and pathogenicity mechanisms of *Salmonella*. In addition, the gene *cdtB* encoding typhoid toxin production was detected in one isolate of *S.* Jangwani. In fact, *cdtB* gene has become commonly detected in NTS isolates from different sources (5, 12, 14, 18, 20, 23). It is noted that typhoid toxin was first found in *S.* Typhi and then several NTS serovars have been reported to carry genes encoding the production of this toxin, especially *cdtB*, suggesting the implication of this gene in the development of invasion non-typhoidal salmonellosis. Moreover, we reported the detection of *spv*, *pef*, and *rck* genes in isolates belonging to serovars Typhimurium and Enteritidis. The genes clustered in the *spv* locus have been demonstrated to possess an essential role in the virulence pathway of NTS (68, 69). The *pef* fimbrial operon mediates adhesion to the murine small intestine (70), while *rck* gene enhances bacterial adhesion and invasion and confers resistance to antimicrobial agents (71). On the other hand, *sodCI* confers resistance to oxidative burst inside macrophages (72, 73). Interestingly, these genes are carried on mobile genetic elements, including plasmids and phages, horizontally transferred between serovars, which may confer a virulence potential to new serovars that have not been reported to cause human gastroenteritis.

Mobile genetic elements are the leading factors for the high spread of antimicrobial resistance by transferring resistance and virulence genes between bacteria. In this study, we detected 18 different plasmids with the dominance of IncFIB(S) and IncFII(S). These plasmids may carry *pef* genes mediated adhesion to the murine on intestine (74), and *spv* genes necessary to the virulence pathway of NTS (75), in addition to their ability to confer hypervirulence and bacterial fitness (76). As known, the distribution of some plasmids is serovar dependent. In this study, we reported the detection of plasmids IncFIB(S) and IncFII(S) in *S.* Enteritidis and *S.* Typhimurium, while the plasmids IncHI2A and IncHI2 were only detected in *S.* I 4, [5], 12:i:–. Moreover, the association between plasmids and antimicrobial resistance genes showed that the plasmid type IncX1 is the leading carrier of the resistance genes *sul2*, *aph (3")-Ib*, *aph (6)-Id*, *tet (A)* in *S.* Enteritdis. These results are in accord with those reported by Li et al. showing that the plasmid IncX1 is the key carrier of antimicrobial resistance determinants like $bla_{\mathrm{TEM-1B}}$, *sul1*, *sul2*, *aph (6)-Id*, *ant (3")-Ia*, *aadA5*, *dfrA17*, *dfrA1*, and *tet(A)* in *S.* Enteritidis (18). Otherwise, Elbediwi et al. reported a strong positive correlation between the plasmids IncHI2 and IncHI2A and the resistance genes *sul1*, *dfrA12*, *armA*, and $bla_{\mathrm{TEM-1B}}$ (20). Therefore, the detection of *Salmonella* isolates harboring plasmids carrying virulence and resistance genes is a significant threat to public health.

## Conclusion

To date, few studies have investigated the epidemiological characteristics of NTS isolated from outpatients in China. Herein, we presented accurate information about the epidemiology of NTS implicated in human salmonellosis

in Shaoxing city, Zhejiang province, China, by using whole-genome sequencing combined with in-depth bioinformatics analysis and cutting-edge phenotypic methods. Fifteen different serovars and 16 STs have been identified with the dominance of *S.* I 4, [5], 12:i:– ST34, *S.* Enteritidis ST11, and *S.* Typhimurium ST19, which were considered the leading cause of non-typhoidal salmonellosis in China and elsewhere. Interestingly, we showed that most isolates are MDR (83.91%) and harbor different antimicrobial genetic determinants carried on transferable plasmids, in addition to critical virulence genes implicated in the pathogenicity pathways of NTS. Hence the high incidence of MDR isolates in clinical NTS is a real issue for public health, threatening the current therapeutic procedures, which requires continuous monitoring of "superbugs" isolates using whole-genome sequencing.

## Data availability statement

The datasets presented in this study can be found in online repositories. The names of the repository/repositories and accession number(s) can be found at: https://www.ncbi.nlm.nih.gov/genbank/, PRJNA844576.

## Author contributions

JC and AE-D analyzed the data and finalized the figures. AE-D and MY wrote the manuscript. HZ and BW did the experiment and data collection. MY and YZ conceived the idea and assisted with data analysis and writing. All authors have read, revised, and approved the final manuscript.

## Funding

This work was supported by the National Program on Key Research Project of China (2019YFE0103900) as well as the European Union's Horizon 2020 Research and Innovation Programme under Grant Agreement No. 861917 – SAFFI, the National Natural Science Foundation of China (31872837 and 32150410374), Zhejiang Provincial Natural Science Foundation of China (LR19C180001), and Zhejiang Provincial Key R&D Program of China (2022C02024; 2021C02008; and 2020C02032).

## Conflict of interest

The authors declare that the research was conducted in the absence of any commercial or financial relationships that could be construed as a potential conflict of interest.

## Publisher's note

All claims expressed in this article are solely those of the authors and do not necessarily represent those of their affiliated organizations, or those of the publisher, the editors and the reviewers. Any product that may be evaluated in this article, or claim that may be made by its manufacturer, is not guaranteed or endorsed by the publisher.

## Supplementary material

The Supplementary Material for this article can be found online at: https://www.frontiersin.org/articles/10.3389/fpubh.2022.988317/full#supplementary-material

## References

1. Humphries RM, Linscott AJ. Practical guidance for clinical microbiology laboratories: diagnosis of bacterial gastroenteritis. *Clin Microbiol Rev.* (2015) 28:3–31. doi: 10.1128/CMR.00073-14

2. Cao RR, Ma XZ, Li WY, Wang BN, Yang Y, Wang HR, et al. Epidemiology of norovirus gastroenteritis in hospitalized children under five years old in western China, 2015–2019. *J Microbiol Immunol Infect.* (2021) 54:918–25. doi: 10.1016/j.jmii.2021.01.002

3. Oppong TB, Yang H, Amponsem-Boateng C, Kyere EKD, Abdulai T, Duan G, et al. Enteric pathogens associated with gastroenteritis among children under 5 years in sub-saharan Africa: a systematic review and meta-analysis. *Epidemiol Infect.* (2020) 148:e64. doi: 10.1017/S0950268820000618

4. Besser JM. *Salmonella* epidemiology: a whirlwind of change. *Food Microbiol.* (2018) 71:55–9. doi: 10.1016/j.fm.2017.08.018

5. Liu Y, Jiang J, Ed-Dra A, Li X, Peng X, Xia L, et al. Prevalence and genomic investigation of *Salmonella* isolates recovered from animal food-chain in Xinjiang, China. *Food Res Int.* (2021) 142:110198. doi: 10.1016/j.foodres.2021.110198

6. Xu Y, Zhou X, Jiang Z, Qi Y, Ed-Dra A, Yue M. Epidemiological investigation and antimicrobial resistance profiles of *Salmonella* isolated from breeder chicken hatcheries in Henan, China. *Front Cell Infect Microbiol.* (2020) 10:497. doi: 10.3389/fcimb.2020.00497

7. Guibourdenche M, Roggentin P, Mikoleit M, Fields PI, Bockemühl J, Grimont PAD, et al. Supplement 2003–2007 (No. 47) to the White-Kauffmann-Le Minor scheme. *Res Microbiol.* (2010) 161:26–9. doi: 10.1016/j.resmic.2009.10.002

8. Pan H, Zhou X, Chai W, Paudyal N, Li S, Zhou X, et al. Diversified sources for human infections by *Salmonella* enterica serovar newport. *Transbound Emerg Dis.* (2019) 66:1044–8. doi: 10.1111/tbed.13099

9. Biswas S, Li Y, Elbediwi M, Yue M. Emergence and dissemination of mcr-carrying clinically relevant *Salmonella typhimurium* monophasic clone st34. *Microorganisms.* (2019) 7:298. doi: 10.3390/microorganisms7090298

10. Elbediwi M, Pan H, Biswas S, Li Y, Yue M. Emerging colistin resistance in *Salmonella enterica* serovar Newport isolates from human infections. *Emerg Microbes Infect.* (2020) 9:535–8. doi: 10.1080/22221751.2020.1733439

11. Paudyal N, Pan H, Wu B, Zhou X, Zhou X, Chai W, et al. Persistent asymptomatic human infections by *Salmonella enterica* serovar Newport in China. *mSphere.* (2020) 5:e00163-20. doi: 10.1128/mSphere.00163-20

12. Xu X, Chen Y, Pan H, Pang Z, Li F, Peng X, et al. Genomic characterization of *Salmonella Uzaramo* for human invasive infection. *Microb genomics.* (2020) 6:mgen000401. doi: 10.1099/mgen.0.000401

13. Elbediwi M, Pan H, Zhou X, Rankin SC, Schifferli DM, Yue M. Detection of mcr-9-harbouring ESBL-producing *Salmonella* Newport isolated from an outbreak in a large-animal teaching hospital in the USA. *J Antimicrob Chemother.* (2021) 76:1107–9. doi: 10.1093/jac/dkaa544

14. Qiu Y, Nambiar RB, Xu X, Weng S, Pan H, Zheng K, et al. Global genomic characterization of *Salmonella enterica* Serovar Telelkebir. *Front Microbiol.* (2021) 12:704152. doi: 10.3389/fmicb.2021.704152

15. Elbediwi M, Shi D, Biswas S, Xu X, Yue M. Changing patterns of *Salmonella enterica* serovar rissen from humans, food animals, and animal-derived foods in China, 1995–2019. *Front Microbiol.* (2021) 12:2011. doi: 10.3389/fmicb.2021.702909

16. Hu B, Hou P, Teng L, Miao S, Zhao L, Ji S, et al. Genomic investigation reveals a community typhoid outbreak caused by contaminated drinking water in China, 2016. *Front Med.* (2022) 9:448. doi: 10.3389/fmed.2022.753085

17. Feasey NA, Dougan G, Kingsley RA, Heyderman RS, Gordon MA. Invasive non-typhoidal *Salmonella* disease: an emerging and neglected tropical disease in Africa. *Lancet.* (2012) 379:2489–99. doi: 10.1016/S0140-6736(11)61752-2

18. Li Y, Kang X, Ed-Dra A, Zhou X, Jia C, Müller A, et al. Genome-based assessment of antimicrobial resistance and virulence potential of isolates of non-pullorum/gallinarum *Salmonella* serovars recovered from dead poultry in China. *Microbiol Spectr.* (2022) e0096522. doi: 10.1128/spectrum.00965-22. [Epub ahead of print].

19. Xu Y, Zhou X, Jiang Z, Qi Y, Ed-Dra A, Yue M. Antimicrobial resistance profiles and genetic typing of *Salmonella* serovars from chicken embryos in china. *Antibiotics.* (2021) 10:1156. doi: 10.3390/antibiotics10101156

20. Elbediwi M, Tang Y, Shi D, Ramadan H, Xu Y, Xu S, et al. Genomic investigation of antimicrobial-resistant *Salmonella enterica* isolates from dead chick embryos in China. *Front Microbiol.* (2021) 12:684400. doi: 10.3389/fmicb.2021.684400

21. Paudyal N, Pan H, Elbediwi M, Zhou X, Peng X, Li X, et al. Characterization of *Salmonella Dublin* isolated from bovine and human hosts. *BMC Microbiol.* (2019) 19:226. doi: 10.1186/s12866-019-1598-0

22. Li Y, Ed-Dra A, Tang B, Kang X, Müller A, Kehrenberg C, et al. Higher tolerance of predominant *Salmonella* serovars circulating in the antibiotic-free feed farms to environmental stresses. *J Hazard Mater.* (2022) 438:129476. doi: 10.1016/j.jhazmat.2022.129476

23. Wu B, Ed-Dra A, Pan H, Dong C, Jia C, Yue M. Genomic investigation of *Salmonella* isolates recovered from pigs slaughtering process in Hangzhou, China. *Front Microbiol.* (2021) 12:704636. doi: 10.3389/fmicb.2021.704636

24. Xu X, Biswas S, Gu G, Elbediwi M, Li Y, Yue M. Characterization of multidrug resistance patterns of emerging *Salmonella enterica* serovar Rissen along the food chain in China. *Antibiotics.* (2020) 9:1–16. doi: 10.3390/antibiotics9100660

25. Liu Q, Chen W, Elbediwi M, Pan H, Wang L, Zhou C, et al. Characterization of *Salmonella Resistome* and plasmidome in pork production system in Jiangsu, China. *Front Vet Sci.* (2020) 7:617. doi: 10.3389/fvets.2020.00617

26. Jiang Z, Anwar TM, Peng X, Biswas S, Elbediwi M, Li Y, et al. Prevalence and antimicrobial resistance of *Salmonella* recovered from pig-borne food products in Henan, China. *Food Control.* (2021) 121:107535. doi: 10.1016/j.foodcont.2020.107535

27. Elbediwi M, Pan H, Jiang Z, Biswas S, Li Y, Yue M. Genomic Characterization of mcr-1-carrying *Salmonella enterica* Serovar 4,[5],12:i:- ST 34 clone isolated from pigs in China. *Front Bioeng Biotechnol.* (2020) 8:663. doi: 10.3389/fbioe.2020.00663

28. Jiang Z, Paudyal N, Xu Y, Deng T, Li F, Pan H, et al. Antibiotic resistance profiles of *Salmonella* recovered from finishing pigs and slaughter facilities in Henan, China. *Front Microbiol.* (2019) 10:1513. doi: 10.3389/fmicb.2019.01513

29. Wang X, Biswas S, Paudyal N, Pan H, Li X, Fang W, et al. Antibiotic resistance in *Salmonella* typhimurium isolates recovered from the food chain through national antimicrobial resistance monitoring system between 1996 and 2016. *Front Microbiol.* (2019) 10:985. doi: 10.3389/fmicb.2019.00985

30. Pan H, Paudyal N, Li X, Fang W, Yue M. Multiple food-animal-borne route in transmission of antibiotic-resistant *Salmonella* newport to humans. *Front Microbiol.* (2018) 9:23. doi: 10.3389/fmicb.2018.00023

31. Elbediwi M, Li Y, Paudyal N, Pan H, Li X, Xie S, et al. Global burden of colistin-resistant bacteria: Mobilized colistin resistance genes study (1980–2018). *Microorganisms.* (2019) 7:461. doi: 10.3390/microorganisms7100461

32. Klemm EJ, Shakoor S, Page AJ, Qamar FN, Judge K, Saeed DK, et al. Emergence of an extensively drug-resistant *Salmonella enterica* serovar typhi clone harboring a promiscuous plasmid encoding resistance to fluoroquinolones and third-generation cephalosporins. *mBio.* (2018) 9:e00105–18. doi: 10.1128/mBio.00105-18

33. Ed-Dra A, Filali FR, Karraouan B, El Allaoui A, Aboulkacem A, Bouchrif B. Prevalence, molecular and antimicrobial resistance of *Salmonella* isolated from sausages in Meknes, Morocco. *Microb Pathog.* (2017) 105:340–5. doi: 10.1016/j.micpath.2017.02.042

34. Collignon P. Superbugs in food: a severe public health concern. *Lancet Infect Dis.* (2013) 13:641–3. doi: 10.1016/S1473-3099(13)70141-5

35. Yu H, Elbediwi M, Zhou X, Shuai H, Lou X, Wang H, et al. Epidemiological and genomic characterization of campylobacter jejuni isolates from a foodborne outbreak at Hangzhou, China. *Int J Mol Sci.* (2020) 21:3001. doi: 10.3390/ijms21083001

36. Peng X, Ed-Dra A, Yue M. Whole genome sequencing for the risk assessment of probiotic lactic acid bacteria. *Crit Rev Food Sci Nutr.* (2022) 1–19. doi: 10.1080/10408398.2022.2087174. [Epub ahead of print].

37. Köser CU, Ellington MJ, Peacock SJ. Whole-genome sequencing to control antimicrobial resistance. *Trends Genet.* (2014) 30:401–7. doi: 10.1016/j.tig.2014.07.003

38. McDermott PF, Tyson GH, Kabera C, Chen Y, Li C, Folster JP, et al. Whole-genome sequencing for detecting antimicrobial resistance in nontyphoidal *Salmonella*. *Antimicrob Agents Chemother.* (2016) 60:5515–20. doi: 10.1128/AAC.01030-16

39. Zhu C, Yue M, Rankin S, Weill FX, Frey J, Schifferli DM. One-step identification of five prominent chicken *Salmonella* serovars and biotypes. *J Clin Microbiol.* (2015) 53:3881–3. doi: 10.1128/JCM.01976-15

40. Grimont P, Weill F-X. *Antigenic Formulae of the Salmonella servovars*. 9th Ed. Paris: Institut Pasteur (2007).

41. CLSI. *Performance Standards for Antimicrobial Susceptibility Testing.* 30th Ed. Clinical and Laboratory Standards Institute (CLSI). (2020).

42. EUCAST (European Committee on Antimicrobial Susceptibility Testing). *Recommendations 2017: Eur Comm Antimicrob Susceptibility Test.* (2017). Available online at: www.sfm-microbiologie.org (accessed July 18, 2020).

43. Magiorakos AP, Srinivasan A, Carey RB, Carmeli Y, Falagas ME, Giske CG, et al. Multidrug-resistant, extensively drug-resistant and pandrug-resistant bacteria: an international expert proposal for interim standard definitions for acquired resistance. *Clin Microbiol Infect.* (2012) 18:268–81. doi: 10.1111/j.1469-0691.2011.03570.x

44. Bolger AM, Lohse M, Usadel B. Trimmomatic: a flexible trimmer for Illumina sequence data. *Bioinformatics.* (2014) 30:2114–20. doi: 10.1093/bioinformatics/btu170

45. Bankevich A, Nurk S, Antipov D, Gurevich AA, Dvorkin M, Kulikov AS, et al. SPAdes: a new genome assembly algorithm and its applications to single-cell sequencing. *J Comput Biol.* (2012) 19:455–77. doi: 10.1089/cmb.2012.0021

46. Seemann T. Prokka: rapid prokaryotic genome annotation. *Bioinformatics.* (2014) 30:2068–9. doi: 10.1093/bioinformatics/btu153

47. Liu B, Zheng D, Jin Q, Chen L, Yang J. VFDB 2019: a comparative pathogenomic platform with an interactive web interface. *Nucleic Acids Res.* (2019) 47:D687–92. doi: 10.1093/nar/gky1080

48. Liu YY, Lin JW, Chen CC. Cano-wgMLST_BacCompare: a bacterial genome analysis platform for epidemiological investigation and comparative genomic analysis. *Front Microbiol.* (2019) 10:1687. doi: 10.3389/fmicb.2019.01687

49. Paudyal N, Pan H, Liao X, Zhang X, Li X, Fang W, et al. Meta-analysis of major foodborne pathogens in Chinese food commodities between 2006 and 2016. *Foodborne Pathog Dis.* (2018) 15:187–97. doi: 10.1089/fpd.2017.2417

50. Yue M, Rankin SC, Blanchet RT, Nulton JD, Edwards RA, Schifferli DM. Diversification of the *Salmonella* Fimbriae: a model of macro- and microevolution. *PLoS One.* (2012) 7:e38596. doi: 10.1371/journal.pone.0038596

51. Yue M, Han X, Masi L De, Zhu C, Ma X, Zhang J, et al. Allelic variation contributes to bacterial host specificity. *Nat Commun.* (2015) 6:1–11. doi: 10.1038/ncomms9754

52. EFSA. The European union one health 2019 zoonoses report. *EFSA J.* (2021) 19:e06406. doi: 10.2903/j.efsa.2021.6406

53. Medalla F, Gu W, Friedman CR, Judd M, Folster J, Griffin PM, et al. Increased incidence of antimicrobial-resistant nontyphoidal *Salmonella* infections, United States, 2004–2016. *Emerg Infect Dis.* (2021) 27:1662–72. doi: 10.3201/eid2706.204486

54. CDC. *National Enteric Disease Surveillance: Salmonella Annual Report, 2016.* (2018). Available online at: https://www.census.gov/geo/pdfs/maps-data/maps/ (accessed April 24, 2021).

55. Pijnacker R, Dallman TJ, Tijsma ASL, Hawkins G, Larkin L, Kotila SM, et al. An international outbreak of *Salmonella* enterica serotype enteritidis linked to eggs from Poland: a microbiological and epidemiological study. *Lancet Infect Dis.* (2019) 19:778–86. doi: 10.1016/S1473-3099(19)30047-7

56. Li S, He Y, Mann DA, Deng X. Global spread of *Salmonella Enteritidis via* centralized sourcing and international trade of poultry breeding stocks. *Nat Commun.* (2021) 12:1–12. doi: 10.1038/s41467-021-25319-7

57. Ke Y, Lu W, Liu W, Zhu P, Chen Q, Zhu Z. Non-typhoidal *Salmonella* infections among children in a tertiary hospital in ningbo, Zhejiang, China, 2012–2019. *PLoS Negl Trop Dis.* (2020) 14:1–18. doi: 10.1371/journal.pntd.0008732

58. Wu LJ, Luo Y, Shi GL, Li ZY. Prevalence, clinical characteristics and changes of antibiotic resistance in children with nontyphoidal *Salmonella* infections from 2009–2018 in Chongqing, China. *Infect Drug Resist.* (2021) 14:1403–13. doi: 10.2147/IDR.S301318

59. Gong B, Li H, Feng Y, Zeng S, Zhuo Z, Luo J, et al. Prevalence, serotype distribution and antimicrobial resistance of non-typhoidal *Salmonella* in hospitalized patients in Conghua District of Guangzhou, China. *Front Cell Infect Microbiol.* (2022) 12:54. doi: 10.3389/fcimb.2022.805384

60. Duong VT, The HC, Nhu TDH, Tuyen HT, Campbell JI, Van Minh P, et al. Genomic serotyping, clinical manifestations, and antimicrobial resistance of nontyphoidal *Salmonella* gastroenteritis in hospitalized children in Ho Chi Minh City, Vietnam. *J Clin Microbiol.* (2020) 58:e01465-20 doi: 10.1128/JCM.01465-20

61. Sinwat N, Angkittitrakul S, Coulson KF, Pilapil FMIR, Meunsene D, Chuanchuen R. High prevalence and molecular characteristics of multidrug-resistant *Salmonella* in pigs,pork and humans in Thailand and Laos provinces. *J Med Microbiol.* (2016) 65:1182–93. doi: 10.1099/jmm.0.000339

62. Teng L, Liao S, Zhou X, Jia C, Feng M, Pan H, et al. Prevalence and genomic investigation of multidrug-resistant *Salmonella* isolates from companion animals in Hangzhou, China. *Antibiot.* (2022) 11:625. doi: 10.3390/antibiotics11050625

63. Alekshun MN, Levy SB. Molecular mechanisms of antibacterial multidrug resistance. *Cell.* (2007) 128:1037–50. doi: 10.1016/j.cell.2007.03.004

64. Ramirez MS, Tolmasky ME. Aminoglycoside modifying enzymes. *Drug Resist Updat.* (2010) 13:151–71. doi: 10.1016/j.drup.2010.08.003

65. Eguale T, Birungi J, Asrat D, Njahira MN, Njuguna J, Gebreyes WA, et al. Genetic markers associated with resistance to beta-lactam and quinolone antimicrobials in non-typhoidal *Salmonella* isolates from humans and animals in central Ethiopia. *Antimicrob Resist Infect Control.* (2017) 6:1–10. doi: 10.1186/s13756-017-0171-6

66. Roberts MC, Schwarz S. Tetracycline and Chloramphenicol Resistance Mechanisms. In: *Antimicrobial Drug Resistance*. Cham: Springer (2017). p. 231–43.

67. Vidovic S, An R, Rendahl A. Molecular and physiological characterization of fluoroquinolone-highly resistant *Salmonella* enteritidis strains. *Front Microbiol.* (2019) 10:729. doi: 10.3389/fmicb.2019.00729

68. Wu S-y, Wang L-d, Li J-l, Xu G-m, He M-l, Li Y-y, et al. *Salmonella* spv locus suppresses host innate immune responses to bacterial infection. *Fish Shellfish Immunol.* (2016) 58:387–96. doi: 10.1016/j.fsi.2016.09.042

69. Guiney DG, Fierer J. The role of the spv genes in *Salmonella pathogenesis*. *Front Microbiol.* (2011) 2:129. doi: 10.3389/fmicb.2011.00129

70. Ledeboer NA, Frye JG, McClelland M, Jones BD. *Salmonella enterica* serovar Typhimurium requires the Lpf, Pef, and tafi fimbriae for biofilm formation on HEp-2 tissue culture cells and chicken intestinal epithelium. *Infect Immun.* (2006) 74:3156–69. doi: 10.1128/IAI.01428-05

71. Futoma-Kołoch B, Bugla-Płoskońska G, Dudek B, Dorotkiewicz-Jach A, Drulis-Kawa Z, Gamian A. Outer membrane proteins of *Salmonella* as potential markers of resistance to serum, antibiotics and biocides. *Curr Med Chem.* (2018) 26:1960–78. doi: 10.2174/0929867325666181031130851

72. Kim B, Richards SM, Gunn JS, Slauch JM. Protecting against antimicrobial effectors in the phagosome allows SodCII to contribute to virulence in *Salmonella enterica* serovar Typhimurium. *J Bacteriol.* (2010) 192:2140–9. doi: 10.1128/JB.00016-10

73. Sly LM, Guiney DG, Reiner NE. *Salmonella enterica* serovar Typhimurium periplasmic superoxide dismutases SodCI and SodCII are required for protection against the phagocyte oxidative burst. *Infect Immun.* (2002) 70:5312–5. doi: 10.1128/IAI.70.9.5312-5315.2002

74. Rychlik I, Gregorova D, Hradecka H. Distribution and function of plasmids in *Salmonella enterica*. *Vet Microbiol.* (2006) 112:1–10. doi: 10.1016/j.vetmic.2005.10.030

75. Kudirkiene E, Andoh LA, Ahmed S, Herrero-Fresno A, Dalsgaard A, Obiri-Danso K, et al. The use of a combined bioinformatics approach to locate antibiotic resistance genes on plasmids from whole genome sequences of *Salmonella enterica* serovars from humans in Ghana. *Front Microbiol.* (2018) 9:1010. doi: 10.3389/fmicb.2018.01010

76. Zhao Q, Feng Y, Zong Z. An integrated IncFIB/IncFII plasmid confers hypervirulence and its fitness cost and stability. *Eur J Clin Microbiol Infect Dis.* (2022) 41:681–4. doi: 10.1007/s10096-022-04407-6

frontiers | Frontiers in Public Health

TYPE Original Research
PUBLISHED 27 September 2022
DOI 10.3389/fpubh.2022.970880



OPEN ACCESS

EDITED BY
Sompong Vongpunsawad,
Chulalongkorn University, Thailand

REVIEWED BY
Zhiqi Zeng,
First Affiliated Hospital of Guangzhou Medical University, China
Guanhao He,
Jinan University, China

*CORRESPONDENCE
Tianmu Chen
13698665@qq.com
Yong Chen
yongchen@xmu.edu.cn
Qin Li
qinlicdc@163.com
Shenggen Wu
15980272757@126.com

†These authors have contributed equally to this work

SPECIALTY SECTION
This article was submitted to Infectious Diseases - Surveillance, Prevention and Treatment, a section of the journal Frontiers in Public Health

RECEIVED 16 June 2022
ACCEPTED 22 August 2022
PUBLISHED 27 September 2022

CITATION
Yang Z, Rui J, Qi L, Ye W, Niu Y, Luo K, Deng B, Zhang S, Yu S, Liu C, Li P, Wang R, Wei H, Zhang H, Huang L, Zuo S, Zhang L, Zhang S, Yang S, Guo Y, Zhao Q, Wu S, Li Q, Chen Y and Chen T (2022) Study on the interaction between different pathogens of Hand, foot and mouth disease in five regions of China.
*Front. Public Health* 10:970880.
doi: 10.3389/fpubh.2022.970880



# Study on the interaction between different pathogens of Hand, foot and mouth disease in five regions of China

Zimei Yang[1†], Jia Rui[1†], Li Qi[2†], Wenjing Ye[3†], Yan Niu[4†], Kaiwei Luo[5], Bin Deng[1], Shi Zhang[1], Shanshan Yu[1], Chan Liu[1], Peihua Li[1], Rui Wang[1], Hongjie Wei[1], Hesong Zhang[1], Lijin Huang[1], Simiao Zuo[1], Lexin Zhang[1], Shurui Zhang[1], Shiting Yang[1], Yichao Guo[1], Qinglong Zhao[6], Shenggen Wu[3]*, Qin Li[2]*, Yong Chen[7]* and Tianmu Chen[1]*

[1]State Key Laboratory of Molecular Vaccinology and Molecular Diagnostics, School of Public Health, Xiamen University, Xiamen, Fujian, China, [2]Chongqing Municipal Center for Disease Control and Prevention, Chongqing, China, [3]Fujian Center for Disease Control and Prevention, Fuzhou, Fujian, China, [4]Chinese Center for Disease Control and Prevention, Beijing, China, [5]Hunan Center for Disease Control and Prevention, Changsha, Hunan, China, [6]Jilin Center for Disease Control and Prevention, Changchun, Jilin, China, [7]Department of Stomatology, School of Medicine, Xiamen University, Xiamen, China

**Objectives:** This study aims to explore the interaction of different pathogens in Hand, foot and mouth disease (HFMD) by using a mathematical epidemiological model and the reported data in five regions of China.

**Methods:** A cross-regional dataset of reported HFMD cases was built from four provinces (Fujian Province, Jiangsu province, Hunan Province, and Jilin Province) and one municipality (Chongqing Municipality) in China. The subtypes of the pathogens of HFMD, including Coxsackievirus A16 (CV-A16), enteroviruses A71 (EV-A71), and other enteroviruses (Others), were included in the data. A mathematical model was developed to fit the data. The effective reproduction number ($R_{eff}$) was calculated to quantify the transmissibility of the pathogens.

**Results:** In total, 3,336,482 HFMD cases were collected in the five regions. In Fujian Province, the $R_{eff}$ between CV-A16 and EV-A71&CV-A16, and between CV-A16 and CV-A16&Others showed statistically significant differences ($P < 0.05$). In Jiangsu Province, there was a significant difference in $R_{eff}$ ($P < 0.05$) between the CV-A16 and Total. In Hunan Province, the $R_{eff}$ between CV-A16 and EV-A71&CV-A16, between CV-A16 and Total were significant ($P < 0.05$). In Chongqing Municipality, we found significant differences of the $R_{eff}$ ($P<0.05$) between CV-A16 and CV-A16&Others, and between Others and CV-A16&Others. In Jilin Province, significant differences of the $R_{eff}$ ($P < 0.05$) were found between EV-A71 and Total, and between Others and Total.

**Conclusion:** The major pathogens of HFMD have changed annually, and the incidence of HFMD caused by others and CV-A16 has surpassed that of EV-A71 in recent years. Cross-regional differences were observed in the interactions between the pathogens.

KEYWORDS

**HFMD, interaction, transmissibility, pathogens, mathematical model**

## Introduction

Hand, foot and mouth disease (HFMD) is a common infectious disease in children that is caused by a variety of enteroviruses. HFMD was first reported in New Zealand on 19 April, 1957 (1), with eight cases noted in children, and has since emerged in other parts of the world. The HFMD was first reported in China in 1974 (2) and formally included in the management of category C statutory infectious diseases in May 2008. Multiple pathogens of enteroviruses can cause HFMD, and the most common causative agents are Coxsackievirus A16 (CV-A16) and Enteroviruses A71 (EV-A71) (3, 4). CV-A16 was first isolated in South Africa in 1955 (5), and can be divided into genotypes A, B1, and B2. EV-A71 was first reported in California in 1969 (6), and usually causes severe cases in large outbreaks.

Currently, the incidence rate of HFMD is on a highly increasing epidemic trend, and the report and fatality rates rank first among Class C infectious diseases throughout the year (7). At the same time, it imposes a heavy disease burden on the patient's family and the socio-medical system, especially in severe cases of premature death. Losses and socioeconomic burden due to premature death increased 2.0 times to 85.104 million yuan from 2013 to 2015 (8). Studies have shown that EV-A71 was the leading pathogen detected in 2009 and 2010, accounting for 63 and 82%, respectively. Since 2011, the proportion of EV-A71 has dropped to 11%; however, the proportion of CV-A16 HFMD has increased to 51%, and the proportion of HFMD caused by other enteroviruses has also risen to 38% (9). To date, other enteroviruses (such as Coxsackievirus A10) have replaced EV-A71 and CV-A16 as the main pathogens in new cases of HFMD in mainland China (10). China launched two inactivated monovalent EV-A71 vaccines in 2016, with other types of viral vaccines still under development (11). The use of the EV-A71 vaccine can provide infants and young children with at least 1 year of protection against moderate and severe diseases of the EV-A71 virus, with an effectivity rate of 97.4% (12). However, it does not provide immunity to other serological viruses. The current National Immunization Program vaccine in China do not include the monovalent EV-A71 vaccine, and the vaccine coverage rate for children aged 6 months to 5 years is <10–50% (13). The application of the EV-A71 vaccine in China may change the trend of the HFMD virus classification. Exploring the interactions between multiple viruses and their regular patterns can provide more accurate decision-making suggestions for the prevention and control of HFMD, and vaccination coverage.

There have been many studies on the different pathogens of HFMD, but most of them have used traditional epidemiological methods, mainly to describe the incidence of different pathogens of HFMD and the detection rates of different virus types (7, 14, 15). Several studies have used mathematical models to calculate transmissibility of HFMD, as well as study seasonal epidemiological trends (16–18). These studies focused on HFMD caused by EV-A71 alone or HFMD related to all pathogens, and did not consider the potential impact of specific pathogen infections on the transmissibility of other pathogens. Few studies have used transmission dynamics models to explore the transmissibility of different subtypes of HFMD and their interactions. Previous studies have used the susceptible–infectious–recovered (SIR) model to study different pathogens to explore the transmission dynamics of HFMD by city (19), and the results showed that there was an interaction between pathogens (CV-A16 and other enterovirus, EV-A71 and other enterovirus). However, other previous studies have shown that the epidemiological characteristics of HFMD and the early warning times of different regions in China are quite different (20–22). The differences in epidemiological characteristics of HFMD among each regions are multiple and may be related to environmental factors, hosts, and pathogen interactions. Some studies have pointed out that meteorological factors such as daily average pressure, daily average relative humidity, daily average temperature were associated with the incidence of HFMD (23). Socioeconomic and population may also have an impact on morbidity of HFMD (24). In addition, differences in the interaction patterns between pathogens need to be considered. We observed interactions between the different types in one city in China, but it is unclear whether there are interactions between pathogens in other regions and whether they follow the same rules of interaction.

In this study, we chose the susceptible–exposed–infectious–asymptomatic–recovered (SEIAR) model with seasonal characteristics and selected a total of 3,336,482 HFMD case data from four provinces and one municipality, which included East China (Fujian Province and Jiangsu Province), the Central of China (Hunan Province), Southwest China (Chongqing Municipality), and Northeastern China (Jilin Province) to conduct a study on the transmission dynamics of different pathogens. This study had a wide range of research areas and a large sample size of research data, which were distributed across several regions of China. The transmissibility of different pathogens and their interactions among different regions were analyzed. We provided countermeasure suggestions for the prevention and control measures of HFMD in various regions of China.

Abbreviations: HFMD, Hand, foot and mouth disease; CV-A16, Coxsackievirus A16; EV-A71, Enterovirus A71; CV-B1, Coxsackievirus B1; SEIAR, susceptible–exposed–infectious–asymptomatic–recovered; SEIR, susceptible–exposed–infectious–recovered; SEIQR, susceptible–exposed–infectious–quarantined–recovered; SEIARW, susceptible–exposed–infectious–asymptomatic–recovered–environment; $R_0$, the basic reproduction number; $R_{eff}$, the Effective reproduction number.

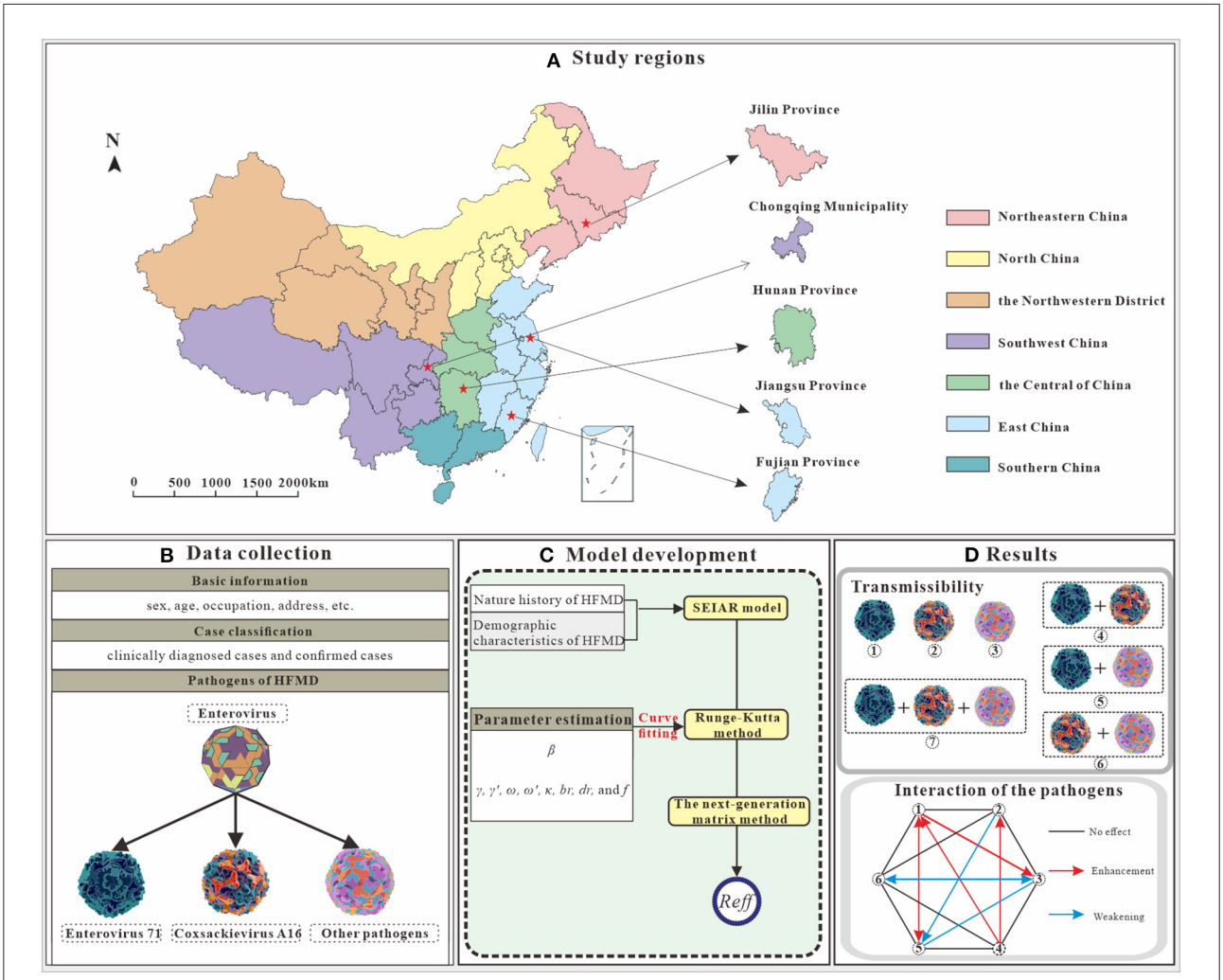


FIGURE 1
Study design on interaction study of major pathogens of HFMD [**(A)** We selected five study areas from four administrative regions. **(B)** Collection of basic information, HFMD incidence and pathogen data. **(C)** A SEIAR model was constructed based on the natural history of HFMD, and incidence rate of HFMD were fitted. **(D)** Clues to pathogen interactions were obtained by comparing the $R_{eff}$ in seven scenarios. Illustrations from https://www.dreamstime.com/stock-illustration-enterovirus-which-causes-hand-foot-mouth-disease-hfmd-colorful-background-d-illustration-model-built-using-data-image81638134, EV-A71; https://www.dreamstime.com/stock-illustration-coxsackievirus-virus-which-causes-respiratory-enteric-brain-infections-enterovirus-isolated-white-background-d-image82681501, CV-A16; https://www.dreamstime.com/stock-illustration-enterovirus-d-which-causes-respiratory-infections-children-isolated-white-background-illustration-model-built-using-image81605888, other enterovirus].

# Methods

## Research design

Based on the literature review, we selected the SEIAR model, and evaluated viral interactions among different pathogens for the purpose of the study. The research design is illustrated in Figure 1.

## Research objects

Fujian Province, Jiangsu Province, Hunan Province, Chongqing Municipality and Jilin Province were selected as the study areas. The time scale of data sets for each region is as follows: January 2008 to December 2020 in Fujian Province (685,463), January 2015 to December 2019 in Jiangsu Province (642,689), January 2008 to December 2018 in Hunan Province (1,364,315), January 2009 to December 2020 in Chongqing Municipality (476,969), and January 2008 to December 2019 in Jilin Province (167,046). A total of 3,336,482 reported cases of HFMD in the five study regions were used as the research objects.

The study consisted of two main datasets, one included the daily reported number of HFMD cases and deaths in five regions. The second dataset was based on laboratory pathogen examinations. Pathogens (CV-A16, EV-A71, and other enteroviruses) were identified by analysis in the Centers

for Disease Control and Prevention (CDC) laboratory using polymerase chain reaction.Both datasets were collected from surveillance data of CDC. Data were collected according to the guidelines for the treatment of HFMD, and the pathogens were classified into three categories (EV-A71, CV-A16, other enterovirus) in the data set. To improve the accuracy of the data, Chinese infectious diseases reporting system conducts regular under-reporting surveys and the data was revised in a timely manner when omissions or false positives were detected.

## Transmission model

In this study, the SEIAR model with seasonal characteristics was selected to fit the daily reported HFMD data in the five study regions. We obtained the transmission rate coefficient ($\beta$) by model fitting and further evaluated the transmissibility of the different pathogens. Model construction and parameter estimation methods were obtained from Huang et al. (25). The natural history of the disease in HFMD and the model hypotheses and model framework is shown in the Additional file 1.

## The model equations for the SEIAR model

$$\begin{aligned} d/dt\,(S) &= brN - \beta S\left(I + kA\right) - drS \\ d/dt\,(E) &= \beta S\left(I + kA\right) - p\omega E - \left(1-p\right)\omega E - drE \\ d/d\,(I) &= p\omega E - \gamma I - \left(dr + f\right) I \\ d/d\,(A) &= \left(1-p\right)\omega E - \gamma' A - drA \\ d/d\,(R) &= \gamma I + \gamma' A - drR \end{aligned}$$

## Estimation of parameters

The definitions and values of the parameters are shown in Table 1.

## The seasonality of the transmission

According to the SEAIR model, the seasonality of HFMD should be dynamic and centered on $\beta$ and the trigonometric functions was adopted for the seasonality in our study with the following equations:

$\beta = \beta_0\left[1 + \sin\left(\frac{2\pi\,(t+\alpha)}{T}\right)\right]$In the equation, $\beta_0$, $t$, $\alpha$ and $T$ refer to the baseline of the transmission rate, time, a constant which adjusts the position of time, and the time span of the season cycle, respectively.

## Assessment of transmissibility

The transmissibility of an infectious disease is usually assessed quantitatively using the basic reproduction number ($R_0$), which is defined as the number of new cases expected to be generated during the communication period when one case is imported into a susceptible population (34). However, $R_0$ quantifies the transmissibility of a disease in an ideal state. In cases where the population is not fully susceptible or is under intervention, the transmissibility of an infectious disease should be expressed as the effective reproduction number ($R_{eff}$). The $R_{eff}$ was defined as the average number of actual secondary cases for a single case at any time during the epidemic period (35). The formula for calculating the value of $R_{eff}$ for the SEIAR model is as follows:

$$R_{eff} = \beta S\left(\frac{1-p}{\gamma + f} + \frac{kp}{\gamma}\right)$$

## Interaction of different pathogens

Seven scenarios were set up in this study based on serological surveillance data: (1) EV-A71 individual transmission (EV-A71), (2) CV-A16 individual transmission (CV-A16), (3) other enterovirus (others), (4) EV-A71 and CV-A16 co-transmission (EV-A71&CV-A16), (5) EV-A71 and other enterovirus co-transmission (EV-A71&others), (6) CV-A16 and other enterovirus co-transmission (CV-A16&others), (7) All-pathogen co-transmission (Total). The above seven scenarios are not real world scenarios, they are simulated scenarios based on laboratory data. The number of daily incidences for different scenarios = Average monthly composition ratio * daily incidence of HFMD. The $R_{eff}$ was estimated for each city and district in the five study areas to quantify the transmissibility of each subgroup.

The interaction pattern between pathogens can be classified as follows (Take pathogen A and pathogen B for example):

1) $R_{eff}$-A $<$ $R_{eff}$-A+B; $R_{eff}$-B $=$ $R_{eff}$-A+B: Pathogen B and pathogen A have a higher transmissibility when present together than when pathogen A was present alone, and did not differ from pathogen B when it was present alone.
2) $R_{eff}$-A $>$ $R_{eff}$-A+B; $R_{eff}$-B $=$ $R_{eff}$-A+B: Pathogen B and pathogen A have a lower transmissibility when present together than when pathogen A was present alone, and did not differ from pathogen B when it was present alone.
3) $R_{eff}$-A $<$ $R_{eff}$-A+B; $R_{eff}$-B $<$ $R_{eff}$-A+B: Pathogen B and pathogen A have a higher transmissibility when present together than when pathogen A or pathogen B was present alone.
4) $R_{eff}$-A $>$ $R_{eff}$-A+B; $R_{eff}$-B $<$ $R_{eff}$-A+B: Pathogen B and pathogen A have a lower transmissibility when present

TABLE 1 Parameter definitions and values.

| Parameters | Description | Unit | Range of value | Value | Method |
|---|---|---|---|---|---|
| $br$ | Birth rate | 1 | 0–1 | – | From National Statistical Yearbook |
| $dr$ | Death rate | 1 | 0–1 | – | From National Statistical Yearbook |
| $\beta$ | Transmission rate coefficient | individual$^{-1}$·day$^{-1}$ | 0–1 | – | Curve fitting |
| $k$ | Relative transmissibility rate of asymptomatic to symptomatic individuals | 1 | 0–1 | 1 | – |
| $p$ | Proportion of the symptomatic | 1 | 0–1 | 0.4423 | References (7, 26, 27) |
| $\omega$ | Incubation relative rate | day$^{-1}$ | 0–1 | 0.2 | References (26, 28) |
| $\gamma$ | Recovery rate of the infectious | day$^{-1}$ | 0–1 | 0.07143 | References (17, 29) |
| $\gamma$' | Recovery rate of the asymptomatic | day$^{-1}$ | 0–1 | 0.04762 | References (7, 28, 30) |
| $f$ | Fatality rate of HFMD cases | 1 | 0–1 | 0.0003 | References (31–33) |

together than when pathogen A or pathogen B was present alone.

## Statistical analysis

Model fitting was performed using Berkeley Madonna software 8.3.18 (developed by Robert Macey and George Oster of the University of California at Berkeley) to analyse the daily incidence rate of HFMD. The fourth-order Runge–Kutta method, with tolerance set at 0.001, was used to perform curve fitting. When the curve is fitted, Berkeley Madonna shows the root mean square deviation between the data and the best run so far. The optimal results were tested for goodness of fit with the actual data, and quantified using the coefficient of determination ($R^2$). SPSS 13.0 (IBM Corp, Armonk, NY, USA) was employed to calculate the $R^2$. The $R_{eff}$ averages for the different scenarios were compared using analysis of variance, with $P < 0.05$ being a statistically significant difference.

# Results

## Composition ratio of different pathogens of HFMD

A total of 3,336,482 reported cases of HFMD in the five study regions were used as the research objects. As the Figure 2 shows the composition ratio of EV-A71 have a significant decrease after 2018 in all regions. And the composition ratio of other enteroviruses has increased in recent years. However, the composition ratio of CV-A16 have not changed.

The laboratory results of HFMD in different regions (Figure 2) show that, during the years of this study, HFMD cases in the southeastern coastal region of East China were mainly caused by EV-A71 and other enterovirus, while fewer were caused by CV-A16. The disease was mostly induced by EV-A71 in the first 5 years, and the composition ratio of other enterovirus increased significantly after 2016. Similarly, the Central of China had a larger composition ratio of EV-A71 and other enterovirus. In Southwest China and the Yellow Sea region of East China, HFMD is mainly caused by other enterovirus. The disease-causing pathogen of HFMD in Northeastern China is mainly CV-A16.

The composition ratios of the different pathogens in the five regions showed certain trends over time. In general, the composition ratio of CV-A16 did not change significantly and was relatively stable, with only a small increase in the Yellow Sea coastal region of East China after 2018. The composition of EV-A71 showed a clear trend over time. At the national level, a relatively large proportion of the composition of EV-A71 was shown until 2016, with a trend of decreasing year by year thereafter.In contrast, the composition ratio of other enterovirus showed an opposite trend over time, with a lower composition of $< 40\%$ in the initial years and a gradual increase in the proportion since 2015.

## Transmissibility of the different pathogens of HFMD

The coefficient of determination ($R^2$) represents the goodness-of-fit of the model used, which is shown in Additional file 2 with a well-fitted effect ($R^2$ in most cities was $> 0.5$, and $P < 0.05$). The $R_{eff}$ values calculated for different scenarios are shown in Figure 3. Overall, the $R_{eff}$ values of HFMD in Jiangsu Province (in the Yellow Sea region of

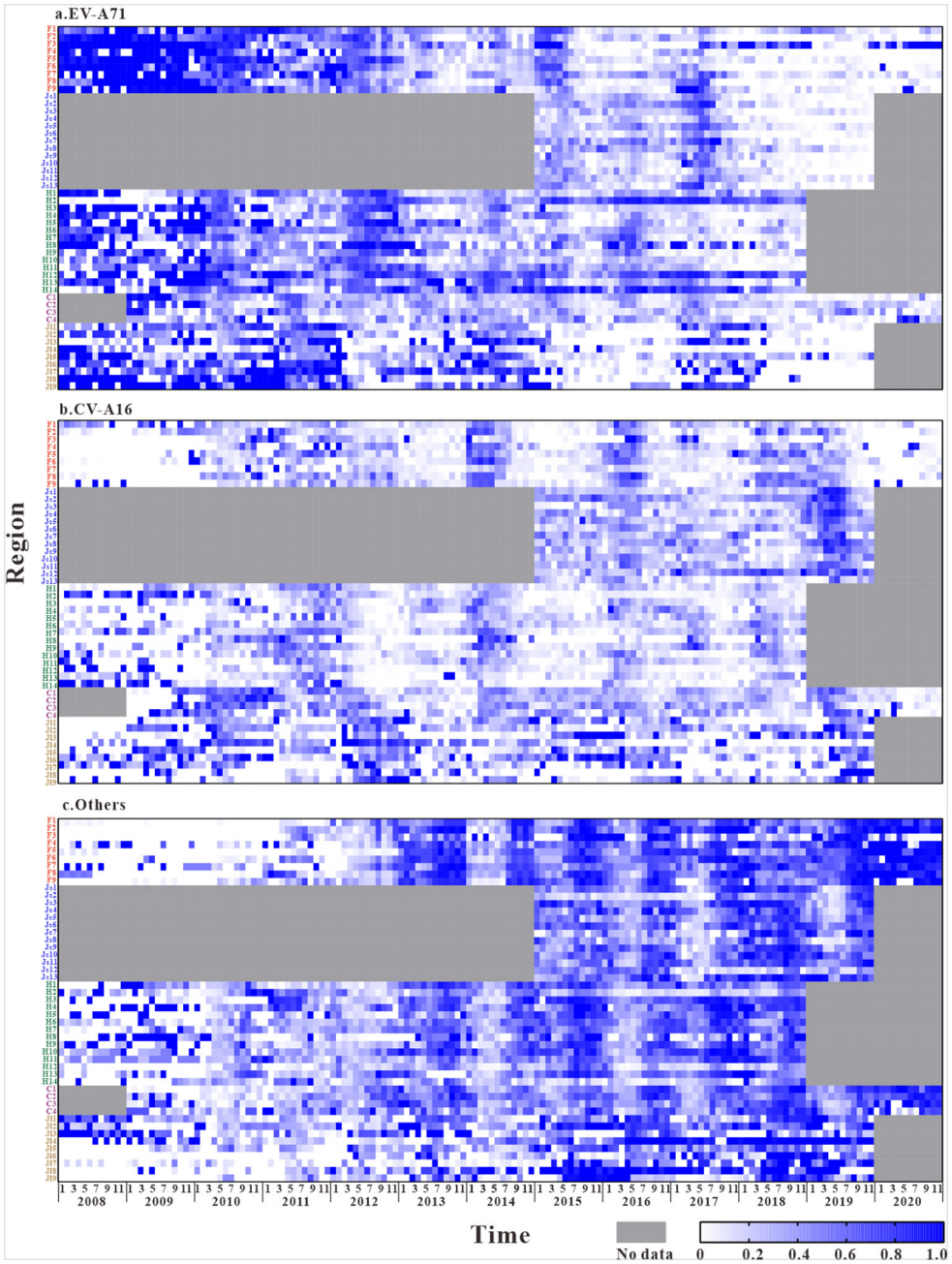


FIGURE 2
The composition ratio characteristics of different pathogens in the five regions (The composition ratio of EV-A71 = Number of EV-A71 tests per month / Total number of laboratory tests per month, The composition ratio of CV-A16 = Number of CV-A16 tests per month / Total number of laboratory tests per month, The composition ratio of Others = Number of Others tests per month / Total number of laboratory tests per month. F1, Fuzhou City; F2, Xiamen City; F3, Putian City; F4, Sanming City; F5, Quanzhou City; F6, Zhangzhou City; F7, Nanping City; F8, Longyan City; F9, Ningde City; Js1, Nanjing City; Js2, Wuxi City; Js3, Xuzhou City; Js4, Changzhou City; Js5, Suzhou City; Js6, Nantong City; Js7, Lianyungang City; Js8, Huaian City; Js9, Yancheng City; Js10, Yangzhou City; Js11, Zhenjiang City; Js12, Taizhou City; Js13, Suqian City; H1, Changsha City; H2, Zhuzhou City; H3, Xiangtan City; H4, Hengyang City; H5, Shaoyang City; H6, Yueyang City; H7, Changde City; H8, Zhangjiajie City; H9, Yiyang City; H10, Chenzhou City; H11, Yongzhou City; H12, Huaihua City; H13, Loudi City; H14, Xiangxi Prefecture; C1, The central urban area of Chongqing; C2, The new area of Chongqing city proper; C3, The city cluster of three gorges reservoir area in northeast Chongqing; C4, The city cluster of Wuling mountain area in southeast Chongqing; Jl1, Changchun City; Jl2, Jilin City; Jl3, Siping City; Jl4, Liaoyuan City; Jl5, Tonghua City; Jl6, Baishan City; Jl7, Songyuan City; Jl8, Baicheng City; Jl9, Yanbian Prefecture).

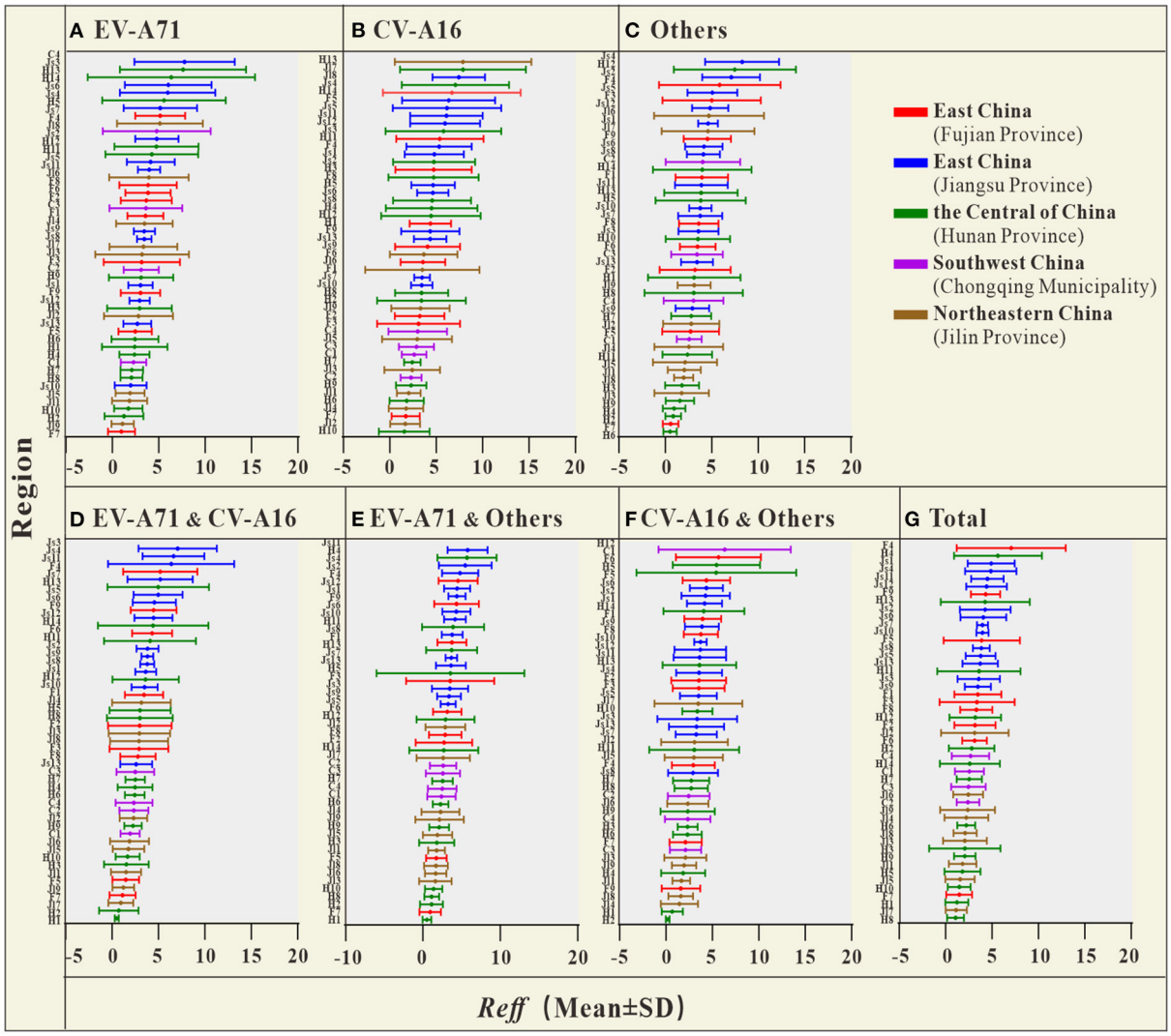


FIGURE 3
The $R_{eff}$ of HFMD in each city, autonomous prefecture, and district [**(A)** $R_{eff}$ average of EV-A71; **(B)** $R_{eff}$ average of CV-A16; **(C)** $R_{eff}$ average of Others; **(D)** $R_{eff}$ average of EV-A71&CV-A16; **(E)** $R_{eff}$ average of EV-A71&Others; **(F)** $R_{eff}$ average of CV-A16&Others; **(G)** $R_{eff}$ average of Total] (F1, Fuzhou City; F2, Xiamen City; F3, Putian City; F4, Sanming City; F5, Quanzhou City; F6, Zhangzhou City; F7, Nanping City; F8, Longyan City; F9, Ningde City; Js1, Nanjing City; Js2, Wuxi City; Js3, Xuzhou City; Js4, Changzhou City; Js5, Suzhou City; Js6, Nantong City; Js7, Lianyungang City; Js8, Huaian City; Js9, Yancheng City; Js10, Yangzhou City; Js11, Zhenjiang City; Js12, Taizhou City; Js13, Suqian City; H1, Changsha City; H2, Zhuzhou City; H3, Xiangtan City; H4, Hengyang City; H5, Shaoyang City; H6, Yueyang City; H7, Changde City; H8, Zhangjiajie City; H9, Yiyang City; H10, Chenzhou City; H11, Yongzhou City; H12, Huaihua City; H13, Loudi City; H14, Xiangxi Prefecture; C1, The central urban area of Chongqing; C2, The new area of Chongqing city proper; C3, The city cluster of three gorges reservoir area in northeast Chongqing; C4, The city cluster of Wuling mountain area in southeast Chongqing; Jl1, Changchun City; Jl2, Jilin City; Jl3, Siping City; Jl4, Liaoyuan City; Jl5, Tonghua City; Jl6, Baishan City; Jl7, Songyuan City; Jl8, Baicheng City; Jl9, Yanbian Prefecture).

East China) were higher than those in the Central of China, Southwest China and Northeastern China.

The results of the study in Table 2 show that, the $R_{eff}$ of HFMD differed significantly between regions. The difference in $R_{eff}$ values between the two provinces in East China was smaller (0.395), but this difference was not statistically significant ($P > 0.05$). The differences in $R_{eff}$ between the two regions of the Central of China, Southwest China and Northeastern China were not statistically significant ($P > 0.05$). In contrast, $R_{eff}$ was significantly different between each of the two provinces in East China and the other three regions ($P < 0.05$).

## Interaction of different pathogens

In this study, we analyzed the interaction between pathogens by comparing the $R_{eff}$ values of different scenarios (Figure 4; Table 3). The results from Fujian Province, the southeastern

TABLE 2 Comparison of the transmissibility of HFMD in the study regions.

| Compare regions | | Difference of $R_{eff}$ | *P*-value |
|---|---|---|---|
| **Region A** | **Region B** | **(A-B)**[a] | |
| East China (Fujian Province) vs. | East China (Jiangsu Province) | −0.395 | 0.574 |
| | Northeastern China (Jilin Province) | 1.621 | 0.000* |
| | the Central of China (Hunan Province) | 1.096 | 0.000* |
| | Southwest China (Chongqing) | 1.198 | 0.000* |
| East China (Jiangsu Province) vs. | Northeastern China (Jilin Province) | 2.016 | 0.000* |
| | the Central of China (Hunan Province) | 1.492 | 0.000* |
| | East China (Fujian Province) | 0.395 | 0.574 |
| | Southwest China (Chongqing) | 1.593 | 0.000* |
| The Central of China (Hunan Province) vs. | East China (Jiangsu Province) | −1.492 | 0.000* |
| | Northeastern China (Jilin Province) | 0.525 | 0.202 |
| | East China (Fujian Province) | −1.096 | 0.000* |
| | Southwest China (Chongqing) | 0.101 | 0.994 |
| Southwest China (Chongqing) vs. | East China (Jiangsu Province) | −1.593 | 0.000* |
| | Northeastern China (Jilin Province) | 0.424 | 0.426 |
| | the Central of China (Hunan Province) | −0.101 | 0.994 |
| | East China (Fujian Province) | −1.198 | 0.000* |
| Northeastern China (Jilin Province) vs. | East China (Jiangsu Province) | −2.016 | 0.000* |
| | the Central of China (Hunan Province) | −0.525 | 0.202 |
| | East China (Fujian Province) | −1.621 | 0.000* |
| | Southwest China (Chongqing) | −0.424 | 0.426 |

*The statistical methods is Analysis of Variance. $P < 0.05$ indicates the difference of $R_{eff}$ between two regions was statistically significant.
[a]Difference of $R_{eff}$ is the $R_{eff}$ mean of region A minus the $R_{eff}$ mean of region B.

coastal region of East China, showed that the differences in $R_{eff}$between CV-A16 (mean of $R_{eff} = 4.13$) and EV-A71&CV-A16 (mean of $R_{eff} = 3.20$), as well as that between CV-A16 (Mean of $R_{eff} = 4.13$) and CV-A16&others (mean of $R_{eff} = 3.20$) scenarios was statistically significant ($P < 0.05$). This significant difference was not observed in the comparison between the other scenarios ($P > 0.05$). In Jiangsu Province, the Yellow Sea region of East China, there was a significant difference in $R_{eff}$ ($P < 0.05$) between the CV-A16 (mean of $R_{eff} = 5.27$) and total (mean of $R_{eff} = 4.13$) scenarios.

In the Central of China (Hunan Province), the difference in $R_{eff}$ between CV-A16 (mean of $R_{eff} = 4.82$) and EV-A71&CV-A16 (mean of $R_{eff} = 2.69$), as well as between CV-A16 (mean of $R_{eff} = 4.82$) and total (mean of $R_{eff} = 2.64$) were statistically significant ($P < 0.05$). The differences in $R_{eff}$ between EV-A71 (mean of $R_{eff} = 3.71$) and EV-A71&CV-A16 (mean of $R_{eff} = 2.69$), EV-A71 (mean of $R_{eff} = 3.71$) and EV-A71&others (mean of $R_{eff} = 2.55$), EV-A71 (mean of $R_{eff} = 3.71$) and total (mean of $R_{eff} = 2.64$) were statistically significant ($P < 0.05$). However, none of the differences among the other scenarios were statistically significant ($P > 0.05$).

Chongqing Municipality, which is located in Southwest China, found statistically significant differences in the $R_{eff}$ between CV-A16 (Mean of $R_{eff} = 2.71$) and CV-A16 & others (Mean of $R_{eff} = 1.81$), as well as between others (Mean of $R_{eff} = 3.30$) and CV-A16 & others (Mean of $R_{eff} = 1.81$) ($P < 0.05$).

On the other hand, in Jilin Province, Northeastern China, statistically significant ($P < 0.05$) differences in $R_{eff}$ were found between EV-A71 (mean of $R_{eff} = 2.94$) and total (mean of $R_{eff} = 4.13$), as well as between others (mean of $R_{eff} = 2.81$) and total (mean of $R_{eff} = 4.13$).

## Discussion

Multiple pathogens of enterovirus can cause HFMD, and are co-transmitted in the population. Previously, in our group's study on different pathogens of HFMD in Changsha City, the reproduction number was used to measure the transmissibility of different pathogens and their interactions (19); however, it was only analyzed for one city in the Central of China. In previous studies, high prevalence of HFMD was found in southwestern and central as well as eastern China (36), differences between regions may be due to different geographical environments (37). The geographical distribution of China varies widely among different regions, with the eastern region dominated by plains, the southeastern coastal cities with higher temperatures, and the southwestern region dominated

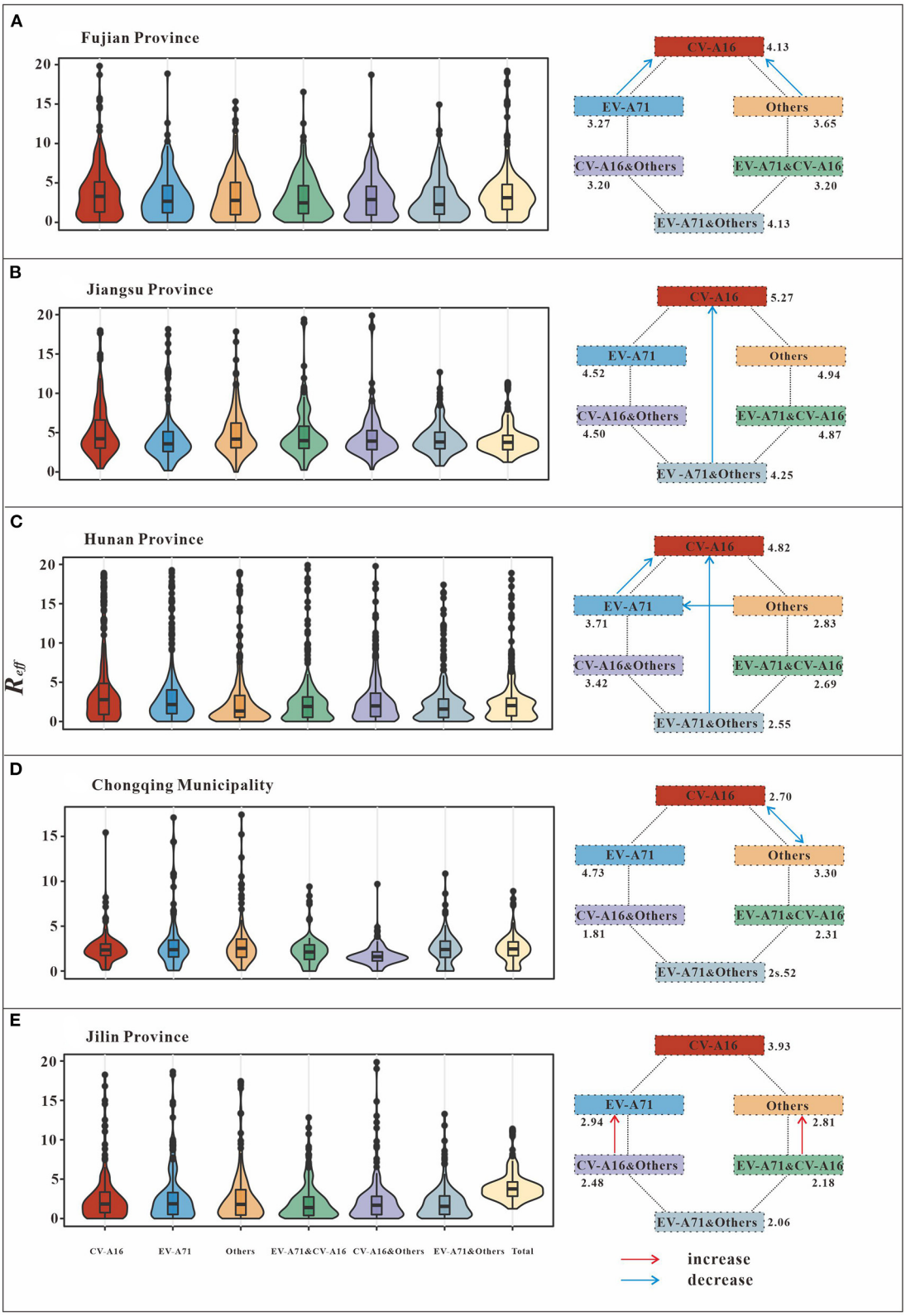


FIGURE 4
Schematic diagram of the interaction among different pathogens of HFMD. **(A)** (Fujian Province) indicates EV-A71 has negative inhibition on CV-A16, while others have negative inhibition on CV-A16. **(B)** (Jiangsu Province) shows that EV-A71 and others are present together to produce negative inhibition of CV-A16. **(C)** (Hunan Province) indicates EV-A71 has negative inhibition on CV-A16. There is negative inhibition of CV-A16 when EV-A71 and others are transmitted simultaneously. In addition to this, others have negative inhibition on EV-A71. **(D)** (Chongqing Municipality) indicates a bidirectional negative inhibition between CV-A16 and other. **(E)** (Jilin Province) indicates that when all-pathogen co-transmission, EV-A71, and other enterovirus get some increase in transmissibility.

TABLE 3 Interaction pattern of different pathogens of HFMD.

| Region | Scenarios | | Difference of $R_{eff}$ (A-B)[a] | *P*-value |
|---|---|---|---|---|
| | A | B | | |
| East China (Fujian Province) | CV-A16 | EV-A71&CV-A16 | 0.931 | 0.039* |
| | CV-A16 | CV-A16&Others | 0.929 | 0.044* |
| | CV-A16 | Total | 0.390 | 0.898 |
| | EV-A71 | EV-A71&CV-A16 | 0.075 | 1.000 |
| | EV-A71 | EV-A71&Others | 0.226 | 0.969 |
| | EV-A71 | Total | −0.466 | 0.594 |
| | Others | CV-A16&Others | 0.451 | 0.705 |
| | Others | EV-A71&Others | 0.605 | 0.356 |
| | Others | Total | −0.088 | 1.000 |
| East China (Jiangsu Province) | CV-A16 | EV-A71&CV-A16 | 0.399 | 0.947 |
| | CV-A16 | CV-A16&Others | 0.773 | 0.361 |
| | CV-A16 | Total | 1.140 | 0.009* |
| | EV-A71 | CV-A16&EV-A71 | −0.350 | 0.981 |
| | EV-A71 | EV-A71&Others | 0.274 | 0.989 |
| | EV-A71 | Total | 0.390 | 0.934 |
| | Others | CV-A16&Others | 0.439 | 0.860 |
| | Others | EV-A71&Others | 0.689 | 0.237 |
| | Others | Total | 0.806 | 0.088 |
| The Central of China (Hunan Province) | CV-A16 | EV-A71&CV-A16 | 2.122 | 0.001* |
| | CV-A16 | CV-A16&Others | 1.394 | 0.435 |
| | CV-A16 | Total | 2.175 | 0.001* |
| | EV-A71 | EV-A71&CV-A16 | 1.015 | 0.050* |
| | EV-A71 | EV-A71&Others | 1.160 | 0.017* |
| | EV-A71 | Total | 1.068 | 0.020* |
| | Others | CV-A16&Others | −0.594 | 0.941 |
| | Others | EV-A71&Others | 0.279 | 0.978 |
| | Others | Total | 0.187 | 0.996 |
| Southwest China (Chongqing) | CV-A16 | EV-A71&CV-A16 | 0.398 | 0.777 |
| | CV-A16 | CV-A16&Others | 0.898 | 0.008* |
| | CV-A16 | Total | 0.168 | 0.996 |
| | EV-A71 | EV-A71&CV-A16 | 2.422 | 0.531 |
| | EV-A71 | EV-A71&Others | 2.215 | 0.637 |
| | EV-A71 | Total | 2.192 | 0.646 |
| | Others | CV-A16&Others | 1.491 | 0.000* |
| | Others | EV-A71&Others | 0.784 | 0.327 |
| | Others | Total | 0.761 | 0.329 |
| Northeastern China (Jilin Province) | CV-A16 | EV-A71&CV-A16 | 1.757 | 0.479 |
| | CV-A16 | CV-A16&Others | 1.453 | 0.715 |
| | CV-A16 | Total | −0.201 | 1.000 |
| | EV-A71 | EV-A71&CV-A16 | 0.765 | 0.340 |
| | EV-A71 | EV-A71&others | 0.885 | 0.161 |
| | EV-A71 | Total | −1.192 | 0.012* |
| | Others | CV-A16&others | 0.331 | 0.979 |
| | Others | EV-A71&others | 0.755 | 0.295 |
| | Others | Total | −1.323 | 0.002* |

*The statistical methods is Analysis of Variance. $P < 0.05$ indicates the difference of $R_{eff}$ between two scenarios was statistically significant.
[a]Difference of $R_{eff}$ is the $R_{eff}$ mean of scenario A minus the $R_{eff}$ mean of scenario B.

by mountainous regions with a subtropical monsoon climate, factors that may favor the outbreak of HFMD (38). In this study, four provinces and one municipality were selected to further exploration of the transmissibility and interaction of different pathogens on a larger scale, including analyse the possible geographical differences. This study was the first to examine the transmission dynamics of different subtypes of HFMD at the provincial level, with a wide study area covering four of the seven administrative regions in China, namely the East China, the Central of China, Southwest China, and Northeastern China. In this study, we analyzed the transmissibility of sub-pathogens based on reliable laboratory results and explored possible interactions between different pathogens of enteroviruses.

The study showed that the predominant pathogen causing the occurrence of severe cases of HFMD in China was overall dominated by EV-A71, but after 2013 and 2015 the percentage of EV-A71 showed a decreasing trend, and in 2018 other enteroviruses became the dominant pathogen (36). In addition, another study showed that during 2008–2016 in China, most EV-A71 was endemic in the eastern, northern, central, and southwestern regions, most CV-A16 was endemic in eastern, southern, and northern China, and other viruses (e.g., CV-A6) were scattered in various regions (39). In this study, a significant trend in the composition ratio of different pathogens over time was observed in all the five study areas. After 2016, there was a significant decrease in the composition ratio of EV-A71 and an increase in the composition ratio of HFMD caused by other enterovirus. This may be because the monovalent EV-A71 virus vaccine was launched in 2016, indicating that the population acquired immunity against EV-A71 with the administration of the vaccine (40). However, other pathogens still have a high transmission rate, which are even higher than that at other time periods.

In China, EV-A71 vaccine is a national class II vaccine, not a mandatory vaccination, and requires self-payment. The optimal age for EV-A71 vaccination is from 6 months to 71 months of age, and full vaccination is encouraged to be completed before the infant reaches 12 months of age (41). The current coverage of EV-A71 vaccine in China is not very high as the previous researches showed that the vaccination coverage rate in Guangdong Province was rose from 3.82 to 10.07% in 2016 and 2017 (42), and the EV71 vaccination rate in Ningbo City was 24.05% among 716,178 children born from 2012 to 2018, with a timely vaccination rate of only 8.61% (43). In Kunming, a central city in southwest China, about 19.16% of children were vaccinated in 2018. Compared to 2015–2016, the number of EV-A71 HFMD cases in Kunming City decreased significantly in 2018 (44). Despite the low vaccination coverage, EV-A71 vaccine implementation continues to have a significant impact on the epidemiological trend of EV-A71 HFMD. In the previous study, we found a significant decrease in the proportion of EV-A71 infections after 2018 in our study of Nanchang City. Correlation analysis showed that EV-A71

vaccination was negatively associated with the incidence of EV-A71 infection (45). Some clinical trials have shown that the EV-A71 vaccine is not protective against HFMD caused by other pathogens (46). In addition, studies have indicated that when vaccination coverage reaches 80–90%, adequate herd immunity can be generated, creating additional social benefits as well (47, 48). Declining vaccination rates can lead to disease outbreaks and epidemics (49, 50). Improving the coverage and timeliness of EV-A71 vaccination is important for disease prevention and control. Meanwhile, it has been suggested that the development of a multivalent HFMD vaccine may be the best strategy, considering the combination of epidemiological, technical, immunological, and economic challenges associated with HFMD (51). Additionally, there are no pharmaceutical interventions for HFMD. Prevention and control is focused on preventing the spread of the virus in the population. Other HFMD prevention and control measures should be given more attention, such as the establishment of a clean, well-hygienic environment in the population, as well as and the timely implementation of isolation of infected cases.

The SEIAR model fitted well with the reported data and the results had good validity. Based on the comparison of HFMD $R_{eff}$, we found that the transmissibility of HFMD was closer between the two provinces in East China, as well as between the Central of China, Southwest China, and Northeastern China. In contrast, there was a significant difference in the $R_{eff}$ values between East China and the other three regions, with the transmissibility of HFMD being higher in East China. The spread of HFMD is closely related to temperature and humidity, and some studies have shown that the incidence rate of HFMD increases with higher average temperatures (52). East China, which has high temperature and humidity, as well as a high population density, may be conducive to the sharp spread of HFMD.

The interaction patterns among the HFMD pathogens differed among the five study regions. In the southeastern coastal region of East China (Fujian Province), CV-A16 has a higher transmissibility when transmitted alone than when transmitted with EV-A71 or other enterovirus together. Similarly, in the Yellow Sea region of eastern China (Jiangsu Province), the transmissibility when CV-A16, EV-A71 and other enterovirus are present together is lower than when CV-A16 is present alone. The interactions between different HFMD pathogens in the Central of China are more complex. When CV-A16 and EV-A71 are present together the transmissibility is lower than when they are each present alone. Also, EV-A71 is more transmissible when present alone than when other enterovirus and EV-A71 are present together. All-pathogen co-transmission conditions have a lower transmissibility than CV-A16 or EV-A71 alone. This result was generally consistent with the interactions between various pathogens in Changsha City during the rising phase of the disease. In Southwest China, CV-A16 and other enterovirus have a much lower transmissibility when present together. Completely different results were observed in Northeastern China. In the case of all-pathogen co-transmission, EV-A71, and other enterovirus increased in transmissibility, whereas CV-A16 did not.

These results show that the interaction of different pathogens varies greatly with geography. There is empirical evidence that infection with a multi-pathogen viral pathogen (e.g., influenza virus) confers transient immunity against other pathogens of the same infection (53). For HFMD, the incidence rate of patients infected with both pathogens is low and there may be a short-term cross-protective effect (54). Although studies have presented evidence for interactions between different HFMD pathogens in terms of transmission dynamics (19), the complexity of these interactions is not known. This may be related to differences in climate (temperature, relative humidity, rainfall, etc.) and cultural and social factors between the regions. The former has a limiting effect on the activity of pathogens, whereas the latter may influence individual lifestyle, hygiene habits, and human contact patterns (55). In conclusion, the interaction between different HFMD pathogens may be highly variable with geography and the mechanisms are complex. Overall, there is a dilution effect of transmission when multiple subtypes of pathogens are transmitted simultaneously, compared to the circulation of just a single predominant subtype. Further studies are required to determine relevant issues.

Of notes, there are several limitations in this study. Firstly, due to the limitations of the data source, this study could only explore the relationship between the three subtypes of HFMD (CV-A16, EV-A71 and other enterovirus). Other enterovirus were not further classified for analysis, which may have prevented meaningful effects of other subtypes from being observed. Analysis of interactions between more pathogens could be considered in future studies. Secondly, although Chinese infectious diseases reporting system provides some control over underreporting and misreporting of HFMD, the possible underreporting and misreporting can have some impact on the analysis of the results. Thirdly, immunity plays an important role in the prevalence of HFMD, but model was not considered due to the unavailability of accurate vaccination rate data for EV71 vaccine in all study areas, which may have an impact on the results of the study. If accurate vaccination rate data are available in the future, immunological issues can be taken into account in future studies. In conclusion, the major pathogens of HFMD have changed annually, with the incidence of HFMD caused by others and CV-A16 surpassing that of EV-A71 in recent years. More attention should be paid to East China because of the high transmissibility of HFMD. Cross-regional differences were observed in the interactions between the pathogens. In most regions of China (East China, the Central of China, and Southwest China), the transmissibility of HFMD was reduced when multiple subtypes of virus were transmitted simultaneously in the population compared with single virus

transmission. In contrast, in Northeastern China, an increase in subtype transmissibility was rarely observed.

## Data availability statement

The datasets presented in this article are not readily available because the data that support the findings of this study are available from Chinese Center for Disease Control and Prevention but restrictions apply to the availability of these data, which were used under license for the current study, and so are not publicly available. Data are however available from the authors upon reasonable request and with permission of Chinese Center for Disease Control and Prevention. Requests to access the datasets should be directed to TC, 13698665@qq.com.

## Author contributions

JR, ZY, TC, and QL made substantial contributions to conception and design. ZY, JR, YN, LQ, and WY collected literature, drafted the manuscript, conceived the experiments, and wrote the manuscript. YN, LQ, WY, QZ, ZY, and JR collected the data. SW, QL, YC, and TC provided technical help and revised it critically for important intellectual content. ZY, ShiZ, HW, HZ, LH, ShuZ, LZ, SiZ, ShanY, and YG conducted the experiments and analyzed the results. ZY, JR, BD, ShanY, ShiY, CL, PL, and HW involved in the visualization of the results. All authors approved the final manuscript and agreed to be accountable for all aspects of the work.

## Funding

This work was supported by the Bill and Melinda Gates Foundation (No: INV-005834), Chongqing Municipal Health Commission (No: 2019GDRC014), Construction of Fujian Provincial Scientific and Technological Innovation Platform (No: 2019Y2001), Provincial Natural Science Foundation of Fujian Province (No: 2013J01268), Public Health Applied Research and Vaccine Preventable Diseases Research Project, Chinese Society of Preventive Medicine (No: 20101801), Science and Technology Plan Project of Hunan Provincial Science and Technology Department (No: 2011FJ3137), Hunan Provincial Natural Science Foundation Joint Project on Science and Health (No: 2019JJ80115), and Chongqing Science and Technology Bureau (CSTC2021jscx-gksb-N0005).

## Conflict of interest

The authors declare that the research was conducted in the absence of any commercial or financial relationships that could be construed as a potential conflict of interest.

## Publisher's note

All claims expressed in this article are solely those of the authors and do not necessarily represent those of their affiliated organizations, or those of the publisher, the editors and the reviewers. Any product that may be evaluated in this article, or claim that may be made by its manufacturer, is not guaranteed or endorsed by the publisher.

## Supplementary material

The Supplementary Material for this article can be found online at: https://www.frontiersin.org/articles/10.3389/fpubh.2022.970880/full#supplementary-material

## References

1. Zhuang ZC, Kou ZQ, Bai YJ, Cong X, Wang LH Li C, et al. Epidemiological research on hand, foot, and mouth disease in Mainland China. *Viruses.* (2015) 7:6400–11. doi: 10.3390/v7122947

2. Leung GM, Xing W, Wu JT, Yu H. Hand, foot, and mouth disease in mainland China–authors' reply. *Lancet Infect Dis.* (2014) 14:1042. doi: 10.1016/S1473-3099(14)70975-2

3. Repass GL, Palmer WC, Stancampiano FF. Hand, foot, and mouth disease: identifying and managing an acute viral syndrome. *Cleve Clin J Med.* (2014) 81:537–43. doi: 10.3949/ccjm.81a.13132

4. Kimmis BD, Downing C, Tyring S. Hand-foot-and-mouth disease caused by coxsackievirus A6 on the rise. *Cutis.* (2018) 102:353–6.

5. Chen X, Tan X, Li J, Jin Y, Gong L, Hong M, et al. Molecular epidemiology of coxsackievirus A16: intratype and prevalent intertype recombination identified. *PLoS ONE.* (2013) 8:e82861. doi: 10.1371/journal.pone.0082861

6. Schmidt NJ, Lennette EH, Ho HH. An apparently new enterovirus isolated from patients with disease of the central nervous system. *J Infect Dis.* (1974) 129:304–9. doi: 10.1093/infdis/129.3.304

7. Xing W, Liao Q, Viboud C, Zhang J, Sun J, Wu JT, et al. Hand, foot, and mouth disease in China, 2008-12: an epidemiological study. *Lancet Infect Dis.* (2014) 14:308–18. doi: 10.1016/S1473-3099(13)70342-6

8. Ya-ming Z. Estimation of social economic burden caused by fatal hand,foot and mouth disease cases in China,2013–2015. *Disease Surveillance.* (2017) 32:516–20.

9. Du J, Wang X, Hu Y, Li Z, Li Y, Sun S, et al. Changing aetiology of hand, foot and mouth disease in Linyi, China, 2009–2011. *Clin Microbiol Infect.* (2014) 20:O47–9. doi: 10.1111/1469-0691.12301

10. Huang J, Liao Q, Ooi MH, Cowling BJ, Chang Z, Wu P, et al. Epidemiology of recurrent hand, foot and mouth disease, China, 2008–2015. *Emerg Infect Dis.* (2018) 24:432–42. doi: 10.3201/eid2403.171303

11. Yang B, Liu F, Liao Q, Wu P, Chang Z, Huang J, et al. Epidemiology of hand, foot and mouth disease in China, 2008 to 2015 prior to the introduction of EV-A71 vaccine. *Euro Surveill.* (2017) 22:16–00824. doi: 10.2807/1560-7917.ES.2017.22.50.16-00824

12. Wu JT, Jit M, Zheng Y, Leung K, Xing W, Yang J, et al. Routine pediatric enterovirus 71 vaccination in China: a cost-effectiveness analysis. *PLoS Med.* (2016) 13:e1001975. doi: 10.1371/journal.pmed.1001975

13. Liu D, Leung K, Jit M, Yu H, Yang J, Liao Q, et al. Cost-effectiveness of bivalent versus monovalent vaccines against hand, foot and mouth disease. *Clin Microbiol Infect.* (2020) 26:373–80. doi: 10.1016/j.cmi.2019.06.029

14. Li X, Liang L, Li B, Wu Y, Chang Q, Xuan W. Analysis of pathogenetic surveillance results of hand, foot and mouth disease in children in Wuwei City from 2008 to 2018. *Public Health Manag China.* (2020) 36:106–9. doi: 10.19568/j.cnki.23-1318.2020.01.027

15. Fan X, Fang S, Chen W, Gao F, Han Z, Xue N, He H. Analysis of pathogenic test results of hand, foot and mouth disease in Urumqi in 2018. *J Trop Med.* (2020) 20:410–3.

16. Wang Y, Feng Z, Yang Y, Self S, Gao Y, Longini IM, et al. Hand, foot, and mouth disease in China: patterns of spread and transmissibility. *Epidemiology.* (2011) 22:781–92. doi: 10.1097/EDE.0b013e318231d67a

17. Takahashi S, Liao Q, Van Boeckel TP, Xing W, Sun J, Hsiao VY, et al. Hand, foot, and mouth disease in china: modeling epidemic dynamics of enterovirus serotypes and implications for vaccination. *PLoS Med.* (2016) 13:e1001958. doi: 10.1371/journal.pmed.1001958

18. Lai CC, Jiang DS, Wu HM, Chen HH. A dynamic model for the outbreaks of hand, foot, and mouth disease in Taiwan. *Epidemiol Infect.* (2016) 144:1500–11. doi: 10.1017/S0950268815002630

19. Luo K, Rui J, Hu S, Hu Q, Yang D, Xiao S, et al. Interaction analysis on transmissibility of main pathogens of hand, foot, and mouth disease: a modeling study (a STROBE-compliant article). *Medicine.* (2020) 99:e19286. doi: 10.1097/MD.0000000000019286

20. Rui J, Luo K, Chen Q, Zhang D, Zhao Q, Zhang Y, et al. Early warning of hand, foot, and mouth disease transmission: a modeling study in mainland, China. *PLoS Negl Trop Dis.* (2021) 15:e0009233. doi: 10.1371/journal.pntd.0009233

21. Xia F, Deng F, Tian H, He W, Xiao Y, Sun X. Estimation of the reproduction number and identification of periodicity for HFMD infections in northwest China. *J Theor Biol.* (2020) 484:110027. doi: 10.1016/j.jtbi.2019.110027

22. Chen S, Yang D, Liu R, Zhao J, Yang K, Chen T. Estimating the transmissibility of hand, foot, and mouth disease by a dynamic model. *Public Health.* (2019) 174:42–8. doi: 10.1016/j.puhe.2019.05.032

23. Zhu HS, Chen S, Wang MZ, Ou JM, Xie ZH, Huang WL, et al. [Analysis on association between incidence of hand foot and mouth disease and meteorological factors in Xiamen, 2013–2017]. *Zhonghua Liu Xing Bing Xue Za Zhi.* (2019) 40:531–6. doi: 10.3760/cma.j.issn.0254-6450.2019.05.008

24. He X, Dong S, Li L, Liu X, Wu Y, Zhang Z, et al. Using a Bayesian spatiotemporal model to identify the influencing factors and high-risk areas of hand, foot and mouth disease (HFMD) in Shenzhen. *PLoS Negl Trop Dis.* (2020) 14:e0008085. doi: 10.1371/journal.pntd.0008085

25. Huang Z, Wang M, Qiu L, Wang N, Zhao Z, Rui J, et al. Seasonality of the transmissibility of hand, foot and mouth disease: a modelling study in Xiamen City, China. *Epidemiol Infect.* (2019) 147:e327. doi: 10.1017/S0950268819002139

26. Koh WM, Bogich T, Siegel K, Jin J, Chong EY, Tan CY, et al. The epidemiology of hand, foot and mouth disease in Asia: a systematic review and analysis. *Pediatr Infect Dis J.* (2016) 35:e285–300. doi: 10.1097/INF.0000000000001242

27. Chang LY, King CC, Hsu KH, Ning HC, Tsao KC, Li CC, et al. Risk factors of enterovirus 71 infection and associated hand, foot, and mouth disease/herpangina in children during an epidemic in Taiwan. *Pediatrics.* (2002) 109:e88. doi: 10.1542/peds.109.6.e88

28. Chang LY, Tsao KC, Hsia SH, Shih SR, Huang CG, Chan WK, et al. Transmission and clinical features of enterovirus 71 infections in household contacts in Taiwan. *JAMA.* (2004) 291:222–7. doi: 10.1001/jama.291.2.222

29. Du Z, Zhang W, Zhang D, Yu S, Hao Y. Estimating the basic reproduction rate of HFMD using the time series SIR model in Guangdong, China. *PLoS ONE.* (2017) 12:e0179623. doi: 10.1371/journal.pone.0179623

30. World Health Organization. *A guide to clinical management and public health response for hand, foot and mouth disease (HFMD)* (2011).

31. Yang Z, Zhang Q, Cowling BJ, Lau EHY. Estimating the incubation period of hand, foot and mouth disease for children in different age groups. *Sci Rep.* (2017) 7:16464. doi: 10.1038/s41598-017-16705-7

32. Liu SL, Pan H, Liu P, Amer S, Chan TC, Zhan J, et al. Comparative epidemiology and virology of fatal and nonfatal cases of hand, foot and mouth disease in mainland China from 2008 to 2014. *Rev Med Virol.* (2015) 25:115–28. doi: 10.1002/rmv.1827

33. Zhang J, Kang Y, Yang Y, Qiu P. Statistical monitoring of the hand, foot and mouth disease in China. *Biometrics.* (2015) 71:841–50. doi: 10.1111/biom.12301

34. Hethcote HW. The mathematics of infectious diseases. (2000) 42:599–653. doi: 10.1137/S0036144500371907

35. Lim JS, Cho SI, Ryu S, Pak SI. Interpretation of the basic and effective reproduction number. *J Prev Med Public Health.* (2020) 53:405–8. doi: 10.3961/jpmph.20.288

36. Ren MR, Cui JZ, Nie TR, Liu FF, Sun JL, Zhang YW, et al. [Epidemiological characteristics of severe cases of hand, foot, and mouth disease in China, 2008–2018]. *Zhonghua Liu Xing Bing Xue Za Zhi.* (2020) 41:1802–7. doi: 10.3760/cma.j.cn112338-20200201-00063

37. Gao Q, Liu Z, Xiang J, Tong M, Zhang Y, Wang S, et al. Forecast and early warning of hand, foot, and mouth disease based on meteorological factors: Evidence from a multicity study of 11 meteorological geographical divisions in mainland China. *Environ Res.* (2021) 192:110301. doi: 10.1016/j.envres.2020.110301

38. Yi X, Chang Z, Zhao X, Ma Y, Liu F, Xiao X. The temporal characteristics of the lag-response relationship and related key time points between ambient temperature and hand, foot and mouth disease: a multicity study from mainland China. *Sci Total Environ.* (2020) 749:141679. doi: 10.1016/j.scitotenv.2020.141679

39. Fu X, Wan Z, Li Y, Hu Y, Jin X, Zhang C. National epidemiology and evolutionary history of four hand, foot and mouth disease-related enteroviruses in China from 2008 to 2016. *Virol Sin.* (2020) 35:21–33. doi: 10.1007/s12250-019-00169-2

40. Xiao J, Zhu Q, Yang F, Zeng S, Zhu Z, Gong D, et al. The impact of enterovirus A71 vaccination program on hand, foot, and mouth disease in Guangdong, China:a longitudinal surveillance study. *J Infect.* (2022). 17:55. doi: 10.1016/j.jinf.2022.06.020

41. Mao QY, Wang YP, Bian LL, Xu M, Liang ZL. EV-A71 vaccine licensure: a first step for multivalent enterovirus vaccine to control HFMD and other severe diseases. *Emerg Microbes Infect.* (2016) 5:e75. doi: 10.1038/emi.2016.73

42. Fen Y, Liang W-J, Sun L-M. Innoculation of enterorirus 71 vaccine and incidence of hand-foot-mouth disease in Guangdong province. *Chin J Public Health.* (2020) 36:351–4. doi: 10.11847/zgggws1119741

43. Ye L, Chen J, Fang T, Ma R, Wang J, Pan X, et al. Vaccination coverage estimates and utilization patterns of inactivated enterovirus 71 vaccine post vaccine introduction in Ningbo, China. *BMC Public Health.* (2021) 21:1118. doi: 10.1186/s12889-021-11198-6

44. Jiang H, Zhang Z, Rao Q, Wang X, Wang M, Du T, et al. The epidemiological characteristics of enterovirus infection before and after the use of enterovirus 71 inactivated vaccine in Kunming, China. *Emerg Microbes Infect.* (2021) 10:619–28. doi: 10.1080/22221751.2021.1899772

45. He F, Rui J, Deng Z, Zhang Y, Qian K, Zhu C, et al. Surveillance, epidemiology and impact of EV-A71 vaccination on hand, foot, and mouth disease in Nanchang, China, 2010–2019. *Front Microbiol.* (2022) 12:811553. doi: 10.3389/fmicb.2021.811553

46. Zhu FC, Meng FY, Li JX, Li XL, Mao QY, Tao H, et al. Efficacy, safety, and immunology of an inactivated alum-adjuvant enterovirus 71 vaccine in children in China: a multicentre, randomised, double-blind, placebo-controlled, phase 3 trial. *Lancet.* (2013) 381:2024–32. doi: 10.1016/S0140-6736(13)61049-1

47. Brewer NT, Chapman GB, Rothman AJ, Leask J, Kempe A. Increasing vaccination: putting psychological science into action. *Psychol Sci Public Interest.* (2017) 18:149–207. doi: 10.1177/1529100618760521

48. Doherty M, Buchy P, Standaert B, Giaquinto C, Prado-Cohrs D. Vaccine impact: benefits for human health. *Vaccine.* (2016) 34:6707–14. doi: 10.1016/j.vaccine.2016.10.025

49. Azimi P, Keshavarz Z, Cedeno Laurent JG, Allen JG. Estimating the nationwide transmission risk of measles in US schools and impacts of vaccination and supplemental infection control strategies. *BMC Infect Dis.* (2020) 20:497. doi: 10.1186/s12879-020-05200-6

50. Habersaat KB, Pistol A, Stanescu A, Hewitt C, Grbic M, Butu C, et al. Measles outbreak in Romania: understanding factors related to suboptimal vaccination uptake. *Eur J Public Health.* (2020) 30:986–92. doi: 10.1093/eurpub/ckaa079

51. Aswathyraj S, Arunkumar G, Alidjinou EK, Hober D. Hand, foot and mouth disease (HFMD): emerging epidemiology and the need for a vaccine strategy. *Med Microbiol Immunol.* (2016) 205:397–407. doi: 10.1007/s00430-016-0465-y

52. Zhang X, Xu C, Xiao G. Spatial heterogeneity of the association between temperature and hand, foot, and mouth disease risk in metropolitan and other areas. *Sci Total Environ.* (2020) 713:136623. doi: 10.1016/j.scitotenv.2020.136623

53. Pitzer VE, Patel MM, Lopman BA, Viboud C, Parashar UD, Grenfell BT. Modeling rotavirus strain dynamics in developed countries to understand the potential impact of vaccination on genotype distributions. *Proc Natl Acad Sci U S A*. (2011) 108:19353–8. doi: 10.1073/pnas.1110507108

54. Li Y, Zhu R, Qian Y, Deng J, Sun Y, Liu L, et al. Comparing Enterovirus 71 with Coxsackievirus A16 by analyzing nucleotide sequences and antigenicity of recombinant proteins of VP1s and VP4s. *BMC Microbiol.* (2011) 11:246. doi: 10.1186/1471-2180-11-246

55. Xu J, Yang M, Zhao Z, Wang M, Guo Z, Zhu Y, et al. Meteorological Factors and the Transmissibility of Hand, Foot, and Mouth Disease in Xiamen City, China. *Front Med.* (2020) 7:597375. doi: 10.3389/fmed.2020.597375

frontiers | Frontiers in Public Health

TYPE Opinion
PUBLISHED 10 October 2022
DOI 10.3389/fpubh.2022.978064



OPEN ACCESS

EDITED BY
Jun Feng,
Shanghai Municipal Center for Disease Control and Prevention (SCDC), China

REVIEWED BY
Mahmoud Almasri,
University of Missouri, United States
Michael Becker,
Public Health Agency of Canada (PHAC), Canada

*CORRESPONDENCE
Jayne Wu
jaynewu@utk.edu
Lei Zheng
lei.zheng@aliyun.com

†These authors have contributed equally to this work

SPECIALTY SECTION
This article was submitted to Infectious Diseases – Surveillance, Prevention and Treatment, a section of the journal Frontiers in Public Health

RECEIVED 25 June 2022
ACCEPTED 22 September 2022
PUBLISHED 10 October 2022

CITATION
Zhang J, Qi H, Wu J, Guan X, Hu Z and Zheng L (2022) Promising on-site and rapid SARS-CoV-2 detection *via* antigens.
*Front. Public Health* 10:978064.
doi: 10.3389/fpubh.2022.978064



# Promising on-site and rapid SARS-CoV-2 detection *via* antigens

Jian Zhang[1,2†], Haochen Qi[1,2†], Jayne Wu[3*], Xiaochun Guan[1], Zhiwen Hu[4] and Lei Zheng[2*]

[1]College of Electrical and Electronic Engineering, Wenzhou University, Wenzhou, China, [2]School of Food and Biological Engineering, Hefei University of Technology, Hefei, China, [3]Department of Electrical Engineering and Computer Science, The University of Tennessee, Knoxville, TN, United States, [4]School of Computer and Information Engineering, Zhejiang Gongshang University, Hangzhou, China

KEYWORDS

**SARS-CoV-2 detection, antigen test, point-of-care diagnosis, on-site detection, spike protein, nucleocapsid protein**

## Challenges and strategies for SARS-CoV-2 diagnosis

COVID-19 pandemic over the past years has shown a great need for rapid, low-cost and on-site detection of severe acute respiratory syndrome coronavirus 2 (SARS-CoV-2). At present, polymerase chain reaction (PCR) based nucleic acid test (NAT) has been a gold standard in clinical practice (1), which has high sensitivity and high throughput. It is capable of providing quantitative results (with qRT-PCR), and recognizing viral mutations with short turnaround (2–4). While NAT plays an irreplaceable role in epidemic prevention around the world, the associated high equipment-cost, the need to operate in a laboratory setting and the longer than desired turnaround time are driving the research effort to achieve low-cost and point-of-care testing of viral infections.

Besides nucleic acids, antibodies and antigens are the two other types of targets for SARS-CoV-2 diagnosis (1). Antibodies such as IgM and IgG are often evaluated using established assays as an auxiliary to NATs, but the appearance of antibodies in the body is a lagging indicator for infection and does not always correlate with the presence of viruses (5). Therefore, antibody tests alone are not reliable for accurate detection of viruses, particularly in the early stage of infection before antibody appearance. Clinically, they have been used for immune evaluation after vaccination and postmortem analysis in asymptomatic individuals (6). To increase the reliability of detection, NAT can be combined with antibody tests to cover a wider range of disease progression. This approach has been employed to detect a variant of SARS-CoV-2 (7), which in fact illustrates that antibody cannot act as an independent indicator for virus presence.

To make the diagnosis more affordable, more convenient and more rapid, antigens from viruses have been attracting attention as biomarkers for SARS-CoV-2 identification (8–10). Generally, there are three common antigens for SARS-CoV-2 detection, i.e., live virion (8), spike (S-) (9) and nucleocapsid (N-) proteins (10) (Figure 1). The latter two are both important structural proteins of the virion. S-protein on the virion surface is responsible for binding to the host cell receptor and fusing the membranes of virus and

cell (11), and N-protein is an abundant RNA-binding protein for viral genome assembly and release (12). Focusing on emerging diagnostic tools, this opinion highlights and summarizes the recent advances in antigen detection techniques, in hope of providing a strategic reference for real-time and high throughput detection of SARS-CoV-2.

## Representative emerging techniques for antigen detection

Few methods have been reported to directly detect live virions of SARS-CoV-2 until a unique aptasensor is developed (8), which can accurately recognize the surface of live virions from the altered surface of inactivated virions. It reaches a limit of detection (LOD) of $10^4$ copies/ml, and the test time is from 30 min to 2 h. This detection is easy to operate with a simple protocol since sample pretreatment is not required. In comparison, some biosensors have been reported with S-protein as the target, such as the one employing human angiotensin-converting enzyme 2 (ACE2) as a probe (9), which successfully recognizes the SARS-CoV-2 UK variant 1.1.7. B. It yields a result within 6.5 min, meeting the requirement of on-site diagnosis, and the cost of this biosensor is only 1.5 US dollars. Another impressive immunosensor is for food quarantine (13), with an ultralow LOD of $10^{-6}$ ng/ml acquired in 20 s. The cost of this sensor is about 1 US dollar. The rapid response and low cost make it possible to realize large-scale and real-time virus screening in food and environmental media.

Due to the long-term preservation of N-proteins in the body, more emerging strategies are based on N-protein detection. One representative technique is a mass spectrometry-based system (14). Although this platform is relatively complex and expensive, it allows multiplexed analysis of four samples within 10 min, enabling the processing of more than 500 samples per day. This method has also been qualitatively and quantitatively validated using 985 specimens previously analyzed by real-time RT-PCR, with an accuracy of 84% and a specificity of 97%. Another typical immunosensor is based on magnetic nanobeads (15), which achieves a LOD of pg/ml level in serum within 1 h. In this research, a smartphone-based diagnostic system has also been developed for point-of-care tests (POCTs). Recently, an aptasensor for ultrasensitive N-protein detection is reported (16) achieving an ultralow LOD of $10^{-6}$ ng/ml, a response time of 15 s, and a cost below 1 US dollar. The matrices include water, saliva, even serum and plasma. This sensor is competitive for low-cost screening and POCT applications.

## Merits of antigen detection

Herein, some prospects of antigen detection strategies are explored based on limited investigation. It is worth noting that ingenious approaches for antigen-based SARS-CoV-2 detection have been extensively researched in the last 2 years. With immunoreactions and key-lock space conformations, the process of recognizing antigens by antibodies, aptamers or enzymes is very fast owing to the binding in several seconds between probes and targets. As a result, antigen detection is rapid, and can even be shortened to dozens of seconds (13, 16). Small, inexpensive, and simple-to-use sensors, as well as innovative sensing mechanisms, make compact platforms possible (9, 13, 16) (Figure 1). Among the antigens, widely adopted N- and S-proteins are of high abundance in not only the respiratory tract, but also blood and other body fluids, and even external matrices (Figure 1), supporting more medium types and analytical methods (8, 9, 16). As we have seen, these studies are forming a hotspot due to the strengths of antigen detection in realizing POCT and large-scale environmental screening of SARS-CoV-2.

Another issue is the quantification of viral load, which is essential to evaluating disease course and infectivity. The samples for SARS-CoV-2 detection are typically collected by swabs, which does not correspond to a well-defined sampling volume. According to existing reports, the viral RNA can hardly be detected in blood in most infected patients (six of 57 patients) (17), while antigen is always found in blood or other body fluids (10). Using suitable protocols, antigen-based detection has been reported to be quantitative and of a wide linear range covering at least three orders of magnitude (8, 9, 13–16).

Over just 2 years, many SARS-CoV-2 mutations, such as Delta and Omicron, have appeared around the world, as expected for an RNA virus, which poses new challenges to their detection, particularly at the beginning of a mutation emergence. In contrast to accurate recognition by RNA sequencing, antigen detection cannot easily distinguish congeneric proteins from different variants. On the other hand, the structural proteins are usually well-preserved, particularly for N-protein (12, 16). Based on this, antigen-testing strategies are capable of broad-spectrum recognition of these variants (Figure 1), which has been verified by many clinical sample tests (9, 18). Due to the lack of specific medicine for particular variants, identifying which mutated strains cause the spread of Covid is of limited importance. In this context, broad-spectrum detection of the virus will be an efficient strategy to screen and identify the infectors.

Similar to all the bioassays, the key figure of merit for SARS-CoV-2 detection should be the accuracy. Presently, a common perception is that the accuracy of antigen tests is low despite these tests being rapid (1). However, this view may not be supported by solid evidence. The accuracy of antigen detection depends on the specific and reliable binding between probe and biomarker, and specific probes can be identified through established antibody and aptamer screening methods. As a result, the reported accuracy of COVID-19 diagnosis using antigen-positive samples has been demonstrated to be good (84%—100%) (9, 14, 15).

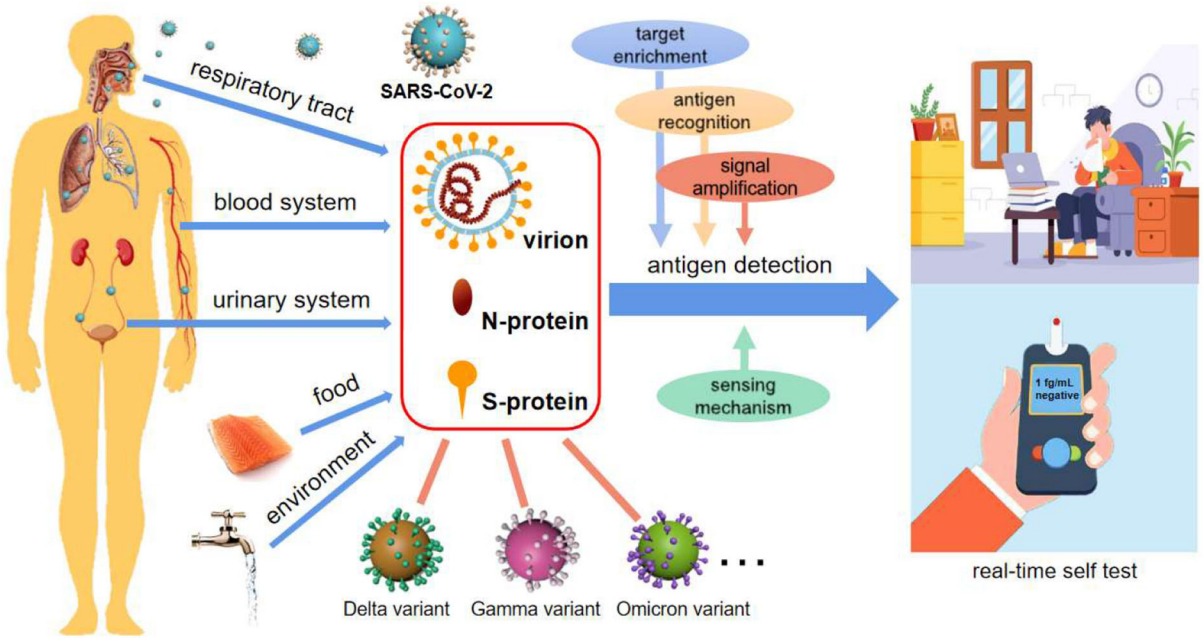


FIGURE 1
SARS-CoV-2 diagnosis *via* antigen test. Antigen detection toward POCTs commonly uses virion, N-protein, and S-protein as targets, potentially integrating with target enrichment, antigen recognition, signal amplification as well as innovative sensing mechanisms. Antigen-based detection strategies may be applicable for various types of body fluids, food, and environmental samples, and are broad-spectrum for SARS-CoV-2 variant recognition. It is also an enabler of real-time self-tests for infectious diseases.

As a matter of fact, a variety of techniques have been implemented for antigen-based detection, which invariably leads to a large variation in sensitivity. Many research groups are working diligently to enhance the detection sensitivity. Advanced techniques, such as microfluidics, have successfully demonstrated enrichment of ultra-trace antigens in unprecedented ways, achieving ultralow LODs of $10^{-6}$ ng/ml for S- and N-proteins (13, 16), i.e., the concentrations of $10^4$ molecules/mL. Assuming that every virion corresponds to 20 protein molecules, the virion concentration is roughly estimated to be 500 #/ml, which is on par with PCR based NATs. Other technological advances, including innovative sensing mechanisms and signal amplifications (13, 15, 16), also contribute to improved sensitivity of sensors and assays.

To concisely and clearly illustrate the main features of antigen tests for SARS-CoV-2 detection, Table 1 presents a summary of the targets, specimens, turnaround time, LOD, time window for test, and brief comments.

## Summary and prospect

Some prospects of antigen detection strategies have been explored based on the limited investigation. First of all, the advantages and importance of NATs are undeniable, which is supported by world-wide adoption of NATs as the primary detection tool of COVID-19. At the same time, considerable efforts have been dedicated to the research and development of a variety of improved or new detection approaches. Only by balancing the advantages and disadvantages of various detection assays according to specific purposes can we obtain the most economical and optimal option. Antigen tests are becoming a promising strategy owing to their merits of rapid response, low cost and simple operation. With the integration of emerging technologies, antigen tests are conducive to be implemented as POCTs on a large scale and as a strong auxiliary test to NATs. Of course, there are still limitations and shortcomings with antigen based techniques at the present stage. One is the large variation in sensitivity from various research groups and developers. The most sensitive technique reports comparable sensitivity to NATs, while the majority of techniques have much higher LODs. Another one is a lack of standard for viral load calibration compared with NATs, which is due to the insufficient products for clinical applications.

Currently, antigen detection technology is undergoing a period of rapid development. Although they have not been popularized around the world, antigen tests hold great promise for low-cost and on-site SARS-CoV-2 screening and diagnosis, particularly in communities and regions with limited resources. We anticipate revolutionary breakthroughs in both academic and clinical fields in near future. In practical applications, multiple methods are often combined to minimize

TABLE 1 Features of antigen tests for SARS-CoV-2 detection.

| SARS-CoV-2 detection strategy | Targets | Specimens | Turnaround time | LOD | Time window for test | Comments |
|---|---|---|---|---|---|---|
| Antigen test | Live virion, N-protein, and S-protein | Upper respiratory secretion, saliva, serum, plasma, other body fluids, water, food | Minutes to hours | fg/ml to ng/ml | Whole disease course | • Easier to implement outside laboratory with portable sensors and apparatuses<br>• Rapid and low-cost assays enabling POCT and large-scale screening<br>• Capable for virus presence test in various matrices<br>• Broad-spectrum response to variants<br>• Lack of direct correlation with viron load<br>• Weak ability to identify specific variants<br>• Not enough products for clinical applications |

the drawbacks of a single method, and antigen tests can be expected to act as a preliminary screening tool, even by self-test, prior to NATs results. With the rapid development of new technologies and methods, we believe that more sensitive, efficient and mature antigen detection methods and products will appear in the near future, which would provide powerful tools for public health.

## Author contributions

JZ and JW wrote the original draft. JW, HQ, and LZ revised the draft. All authors contributed to the article and approved the submitted version.

## Funding

This work was funded by the National Natural Science Foundation of China (62074047 and 32072306) and USDA NIFA (The United States Department of Agriculture, the National Institute of Food and Agriculture) (Grant No. 2017-67007-26150).

## Conflict of interest

The authors declare that the research was conducted in the absence of any commercial or financial relationships that could be construed as a potential conflict of interest.

## Publisher's note



## References

1. Valera E, Jankelow A, Lim J, Kindratenko V, Ganguli A, White K, et al. COVID-19 point-of-care diagnostics: present and future. *ACS Nano*. (2021) 15:7899–906. doi: 10.1021/acsnano.1c02981

2. Zhou Y, Zhang L, Xie YH, Wu J. Advancements in detection of SARS-CoV-2 infection for confronting COVID-19 pandemics. *Lab Invest*. (2022) 102:4–13. doi: 10.1038/s41374-021-00663-w

3. Shen M, Zhou Y, Ye J, Al-Maskri AAA, Kang Y, Zeng S, et al. Recent advances and perspectives of nucleic acid detection for coronavirus. *J Pharm Anal*. (2020) 10:97–101. doi: 10.1016/j.jpha.2020.02.010

4. Vega-Magaña N, Sánchez-Sánchez R, Hernández-Bello J, Venancio-Landeros AA, Peña-Rodríguez M, Vega-Zepeda RA, et al. RT-qPCR assays for rapid detection of the N501Y, 69-70del, K417N, and E484K SARS-CoV-2 mutations: a screening strategy to identify variants with clinical impact. *Front Cell Infect Microbiol*. (2021) 11:672562. doi: 10.3389/fcimb.2021.672562

5. Isho B, Abe KT, Zuo M, Jamal AJ, Rathod B, Wang JH, et al. Persistence of serum and saliva antibody responses to SARS-CoV-2 spike antigens in COVID-19 patients. *Sci Immunol*. (2020) 5:abe5511 doi: 10.1126/sciimmunol.abe5511

6. Petherick A. Developing antibody tests for SARS-CoV-2. *Lancet*. (2020) 395:1101–2. doi: 10.1016/S0140-6736(20)30788-1

7. Mlcochova P, Collier D, Ritchie A, Assennato SM, Hosmillo M, Goel N, et al. Combined point-of-care nucleic acid and antibody testing for SARS-CoV-2 following emergence of D614G spike variant. *Cell Rep Med*. (2020) 1:100099. doi: 10.1016/j.xcrm.2020.100099

8. Peinetti AS, Lake RJ, Cong W, Cooper L, Wu Y, Ma Y, et al. Direct detection of human adenovirus or SARS-CoV-2 with ability to inform infectivity using DNA aptamer-nanopore sensors. *Sci Adv*. (2021) 7:eabh2848 doi: 10.1126/sciadv.abh2848

9. de Lima LF, Ferreira AL, Torres MDT, de Araujo WR, de la Fuente-Nunez C. Minute-scale detection of SARS-CoV-2 using a low-cost biosensor composed of pencil graphite electrodes. *Proc Natl Acad Sci USA*. (2021) 118:e2106724118 doi: 10.1073/pnas.2106724118

10. Shan D, Johnson JM, Fernandes SC, Suib H, Hwang S, Wuelfing D, et al. N-protein presents early in blood, dried blood and saliva during asymptomatic and symptomatic SARS-CoV-2 infection. *Nat Commun.* (2021) 12:1931. doi: 10.1038/s41467-021-22072-9

11. Walls AC, Park YJ, Tortorici MA, Wall A, McGuire AT, Veesler D. Structure, function, and antigenicity of the SARS-CoV-2 spike glycoprotein. *Cell*. (2020) 181:281–92 doi: 10.1016/j.cell.2020.02.058

12. Cubuk J, Alston JJ, Incicco JJ, Singh S, Stuchell-Brereton MD, Ward MD, et al. The SARS-CoV-2 nucleocapsid protein is dynamic, disordered, and phase separates with RNA. *Nat Commun.* (2021) 12:1936. doi: 10.1038/s41467-021-21953-3

13. Zhang J, Fang X, Mao Y, Qi H, Wu J, Liu X, et al. Real-time, selective, and low-cost detection of trace level SARS-CoV-2 spike-protein for cold-chain food quarantine. *NPJ Sci Food*. (2021) 5:12 doi: 10.1038/s41538-021-00094-3

14. Cardozo KHM, Lebkuchen A, Okai GG, Schuch RA, Viana LG, Olive AN, et al. Establishing a mass spectrometry-based system for rapid detection of SARS-CoV-2 in large clinical sample cohorts. *Nat Commun.* (2020) 11:6201. doi: 10.1038/s41467-020-19925-0

15. Li J, Lillehoj PB. Microfluidic magneto immunosensor for rapid, high sensitivity measurements of SARS-CoV-2 nucleocapsid protein in serum. *ACS Sensors.* (2021) 6:1270–8. doi: 10.1021/acssensors.0c02561

16. Qi H, Hu Z, Yang Z, Zhang J, Wu JJ, Cheng C, et al. Capacitive aptasensor coupled with microfluidic enrichment for real-time detection of trace SARS-CoV-2 nucleocapsid protein. *Anal Chem.* (2022) 94:2812–9. doi: 10.1021/acs.analchem.1c04296

17. Chen W, Lan Y, Yuan X, Deng X, Li Y, Cai X, et al. Detectable 2019-nCoV viral RNA in blood is a strong indicator for the further clinical severity. *Emerg Microbes Infect.* (2020) 9:469–73. doi: 10.1080/22221751.2020.1732837

18. Bekliz M, Adea K, Essaidi-Laziosi M, Sacks JA, Escadafal C, Kaiser L, et al. SARS-CoV-2 rapid diagnostic tests for emerging variants. *Lancet Microbe.* (2021) 2:e351. doi: 10.1016/S2666-5247(21)00147-6

frontiers | Frontiers in Medicine

TYPE Original Research
PUBLISHED 13 October 2022
DOI 10.3389/fmed.2022.991807



OPEN ACCESS

EDITED BY
Kun Yin,
Shanghai Jiao Tong University, China

REVIEWED BY
Colby T. Ford,
University of North Carolina at Charlotte, United States
Remington Nevin,
Johns Hopkins University, United States

*CORRESPONDENCE
Edwin Kamau
edwin.kamau.mil@health.mil;
ashford.kamau@gmail.com

†These authors have contributed equally to this work

SPECIALTY SECTION
This article was submitted to Infectious Diseases – Surveillance, Prevention and Treatment, a section of the journal Frontiers in Medicine

RECEIVED 12 July 2022
ACCEPTED 27 September 2022
PUBLISHED 13 October 2022

CITATION
Andagalu B, Lu P, Onyango I, Bergmann-Leitner E, Wasuna R, Odhiambo G, Chebon-Bore LJ, Ingasia LA, Juma DW, Opot B, Cheruiyot A, Yeda R, Okudo C, Okoth R, Chemwor G, Campo J, Wallqvist A, Akala HM, Ochiel D, Ogutu B, Chaudhury S and Kamau E (2022) Age-dependent antibody profiles to plasmodium antigens are differentially associated with two artemisinin combination therapy outcomes in high transmission setting.
*Front. Med.* 9:991807.
doi: 10.3389/fmed.2022.991807

# Age-dependent antibody profiles to plasmodium antigens are differentially associated with two artemisinin combination therapy outcomes in high transmission setting

Ben Andagalu[1†], Pinyi Lu[2,3†], Irene Onyango[1], Elke Bergmann-Leitner[4], Ruth Wasuna[1], Geoffrey Odhiambo[1], Lorna J. Chebon-Bore[1], Luicer A. Ingasia[1], Dennis W. Juma[1], Benjamin Opot[1], Agnes Cheruiyot[1], Redemptah Yeda[1], Charles Okudo[1], Raphael Okoth[1], Gladys Chemwor[1], Joseph Campo[5], Anders Wallqvist[2], Hoseah M. Akala[1], Daniel Ochiel[1], Bernhards Ogutu[6], Sidhartha Chaudhury[2,7] and Edwin Kamau[1,8,9*]

[1]Department of Emerging and Infectious Diseases (DEID), United States Army Medical Research Directorate-Africa (USAMRD-A), Kenya Medical Research Institute (KEMRI)/Walter Reed Project, Kisumu, Kenya, [2]Biotechnology High Performance Computing Software Applications Institute, Telemedicine and Advanced Technology Research Center, U.S. Army Medical Research and Development Command, Fort Detrick, MD, United States, [3]Henry M. Jackson Foundation for the Advancement of Military Medicine Inc., Bethesda, MD, United States, [4]Biologics Research and Development, Walter Reed Army Institute of Research, Silver Spring, MD, United States, [5]Antigen Discovery Inc., Irvine, CA, United States, [6]Kenya Medical Research Institute (KEMRI), Nairobi, Kenya, [7]Center for Enabling Capabilities, Walter Reed Army Institute of Research, Silver Spring, MD, United States, [8]U.S. Military HIV Research Program, Walter Reed Army Institute of Research, Silver Spring, MD, United States, [9]Department of Pathology and Laboratory Medicine, David Geffen School of Medicine, University of California, Los Angeles, Los Angeles, CA, United States

The impact of pre-existing immunity on the efficacy of artemisinin combination therapy is largely unknown. We performed in-depth profiling of serological responses in a therapeutic efficacy study [comparing artesunate-mefloquine (ASMQ) and artemether-lumefantrine (AL)] using a proteomic microarray. Responses to over 200 *Plasmodium* antigens were significantly associated with ASMQ treatment outcome but not AL. We used machine learning to develop predictive models of treatment outcome based on the immunoprofile data. The models predict treatment outcome for ASMQ with high (72–85%) accuracy, but could not predict treatment outcome for AL. This divergent treatment outcome suggests that humoral immunity may synergize with the longer mefloquine half-life to provide a prophylactic effect at 28–42 days post-treatment, which was further supported by simulated

pharmacokinetic profiling. Our computational approach and modeling revealed the synergistic effect of pre-existing immunity in patients with drug combination that has an extended efficacy on providing long term treatment efficacy of ASMQ.

KEYWORDS

artemisinin combination therapy, machine learning, modeling, immunoprofiling, malaria, artesunate-mefloquine, artemether-lumefantrine, computational analysis

## Introduction

Therapeutic efficacy studies (TESs) are used to monitor efficacy of antimalarial drugs including assessment of clinical and parasitological outcome for artemisinin-based combination therapies (ACTs), the first-line treatment for uncomplicated *Plasmodium falciparum* malaria. TESs conducted at regular intervals in the same location can be used for the detection of the decline of drug efficacy over time. Key indicators monitored during ACTs TESs include proportion of patients who are parasitemic on day 3, and treatment failure by days 28 or 42 (1). Naturally acquired immunity is a key determinant of antimalarial therapeutic response (2), which is highly influenced by transmission intensity (3), and age of the patient (4). Pharmacokinetics (PK) and pharmacodynamics of artemisinin derivatives and partner drugs in ACTs are also important when interpreting TES data.

Artemether-lumefantrine (AL) is the most widely used ACTs in sub-Saharan Africa (sSA), followed by artesunate-amodiaquine (ASAQ) (5). A study that investigated clinical determinants of early parasitological response to ACTs in African patients found that risks of persistent parasitemia on the first and the second day were higher in patients treated with AL compared to those treated with dihydroartemisinin-piperaquine (DP) and ASAQ (6). However, on the third day, the difference was not apparent. Artesunate-mefloquine (ASMQ) has been extensively used in Asia and Latin America but not in sSA because of the availability of other more affordable ACTs (7), concerns for mefloquine resistance seen in Southeast Asia (SEA) (8), and side effects such as excessive vomiting in children (9).

The power of computational tools and mathematical modeling in resolving complex biological questions such as identifying correlates of protection (10–12) or biomarkers of disease (13–16) is now apparent. We have previously used computational integration of immunoprofiling data and modeling to identify immune signature of vaccine adjuvants (10, 17) and vaccine-induced immune correlates of protection (12, 18). In a previous study, we explored the association between the antibody profiles to five Plasmodium antigens and parasite clearance kinetics using part of the TES data presented here (19). Although the scope of this pilot study was limited to five Plasmodium antigens and focused on parasite clearance kinetics in the first 3 days of treatment, it revealed that pre-existing immunity does play a role in treatment outcome thus laying the foundation for the present work. The present, in-depth report on the TES data demonstrates the power of bioinformatics by integrating microarray data and clinical drug and modeling that led to the identification of biomarkers (antigens) associated with a specific treatment outcome within the context of ACTs TES following natural infections.

## Materials and methods

### Study design and participants

This was a randomized, open-label, two-cohort trial, each with two arms conducted in western Kenya, a high transmission, holoendemic region. The study was approved by Institutional Review Boards (IRBs) and Human Subjects Protection Branch, and was registered at clinicaltrials.gov (NCT01976780). Cohort I study was conducted between June 2013 and November 2014, and assessed ASMQ and AL, while cohort II study was conducted between December 2014 and July 2015, and assessed DP and AL. Potential study participants (age 6 months- 65 years) with uncomplicated malaria were identified using malaria rapid diagnostic test (mRDT). Informed consent/assent from the participants, parents or legally authorized representatives was obtained prior to screening procedures. Study details are described in **Supplementary material**.

### Study procedures

Enrolled participants were randomized for malaria treatments and treated with DP (Duo-cotecxin®—Holly Cotec Pharmaceuticals, China), ASMQ or AL (Coartem®—Novartis Pharma Ag, Switzerland). Details of drug treatment scheduling, dosing, and administration are provided in **Supplementary Method**.

During the treatment phase of the studies, blood samples were collected at hours 0, 4, 8, 12, 18, 24, and thereafter, every 6 h until two consecutive negative smears for malaria were obtained. Upon completion of study treatment, participants were followed up weekly from day 7 through day 42.

## Study outcomes

WHO definitions for treatment outcomes in malaria drug efficacy studies were used (1). Parasite clearance rates were calculated using the WWARN, PCE tool located at http://www.wwarn.org/toolkit/data-management/parasite-clearance-estimator. Log transformed parasite density was plotted against time in hours to generate the slope half-life which is defined as the time needed for parasitemia to be reduced by half.

## Laboratory procedures

Malaria microscopy was performed using standardized procedures. *In vitro* drug sensitivity testing was conducted on day 0 (pre-treatment samples) as well as on samples collected from participants who had reappearance of parasites on follow-up visits as previously described (20). Molecular testing was performed as previously described (20).

## Protein microarrays and antibody profiles

A protein microarray containing a total of 1,087 *P falciparum* antigens [3D7 proteome (Antigen Discovery Inc., USA)] was used as previously described (21) to establish the antibody profile of pre-treatment sera for cohort I (ASMQ and AL arms) and perform bioinformatics, data analysis, and modeling. Details on the methodology are provided in **Supplementary material**.

## Bioinformatics, data analysis, and modeling

Detailed bioinformatics, data analysis, and modeling methods can be found in **Supplementary material**. Briefly, to identify antibody signal intensities that differed with respect to different treatment outcomes, univariate analysis was conducted for each antibody signal in the immunoprofile. ASMQ and AL study arms were analyzed separately. Within each arm, participants were further classified as treatment success or treatment failure based on non-PCR-corrected Adequate Clinical and Parasitological Response (nPC-ACPR) on day 28 and 42 per World Health Organization (WHO) definition and guidance for the treatment of malaria (1). Each antibody signal was compared between treatment success (nPC-ACPR = 1) and treatment failure (nPC-ACPR = 0). Random forest and logistic regression were applied to build machine learning models using all antibody signals to predict individual participants' treatment outcome (nPC-ACPR). To evaluate the predictive accuracy of random forest models, cross-validation was utilized, where data samples were subsampled by up-sampling. This aggregation for training and prediction performance was evaluated on data samples that were not used in training. Models' performance was expressed as both a percentage of correctly predicted outcomes with a Cohen's kappa value, and as the area under the curve of the receiver operating characteristic (AUCROC). Cohen's kappa statistic is a measure that can handle imbalanced class problems. A kappa value larger than 0.4 can indicate that the classifier is performing better than a classifier that guesses at random according to the frequency of each class. To assess the statistical significance of the models and check the overfitting that might occur in the machine learning process, AUCROC-based permutation tests were carried out. Relative importance scores of each antibody signal were calculated using random forest models. Principal component analysis (PCA) was applied to all the antibody signals with relative importance scores higher than 50. Antibody signal intensities of participants in the ASMQ arm were plotted using principal component (PC)1 and PC2. We constructed one-compartment PK models for artemether, artesunate, lumefantrine and mefloquine, respectively, using the *linpk* R package. The values of PK parameters, including bioavailable fraction, central clearance, central volume, and first-order absorption rate, were obtained from a previous study (22). All statistical analyses were performed using the R *stats* package and STATA version 13 (StataCorp) while machine learning was carried out using the R *caret* package. The R codes are available in GitHub[1] and datasets are available on request.

# Results

## Differences in anti-parasitic efficacy of the drug combinations

A total of 236 study participants ($n$ = 118 in each cohort) were enrolled of which 200 (84.7%) participants completed 42-day follow-up, 100 from each cohort; 52 in ASMQ arm and 48 in AL arm in cohort I and 50 in each arm in cohort II (**Supplementary Figure 1** for study disposition chart). There were no notable differences in the baseline characteristics of the enrolled participants (**Supplementary Table 1**), and no cases of early treatment failure (**Figure 1**). All study participants

1 https://github.com/BHSAI/immstat2

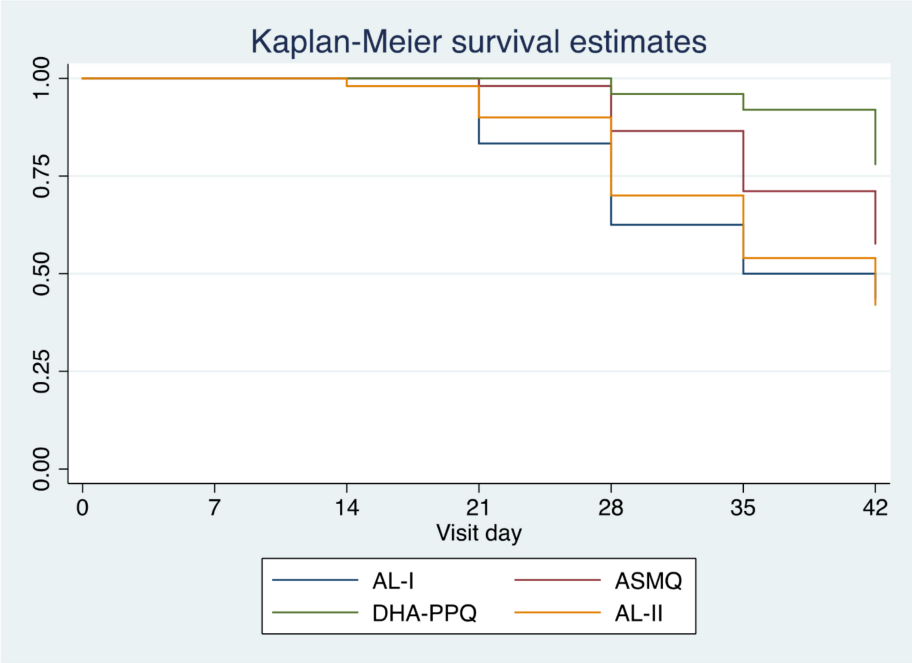


FIGURE 1
Kaplan-Meier survival estimate for time to malaria infection following ACT treatment. Survival curves are shown for Cohort 1, AL subjects (blue), ASMQ subjects (red) and Cohort II AL subjects (orange), and DHA-PPQ subjects (purple) as a function of days post-treatment.

achieved 100% PCR-corrected ACPR (PC-ACPR) rates at day 28 and 42 (Table 1). There were no significant differences in the parasite clearance half-lives between the study arms (Table 2). The maximum parasite clearance slope half-lives observed for both cohorts were 4.2 (AL arm in cohort I) and 4.3 (AL arm in cohort II) hours falling within the WHO recommended cut-off for suspected artemisinin resistance (1). However, PC50 and PC99 data (time for the initial parasite density to fall by 50 or 99%) revealed ASMQ and DP outperformed AL by clearing parasites faster (Table 2). Further, participants who received ASMQ and DP achieved better nPC-ACPR at day 28 and 42 compared to those who received AL (Table 1), with significant difference present in cohort I for ASMQ vs. AL on day 28 ($p$ = 0.042) but not on day 42 ($p$ = 0.280), and in cohort II, a significant difference was present for DP vs. AL on day 28 ($p$ = 0.001) and on day 42 ($p$ = 0.008). Of note, none of the study participants developed side effects including those in ASMQ arm.

## *In vitro* and molecular analyses

*In vitro* susceptibility testing to AL component drugs (artemether and lumefantrine) was successfully performed in some of the parasite isolates (Supplementary Figure 2). The parasite isolates IC50 values for both drugs remained unchanged, similarly to the published IC50 (17). K13 mutations were present, but none of the K13 mutations identified as markers of artemisinin resistance in SEA. We investigated the polymorphisms in pfcrt (K76) and pfmdr1 (N86, 184F and D1246), and pfmdr1 copy numbers, which are associated with AL selection in sSA parasites (17). The frequencies of these mutations and pfmdr1 copy number variation were similar in both cohorts and to the previously published data (17).

## Wider breadth of humoral immunity confers better non-PCR-corrected adequate clinical and parasitological response outcome in artesunate-mefloquine arm

Since the variances in the response to drug treatment were not due to differences in parasite genetic diversity profiles, we sought to determine whether distinct immunoprofiles in participants treated with the different drug combinations impacted the clinical and parasitological outcome in cohort I. Although there were no significant differences in the parasite clearance half-lives between the study arms regardless of the treatment used, the parasite clearance kinetics based on PC50/PC99 clearly demonstrated there was a lag phase in AL treatment compared to ASMQ and DP (Table 2).

TABLE 1 Rates of adequate clinical and parasitological response (ACPR) with and without PCR corrections.

| | ASMQ | AL | Difference% (95% CI) | DP | AL | Difference% (95% CI) |
|---|---|---|---|---|---|---|
| Day 42 | ***n* = 52** | ***n* = 48** | | ***n* = 50** | ***n* = 50** | |
| PC-ACPR | 52 (100%) | 48 (100%) | | 50 (100%) | 50 (100%) | |
| nPC-ACPR | 30 (57.7%) | 21 (43.8%) | −13.9% (−33.4 to 5.5) | 39 (78.0%) | 21 (42.0%) | −36% (−53.8 to −18.1) |
| Day 28 | ***n* = 53** | ***n* = 51** | | ***n* = 53** | ***n* = 51** | |
| PC-ACPR | 53 (100%) | 51 (100%) | | 53 (100%) | 51 (100%) | |
| nPC-ACPR | 45 (84.9%) | 32 (62.8%) | −22.2% (−38.6 to −5.8) | 50 (96.2%) | 36 (70.6%) | −25.6% (−39.1 to −12.0) |

TABLE 2 Parasite clearance rates.

| Parameters | ASMQ | AL-I | DP | AL-II |
|---|---|---|---|---|
| **Total analyzed for $T_{1/2}$** | **58** | **50** | **57** | **53** |
| Slope half-life median (IQR) | 2.3 (1.8–2.7) | 2.5 (2.2–3.0) | 2.2 (1.9–2.5) | 2.3 (2.0–2.9) |
| Slope half-life mean (range) | 2.2 (0.98–3.6) | 2.6 (1.5–4.2) | 2.2 (1.2–3.6) | 2.4 (1.4–4.3) |
| PC50 median (IQR) | 4.0 (2.6–6.0) | 7.4 (4.8–9.6) | 4.1 (3.2–6.0) | 6.7 (4.4–8.8) |
| PC50 mean (range) | 4.2 (0.28–11.1) | 7.4 (0.5–15.3) | 4.6 (0.27–11.3) | 6.5 (0.24–11.6) |
| PC99 median (IQR) | 17.0 (13.4–19.2) | 21.5 (18.3–24.8) | 16.8 (14.6–19.5) | 20.1 (17.5–22.1) |
| PC99 mean (range) | 16.6 (6.5–25.6) | 21.9 (10.0–33.0) | 17.0 (7.3–27.9) | 20.0 (9.1–30.5) |

Data shows parasite slope half-lives and parasite clearance rates for cohort I (ASMQ and AL-I) and cohort II (DP and AL-II) in hours.

We used nPC-ACPR as endpoint data to dichotomize study participants' response to treatment regardless of whether it was reinfection or recrudescence because it indicated differences in the ability of the study participants to control parasites likely due to existing anti-Plasmodial antibodies. Microarrays analyses to establish the Plasmodium-specific antibody profiles were successfully performed for 91 (46 in ASMQ and 45 in AL) of the 104 participants who completed day 28 follow-up, and 87 (45 in ASMQ and 42 in AL) of 100 participants who completed day 42. We carried out univariate analyses to compare the antibody profiles established by the microarrays between participants in ASMQ and AL arms who achieved nPC-ACPR vs. those who did not, on day 28 and 42. Significant nPC-ACPR associated differences were present in the ASMQ arm (**Figures 2A,B**), but not in the AL arm (**Figures 2C,D**). In the ASMQ arm, antibody responses to 277 antigens with $P < 0.05$ and adjusted $P < 0.1$ (**Figure 2A**) were significantly different between participants that showed nPC-ACPR on day 28 compared to those who did not. On day 42, significant differences were observed for antibody responses to 10 antigens with $P < 0.05$ and adjusted $P < 0.1$ (**Figure 2B**). The right-skewed pattern in the volcano plots (**Figures 2A,B**) indicates that participants maintaining nPC-ACPR in the ASMQ arm had higher humoral immunity to *P falciparum* antigens compared those who did not. The specific antigens that correspond to these antibody responses are listed in **Supplementary Table 2**, ranked by corresponding Benjamini-Hochberg adjusted *P*-values. To determine whether distinct immunoprofiles are associated with parasitological outcome, microarray and treatment outcome data were integrated and a PCA was performed. In the ASMQ arm, participants clustered separately based on their treatment outcome, showing clear systematic differences in immune responses (**Figures 3A,B**). However, there was no separation in the AL arm (**Figures 3C,D**).

## Antibody responses associated with non-PCR-corrected adequate clinical and parasitological response are age dependent

To investigate the magnitude of immune responses with age, we compared antibody signal intensities of the study participants in different age groups (5 or younger, 5–12, and 12 or older) in the ASMQ arm. Normalizing the mean signal intensities to *P falciparum* proteins from participants at varying ages against the mean intensities for the oldest study participant group revealed that the magnitude of antibody responses to these antigens increased with age (**Figure 4**). Among antibody responses associated with nPC-ACPR on day 28, children (participants < 12 years) showed approximately half the magnitude of antibody responses as older participants (≥12 years), as indicated by the slope. This effect was more pronounced in antibody responses associated with nPC-ACPR on day 42, where children showed approximately a third of the magnitude of responses as older participants.

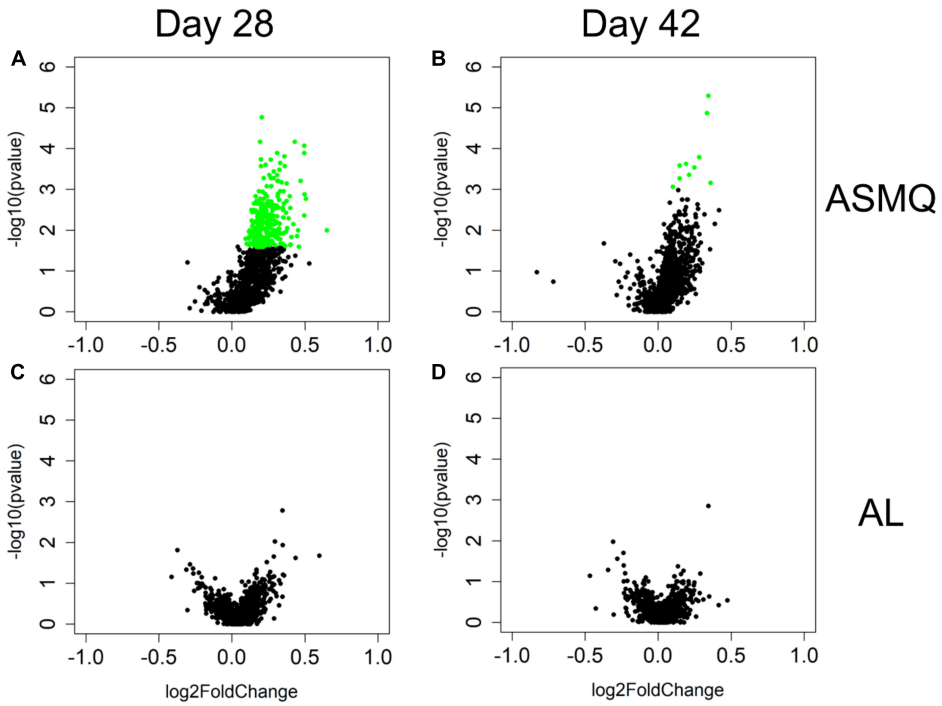


FIGURE 2
nPC-ACPR-associated differences in subjects' humoral immunity to malaria in the ASMQ and AL arms. Univariate analyses were applied to identify differences in subjects' humoral immunity associated with ASMQ outcomes on day 28 **(A)** and day 42 **(B)**, and with AL outcomes on day 28 **(C)** and day 42 **(D)**, respectively. Volcano plots were used to present analysis results. The *x*-axis is log2 ratio of malaria antigen-specific antibody signals of subjects presenting nPC-ACPR to those of subjects not presenting nPC-ACPR. The *y*-axis is *P*-values based on −log10. The green dots represent the antibody responses with $P < 0.05$ and Benjamini-Hochberg adjusted $P < 0.1$.

## Machine learning can predict treatment outcome for artesunate-mefloquine using humoral immunity data

Machine learning methods (random forest models confirmed by logistic regression models) were used to assess the degree to which humoral immunity to malaria could predict treatment outcome. For the ASMQ arm, 100 random forest models were built for predicting treatment outcome using antibody signals that were significantly different between participants that showed nPC-ACPR compared to those who did not. Models built for predicting treatment outcomes on day 28 achieved 85% accuracy (Kappa: 0.40) with an average AUCROC of 0.85 (**Figures 5A,E**), and on day 42, the accuracy was 72% (Kappa: 0.43) with an average AUCROC of 0.83 (**Figures 5B,F**). Randomly shuffled nPC-ACPR outcomes across participants to remove any possible link between humoral immunity and outcome were used as negative control for the machine learning analysis to test for overfitting. The average AUCROC for using the randomly shuffled data for day 28 and 42 in ASMQ arm were 0.54 and 0.53, which were significantly lower than the average AUCROC of actual models (**Figures 5A,B**).

In the AL arm, machine learning models could not predict nPC-ACPR outcome on day 28 or 42, achieving accuracies of 53% (Kappa: 0.02) and 61% (Kappa: 0.05), respectively, with an average AUCROC of 0.51, indicating an accuracy no better than random chance (**Figures 5C,D,G,H**). Relative importance scores of each antibody signal were calculated only for the ASMQ arm using random forest models, which could not only help get a better understanding of the model's logic, but also help identify antibody signals more related to the therapeutic efficacy of ASMQ (**Supplementary Table 3**).

## Simulation of artesunate-mefloquine and artemether-lumefantrine pharmacokinetics profiles

To explore how humoral immunity and treatment interact, we simulated PK profile of ASMQ and AL out to day 28 and 42. The PK profiles of both regimens show that the concentration of artemisinin derivative drugs clears within 6 days post-treatment. In the AL regimen, lumefantrine is cleared by day 11 post-treatment, therefore is unlikely to have a major impact on day 28 and 42 outcomes (**Figure 6A** and **Supplementary Figure 3**). By comparison, in the ASMQ regimen, mefloquine has a

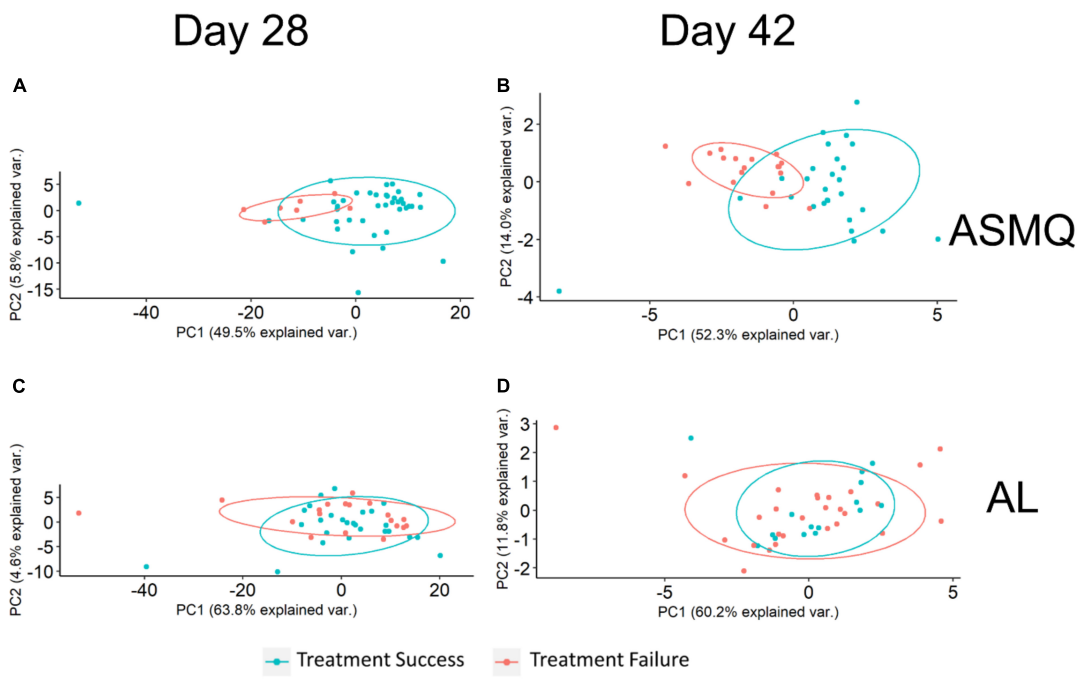


FIGURE 3
Principal Component Analysis (PCA) plots of treatment outcome-specific differences. **(A,B)**. PCA used antibody signals with adjusted $P < 0.1$ to visualize treatment outcome-specific differences in the ASMQ arm, which were identified by univariate analyses applied to identify differences in subjects' humoral immunity associated with ASMQ outcomes on day 28 and 42, respectively. **(C,D)**. PCA used the same antibody signals as **(A,B)** to visualize treatment outcome-specific differences in the AL arm.

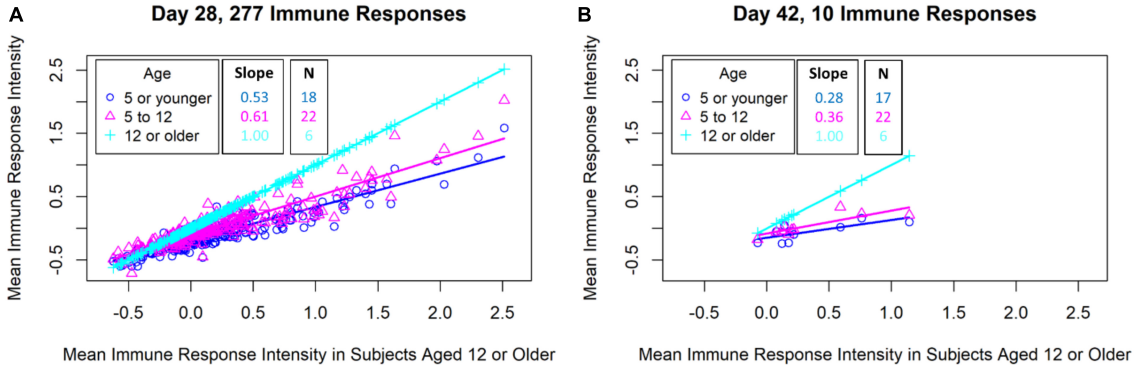


FIGURE 4
Comparison of malaria antigen-specific antibody responses of subjects in different age groups. The mean antigen-specific antibody signal intensities to *P falciparum* proteins (identified through univariate analyses) from subjects in varying ages (*y*-axis) were plotted against the mean intensities for the oldest subject group (*x*-axis). **(A)** Scatterplot of mean antibody signal intensities of 277 *P falciparum* proteins associated with ASMQ outcomes on day 28. **(B)** Scatterplot of mean antibody signal intensities of 10 *P falciparum* proteins associated with ASMQ outcomes on day 42.

much longer apparent half-life, with concentrations relative to peak concentration of 30.9% at day 28, and 3.3% at day 42 (Figure 6A), representing 3- and 30-fold reductions from the peak concentrations.

Based on this data we formulated the hypothesis that humoral immunity augments the efficacy of mefloquine when it is at sub-therapeutic concentrations. The minimum inhibitory concentration (MIC) of the drug required to be effective is likely to vary between individuals. Given that all participants showed nPC-ACPR at day 7, for participants that showed nPC-ACPR failure by day 28, it is plausible the drug concentration fell below individual's MIC between day 7 and 28. Based on our simulated PK profiles, the average mefloquine concentration during that time span was 2.35 mg/l. Likewise, for participants that showed

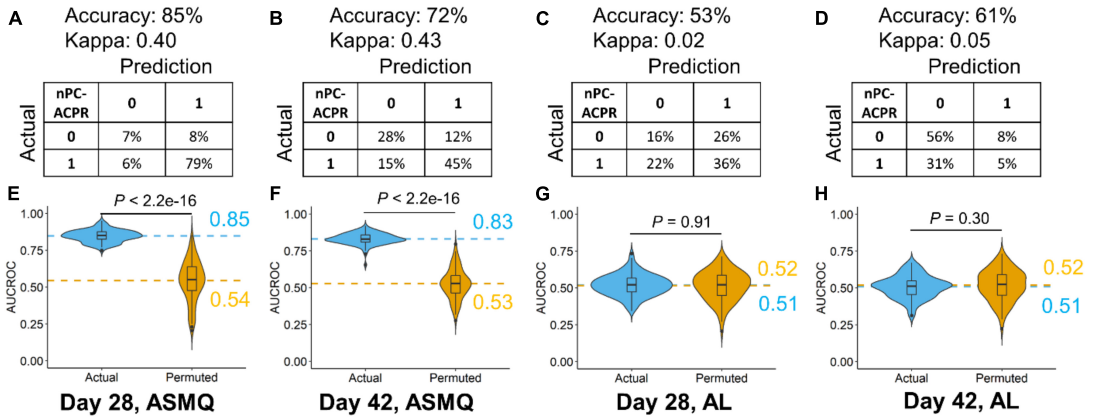


FIGURE 5
Performance evaluation of random forest models predicting ASMQ outcomes on day 28 and 42 **(A–D)**. Prediction accuracy, kappa, and confusion matrices. The rows of confusion matrices represent the actual treatment outcomes, whereas the columns indicate the predicted treatment outcomes **(E–H)**. Comparison of AUCROC values from 100 repetitions of 100 times repeated fivefold cross-validation using actual (blue) vs. permutated (yellow) nPC-ACPR labels. Dashed line represented the mean AUCROC values. Significance is determined using Mann-Whitney-Wilcoxon test.

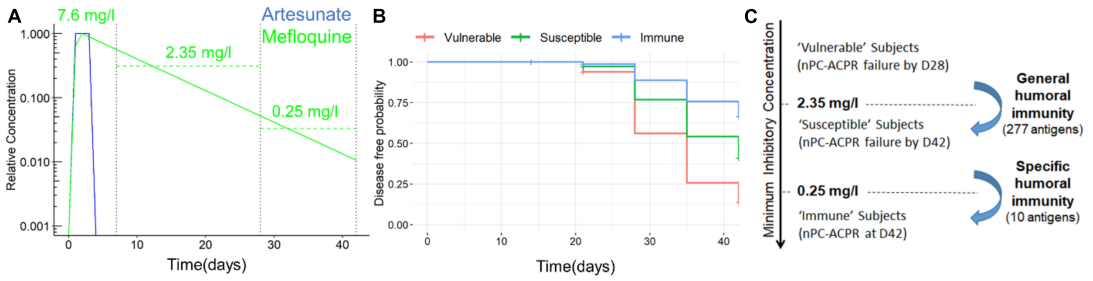


FIGURE 6
PK profile of ASMQ and estimation of MIC of mefloquine. **(A)** Simulated PK profile of ASMQ for artesunate (blue) and mefloquine (green). Estimated peak concentration, and average concentration between day 7 and 28, and day 28 and 42 are shown for mefloquine are labeled. **(B)** Estimated disease-free probability for all ASMQ subjects classified as "susceptible," "intermediate," and "immune" based on humoral immunity using the day 28 and 42 predictive models. **(C)** Relationship between humoral immunity and MIC of mefloquine based on ACPR outcome, univariate analysis, and simulated PK profiles.

nPC-ACPR at day 28, but nPC-ACPR failure by day 42, the mefloquine concentration fell below their MIC within the time span of day 28 and 42, during which an average concentration was estimated to be 0.25 mg/l. Therefore, based on our estimates, "vulnerable" participants who had nPC-ACPR failure by day 28 have an average MIC > 2.35 mg/l, while immune participants who show nPC-ACPR even out to day 42 have an average MIC of < 0.25 mg/l. In addition, Cox regression analysis showed a strong association ($P < 0.01$) between the time to malaria re-infection and classes of participants identified by machine learning models (Figures 6B,C).

## Discussion

Our study provides crucial findings on the efficacy of ACTs in treatment of uncomplicated *P falciparum* in high transmission settings. To the best of our knowledge, this is the first study to demonstrate divergent impact of serological immune profiles on treatment outcomes based on ACT treatment using a computational approach. Machine learning approaches identified *P falciparum* antigens that are highly predictive of successful ASMQ treatment outcome. Our modeling data suggest that at sub-therapeutic concentrations, mefloquine acts synergistically with Plasmodium-specific antibody responses to provide extended protection against clinical and parasitological failure. In sSA, there is a need to deploy additional ACTs or new class of antimalarial drugs to avoid development of resistance to the current first-line treatments. By identifying specific antigens associated with, and predictive of treatment outcome for specific antimalarial drugs, our data support the notion of smart deployment of new ACTs and other antimalarial drugs, where decisions are informed

by individual and population immune profiles, and therefore strategically prioritized for each region or a country.

The high efficacy of all the ACTs tested in this study can be attributed to high transmission rates and prevalent immunity. We showed ASMQ and DP outperformed AL on day 28, as well as day 42, corroborating other studies (6, 23). This has previously been attributed to the long half-lives of mefloquine and piperaquine, which are thought to provide 4–6 weeks prophylaxis after treatment compared to 3–4 days for lumefantrine (24). Using PK modeling, we estimated mefloquine concentrations to be at 30% of peak concentration on day 28, while lumefantrine was completely cleared by 14 days, confirming the persistence of mefloquine and its role in the apparent post-treatment prophylaxis observed in the ASMQ cohort.

Host immunity is an important determinant of treatment outcome in *P falciparum* malaria infections (2), with the magnitude of immunological response increasing with age (4). In this study, we show that the interaction between humoral immunity and residual mefloquine concentration is important in providing protection and predicting treatment outcome. This is supported by the following observations: First, if humoral immunity alone was sufficient for nPC-ACPR out to day 28 and 42, then immunity would have predicted protection in AL arm as well; second, if residual mefloquine concentration alone was sufficient to determine nPC-ACPR outcome, then humoral immunity wouldn't have predicted outcome in ASMQ; and third, immunity is likely the only explanation for differences in nPC-ACPR based on age, as age-specific differences in PK profiles of AL and ASMQ have not been reported. Machine learning identified three classes of patients (vulnerable, susceptible, and immune) in the ASMQ arm based on immune data (**Figure 6B**). Our findings suggest that general humoral immunity to a wide range of Plasmodium antigens is sufficient to provide protection in the presence of residual mefloquine concentrations out to day 28, while specific immunity to a handful of select antigens is necessary to provide protection in very low residual mefloquine concentrations out to day 42.

Reports of mefloquine side-effects including early vomiting, mental and neurological concerns might be contributing to the poor scale-up of ASMQ in Africa (9, 23, 25). Dosing and timing of when mefloquine is administered as a combination therapy is important, impacts drug efficacy, and the side effects experienced by the patients. Ter Kuile et al., showed that in children $\leq$ 2 years, vomiting was reduced by 40% when mefloquine dose of 25 mg/kg was split over 2 days, and by 50% when given on the second day (9). By administering artesunate first, and then mefloquine 24 h later, this reduced vomiting because the patients had recovered clinically and were more likely to tolerate mefloquine. Further, delaying the dose of mefloquine for 24 h after artesunate administration increases mefloquine oral bioavailability substantially probably due to rapid clinical improvement (26). In our study, administration of three doses of artesunate in the first 48 h, and then mefloquine at 72 and 96 h eliminated vomiting and dramatically reduced side effects. As a fixed-dose or non-fixed-dose combination therapy, ASMQ is given over a 3-day period once or twice daily (25, 27–29). Since fixed-dose medication improved compliance, we propose creation of a fixed-dose ASMQ combination that delivers mefloquine after the first 24 or 48 h to allow ample time for clinical recovery of the patient.

This study has limitations: (1) relatively small sample size; our univariate analysis statistical test accounts for sample size and utilizes a multiple test correction to account for the large number of parameters being measured. The immune correlates of outcome were identified in ASMQ cohorts, but not in AL cohorts. This would not have been possible in an under-powered study. (2) The small number of correlates identified in the ASMQ Day 42 cohort could be the result of the waning impact of immunity over time, post-treatment, as the mefloquine concentration decreases. In the future, it will be important to repeat these analyses using other ACTs especially DP due to its high efficacy and the long prophylactic life-span of piperaquine.

## Conclusion

In conclusion, we have demonstrated that data integration, machine learning, and modeling provide a comprehensive approach capturing the underlying complexity of malaria control in sSA. Further, we have shown ASMQ is a highly effective drug, making it an appropriate choice of possible first-line treatment in western Kenya, a region which account for most malaria transmission in the country.

## Data availability statement

The original contributions presented in this study are included in the article/**Supplementary material**, further inquiries can be directed to the corresponding author.

## Ethics statement

The studies involving human participants were reviewed and approved by the Kenya Medical Research Institute Scientific and Ethical Review Unit (KEMRI-SERU)—KEMRI SSC numbers 2518 and 2722, as well as the Walter Reed Army Institute of Research Institutional Review Board (WRAIR IRB)—WRAIR numbers 1935 and 1935A. The patients/participants provided their written informed consent to participate in this study.

## Author contributions

BA: study principal investigator (PI), funding, data analysis, manuscript draft writing, and reviewing. PL: bioinformatics analysis and draft review. IO: study oversite and recruitment of study participants. EB-L: data analysis, draft writing, and reviewing. RW: study pharmacists. GO, LC-B, LI, DJ, BenO, AC, RY, CO, RO, and GC: laboratory analysis of specimens. JC: immunological data analysis, funding, and manuscript review. AW: bioinformatics analysis and team lead. HA: specimen and personnel management, data analysis, and draft review. DO: data analysis and manuscript review. BerO: consultation and manuscript review. SC: bioinformatics analysis, draft writing, and reviewing. EK: study and team management, concept refinement, draft writing, and reviewing. All authors contributed to the article and approved the submitted version.

## Funding

This study was funded by the Armed Forces Health Surveillance Branch (AFHSB) and its Global Emerging Infections Surveillance (GEIS) Section (Grant no. P0126_13_KY).

## Acknowledgments

We thank Drs. Veronica Manduku, KEMRI Center for Clinical Research; LTC Claire A Cornelius, Douglas Shaffer, Directors, USAMRD-A/K, and Steve Munga, KEMRI Center for Global Health Research, for supporting this study and giving their permission to publish these data. We also thank all clinical staff at Kombewa District Hospital for their assistance. But most importantly, we express our heartfelt gratitude to the study participants who sacrificed a lot to participate in our studies for the betterment of the community, thank you!

## Conflict of interest

Author PL was employed by the Henry M. Jackson Foundation for the Advancement of Military Medicine Inc. Author JC was employed by the Antigen Discovery Inc.

The remaining authors declare that the research was conducted in the absence of any commercial or financial relationships that could be construed as a potential conflict of interest.

## Publisher's note

All claims expressed in this article are solely those of the authors and do not necessarily represent those of their affiliated organizations, or those of the publisher, the editors and the reviewers. Any product that may be evaluated in this article, or claim that may be made by its manufacturer, is not guaranteed or endorsed by the publisher.

## Author disclaimer

Material has been reviewed and approved for public release with unlimited distribution by the Walter Reed Army Institute of Research and The Henry M. Jackson Foundation for Advancement of Military Medicine, Inc. (HJF). This manuscript has been approved for public release with unlimited distribution. The investigators have adhered to the policies for protection of human subjects as prescribed in AR 70–25. EB-L, SC, and EK were government employees, and this work was prepared as part of their official duties. Title 17 U.S.C. §105 provides that copyright protection under this title is not available for any work of the U.S. Government. The opinions or assertions contained herein are the private views of the author, and are not to be construed as official, or as reflecting true views of the Department of the Army, the U.S. Department of Defense, or HJF.

## Supplementary material

The Supplementary Material for this article can be found online at: https://www.frontiersin.org/articles/10.3389/fmed.2022.991807/full#supplementary-material

## References

1. World Health Organization. *Guidelines for the treatment of malaria*. Geneva: World Health Organization (2015).

2. Rogerson SJ, Wijesinghe RS, Meshnick SR. Host immunity as a determinant of treatment outcome in *Plasmodium falciparum* malaria. *Lancet Infect Dis.* (2010) 10:51–9. doi: 10.1016/s1473-3099(09)70322-6

3. Snow RW, Marsh K. New insights into the epidemiology of malaria relevant for disease control. *Br Med Bull.* (1998) 54:293–309. doi: 10.1093/oxfordjournals.bmb.a011689

4. Marsh K, Kinyanjui S. Immune effector mechanisms in malaria. *Parasite Immunol.* (2006) 28:51–60. doi: 10.1111/j.1365-3024.2006.00808.x

5. World Health Organization. *World malaria report 2018*. Geneva: World Health Organization (2018).

6. Das D, Price RN, Bethell D, Guerin PJ, Stepniewska K. Early parasitological response following artemisinin-containing regimens: A critical review of the literature. *Malar J.* (2013) 12:125. doi: 10.1186/1475-2875-12-125

7. Wells S, Diap G, Kiechel JR. The story of artesunate-mefloquine (ASMQ), innovative partnerships in drug development: Case study. *Malar J.* (2013) 12:68. doi: 10.1186/1475-2875-12-68

8. Fontanet AL, Johnston DB, Walker AM, Rooney W, Thimasarn K, Sturchler D, et al. High prevalence of mefloquine-resistant *falciparum* malaria in eastern Thailand. *Bull World Health Organ.* (1993) 71:377–83.

9. ter Kuile FO, Nosten F, Luxemburger C, Kyle D, Teja-Isavatharm P, Phaipun L, et al. Mefloquine treatment of acute *falciparum* malaria: A prospective study of non-serious adverse effects in 3673 patients. *Bull World Health Organ.* (1995) 73:631–42.

10. Chaudhury S, Duncan EH, Atre T, Dutta S, Spring MD, Leitner WW, et al. Combining immunoprofiling with machine learning to assess the effects of adjuvant formulation on human vaccine-induced immunity. *Hum Vaccin Immunother.* (2020) 16:400–11. doi: 10.1080/21645515.2019.1654807

11. Chaudhury S, Regules JA, Darko CA, Dutta S, Wallqvist A, Waters NC, et al. Delayed fractional dose regimen of the RTS,S/AS01 malaria vaccine candidate enhances an IgG4 response that inhibits serum opsonophagocytosis. *Sci Rep.* (2017) 7:7998. doi: 10.1038/s41598-017-08526-5

12. Pallikkuth S, Chaudhury S, Lu P, Pan L, Jongert E, Wille-Reece U, et al. A delayed fractionated dose RTS,S AS01 vaccine regimen mediates protection *via* improved T follicular helper and B cell responses. *eLife.* (2020) 9:e51889. doi: 10.7554/eLife.51889

13. Ceballos GA, Hernandez LF, Paredes D, Betancourt LR, Abdulreda MH. A machine learning approach to predict pancreatic islet grafts rejection versus tolerance. *PLoS One.* (2020) 15:e0241925. doi: 10.1371/journal.pone.0241925

14. Penney KL, Tyekucheva S, Rosenthal J, El Fandy H, Carelli R, Borgstein S, et al. Metabolomics of prostate cancer gleason score in tumor tissue and serum. *Mol Cancer Res.* (2020) 19:475–84. doi: 10.1158/1541-7786.Mcr-20-0548

15. Tavolara TE, Niazi MKK, Ginese M, Piedra-Mora C, Gatti DM, Beamer G, et al. Automatic discovery of clinically interpretable imaging biomarkers for *Mycobacterium tuberculosis* supersusceptibility using deep learning. *EBioMedicine.* (2020) 62:103094. doi: 10.1016/j.ebiom.2020.103094

16. Ungaro RC, Hu L, Ji J, Nayar S, Kugathasan S, Denson LA, et al. Machine learning identifies novel blood protein predictors of penetrating and stricturing complications in newly diagnosed paediatric Crohn's disease. *Aliment Pharmacol Ther.* (2020) 53:281–90. doi: 10.1111/apt.16136

17. Chaudhury S, Duncan EH, Atre T, Storme CK, Beck K, Kaba SA, et al. Identification of immune signatures of novel adjuvant formulations using machine learning. *Sci Rep.* (2018) 8:17508. doi: 10.1038/s41598-018-35452-x

18. Hickey B, Teneza-Mora N, Lumsden J, Reyes S, Sedegah M, Garver L, et al. IMRAS-A clinical trial of mosquito-bite immunization with live, radiation-attenuated P. *falciparum* sporozoites: Impact of immunization parameters on protective efficacy and generation of a repository of immunologic reagents. *PLoS One.* (2020) 15:e0233840. doi: 10.1371/journal.pone.0233840

19. Odhiambo G, Bergmann-Leitner E, Maraka M, Wanjala CNL, Duncan E, Waitumbi J, et al. Correlation between malaria-specific antibody profiles and responses to artemisinin combination therapy for treatment of uncomplicated malaria in Western Kenya. *J Infect Dis.* (2019) 219:1969–79. doi: 10.1093/infdis/jiz027

20. Akala HM, Eyase FL, Cheruiyot AC, Omondi AA, Ogutu BR, Waters NC, et al. Antimalarial drug sensitivity profile of western Kenya *Plasmodium falciparum* field isolates determined by a SYBR Green I *in vitro* assay and molecular analysis. *Am J Trop Med Hyg.* (2011) 85:34–41. doi: 10.4269/ajtmh.2011.10-0674

21. Crompton PD, Kayala MA, Traore B, Kayentao K, Ongoiba A, Weiss GE, et al. A prospective analysis of the Ab response to Plasmodium falciparum before and after a malaria season by protein microarray. *Proc Natl Acad Sci U.S.A.* (2010) 107:6958–63. doi: 10.1073/pnas.1001323107

22. Guidi M, Mercier T, Aouri M, Decosterd LA, Csajka C, Ogutu B, et al. Population pharmacokinetics and pharmacodynamics of the artesunate-mefloquine fixed dose combination for the treatment of uncomplicated *falciparum* malaria in African children. *Malar J.* (2019) 18:139. doi: 10.1186/s12936-019-2754-6

23. Whegang Youdom S, Tahar R, Basco LK. Comparison of anti-malarial drugs efficacy in the treatment of uncomplicated malaria in African children and adults using network meta-analysis. *Malar J.* (2017) 16:311. doi: 10.1186/s12936-017-1963-0

24. Djimde A, Lefevre G. Understanding the pharmacokinetics of Coartem. *Malar J.* (2009) 8(Suppl. 1):S4. doi: 10.1186/1475-2875-8-S1-S4

25. Sirima SB, Ogutu B, Lusingu JPA, Mtoro A, Mrango Z, Ouedraogo A, et al. Comparison of artesunate-mefloquine and artemether-lumefantrine fixed-dose combinations for treatment of uncomplicated *Plasmodium falciparum* malaria in children younger than 5 years in sub-Saharan Africa: A randomised, multicentre, phase 4 trial. *Lancet Infect Dis.* (2016) 16:1123–33. doi: 10.1016/S1473-3099(16)30020-2

26. Hellgren U, Berggren-Palme I, Bergqvist Y, Jerling M. Enantioselective pharmacokinetics of mefloquine during long-term intake of the prophylactic dose. *Br J Clin Pharmacol.* (1997) 44:119–24. doi: 10.1046/j.1365-2125.1997.00633.x

27. Agomo PU, Meremikwu MM, Watila IM, Omalu IJ, Odey FA, Oguche S, et al. Efficacy, safety and tolerability of artesunate-mefloquine in the treatment of uncomplicated *Plasmodium falciparum* malaria in four geographic zones of Nigeria. *Malar J.* (2008) 7:172. doi: 10.1186/1475-2875-7-172

28. Faye B, Ndiaye JL, Tine R, Sylla K, Gueye A, Lo AC, et al. A randomized trial of artesunate mefloquine versus artemether lumefantrine for the treatment of uncomplicated *Plasmodium falciparum* malaria in Senegalese children. *Am J Trop Med Hyg.* (2010) 82:140–4. doi: 10.4269/ajtmh.2010.09-0265

29. Sagara I, Diallo A, Kone M, Coulibaly M, Diawara SI, Guindo O, et al. A randomized trial of artesunate-mefloquine versus artemether-lumefantrine for treatment of uncomplicated Plasmodium falciparum malaria in Mali. *Am J Trop Med Hyg.* (2008) 79:655–61.

frontiers | Frontiers in Public Health

TYPE Opinion
PUBLISHED 20 October 2022
DOI 10.3389/fpubh.2022.1001666



OPEN ACCESS

EDITED BY
Hui Chen,
Brigham and Women's Hospital and Harvard Medical School, United States

REVIEWED BY
Binsen Li,
UCLA Health System, United States
Sahar Rostamian,
Brigham and Women's Hospital and Harvard Medical School, United States

*CORRESPONDENCE
Nuriye Nuray Ulusu
nulusu@ku.edu.tr
Duygu Aydemir
daydemir16@ku.edu.tr

SPECIALTY SECTION
This article was submitted to Infectious Diseases–Surveillance, Prevention and Treatment, a section of the journal Frontiers in Public Health

RECEIVED 23 July 2022
ACCEPTED 30 September 2022
PUBLISHED 20 October 2022

CITATION
Aydemir D and Ulusu NN (2022) The possible importance of the antioxidants and oxidative stress metabolism in the emerging monkeypox disease: An opinion paper. *Front. Public Health* 10:1001666. doi: 10.3389/fpubh.2022.1001666



# The possible importance of the antioxidants and oxidative stress metabolism in the emerging monkeypox disease: An opinion paper

Duygu Aydemir[1,2]* and Nuriye Nuray Ulusu[1,2]*

[1]Department of Medical Biochemistry, School of Medicine, Koc University, Istanbul, Turkey, [2]Koc University Research Center for Translational Medicine (KUTTAM), Istanbul, Turkey

KEYWORDS

**antioxidant molecules, monkeypox, MPXV infection, oxidative stress, immune response, antioxidant enzymes**

## Introduction

The world has been struggling with a major public health problem since December 2019: an infectious disease caused by a novel coronavirus called severe acute respiratory syndrome coronavirus 2 (SARS-CoV-2). Despite vaccination, people are still infected and die because of COVID-19 since the virus mutates very quickly (1, 2). While the world is struggling with the COVID-19 pandemic, a new virus called Monkeypox (MPXV) alerts scientists about whether a new pandemic will arise. Monkeypox is a zoonotic, neglected, and emerging disease caused by the MPXV belonging to the *Orthopoxvirus* genus of the *Poxviridae* family. MPXV was first identified in Macaca irus wild monkeys in 1958 in Denmark; it was the first time specified in humans in 1970 in the Democratic Republic of the Congo in a 9-month-old boy (3, 4). However, several rodent species were also reported as reservoirs of this virus (5). Monkeypox disease has been reported as an emerging outbreak affecting 43 countries with 2103 confirmed cases (6).

The transmission ways of MPXV are direct contact with an infected animal or infected person *via* body fluids, using contaminated objects, and inhaling virus-containing respiratory droplets. The incubation time of the disease takes 5–21 days, where the symptoms of MPXV infection are reported as headache, fever, muscle pain, back pain, swollen lymph nodes, chills, adenopathy, maculopapular rash, especially on the palms, and exhaustion. Lesions such as macules, papules, vesicles, pustules, and scabs have been reported mainly in the palms of the hands and the soles of the feet. There is no treatment for MPXV infection; however, smallpox vaccination is considered a treatment option (7, 8). The MPXV infection begins like other viral infections with the entry of the virus into the cells and replication, leading to the immune response in the host cells, such as blocking the antiviral T-cell activation and inflammatory cytokine production. However, cellular mechanisms of MPXV infection, host cell interactions, immune responses, and destruction are not fully understood in humans despite animals (9).

## Metabolism of virally infected cells

Viral infection and replication are tightly associated with the dysregulated immune system and inflammatory response. Since humans have complicated defense mechanisms against pathogens, viruses can quickly adapt to changing conditions such as the host's immune system and drug treatments. For instance, viruses deregulate cellular signaling pathways, including oxidative stress metabolism and cell death mechanisms, to escape the host's immune system (10, 11). The crucial step for virus replication is escaping from the cellular defense mechanism of the host cell (12, 13). Viruses are disparate from all living things; they don't inherently have their metabolism. Major cytosolic and mitochondrial metabolic pathways are altered in virus-infected cells (14, 15). Specific anabolic pathways such as glycolysis, glycogenolysis, pentose phosphate pathway (PPP), lipogenesis, cholesterol synthesis, one-carbon metabolism, and various transporters such as glucose and glutamine transporters are upregulated in virally infected cells (16, 17). It has also been investigated that the Warburg effect, which can be seen in cancer cells using glucose and producing lactate under normoxia conditions, can also be in the virus metabolism (18).

## Importance of the antioxidant defense and antioxidant molecules in the viral infections

Various intrinsic and extrinsic factors regulate oxidative stress metabolism by balancing reactive oxygen species (ROS) and antioxidant capacity. Antioxidant metabolism is one of the major defense systems in many pathological conditions, including viral infections. PPP plays a vital role in antioxidant defense by regulating different enzymes. Glucose 6-phosphate dehydrogenase (G6PD) is the rate-limiting enzyme in the PPP involved in glutathione metabolism, antioxidant response, and bioenergetic and biosynthetic pathways (19–22).

The cytosolic hexokinase enzyme rapidly converts glucose to glucose-6-phosphate (G6P) to trap the glucose inside the cell by using an ATP molecule. This enzymatic reaction is not just specific to glucose; the hexokinase enzyme phosphorylates all the six-carbon sugars. After the phosphorylation of these sugar phosphates, many cellular conditions, such as hormones, energy status, infections, and all cellular signals, determine the fate of the phosphorylated molecule. It would enter breakdown or synthesis pathways according to the metabolic signals (23–30). G6PD enzyme is found in all cells and regulates the $NADP^+$/NADPH ratio involved in fatty acid, cholesterol, and neurotransmitter biosynthesis. Additionally, NADPH is the essential coenzyme in detoxification reactions *via* regulation of the balance between the oxidized glutathione (GSSG)/reduced glutathione (GSH) by involving in the glutathione reductase (GR)-catalyzed enzymatic and non-enzymatic reactions (31–34).

Furthermore, the reduced form of NADPH is also vital in cytochrome p450 superfamily-catalyzed reactions, such as cytochrome p450 monooxygenases and NADPH-cytochrome P450 reductase responsible for the xenobiotic detoxification, antioxidant-defense system, and cellular redox homeostasis. Since GSH/GSSG ratio is the major biomarker for oxidative stress, preserving the GSH pool is vital to maintaining antioxidant defense in the cell (35). Virus-infected cells also affect the mitochondrial pathways due to the high demand for biosynthetic processes such as the proliferation of virions. Mitochondria is the major source of ROS and enhanced ROS induces mitochondrial dysfunction leading to impaired electron transport chain (ETC) and energy metabolism (36). However, NADPH also protects mitochondria stress *via* a mitochondrial membrane from the effects of ROS *via* NADPH-dependent antioxidant enzymes (37). Human viral diseases, including COVID-19, increase the production of ROS and impair antioxidant mechanisms leading to the impairment of the immune system (38). On the other hand, virus-induced immune response contributes to oxidative stress as well, where oxidative stress increases inflammation, leading to enhanced oxidative stress as a vicious cycle (39). Danger signals trigger the immune system through pattern recognition receptors (PRRs) belonging to the Toll-like (TLRs) and the NOD-like (NLRs) families, where oxidative stress involves in these processes at several levels, including the release of danger molecules, activation by PRRs, and their downstream pathways (40). All viral infections cause redox imbalance in the host; for instance, prototypic poxvirus vaccinia virus (VACV) enhances ROS production at the side of the infection to promote viral replication. Additionally, high levels of ROS are required for VACV infection (41).

Antioxidant administration has been reported to ameliorate virus-induced side effects or to reduce viral replication yield, according to various studies. For instance, N-acetyl-L-cysteine (NAC) inhibits pro-inflammatory mediators in the alveolar cells infected with influenza virus A and B and with the respiratory syncytial virus (RSV) (42). The antioxidant molecule butylated hydroxyanisole (BHA) treatment ameliorates RSV-induced lung inflammation (43). Terameprocol (TMP) is a methylated derivative of nordihydroguaiaretic acid, which is a phenolic antioxidant derived from creosote bush. TMP showed antiviral and anti-inflammatory effects *via* potently inhibiting the growth of both cowpox virus and vaccinia virus *in vitro*, where TMP treatment effectively reduced the infectious virus yield (44). On the other hand, resveratrol altered genome replication and post-replicative gene expression of MXPV (45). Resveratrol (RV) is a natural polyphenol non-flavonoid compound found in grapes, berries, and several other plants. RV is accepted as one of the powerful polyphenols with many positive effects on metabolism and health and

significantly reduces the replication of MPXV (46, 47). No studies reveal the antioxidant's impact on the MPXV infection in humans since monkeypox is an emerging disease worldwide. Thus, the possible effect of the antioxidants on the MPXV infection in humans can be investigated to develop antioxidant-based therapeutic approaches to ease the severe symptoms.

## Conclusion

All viruses depend entirely on the host's cell cellular metabolism, and every virus family has different molecular machinery to enter, using the host cells' energy and metabolic pathways multiplication and all steps in viral infection. However, we need novel studies to increase our knowledge on virus and virus-infected host cell metabolism, especially during the pandemic and the Monkeypox outbreak. Since antioxidants can reduce MPXV replication *in vitro*, according to the studies, antioxidant molecules can be investigated to develop therapeutic approaches or to ease the symptoms of MPXV infection.

## Author contributions

DA and NU are responsible for the conceptualization and writing the manuscript. All authors contributed to the article and approved the submitted version.

## Acknowledgments

The authors gratefully acknowledge the use of the services and facilities of the Koc University Research Center for Translational Medicine (KUTTAM), funded by the Presidency of Turkey, the Presidency of Strategy and Budget.

## Conflict of interest

The authors declare that the research was conducted in the absence of any commercial or financial relationships that could be construed as a potential conflict of interest.

## Publisher's note

All claims expressed in this article are solely those of the authors and do not necessarily represent those of their affiliated organizations, or those of the publisher, the editors and the reviewers. Any product that may be evaluated in this article, or claim that may be made by its manufacturer, is not guaranteed or endorsed by the publisher.

## Author disclaimer

The content is solely the responsibility of the authors and does not necessarily represent the official views of the Presidency of Strategy and Budget.

## References

1. Aydemir D, Ulusu NN. Correspondence: angiotensin-converting enzyme 2 coated nanoparticles containing respiratory masks, chewing gums and nasal filters may be used for protection against COVID-19 infection. *Travel Med Infect Dis.* (2020) 37:101697. doi: 10.1016/j.tmaid.2020.101697

2. Harapan H, Itoh N, Yufika A, Winardi W, Keam S, Te H, et al. Coronavirus disease 2019 (COVID-19): a literature review. *J Infect Public Health.* (2020) 13:667–73. doi: 10.1016/j.jiph.2020.03.019

3. Parker S, Buller RM. A review of experimental and natural infections of animals with monkeypox virus between 1958 and 2012. *Fut Virol.* (2013) 8:129–57. doi: 10.2217/fvl.12.130

4. Alakunle E, Moens U, Nchinda G, Okeke MI. Monkeypox virus in nigeria: infection biology, epidemiology, and evolution. *Viruses.* (2020) 12:1257. doi: 10.3390/v12111257

5. Silva NIO, de Oliveira JS, Kroon EG, Trindade GS, Drumond BP. Here, there, and everywhere: the wide host range and geographic distribution of zoonotic orthopoxviruses. *Viruses.* (2020) 13:43. doi: 10.3390/v13010043

6. WHO. Multi-Country Monkeypox Outbreak: Situation Update. WHO. Available online at: https://www.who.int/emergencies/disease-outbreak-news/item/2022-DON393

7. Cann JA, Jahrling PB, Hensley LE, Wahl-Jensen V. Comparative pathology of smallpox and monkeypox in man and macaques. *J Comp Pathol.* (2013) 148:6–21. doi: 10.1016/j.jcpa.2012.06.007

8. Peter OJ, Kumar S, Kumari N, Oguntolu FA, Oshinubi K, Musa R. Transmission dynamics of monkeypox virus: a mathematical modelling approach. *Model Earth Syst Environ.* (2021) 8:3423–34. doi: 10.1007/s40808-021-01313-2

9. Tortorella D, Gewurz BE, Furman MH, Schust DJ, Ploegh HL. Viral subversion of the immune system. *Annu Rev Immunol.* (2000) 18:861–926. doi: 10.1146/annurev.immunol.18.1.861

10. Hanada S, Pirzadeh M, Carver KY, Deng JC. Respiratory viral infection-induced microbiome alterations and secondary bacterial pneumonia. *Front Immunol.* (2018) 9:2640. doi: 10.3389/fimmu.2018.02640

11. Pratheek BM, Saha S, Maiti PK, Chattopadhyay S, Chattopadhyay S. Immune regulation and evasion of mammalian host cell immunity during viral infection. *Indian J Virol.* (2013) 24:1–15. doi: 10.1007/s13337-013-0130-7

12. de Beeck AO, Caillet-Fauquet P. Viruses and the cell cycle. In: *Progress in Cell Cycle Research.* Boston, MA: Springer US (1997). p. 1–19. doi: 10.1007/978-1-4615-5371-7_1

13. Meylan E, Tschopp J. Toll-Like receptors and RNA helicases: two parallel ways to trigger antiviral responses. *Mol Cell.* (2006) 22:561–9. doi: 10.1016/j.molcel.2006.05.012

14. Morrison AJ. Cancer cell metabolism connects epigenetic modifications to transcriptional regulation. *FEBS J.* (2022) 289:1302–14. doi: 10.1111/febs.16032

15. Gusev E, Zhuravleva Y. Inflammation: a new look at an old problem. *Int J Mol Sci.* (2022) 23:4596. doi: 10.3390/ijms23094596

16. Perła-Kaján J, Jakubowski H. COVID-19 and one-carbon metabolism. *Int J Mol Sci.* (2022) 23:4181. doi: 10.3390/ijms23084181

17. Mayer KA, Stöckl J, Zlabinger GJ, Gualdoni GA. Hijacking the supplies: metabolism as a novel facet of virus-host interaction. *Front Immunol.* (2019) 10:1533. doi: 10.3389/fimmu.2019.01533

18. Icard P, Lincet H, Wu Z, Coquerel A, Forgez P, Alifano M, et al. The key role of Warburg effect in SARS-CoV-2 replication and associated inflammatory response. *Biochimie.* (2021) 180:169–77. doi: 10.1016/j.biochi.2020.11.010

19. Aydemir D, Ulusu NN. Is glucose-6-phosphate dehydrogenase enzyme deficiency a factor in Coronavirus-19 (COVID-19) infections and deaths? *Pathog Glob Health.* (2020) 114:109–10. doi: 10.1080/20477724.2020.1751388

20. Aydemir D, Daglioglu G, Candevir A, Kurtaran B, Bozdogan ST, Inal TC, et al. COVID-19 may enhance risk of thrombosis and hemolysis in the G6PD deficient patients. *Nucleosides Nucleotides Nucleic Acids.* (2021) 40:505–17. doi: 10.1080/15257770.2021.1897457

21. Lee SR, Roh JY, Ryu J, Shin HJ, Hong EJ. Activation of TCA cycle restrains virus-metabolic hijacking and viral replication in mouse hepatitis virus-infected cells. *Cell Biosci.* (2022) 12:7. doi: 10.1186/s13578-021-00740-z

22. Moreno-Altamirano MMB, Kolstoe SE, Sánchez-García FJ. Virus control of cell metabolism for replication and evasion of host immune responses. *Front Cell Infect Microbiol.* (2019) 9:95. doi: 10.3389/fcimb.2019.00095

23. Aydemir D, Öztaşci B, Barlas N, Ulusu NN. Effects of butylparaben on antioxidant enzyme activities and histopathological changes in rat tissues. *Arch Indust Hyg Toxicol.* (2019) 70:315–24. doi: 10.2478/aiht-2019-70-3342

24. Gök M, Ulusu NN, Tarhan N, Tufan C, Ozansoy G, Ari N, et al. Flaxseed protects against diabetes-induced glucotoxicity by modulating pentose phosphate pathway and glutathione-dependent enzyme activities in rats. *J Diet Suppl.* (2016) 13:339–51. doi: 10.3109/19390211.2015.1036188

25. Nóbrega-Pereira S, Fernandez-Marcos PJ, Brioche T, Gomez-Cabrera MC, Salvador-Pascual A, Flores JM, et al. G6PD protects from oxidative damage and improves healthspan in mice. *Nat Commun.* (2016) 7:10894. doi: 10.1038/ncomms10894

26. Bermúdez-Muñoz JM, Celaya AM, Hijazo-Pechero S, Wang J, Serrano M, Varela-Nieto I. *G6PD* overexpression protects from oxidative stress and age-related hearing loss. *Aging Cell.* (2020) 19:e13275. doi: 10.1111/acel.13275

27. Dashty M. A quick look at biochemistry: carbohydrate metabolism. *Clin Biochem.* (2013) 46:1339–52. doi: 10.1016/j.clinbiochem.2013.04.027

28. Judge A, Dodd MS. Metabolism. *Essays Biochem.* (2020) 64:607–47. doi: 10.1042/EBC20190041

29. Tandogan B, Kuruüzüm-Uz A, Sengezer C, Güvenalp Z, Demirezer LÖ, Nuray Ulusu N. *In vitro* effects of rosmarinic acid on glutathione reductase and glucose 6-phosphate dehydrogenase. *Pharm Biol.* (2011) 49:587–94. doi: 10.3109/13880209.2010.533187

30. Ulusu NN. Glucose-6-phosphate dehydrogenase deficiency and Alzheimer's disease: partners in crime? The hypothesis. *Med Hypotheses.* (2015) 85:219–23. doi: 10.1016/j.mehy.2015.05.006

31. Aydemir D, Hashemkhani M, Durmusoglu EG, Acar HY, Ulusu NN. A new substrate for glutathione reductase: glutathione coated Ag2S quantum dots. *Talanta.* (2019) 194:501–6. doi: 10.1016/j.talanta.2018.10.049

32. Ulusu NN, Acan NL, Turan B, Tezcan EF. Inhibition of glutathione reductase by cadmium ion in some rabbit tissues and the protective role of dietary selenium. *Biol Trace Elem Res.* (2003) 91:151–6. doi: 10.1385/BTER:91:2:151

33. Ulusu NN, Tandogan B. Purification and kinetic properties of glutathione reductase from bovine liver. *Mol Cell Biochem.* (2007) 303:45–51. doi: 10.1007/s11010-007-9454-1

34. Aydemir D, Ulusu NN. Comment on the: molecular mechanism of CAT and SOD activity change under MPA-CdTe quantum dots induced oxidative stress in the mouse primary hepatocytes (Spectrochim Acta A Mol Biomol Spectrosc. 2019 Sep 5; 220:117104). *Spectrochim Acta A Mol Biomol Spectrosc.* (2020) 229:117792. doi: 10.1016/j.saa.2019.117792

35. Manikandan P, Nagini S. Cytochrome P450 structure, function and clinical significance: a review. *Curr Drug Targets.* (2018) 19:38–54. doi: 10.2174/1389450118666170125144557

36. Combs JA, Norton EB, Saifudeen ZR, Bentrup KHZ, Katakam P v., Morris CA, et al. Human cytomegalovirus alters host cell mitochondrial function during acute infection. *J Virol.* (2020) 94:e01183–19. doi: 10.1128/JVI.01183-19

37. Tarafdar A, Pula G. The role of NADPH oxidases and oxidative stress in neurodegenerative disorders. *Int J Mol Sci.* (2018) 19:3824. doi: 10.3390/ijms19123824

38. Hejrati A, Nurzadeh M, Roham M. Association of coronavirus pathogencity with the level of antioxidants and immune system. *J Fam Med Prim Care.* (2021) 10:609. doi: 10.4103/jfmpc.jfmpc_1007_20

39. Aydemir D, Ulusu NN. People with blood disorders can be more vulnerable during COVID-19 pandemic: a hypothesis paper. *Transfus Apher Sci.* (2021) 60:103080. doi: 10.1016/j.transci.2021.103080

40. Lugrin J, Rosenblatt-Velin N, Parapanov R, Liaudet L. The role of oxidative stress during inflammatory processes. *Biol Chem.* (2014) 395:203–30. doi: 10.1515/hsz-2013-0241

41. Bidgood SR, Samolej J, Novy K, Collopy A, Albrecht D, Krause M, et al. Poxviruses package viral redox proteins in lateral bodies and modulate the host oxidative response. *PLoS Pathog.* (2022) 18:e1010614. doi: 10.1371/journal.ppat.1010614

42. Mata M, Morcillo E, Gimeno C, Cortijo J. N-acetyl-l-cysteine (NAC) inhibit mucin synthesis and pro-inflammatory mediators in alveolar type II epithelial cells infected with influenza virus A and B and with respiratory syncytial virus (RSV). *Biochem Pharmacol.* (2011) 82:548–55. doi: 10.1016/j.bcp.2011.05.014

43. Castro SM, Guerrero-Plata A, Suarez-Real G, Adegboyega PA, Colasurdo GN, Khan AM, et al. Antioxidant treatment ameliorates respiratory syncytial virus–induced disease and lung inflammation. *Am J Respir Crit Care Med.* (2006) 174:1361–9. doi: 10.1164/rccm.200603-319OC

44. Pollara JJ, Laster SM, Petty ITD. Inhibition of poxvirus growth by terameprocol, a methylated derivative of nordihydroguaiaretic acid. *Antiviral Res.* (2010) 88:287–95. doi: 10.1016/j.antiviral.2010.09.017

45. Abdelkhalek A, Salem MZM, Kordy AM, Salem AZM, Behiry SI. Antiviral, antifungal, and insecticidal activities of eucalyptus bark extract: HPLC analysis of polyphenolic compounds. *Microb Pathog.* (2020) 147:104383. doi: 10.1016/j.micpath.2020.104383

46. Salehi B, Mishra A, Nigam M, Sener B, Kilic M, Sharifi-Rad M, et al. Resveratrol: a double-edged sword in health benefits. *Biomedicines.* (2018) 6:91. doi: 10.3390/biomedicines6030091

47. Cao S, Realegeno S, Pant A, Satheshkumar PS, Yang Z. Suppression of poxvirus replication by resveratrol. *Front Microbiol.* (2017) 8:2196. doi: 10.3389/fmicb.2017.02196

frontiers | Frontiers in Public Health

TYPE Case Report
PUBLISHED 21 October 2022
DOI 10.3389/fpubh.2022.1028920



OPEN ACCESS

EDITED BY
Kun Yin,
Shanghai Jiao Tong University, China

REVIEWED BY
Abdelaziz Ed-Dra,
Zhejiang University, China
Sarunyou Chusri,
Prince of Songkla University, Thailand

*CORRESPONDENCE
Linlin Zhang
abluelemon@163.com
Jian-Xin Zhou
zhoujx.cn@icloud.com

†These authors have contributed equally to this work and share last authorship

SPECIALTY SECTION
This article was submitted to Infectious Diseases – Surveillance, Prevention and Treatment, a section of the journal Frontiers in Public Health

RECEIVED 26 August 2022
ACCEPTED 10 October 2022
PUBLISHED 21 October 2022

CITATION
Tian Y, Xia H, Zhang L and Zhou J-X (2022) Detection of multidrug-resistant *Acinetobacter baumannii* by metagenomic next-generation sequencing in central nervous system infection after neurosurgery: A case report. *Front. Public Health* 10:1028920. doi: 10.3389/fpubh.2022.1028920



# Detection of multidrug-resistant *Acinetobacter baumannii* by metagenomic next-generation sequencing in central nervous system infection after neurosurgery: A case report

Ying Tian[1], Han Xia[2], Linlin Zhang[1,3*†] and Jian-Xin Zhou[1,3,4*†]

[1]Department of Critical Care Medicine, Beijing Tiantan Hospital, Capital Medical University, Beijing, China, [2]Department of Scientific Affairs, Hugo Biotechnologies, Co., Ltd, Beijing, China, [3]Beijing Engineering Research Center of Digital Healthcare for Neurological Diseases, Beijing, China, [4]Beijing Shijitan Hospital, Capital Medical University, Beijing, China

**Background:** Central nervous system (CNS) infection is one of the most serious complications after neurosurgery. Traditional clinical methods are difficult to diagnose the pathogen of intracranial infection. Due to recent advances in genomic approaches, especially sequencing technologies, metagenomic next-generation sequencing (mNGS) has been applied in many research and clinical settings.

**Case presentation:** Here, we report a case of CNS infection with *Acinetobacter baumannii* in a 15-year-old woman, who previously underwent surgery for recurrence of ependymoma in the fourth ventricle. On the eleventh postoperative day, the patient had a high fever and leukocytosis in the cerebrospinal fluid (CSF). mNGS using CSF rapidly and accurately identified the causative pathogen as *A. baumannii* with carbapenem resistance genes *blaOXA-23* and *blaOXA-51*, which were confirmed by subsequent culture and susceptibility tests within 5 days. During the disease, mNGS, culture, and drug susceptibility testing were continued to monitor changes in pathogenic bacteria and adjust medication. At present, there are no case reports on to the use of mNGS for detecting pathogens in postoperative infection with ependymoma and guide medication.

**Conclusion:** mNGS has great advantages in pathogen identification and even pathogen resistance prediction. Multiple mNGS examinations during the course of the disease play an important role in the dynamic monitoring of pathogens.

KEYWORDS

***Acinetobacter baumannii*, central nervous system infections, metagenomic next-generation sequencing, cerebrospinal fluid, resistance genes**

## Background

Central nervous system (CNS) infection is caused by pathogenic microorganisms invading the CNS, manifesting as a class of inflammatory or non-inflammatory diseases with acute or chronic symptoms. The pathogenic microorganisms of CNS infection mainly include viruses, bacteria, fungi, and parasites. CNS infections can be community-acquired or hospital-acquired. Patients with a history of neurosurgery, severe neurotrauma, or indwelling cerebrospinal fluid (CSF) drainage experience a high risk for hospital-acquired CNS infections (1). Despite current advances in clinical diagnosis and treatment, CNS infections still have a high morbidity and mortality, with an estimated 320,000 deaths due to meningitis worldwide in 2016 (2).

Metagenomic next-generation sequencing (mNGS) technology, capable of deciphering millions of DNA and RNA sequences in parallel, has shown promise for detecting pathogens in clinical samples (3). A major advantage of mNGS is the unbiased simultaneous detection of multiple pathogens, its broad identification of known and unexpected pathogens, and the discovery of new organisms (4). The unbiased nature of mNGS aids neurologists in evaluating complex clinical cases with incomplete information. Another advantage of mNGS is that it can provide auxiliary genomic information needed for evolutionary tracking, strain identification, and resistance prediction (5–8). mNGS can quantify or semi-quantify the concentration of organisms in a sample, which is useful for multiple microbial samples or when more than one pathogen is involved in the disease process (9).

*Acinetobacter baumannii* (*A. baumannii*) is a non-enteric gram-negative bacillus characterized by low virulence. As an opportunistic nosocomial pathogen, *A. baumannii* has been one of the most important multidrug-resistant (MDR) microorganisms in hospitals worldwide. This human pathogen causes a variety of infections, of which ventilator-associated pneumonia and bloodstream infections are the most common, with a mortality rate of 35% (10). *A. baumannii* associated CNS infection is common in patients with brain surgery and extra ventricular drainage through a catheter (11). The ability of *A. baumannii* to develop resistance to currently used antibiotics is quite high compared to other bacteria (12). Intrathecal or intracerebroventricular administration of colistin has become an increasingly common approach for the treatment of MDR or extensive drug-resistant (XDR) *A. baumannii* associated CNS infections (13–15).

## Case presentation

Here, we report a 15-year-old female patient who was presented to a local hospital in 2018 due to headache and vomiting (Supplementary Figure 1). Magnetic resonance imaging (MRI) showed an intracranial occupying lesion. Subsequently, she underwent a quadruple ventricular tumor resection in a Beijing hospital. The pathology report of the tumor was WHO grade II ventricular meningioma. The patient recovered well after the operation.

However, in June 2021, the patient developed pulsating headaches with dizziness and vomiting again, and the symptoms gradually worsened. Therefore, she came to Beijing Tiantan Hospital for further treatment. MRI (Figure 1) of the head at our hospital showed bilateral cerebellopontine angle (CPA) and fourth ventricle occupying lesions with a high likelihood of ventricular meningioma recurrence and hydrocephalus. After a series of preoperative examinations, the patient underwent a posterior median craniotomy and artificial dural repair under general anesthesia. Postoperatively, she was kept in the intensive care unit with tracheal intubation and mechanical ventilation to assist breathing, followed by airway care, hormones, dehydration, rehydration, and symptomatic treatment.

Postoperative cranial Computed Tomography (CT) showed a "post-occipital craniotomy" status, enlargement of the ventricular system, and a slight intracerebroventricular hyperintensity (Figures 2A,B). The patient was conscious on the first postoperative day, with a temperature of 39°C, absolute white blood cell (WBC) value of 20.99 × $10^9$/L, and granulocyte (GR) value of 96.9%. Considering that the elevated body temperature and absolute WBC values might be related to postoperative stress, the patient was given physical cooling and anti-infective treatment with cefuroxime (1.5 g, q12h). After symptomatic treatment, the patient's vital signs were stable, the temperature dropped to 36.5°C, and the inflammatory indexes gradually decreased to normal levels on the sixth postoperative day. Therefore, ventilator withdrawal was attempted on the sixth postoperative day, and transoral tracheal intubation was removed, but the patient's blood oxygen level decreased, and her respiratory rhythm was irregular. So, transnasal tracheal intubation with continuous T-tube oxygenation was performed again.

On the eleventh postoperative day, the patient's consciousness was clear, but the body temperature rose to 39.5°C, with the pulse rate of 130 beats/min and WBC of 33.08 × $10^9$/L. Infection of the patient was considered. CSF and blood were drawn from the patient for routine testing and cultures. CSF routine results revealed orange-red, cloudy CSF in appearance with total cells of 3,585/μl, pericytes of 1,085/μl,

Abbreviations: CNS, Central nervous system; mNGS, Metagenomic next-generation sequencing; CSF, Cerebrospinal fluid; *A. baumannii*, *Acinetobacter baumannii*; MDR, Multidrug-resistant; XDR, Extensive drug-resistant; MRI, Magnetic resonance imaging; CPA, Cerebellopontine angle; CT, Computed Tomography; WBC, White blood cell; GR, Granulocyte; ESI-MS, Electro Spray Ionization-Mass Spectroscopy; PCR, Polymerase chain reaction.

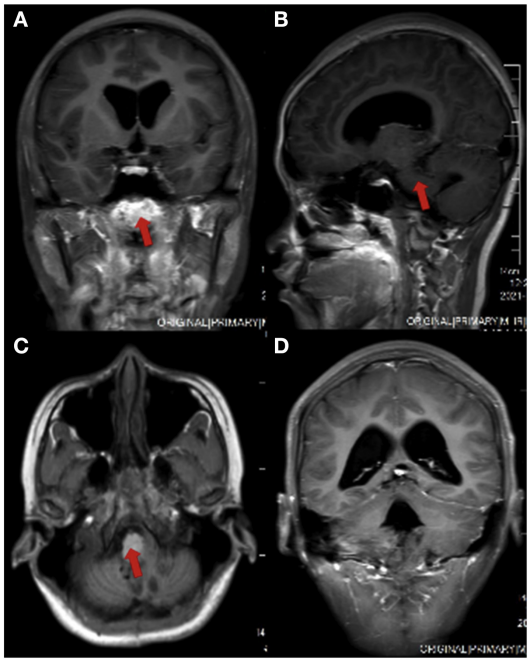


FIGURE 1
Head MRI of the patient before surgery. **(A)** coronal view; **(B)** sagittal section view; **(C)** axial view; **(D)** ventricular enlargement in coronal view

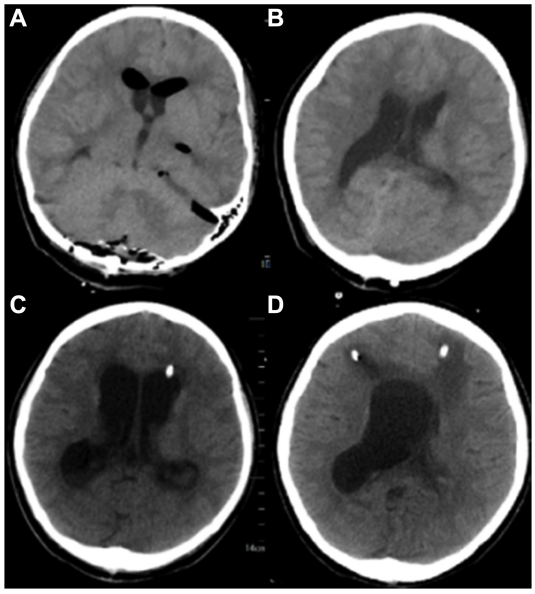


FIGURE 2
Brain CT of the patient in different stages of the disease. **(A, B)**: Postoperative CT of the patient. **(C)** On the 17th postoperative day, the patient's head CT after left ventriculocentesis. **(D)** On the 27th postoperative day, the patient's head CT after left ventriculocentesis.

multinucleated cells ratio of 97.9%, mononuclear cells ratio of 2.1%, glucose of 0.68 mmol/L, protein of 413.6 mg/dL, chloride of 106 mmol/L, and Lactate of 18.6 mmol/L. The presence of intracranial infection in the patient could not be excluded. The patient was given an antibiotic regimen of vancomycin hydrochloride (1000 mg, q12h) and meropenem (2 g IV q8h). On the twelfth day after surgery, the patient's temperature and pulse decreased (37.5°C and 110 beats/min), but the WBC was still high ($64.58 \times 10^9$/L). The patient's vital signs were assessed by a neurosurgeon, and then a lumbar pool tube was placed to drain CSF on the same day, which was immediately sent for mNGS by illumina's NextSeq550DX (Hugobiotech, Beijing, China). On the fourteenth postoperative day, the CSF mNGS results revealed 99,343 specific sequences of *A. baumannii,* with a coverage of 54.3% (Figure 3A). Carbapenem resistance genes *blaOXA-23* (36 reads) and *blaOXA-51* (15 reads) were also detected (Table 1). We discontinued vancomycin and added polymyxin (500,000 units, q12h) following the guidelines for the treatment of *A. baumannii* in The Sanford Guide to antimicrobial therapy. The CSF culture and drug susceptibility test on the sixteenth postoperative day confirmed the mNGS results, indicating intracranial reinfection caused by MDR *A. baumannii* (Table 1). Her blood culture was negative. Therefore, we stopped using meropenem and added tigecycline injection (50 mg, q12h), along with intrathecal polymyxin (50,000 units, q12h). The dynamic monitoring of CSF-related indicators continued in this patient.

On the seventeenth postoperative day, the conditions of the patient improved but were still higher than the normal range, with a body temperature of 37.6°C, WBC of $14.19 \times 10^9$/L, and GR of 86.4%. CSF routine showed pale yellow and clear in appearance, with total cells of 1137/μl, pericytes of 237/μl, multinucleated cells of 85.6%, mononuclear cells of 14.4%, glucose of 1.19 mmol/L, protein of 100.9 mg/dL, chloride of 119 mmol/L, and lactate of 7.8 mmol/L. To further monitor the progression, mNGS and culture using CSF and blood samples were performed again on the seventeenth postoperative day. The second CSF mNGS result still revealed *A. baumannii* with 88,618 specific sequences and 68.32% coverage (Figure 3B). Besides, drug-resistant genes, including *blaOXA-23* (56 reads), *blaOXA-51* (34 reads), *parC* (98 reads), *gyrA* (93 reads), *oprD* (17 reads) and *ampC* beta-lactamase (9 reads), were detected, suggesting they might resist to both fluoroquinolones and carbapenems, consistent with the results of subsequent CSF culture (Table 1). By contrast, mNGS and culture of blood were negative. Therefore, the current treatment regimen was continued.

A left ventricular puncture and drainage procedure was performed due to the progressive hydrocephalus (Figure 2C) on the seventeenth postoperative day. Postoperative monitoring showed the patient's body temperature, blood routine, CSF routine, and biochemistry were slightly better than before. However, right ventricular puncture and drainage was

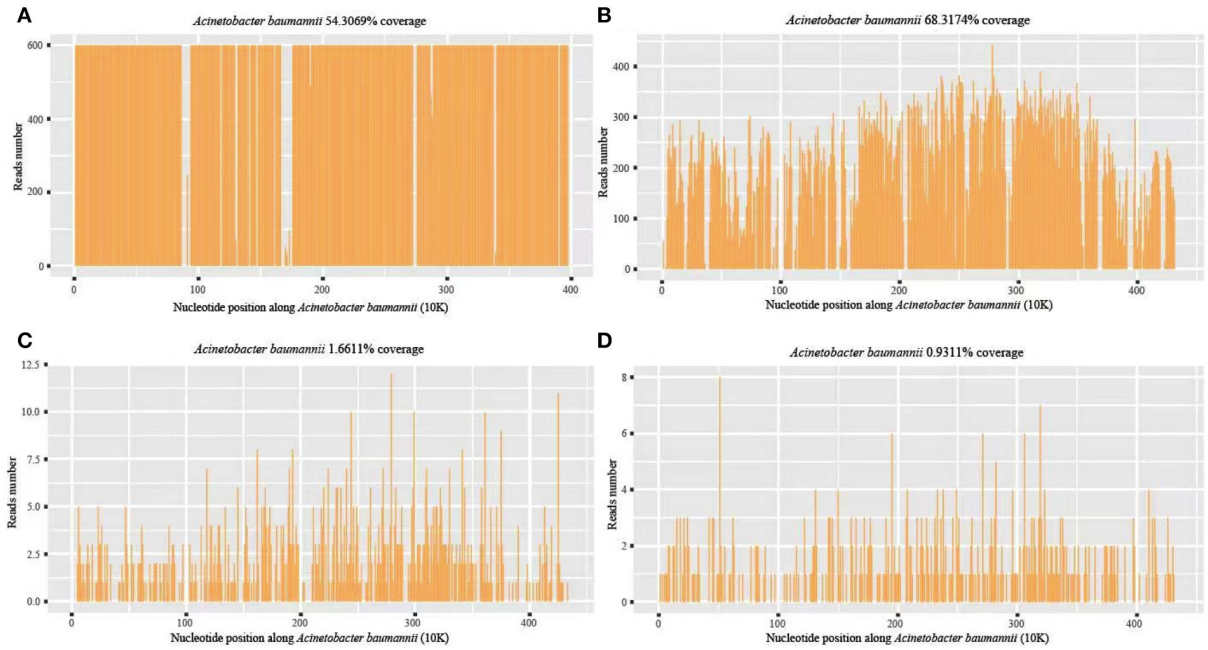


FIGURE 3
*A. baumannii* coverage map of mNGS detection in different periods. **(A)** The first mNGS of CSF: 99,343 specific sequences of *A. baumannii*, with a coverage of 54.3%; **(B)** The second mNGS of CSF: 88,618 specific sequences and 68.32% coverage; **(C, D)** The third mNGS of CSF and blood: 857 (coverage 1.66%) and 446 (coverage 0.93%) specific reads, respectively.

performed on the twenty-seventh postoperative day due to suspected hydrocephalus according to head CT, which showed an enlarged right ventricle (Figure 2D). The patient's temperature was 37.8°C, with WBC of $12.36 \times 10^9$/L and GR of 74%. Right ventricular drainage CSF routine revealed yellowish in appearance, cloudy in nature, total cells of 2231/μl, pericytes of 331/μl, multinucleated cells of 71.3%, mononuclear cells of 28.7%, glucose of 3.07 mmol /L, protein of 363.19 mg/dL, chloride of 115 mmol/L, and lactate of 4.6 mmol/L. The third mNGS using blood and right ventricle CSF was performed on the twenty-seventh postoperative day, revealing 857 (coverage 1.66%) and 446 (coverage 0.93%) specific reads of *A. baumannii*, respectively. Drug-resistant genes (*gyrA* by CSF, and *parC* and *gyrA* by blood, all were 1 sequence) were also detected by both blood and CSF mNGS (Figures 3C,D). The current anti-infective treatment regimen continued.

Two days later, the patient was transferred to a local hospital according to her family's request. She received conservative treatment and was discharged with stable vital signs. The patient was followed up 3 months after discharge with a Glasgow Outcome Scale (GOS) score of 4.

## Discussion and conclusions

Ventricular meningioma is a glioma with ventricular meningeal cell differentiation that can occur in the ventricles and spinal cord. It can be classified into three grades according to 2016 WHO classification criteria, including subventricular and mucinous papillary ventricular meningiomas (grade I), ventricular meningiomas (grade II), and mesenchymal ventricular meningiomas (grade III). Recurrence of primary ventricular meningioma after surgery is common, and younger age, incomplete tumor resection, and high-grade or mucinous papillary ventricular meningioma are the risk factors (16). Surgery for tumors presenting in the fourth ventricle is more challenging, with a probability of postoperative infection of approximately 4.5% (17). The current case is a WHO grade II ventricular meningioma in the fourth ventricle, which recurred 3 years after total tumor resection. There were no metastases elsewhere, but respiratory and circulatory failure and infection after reoperation.

*A. baumannii* is a Gram-negative ESKAPE microorganism with MDR due to widespread antibiotic abuse and mismanagement (18). Immunocompromised and severely ill hosts are susceptible to invasive infections by *A. baumannii*. Carbapenems were once considered the drugs of choice for the empirical treatment of *A. baumannii* infections. However, previous studies have shown that most MDR *A. baumannii* strains (98.1%) were resistant to imipenem, and about 50% were resistant to meropenem, amikacin, and gentamicin. Potent carbapenemase genes were detected in almost all strains, such as *blaOXA-51* (89.3%) and *blaOXA-23* (68.9%) (19). In this case, the patient was in a postoperative state

10.3389/fpubh.2022.1028920

TABLE 1 Drug resistance results of culture and mNGS.

| | CSF culture (twelfth postoperative day) | | CSF culture (seventeenth postoperative day) | |
|---|---|---|---|---|
| | **Sensitivity** | **MIC** | **Sensitivity** | **MIC** |
| Piperacillin-tazobactam | R | ≥128.0 | R | ≥128.0 |
| Ceftazidime | R | ≥64.0 | R | ≥64.0 |
| Cefoperazone sulbactam | S | 16.0 | S | 16.0 |
| Cefepime | R | ≥32.0 | R | ≥32.0 |
| Imipenem | R | ≥16.0 | R | ≥16.0 |
| Meropenem | R | ≥16.0 | R | ≥16.0 |
| Tobramycin | R | ≥16.0 | R | ≥16.0 |
| Ciprofloxacin | R | ≥4.0 | R | ≥4.0 |
| Levofloxacin | R | ≥8.0 | R | ≥8.0 |
| Doxycycline | R | ≥16.0 | R | ≥16.0 |
| Minocycline | S | 4.0 | S | 4.0 |
| Tigecycline | S | 1.0 | S | 1.0 |
| Polymyxin | S | ≤0.5 | S | ≤0.5 |
| Compound Sulfonamide | S | ≤20.0 | S | ≤20.0 |
| | CSF mNGS (twelfth postoperative day) | CSF mNGS (seventeenth postoperative day) | CSF mNGS (twenty-seventh postoperative day) | Blood mNGS (twenty-seventh postoperative day) |
| blaOXA-23 | 36 reads | 56 reads | - | - |
| blaOXA-51 | 15 reads | 34 reads | - | - |
| parC | 101 reads | 98 reads | 1 reads | 1 reads |
| gyrA | 108 reads | 93 reads | - | 1 reads |
| OprD | 13 reads | 17 reads | - | - |
| ampC beta-lactamase | 23 reads | 9 reads | - | - |

for ventricular meningioma and was vulnerable to XDR *A. baumannii*. The carbapenem resistance gene of *A. baumannii* was detected in the first and second CSF mNGS, suggesting that the strain may be resistant to imipenem and meropenem. And the second and third CSF mNGS also detected the gene encoding DNA gyrase (*gyrA*) and the gene encoding topoisomerase IV (*parC*) at the target site of fluoroquinolone drug action, and mutations at different sites, suggesting that the strain may escape from fluoroquinolones (20). However, these mutations have not yet been reported in the literature on whether they are related to fluoroquinolone resistance. Therefore, we did not adjust the antibiotic treatment plan according to the resistance genes detected by mNGS.

An accurate etiologic diagnosis is important for the treatment of postoperative complications, including serious infections and infections caused by drug-resistant organisms. Raper et al. reported a rare case of herpes simplex virus encephalitis after ventriculotomy, the rapid detection of HSV infection by mNGS played a key role in the timely antiviral treatment of the patient (21). Farrell et al. reported a case of *Enterococcus faecalis* infection detected by polymerase chain reaction (PCR) combined with Electro Spray Ionization-Mass Spectroscopy (ESI-MS) in CSF from a patient with concurrent bacterial meningitis after ventriculoma resection, and emphasized the importance of accurate pathogenic diagnosis and dynamic monitoring of ongoing infection in postoperative CNS infections (22). In this case, the patient had a significantly elevated CSF leukocyte 11 days after ventricular meningioma surgery. We took CSF for culture and mNGS testing at the same time. The mNGS results reported MDR *A. baumannii* 2 days later, while the CSF culture results returned MDR *A. baumannii* 5 days later. Interestingly, the drug resistance genes by mNGS and the phenotypes of the drug susceptibility test were essentially identical. This demonstrates the ability of mNGS to detect pathogens and predict drug resistance factors rapidly and accurately. The progressive decrease of specific reads of the pathogen detected by mNGS during the course also indirectly indicated the effectiveness of adjusted anti-infective therapy. It is worth noting that the third CSF cultures were negative compared to mNGS, possibly since cultures are more susceptible to antibiotic use.

Interestingly, the third blood mNGS on the twenty-seventh postoperative day was positive for *A. baumannii*, which was

negative in previous blood mNGS detections. One possible reason is that the blood-brain barrier was damaged due to the patient's multiple open cranial surgeries or other factors, such as inflammation and tumors (18). Pathogens enter the blood through the damaged blood-brain barrier. However, the patient had no obvious signs of systemic infection by *A. baumannii*. It may be because the antibiotics given to the patient also inhibited the growth of *A. baumannii* in the blood. Another possible reason is that the nucleic acids of the pathogen entered the blood *via* the damaged blood-brain barrier. Nevertheless, this case reminds us real-time monitoring of blood pathogens in patients after craniotomy is necessary.

Intravenous and intrathecal polymyxin and tigecycline are often the choices of MDR/XDR *A. baumannii* CNS infection (23). Maintaining patency of CSF drainage and ventricular lavage is also crucial in the treatment of *A. baumannii* intracranial infections. Intrathecal injection of drugs combined with continuous drainage of the lumbar pool is more clinically effective than treatment with intravenous antibiotics only (24). In this case, the patient was treated with both intrathecal polymyxin and tigecycline injections immediately after the pathogenetic evidence was clarified.

In conclusion, infection remains one of the most important complications after ventricular meningioma surgery, seriously affecting the patient's prognosis. mNGS allows early and accurate identification of the responsible causative agent and prediction of drug resistance or virulence factors. In addition, the application of multiple mNGS tests during the course can monitor the state of illness and assess the treatment efficacy.

## Data availability statement

The datasets for this article are not publicly available due to concerns regarding participant/patient anonymity. Requests to access the datasets should be directed to the corresponding author.

## Ethics statement

The studies involving human participants were reviewed and approved by IRB of Beijing Tiantan Hospital, Capital Medical University. Written informed consent to participate in this study was provided by the participants' legal guardian/next of kin. Written informed consent was obtained from the minor(s)' legal guardian/next of kin for the publication of any potentially identifiable images or data included in this article.

## Author contributions

YT was involved in the collection of data. YT, LZ, and J-XZ were involved in drafting and editing the manuscript. HX performed the mNGS. All authors have read and approved the manuscript.

## Funding

This work was supported by the Beijing Municipal Commission of Science and Technology (Grant No. Z201100005520050). Funders had no role in this case, data collection and analysis, publication decisions, or manuscript preparation.

## Acknowledgments

We acknowledge all healthcare workers involved in the diagnosis and treatment of the patient.

## Conflict of interest

Author HX was employed by Hugobiotech Co., Ltd.

The remaining authors declare that the research was conducted in the absence of any commercial or financial relationships that could be construed as a potential conflict of interest.

## Publisher's note



## Supplementary material

The Supplementary Material for this article can be found online at: https://www.frontiersin.org/articles/10.3389/fpubh.2022.1028920/full#supplementary-material

# References


1. Brouwer MC, van de Beek D. Management of bacterial central nervous system infections. *Handb Clin Neurol.* (2017) 140:349–64. doi: 10.1016/B978-0-444-63600-3.00019-2

2. Zhang Y, Cui P, Zhang HC, Wu HL, Ye MZ, Zhu YM, et al. Clinical application and evaluation of metagenomic next-generation sequencing in suspected adult central nervous system infection. *J Transl Med.* (2020) 18:199. doi: 10.1186/s12967-020-02360-6

3. Goldberg B, Sichtig H, Geyer C, Ledeboer N, Weinstock GM. Making the leap from research laboratory to clinic: challenges and opportunities for next-generation sequencing in infectious disease diagnostics. *MBio.* (2015) 6:e01888–01815. doi: 10.1128/mBio.01888-15

4. Chiu CY. Viral pathogen discovery. *Curr Opin Microbiol.* (2013) 16:468–78. doi: 10.1016/j.mib.2013.05.001

5. Gire SK, Goba A, Andersen KG, Sealfon RS, Park DJ, Kanneh L, et al. Genomic surveillance elucidates Ebola virus origin and transmission during the 2014 outbreak. *Science.* (2014) 345:1369–72. doi: 10.1126/science.1259657

6. Salipante SJ, SenGupta DJ, Cummings LA, Land TA, Hoogestraat DR, Cookson BT. Application of whole-genome sequencing for bacterial strain typing in molecular epidemiology. *J Clin Microbiol.* (2015) 53:1072–9. doi: 10.1128/JCM.03385-14

7. Deurenberg RH, Bathoorn E, Chlebowicz MA, Couto N, Ferdous M, Garcia-Cobos S, et al. Application of next generation sequencing in clinical microbiology and infection prevention. *J Biotechnol.* (2017) 243:16–24. doi: 10.1016/j.jbiotec.2016.12.022

8. Sahoo MK, Lefterova MI, Yamamoto F, Waggoner JJ, Chou S, Holmes SP, et al. Detection of cytomegalovirus drug resistance mutations by next-generation sequencing. *J Clin Microbiol.* (2013) 51:3700–10. doi: 10.1128/JCM.01605-13

9. Salipante SJ, Hoogestraat DR, Abbott AN, SenGupta DJ, Cummings LA, Butler-Wu SM, et al. Coinfection of Fusobacterium nucleatum and Actinomyces israelii in mastoiditis diagnosed by next-generation DNA sequencing. *J Clin Microbiol.* (2014) 52:1789–92. doi: 10.1128/JCM.03133-13

10. Ceylan B, Arslan F, Sipahi OR, Sunbul M, Ormen B, Hakyemez IN, et al. Variables determining mortality in patients with *Acinetobacter baumannii* meningitis/ventriculitis treated with intrathecal colistin. *Clin Neurol Neurosurg.* (2017) 153:43–9. doi: 10.1016/j.clineuro.2016.12.006

11. Navon-Venezia S, Ben-Ami R, Carmeli Y. Update on Pseudomonas aeruginosa and *Acinetobacter baumannii* infections in the healthcare setting. *Curr Opin Infect Dis.* (2005) 18:306–13. doi: 10.1097/01.qco.0000171920.44809.f0

12. Fournier PE, Vallenet D, Barbe V, Audic S, Ogata H, Poirel L, et al. Comparative genomics of multidrug resistance in Acinetobacter baumannii. *PLoS Genet.* (2006) 2:e7. doi: 10.1371/journal.pgen.0020007

13. Antunes LC, Visca P, Towner KJ. *Acinetobacter baumannii*: evolution of a global pathogen. *Pathog Dis.* (2014) 71:292–301. doi: 10.1111/2049-632X.12125

14. Dersch R, Robinson E, Beume L, Rauer S, Niesen WD. Full remission in a patient with catheter-associated ventriculitis due to *Acinetobacter baumannii* treated with intrathecal and intravenous colistin besides coinfections with other multidrug-resistant bacteria. *Neurol Sci.* (2015) 36:633–4. doi: 10.1007/s10072-014-2031-y

15. Fotakopoulos G, Makris D, Chatzi M, Tsimitrea E, Zakynthinos E, Fountas K. Outcomes in meningitis/ventriculitis treated with intravenous or intraventricular plus intravenous colistin. *Acta Neurochir (Wien).* (2016) 158:603–10; discussion 610. doi: 10.1007/s00701-016-2702-y

16. Witt H, Mack SC, Ryzhova M, Bender S, Sill M, Isserlin R, et al. Delineation of two clinically and molecularly distinct subgroups of posterior fossa ependymoma. *Cancer Cell.* (2011) 20:143–57. doi: 10.1016/j.ccr.2011.07.007

17. Winkler EA, Birk H, Safaee M, Yue JK, Burke JF, Viner JA, et al. Surgical resection of fourth ventricular ependymomas: case series and technical nuances. *J Neurooncol.* (2016) 130:341–9. doi: 10.1007/s11060-016-2198-6

18. Avci FG, Tastekil I, Jaisi A, Ozbek Sarica P, Sariyar Akbulut B. A review on the mechanistic details of OXA enzymes of ESKAPE pathogens. *Pathog Glob Health.* (2022) 1–16. doi: 10.1080/20477724.2022.2088496

19. AlAmri AM, AlQurayan AM, Sebastian T, AlNimr AM. Molecular Surveillance of Multidrug-Resistant *Acinetobacter baumannii*. *Curr Microbiol.* (2020) 77:335–42. doi: 10.1007/s00284-019-01836-z

20. Kyriakidis I, Vasileiou E, Pana ZD, Tragiannidis A. *Acinetobacter baumannii* Antibiotic Resistance Mechanisms. *Pathogens.* (2021) 10:373. doi: 10.3390/pathogens10030373

21. Raper DM, Wong A, McCormick PC, Lewis LD. Herpes simplex encephalitis following spinal ependymoma resection: case report and literature review. *J Neurooncol.* (2011) 103:771–6. doi: 10.1007/s11060-010-0438-8

22. Farrell JJ, Tsung AJ, Flier L, Martinez DL, Beam SB, Chen C, et al. PCR and electrospray ionization mass spectrometry for detection of persistent enterococcus faecalis in cerebrospinal fluid following treatment of postoperative ventriculitis. *J Clin Microbiol.* (2013) 51:3464–6. doi: 10.1128/JCM.01343-13

23. Wu Y, Chen K, Zhao J, Wang Q, Zhou J. Intraventricular administration of tigecycline for the treatment of multidrug-resistant bacterial meningitis after craniotomy: a case report. *J Chemother.* (2018) 30:49–52. doi: 10.1080/1120009X.2017.1338846

24. Wang J, Liu H, Zheng K, Zhang S, Dong W. Clinical effect of intrathecal injection of medicine combined with continuous lumbar cistern drainage on intracranial infection after intracranial tumor surgery. *Pak J Pharm Sci.* (2021) 34:65–7

frontiers | Frontiers in Public Health

TYPE Original Research
PUBLISHED 21 October 2022
DOI 10.3389/fpubh.2022.1010172



OPEN ACCESS

EDITED BY
Gisely Melo,
Fundação de Medicina Tropical Doutor Heitor Vieira Dourado (FMT-HVD), Brazil

REVIEWED BY
Laila Rowena Albuquerque Barbosa,
Heitor Vieira Dourado Tropical Medicine Foundation, Brazil
Ari Winasti Satyagraha,
Eijkman Institute for Molecular Biology, Indonesia

*CORRESPONDENCE
Xinyu Feng
fengxinyu2013@163.com
Guangze Wang
wangguangze63@126.com
Dingwei Sun
sdw_bmjc@163.com

†These authors have contributed equally to this work

SPECIALTY SECTION
This article was submitted to Infectious Diseases–Surveillance, Prevention and Treatment, a section of the journal Frontiers in Public Health

RECEIVED 02 August 2022
ACCEPTED 30 September 2022
PUBLISHED 21 October 2022

CITATION
Zeng W, Liu N, Li Y, Gao A, Yuan M, Ma R, Jiang N, Sun D, Wang G and Feng X (2022) Prevalence of glucose-6-phosphate dehydrogenase deficiency (G6PDd) and clinical implication for safe use of primaquine in malaria-endemic areas of Hainan Province, China.
*Front. Public Health* 10:1010172.
doi: 10.3389/fpubh.2022.1010172



# Prevalence of glucose-6-phosphate dehydrogenase deficiency (G6PDd) and clinical implication for safe use of primaquine in malaria-endemic areas of Hainan Province, China

Wen Zeng[1†], Ning Liu[2†], Yuchun Li[1†], Ai Gao[3†], Mengyi Yuan[3†], Rui Ma[3], Na Jiang[3], Dingwei Sun[1*], Guangze Wang[1*] and Xinyu Feng[4,5*]

[1]Department of Tropic Disease, Hainan Center for Disease Control and Prevention, Haikou, China, [2]Department of Gastrointestinal Surgery, Hainan General Hospital, Hainan Affiliated Hospital of Hainan Medical University, Haikou, China, [3]Department of Biology, College of Life Sciences, Inner Mongolia University, Hohhot, China, [4]National Institute of Parasitic Diseases, Chinese Center for Disease Control and Prevention (Chinese Center for Tropical Diseases Research), NHC Key Laboratory of Parasite and Vector Biology, WHO Collaborating Centre for Tropical Diseases, National Center for International Research on Tropical Diseases, Joint Research Laboratory of Genetics and Ecology on Parasite-Host Interaction, Fudan University, Shanghai, China, [5]School of Global Health, Chinese Center for Tropical Diseases Research, Shanghai Jiao Tong University School of Medicine, One Health Center, Shanghai Jiao Tong University-The University of Edinburgh, Shanghai, China

Primaquine, the only licensed antimalarial drug for eradication of *Plasmodium vivax* and *Plasmodium ovale* malaria, may cause acute hemolytic anemia in individuals with glucose-6-phosphate dehydrogenase deficiency (G6PDd) during treatment. The different prevalence and distribution patterns of G6PDd in Hainan, the ancient malaria-endemic area, are unclear. This study included 5,622 suspected malaria patients between 2009 and 2011 in 11 counties of Hainan. Glucose-6-phosphate dehydrogenase deficiency prevalence was determined using the fluorescent spot test (FST) and malaria patients was confirmed by a positive light microscopy. The G6PDd prevalence for different ethnic groups, genders, and counties were calculated and compared using $\chi^2$-test. Spatial cluster and Spearman rank correlation of G6PDd prevalence and malaria incidence were analyzed. The overall G6PDd prevalence of study population was 7.45%. The G6PDd prevalence of males, Li ethnic minority, and malaria patients was significantly higher than that of females, Han ethnic majority, and non-malarial patients ($p < 0.01$), respectively. The spatial cluster of G6PDd and malaria located in south-western and central-southern Hainan, respectively, with no significant correlation. The study provides essential information on G6PDd prevalence in ancient malaria-endemic areas of Hainan

Province. We also highlight the need for a better understanding of the mechanisms underlying the relationship between G6PDd prevalence and malaria incidence. These findings provide a reference for the safety of the primaquine-based intervention, even after malaria elimination.

KEYWORDS

**G6PD, primaquine, *vivax* malaria, spatial cluster, prevalence**

## Introduction

The malaria elimination program started in 2010 (1) and succeeded in 2021 in China. Throughout the journey, Hainan Province, the most southern province of China and the most seriously affected malaria-endemic area was always the hot spot for the campaign. Since 2010, no falciparum malaria cases have been reported in the area. However, *Plasmodium vivax* malaria sustained endemic for another 2 years, presenting a critical barrier to elimination in Hainan Province and other countries planning to eliminate malaria. Notably, *P. vivax* malaria often occurs with low parasitemia and can be missed under routine surveillance. Furthermore, it has gradually become a consensus that *P. vivax* malaria can be as debilitating as falciparum malaria. Recently, imported *P. vivax* malaria has been documented and accounted for more than 80% of reported malaria cases. Therefore, additional measures are still needed to extend the comprehensive response to *P. vivax* malaria control by reducing *P. vivax* transmission/relapse, and meanwhile, protecting the most vulnerable populations.

There is increasing use of chemopreventive agents for the eradication of malaria toward malaria-free status. In China, primaquine is the only drug approved by the State Food and Drug Administration (SFDA) of China to prevent malaria relapse. It is one of the critical components of the nationwide malaria elimination program (2). Therefore, a massive primaquine administration was expected and applied in malaria-endemic regions. However, primaquine may cause acute hemolytic anemia in individuals with glucose-6-phosphate dehydrogenase deficiency (G6PDd), a common congenital X-linked hereditary enzyme deficiency widespread across most malaria-endemic countries (3). In order to improve the compliance rate of primaquine for the radical cure of malaria, it is urgent to understand better the distribution pattern of G6PDd in main malaria-endemic areas in China.

Previous studies have revealed a relatively low incidence of G6PDd, about 3–7% in China (3); however, there may still be a large number of people with G6PDd in the country, considering its large population. In addition, G6PDd prevalence varied significantly among ethnic groups (4–6). For example, the G6PDd prevalence of the ethnic minorities is different from that of the Han ethnic majority in Yunnan Province, one of the ancient malaria-endemic areas in China (7, 8). Hainan Province still has a multi-ethnic population, but the G6PDd prevalence of its various ethnic minorities remains unclear.

Generally speaking, G6PDd confers a protective effect against both falciparum malaria and vivax malaria episodes (9), lending to a presumptive consensus that wide geographical distribution of G6PDd in human populations is derived by the epidemic (9). Interestingly, there is ecological overlap between G6PDd and malaria endemic areas, as shown in Africa, southern Europe, the middle east, southeast Asia, and the central and southern Pacific islands (10, 11). Therefore, information on the prevalence of G6PDd is critical to optimize the malaria elimination strategy, especially for radical treatment of *P. vivax* malaria using primaquine. It is necessary to determine the G6PDd distribution patterns in malaria-endemic areas and further analyze the unveiled relationship between malaria incidence and the G6PDd prevalence.

The present study presented the most recently updated information on G6PDd in Hainan, China. We also analyzed and compared the G6PDd distribution patterns among different counties, ethnic groups, and genders and explored the relationship between the spatial distribution of malaria cases and G6PDd status in the minority area. These results would be beneficial for optimizing existing tools against *P. vivax*, and deploying more effective measures for protecting the most vulnerable populations.

## Materials and methods

### Study area

The study areas were located on the main island of Hainan Province, 18°10′-20°10′ north latitude and 108°37′-111°03′ east longitude, in southern China. This region has a land area of 33,900 $km^2$ with a population of 8.26 million. There are multi-ethnic populations, including Li, Miao, and Hui ethnic minorities living together in the central and southern mountainous areas. The Han ethnic majority distributes throughout the island. The Li ethnic minority is one of the earliest inhabitants and the most populous ethnic minority in Hainan.

## Ethics statement

This clinical study protocol was reviewed and approved by the Ethics Review Committee of the Hainan Center for Disease Control and Prevention. Each participant provided informed consent (in Chinese) before participating in this study. In most cases, the participants provided their written informed consent. The consent was verbal for patients who could not read or write standard Chinese. In these cases, the research nurse documented the participant's consent in writing, including the contents and methods of information provided to the participant and the date and time of the verbal consent, which was then witnessed and signed by another nurse who was not in the research team. The informed consent record, either written or verbal, was kept in the participant's hospital chart. The Ethics mentioned above Committee reviewed and approved this consent procedure.

## Participants and data collection

We selected 11 malaria-endemic counties (Baisha, Baoting, Changjiang, Dongfang, Ledong, Lingshui, Qionghai, Qiongzhong, Sanya, Wanning, and Wuzhishan) in Hainan according to the reported malaria incidence in the previous 5 years (2004–2009). We selected one comprehensive county-level hospital in each county as the investigation sites. Patients with malaria-like symptoms such as fever, shivering, and perspiring seeking medical service in these 11 hospitals between January 1, 2009 and December 31, 2011 were enrolled. Each participant's demographic and clinical information was collected, including the ethnic group, sex, age, location of residence, clinical symptom, and the routine test.

## Procedure for detection of G6PDd

The peripheral blood sample (5 ml) was obtained from each participant by forearm venipuncture and tested for G6PDd using the fluorescent spot test (FST) method as previously described (12, 13). Briefly, 10 μl of blood sample was added to 100 μl test reagents and incubated at 37°C for 30 min; a spot was made on ordinary filter paper and was permitted to dry; the spots were then visualized under an ultraviolet (UV) light. Spots that showed fluorescence were classified as normal G6PD, and spots that failed to show fluorescence were classified as G6PDd. After being used for G6PDd test, microscopy test, and blood routine test, the remaining blood samples were stored in Hainan CDC for further confirmation assays. The microscopy examined all patients to confirm or rule out a malaria diagnosis.

## G6PDd prevalence and spatial distribution analysis

The G6PDd prevalence for various groups, including different ethnic groups, genders, counties, malaria patients, and patients without malaria, were calculated and compared using the $\chi^2$-test. In order to avoid the confounding effects caused by ethnicity in different counties, we calculated the ethnic-standardized G6PD prevalence. The ethnic-standardized G6PDd prevalence of the study area and each county were calculated and compared with their corresponding general G6PDd prevalence using the $\chi^2$-test. The malaria incidence of the study participants in each county were calculated.

The G6PDd prevalence of each county were first categorized into three levels, i.e., 0–5.00%, 5.01–10.00%, and 10.01–15.00%, respectively, and then geo-coded and matched to the corresponding polygon on a digital map of Hainan, which was marked with different colors to represent the different levels of the G6PDd prevalence. The spatial autocorrelations of the G6PDd prevalence and ethnic-standardized G6PDd prevalence across the study area was estimated using Moran's I statistic program to determine whether G6PDd was randomly distributed among the counties. The spatial analyses were conducted using the Spatial Analyst Model with ArcGIS 9.2 software (ArcGIS 9.2, Environmental Systems Research Institute, Redlands, CA, USA).

## Cluster analysis

The spatial cluster analyses of malaria incidence and G6PDd prevalence were conducted between 2009 and 2011. In order to detect and compare the counties with a high risk of malaria and G6PDd at different spatial scales, maximum spatial cluster sizes of 20%, 30%, and 40% of the entire population were specified for both malaria incidence and G6PDd prevalence. The cluster window with the highest likelihood ratio (LLR) was the most likely cluster to have the highest risk of malaria or G6PDd. The cluster window with the next to maximum LLR was the secondary likely cluster with the second-highest risk of malaria or G6PDd. The relative risks of malaria or G6PDd within and outside these windows were calculated to evaluate the degree of risk. The cluster analysis was performed using SatScan 7.0.3 (SatScan 7.0.3, Information Management Services Inc., Boston, MA, USA). Clustering was performed using purely spatial and a Poisson model was used during the analysis.

## Correlation analysis

Spearman rank correlation analysis was conducted to detect the relationship between G6PDd prevalence and malaria incidence in the study areas. The index $r > 0$ denoted a positive

TABLE 1 The G6PDd prevalence in different groups in Hainan, China, 2009–2011.

| Variable | Subgroup (*N*) | G6PDd (%) | Prevalence (%) | $\chi^2$ | *P* |
|---|---|---|---|---|---|
| Ethnicity | Li ($N = 3,009$) | 268 | 8.91 | 19.84 | <0.01 |
| | Han ($N = 2,613$) | 151 | 5.87 | | |
| Gender | Male ($N = 2,178$) | 262 | 12.03 | 107.96 | <0.01 |
| | Female ($N = 3,444$) | 157 | 4.65 | | |
| Malaria status | Malaria ($N = 670$) | 83 | 12.39 | 26.86 | <0.01 |
| | Non-malaria ($N = 4,952$) | 336 | 6.79 | | |

correlation, while $r < 0$ denoted a negative correlation. The correlation was considered significant when $P < 0.05$.

# Results

## Characteristics of the participants

Among the 5,622 participants in the present study, 3,444 were Han Chinese and 2,178 were Li Chinese, including 3,009 males and 2,613 females, and 670 were malaria patients (including 667 *P. vivax malaria* patients and 3 *Plasmodium falciparum* malaria patients) and 4,952 were patients without malaria (Supplementary Table S1). The age of the 5,622 participants ranged from 19 to 72 years old (median = 39 years, IQR 26–52 years). There were 634 (94.63%) malaria patients with a body temperature higher than 37.5°C, 571 (85.22%) with shivering, 595 (88.81%) with perspire, 206 (30.75%) with abdominal pain, 113 (16.87%) with nausea, and 105 (15.67%) with vomiting. The median WBC, RBC, and hemoglobin of the 670 malaria patients were $8.2 \times 10^9$/L ($4.6–11.3 \times 10^9$/L), $4.3 \times 10^{12}$/L ($3.5–5.2 \times 10^{12}$/L), and 121 g/L (102–139 g/L).

## G6PDd prevalence

The overall G6PDd prevalence was 7.45% (419/5,622). The G6PDd prevalence of males was significantly higher than that of females (8.91% vs. 5.78%; $\chi^2 = 19.84$, $P < 0.01$, Table 1). The G6PDd prevalence of the Li ethnic minority was significantly higher than that of the Han ethnic majority (12.03% vs. 4.56%; $\chi^2 = 107.96$, $P < 0.01$, Table 1). The G6PDd prevalence of malaria patients was significantly higher than that of patients without malaria (12.39% vs. 6.79%; $\chi^2 = 26.86$, $P < 0.01$, Table 1). The G6PDd prevalence of male patients was significantly higher than that of patients without malaria (12.88% vs. 8.36%; $\chi^2 = 8.07$, $P < 0.01$). After a careful comparative analysis of the subgroups, Li ethnic group, male gender, and G6PDd were at risk of malaria. There was no significant difference between the G6PDd prevalence and the ethnic-standardized G6PDd prevalence of the entire study population (7.45% vs. 8.29%; $\chi^2 = 3.55$, $P > 0.05$).

## Spatial distribution pattern of G6PDd

The G6PDd prevalence varied from 2.96% in Qionghai County to 14.48% in Dongfang County, and the ethnic-standardized G6PDd prevalence varied from 2.11% in Wuzhishan County to 14.82% in Dongfang County (Table 2). There were significant differences in both G6PDd prevalence and ethnic-standardized G6PDd prevalence among the 11 counties (Table 2, $\chi^2 = 121.16$, $P < 0.01$; $\chi^2 = 110.65$, $P < 0.01$). In addition, significantly positive spatial autocorrelations of G6PDd prevalence and ethnic-standardized G6PDd prevalence across the 11 counties [Moran's I = 0.49, Z (I) = 2.62, $P < 0.05$; Moran's I = 0.53, Z (I) = 2.71, $P < 0.05$] was observed. However, there was no significant difference between the G6PDd prevalence and the ethnic-standardized G6PDd prevalence in each county. The spatial distribution pattern of the G6PDd prevalence of the 11 counties was heterogeneous (Figure 1).

## Spatial clusters of G6PDd prevalence and malaria incidence

We limit the maximum spatial cluster size to 20% of the population size at risk, three counties constituted the most likely cluster of G6PDd (Baisha Changjiang and Dongfang) and one county constituted the secondary likely cluster (Lingshui) (Figure 1A). When the maximum spatial cluster size was 20% of the population size, four counties constituted the most likely cluster of malaria (Lingshui, Qiongzhong, Wuzhishan, and Baoting), and one county constituted the secondary likely cluster (Baisha) (Figure 1B). These results further indicated that the distribution patterns of G6PDd and malaria were significantly different among the studied counties.

## Correlation between G6PDd prevalence and malaria incidence

Correlation analysis indicated no significant correlation between the G6PDd prevalence and malaria incidence during 2009–2011 in the study areas ($r = 0.46$, $P > 0.05$).

10.3389/fpubh.2022.1010172

TABLE 2 The G6PDd prevalence, ethnic-adjusted G6PDd prevalence, and malaria incidence in 11 counties in Hainan, China, 2009–2011.

| County | Number of study participants | Number of malaria cases | Malaria incidence (%) | Number of G6PDd cases | G6PDd prevalence (%) | $\chi^2$ | *P* | Ethnic-adjusted G6PDd prevalence (%) | $\chi^2$ | *P* | $\chi^{2*}$ | *P** |
|---|---|---|---|---|---|---|---|---|---|---|---|---|
| Baisha | 423 | 102 | 24.11 | 60 | 14.18 | 121.16 | <0.01 | 11.33 | 110.65 | <0.01 | 1.53 | 0.22 |
| Baoting | 469 | 126 | 26.87 | 29 | 6.18 | | | 5.03 | | | 0.50 | 0.48 |
| Changjiang | 566 | 58 | 10.25 | 43 | 7.60 | | | 8.94 | | | 0.74 | 0.39 |
| Dongfang | 504 | 70 | 13.89 | 73 | 14.48 | | | 14.82 | | | 0.03 | 0.86 |
| Ledong | 485 | 42 | 8.66 | 22 | 4.54 | | | 4.97 | | | 0.09 | 0.76 |
| Lingshui | 388 | 59 | 15.21 | 49 | 12.63 | | | 10.56 | | | 0.80 | 0.37 |
| Qionghai | 608 | 36 | 5.92 | 18 | 2.96 | | | 4.88 | | | 3.12 | 0.08 |
| Qiongzhong | 460 | 79 | 17.17 | 29 | 6.30 | | | 5.17 | | | 0.50 | 0.48 |
| Sanya | 489 | 20 | 4.09 | 40 | 8.18 | | | 8.55 | | | 0.05 | 0.82 |
| Wanning | 450 | 42 | 9.33 | 25 | 5.56 | | | 7.19 | | | 0.92 | 0.34 |
| Wuzhishan | 780 | 36 | 4.62 | 31 | 3.97 | | | 2.11 | | | 4.94 | 0.03 |

*$\chi^2$-test of the difference between the G6PDd prevalence and the ethnic-adjusted G6PDd prevalence in each county.

## Discussion

It has been estimated that more than 400 million people are affected by G6PDd in malaria-endemic regions worldwide (10). Moreover, G6PDd prevalence in the ethnic minority areas is most likely underestimated due to no universal access to diagnosis or high expenditure (7, 14–18). So, the actual G6PDd prevalence may need continuous updates leading to additional difficulty in combating malaria (3, 19). The present study demonstrated that the population in Hainan has a significantly higher G6PDd prevalence compared with other areas in China (8, 9, 20).

Though currently, Hainan has eliminated *P. vivax* malaria, the current undated data on G6PDd prevalence has important implications for treating imported *P. vivax* malaria and preventing re-transmission in the future.

Glucose-6-phosphate dehydrogenase (G6PD) deficiency is a common X-linked genetic trait, and thus affects mainly males. Link between G6PDd and gender revealed that the prevalence in males is usually higher than that of females. The G6PD test classifies the heterozygous females as normal because they have both normal and deficient G6PD red blood cells. From the genetic point of view, our result confirmed that the G6PDd prevalence of males is significantly higher than that of females overall (12.03% vs. 4.56%) or at the group level (both in Li ethnic group and Han ethnic group). On the other hand, males are more likely to become infected with malaria because of some social and behavioral characteristics. For example, males are more likely exposed to the environment of Anopheles mosquitoes, and females are more likely to use mosquito nets than males as they tend to protect their young children. Where feasible, particular attention should be paid to the males, especially in the endemic area or where an outbreak happens when massive primaquine is used.

Knowing the G6PDd prevalence is crucial to determining whether primaquine is contraindicated in patients (21, 22). Hainan Province is multi-ethnic with variant genetic backgrounds, while Han and Li are the two main ethnic groups. According to a national survey, the G6PDd prevalence among ethnic groups is usually greater than among ethnic Han Chinese. In the present study, we also found the different G6PDd prevalence among ethnic groups. For example, the G6PDd prevalence (8.91%) of the Li ethnic minority was significantly higher than that of the Han ethnic majority and was also higher than that of other ethnic minority populations reported from other areas in China (8, 20, 23). Li ethnic minority group was the second largest population with unique genetic traits on Hainan Island. However, the G6PDd studies on Hainan Li population are still insufficient because Li populations live in remote or hard-to-reach areas and have limited access to health facilities. Particular attention should be paid to high-risk groups vulnerable to drug reactions, especially when their genetic variants are unknown.

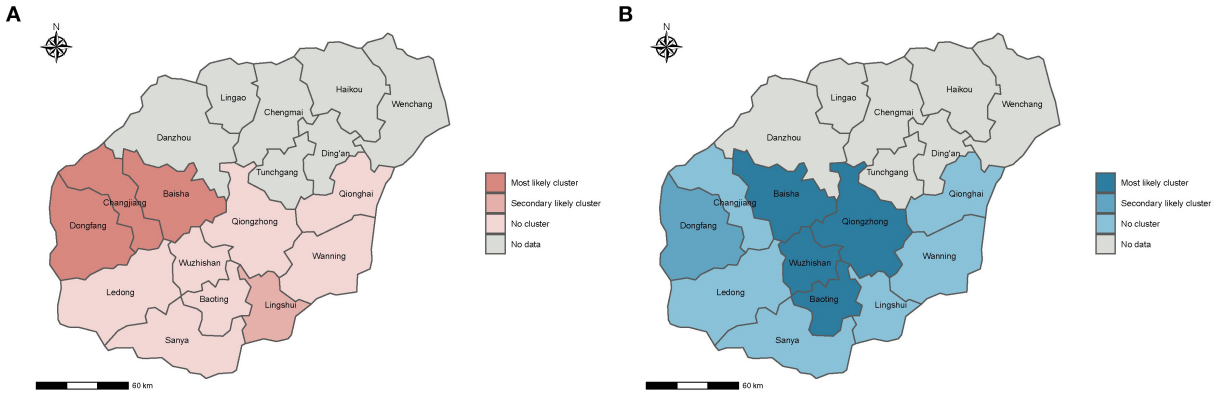


FIGURE 1
Spatial distribution of clusters with high G6PDd risk and high malaria risk in Hainan, China, 2009–2011. **(A,B)** is the spatial distribution of clusters with high G6PDd risk and high malaria risk, respectively. The risk of G6PDd and malaria were ordered using the likelihood ratio (LLR). The most likely cluster indicates the area with the highest risk of G6PDd and malaria, and the secondary likely cluster indicates the area with the second highest risk of G6PDd and malaria.

Glucose-6-phosphate dehydrogenase deficiency can provide protection from severe malaria (24). There is significant selective pressure on the *G6PD* gene in malaria-endemic areas resulting G6PDd prevalence is exceptionally high in some areas of Africa, the Middle East, and South Asia (25). The present study also found that the G6PDd prevalence in malaria patients was more remarkable when compared with that in the non-malaria patient. However, its protective effect on preventing severe malaria needs further evaluation because we did not find such patients in our investigation period. Additionally, the relationship between parasite density and G6PDd status has yet to be explored.

We also found that the distribution patterns of G6PDd were not consistent with the malaria incidence by cluster analysis. These results suggest that the spatial correlation between G6PDd prevalence and malaria incidence is not evident in our study. Similarly, Rosalind et al. established a geostatistical model based on G6PDd prevalence, estimated affected populations, and found that G6PDd was spatially heterogeneous. However, cluster analysis revealed that malaria patients were mainly distributed in the central-southern counties of Hainan, consistent with the epidemic situation during the study period (26). Identification of distribution pattern of G6PD and malaria incidence can provide valuable insights for deliberating the relatedness.

Of note, the present study also has some limitations. Firstly, we only included a small number of participants from 11 counties, which may not reflect the true representative of the overall demographic sample. Secondly, we only focused on the two largest ethnic groups but not include other ethnic minorities. The G6PDd patterns and factors influencing the associations with malaria incidence are needed to examine in a stratified sampling method. Thirdly, the enrolled participants were selected from the hospital instead of the community, which may lead to bias.

## Conclusion

In summary, the results of this study represent the actual G6PDd status in malaria-endemic areas of Hainan. The Li ethnic minority had a higher G6PDd prevalence, especially in males and malaria patients. The G6PDd prevalence was not spatially correlated with the malaria incidence. Thus, in order to mitigate the risk of primaquine-induced hemolysis, special attention should be paid to minority populations in Hainan. More efficient and convenient diagnostic testing tools, such as point-of-care field tests, are expected to inform the potential risk of primaquine-associated harm.

## Data availability statement

The original contributions presented in the study are included in the article/Supplementary material, further inquiries can be directed to the corresponding authors.

## Ethics statement

This clinical study protocol was reviewed and approved by the Ethics Review Committee of the Hainan Center for Disease Control and Prevention. Each participant provided informed consent (in Chinese) before participating in this study. In most cases, the participants provided their written informed consent. The consent was verbal for patients who could not read or write standard Chinese. In these cases, the research nurse documented the participant's consent in writing, including the contents and methods of information provided to the participant and the date and time of the verbal consent,

which was then witnessed and signed by another nurse who was not in the research team. The informed consent record, either written or verbal, was kept in the participant's hospital chart. The Ethics mentioned above Committee reviewed and approved this consent procedure. The patients/participants provided their written informed consent to participate in this study.

## Author contributions

WZ, YL, and GW contributed to the original idea and conceived the paper. GW, NL, AG, MY, RM, and NJ wrote the initial draft of the paper. XF, DS, and GW contributed to the revision of the manuscript. XF reviewed the final version. All authors approved the final manuscript.

## Funding

This study was supported by the Key Medical Research Project of the Health Department of Hainan Province (2010Qiong-36) and the Hainan Provincial Scientific Research Grant (813251). This study was also supported by Hainan Provincial Basic and Applied Basic Research Program (Natural Science Foundation) for High-level Talents in 2019 (2019RC394).

## Conflict of interest

The authors declare that the research was conducted in the absence of any commercial or financial relationships that could be construed as a potential conflict of interest.

## Publisher's note

All claims expressed in this article are solely those of the authors and do not necessarily represent those of their affiliated organizations, or those of the publisher, the editors and the reviewers. Any product that may be evaluated in this article, or claim that may be made by its manufacturer, is not guaranteed or endorsed by the publisher.

## Supplementary material

The Supplementary Material for this article can be found online at: https://www.frontiersin.org/articles/10.3389/fpubh.2022.1010172/full#supplementary-material

## References

1. Chinese Military of Public Health. *Plan of Action for the Elimination of Malaria (2010–2020)* (2010). Available online at: http://www.nhfpc.gov.cn/zhuzhan/wsbmgz/201304/15a4cc7a40b0452191fe409590ca99d8.shtml (accessed March 26, 2014).

2. Baird JK. Eliminating malaria-all of them. *Lancet.* (2010) 376:1883–5. doi: 10.1016/S0140-6736(10)61494-8

3. Howes RE, Pie FB, Patil AP, Nyangiri OA, Gething PW, Dewi M, et al. G6PD deficiency prevalence and estimates of affected populations in malaria endemic countries: a geostatistical model-based map. *PLoS Med.* (2012) 9:e1001339. doi: 10.1371/journal.pmed.1001339

4. Phompradit P, Kuesap J, Chaijaroenkul W, Rueangweerayut R, Hongkaew Y, Yamnuan R, et al. Prevalence and distribution of glucose-6-phosphate dehydrogenase (G6PD) variants in Thai and Burmese populations in malaria endemic areas of Thailand. *Malar J.* (2011) 10:368. doi: 10.1186/1475-2875-10-368

5. Amini F, Ismail E, Zilfalil BA. Prevalence and molecular study of G6PD deficiency in Malaysian Orang Asli. *Intern Med J.* (2011) 41:351–3. doi: 10.1111/j.1445-5994.2011.02456.x

6. Tantular IS, Matsuoka H, Kasahara Y, Pusarawati S, Kanbe T, Tuda JS, et al. Incidence and mutation analysis of glucose-6-phosphate dehydrogenase deficiency in eastern Indonesian populations. *Acta Med Okayama.* (2010) 64:367–73. doi: 10.18926/AMO/41322

7. Leslie T, Moiz B, Mohammad N, Amanzai O, Ur Rasheed H, Jan S, et al. Prevalence and molecular basis of glucose-6-phosphate dehydrogenase deficiency in Afghan populations: implications for treatment policy in the region. *Malar J.* (2013) 12:230. doi: 10.1186/1475-2875-12-230

8. Li H, Zhu J, Che Y, Dao T, Zhao S. Screening of glucose-6-phosphate dehydrogenase (G6PD) deficiency in minority nationalities in high malaria endemic areas of Xishuangbanna prefecture. *China Trop Med.* (2012). 12:137–48. doi: 10.13604/j.cnki.46-1064/r.2012.02.031

9. Cappellini MD, Fiorelli G. Glucose-6-phosphate dehydrogenase deficiency. *Lancet.* (2008) 371:64–74. doi: 10.1016/S0140-6736(08)60073-2

10. Beutler E, Duparc S, G6PD Deficiency Working Group. Glucose-6-phosphate dehydrogenase deficiency and antimalarial drug development. *Am J Trop Med Hyg.* (2007) 77:779–89. doi: 10.4269/ajtmh.2007.77.779

11. Leslie T, Briceño M, Mayan I, Mohammed N, Klinkenberg E, Sibley CH, et al. The impact of phenotypic and genotypic G6PD deficiency on risk of *Plasmodium vivax* infection: a case-control study amongst Afghan refugees in Pakistan. *PLoS Med.* (2010) 7:e1000283. doi: 10.1371/journal.pmed.1000283

12. Beutler E, Mitchell M. Special modifications of the fluorescent screening method for glucose-6-phosphate dehydrogenase deficiency. *Blood.* (1968) 32:816–8. doi: 10.1182/blood.V32.5.816.816

13. Roca-Feltrer A, Khim N, Kim S, Chy S, Canier L, Kerleguer A, et al. Field trial evaluation of the performances of point-of-care tests for screening G6PD deficiency in Cambodia. *PLoS ONE.* (2015) 9:e116143. doi: 10.1371/journal.pone.0116143

14. von Fricken ME, Weppelmann TA, Eaton WT, Alam MT, Carter TE, Schick L, et al. Prevalence of glucose-6-phosphate dehydrogenase (G6PD) deficiency in the Ouest and Sud-Est departments of Haiti. *Acta Trop.* (2014) 135:62–6. doi: 10.1016/j.actatropica.2014.03.011

15. Khim N, Benedet C, Kim S, Kheng S, Siv S, Leang R, et al. G6PD deficiency in *Plasmodium falciparum* and *Plasmodium vivax* malaria-infected Cambodian patients. *Malar J.* (2013) 12:171. doi: 10.1186/1475-2875-12-171

16. Herdiana H, Fuad A, Asih PB, Zubaedah S, Arisanti RR, Syafruddin D, et al. Progress towards malaria elimination in Sabang Municipality, Aceh, Indonesia. *Malar J.* (2013) 12:42. doi: 10.1186/1475-2875-12-42

17. Asih PB, Rozi IE, Herdiana, Pratama NR, Hidayati AP, Marantina SS, et al. The baseline distribution of malaria in the initial phase of elimination in Sabang Municipality, Aceh Province, Indonesia. *Malar J.* (2012) 11:291. doi: 10.1186/1475-2875-11-291

18. Millimono TS, Loua KM, Rath SL, Relvas L, Bento C, Diakite M, et al. High prevalence of hemoglobin disorders and glucose-6-phosphate dehydrogenase

(G6PD) deficiency in the Republic of Guinea (West Africa). *Hemoglobin.* (2012) 36:25–37. doi: 10.3109/03630269.2011.600491

19. Nkhoma ET, Poole C, Vannappagari V, Hall SA, Beutler E. The global prevalence of glucose-6-phosphate dehydrogenase deficiency: a systematic review and meta-analysis. *Blood Cells Mol Dis.* (2009) 42:267–78. doi: 10.1016/j.bcmd.2008.12.005

20. Yao LQ, Zou TB, Wang XT, Quan X, Chen Q, Yang FB, et al. G6PD deficiency among children under 7 years old from Yunnan with unique ethnic m inority origin. *Chin J Med Genet.* (2013) 30:189–94. doi: 10.3760/cma.j.issn.1003-9406.2013.04.015

21. Lyon MF. Gene action in the X-chromosome of the mouse (*Mus musculus* L.). *Nature.* (1961) 190:372–3. doi: 10.1038/190372a0

22. Beutler E, Yeh M, Fairbanks VF. The normal human female as a mosaic of X-chromosome activity: studies using the gene for C-6-PD-deficiency as a marker. *Proc Natl Acad Sci USA.* (1962) 48:9–16. doi: 10.1073/pnas.48.1.9

23. Hu L, Yang H, Ou C, Zou T, Yao L, Liu J. Yunnan Nujiang Lisu, Clan and Primi, Dulong population children under the age of seven G6PD deficiency investigation. *Zhongguo Yousheng Yu Yichuan Zazhi.* (2011) 19:128–9. doi: 10.13404/j.cnki.cjbhh.2011.12.065

24. Ruwende C, Khoo SC, Snow RW, Yates SN, Kwiatkowski D, Gupta S, et al. Natural selection of hemi-and heterozygotes for G6PD deficiency in Africa by resistance to severe malaria. *Nature.* (1995) 376:246–9. doi: 10.1038/376246a0

25. Xiao D, Long Y, Wang S, Wu K, Xu D, Li H, et al. Epidemic distribution and variation of *Plasmodium falciparum* and *Plasmodium vivax* malaria in Hainan, China during 1995–2008. *Am J Trop Med Hyg.* (2012) 87:646–54. doi: 10.4269/ajtmh.2012.12-0164

26. Xiao D, Long Y, Wang S, Fang L, Xu D, Wang G, et al. Spatiotemporal distribution of malaria and the association between its epidemic and climate factors in Hainan, China. *Malar J.* (2010) 9:185. doi: 10.1186/1475-2875-9-185

frontiers | Frontiers in Medicine

TYPE Case Report
PUBLISHED 28 October 2022
DOI 10.3389/fmed.2022.1017074



OPEN ACCESS

EDITED BY
Hui Chen,
Brigham and Women's Hospital and Harvard Medical School, United States

REVIEWED BY
Yue Zheng,
Dana-Farber/Brigham and Women's Cancer Center, United States
Sahar Rostamian,
Brigham and Women's Hospital and Harvard Medical School, United States
Xiangxiang Hu,
University of North Carolina at Chapel Hill, United States
Xun Li,
University of Maryland, Baltimore, United States

*CORRESPONDENCE
Li Peng
pli1228@163.com
Rui Guo
guo.rui.cqmu@gmail.com

†These authors have contributed equally to this work and share first authorship

‡These authors have contributed equally to this work

SPECIALTY SECTION
This article was submitted to Infectious Diseases – Surveillance, Prevention and Treatment, a section of the journal Frontiers in Medicine

RECEIVED 11 August 2022
ACCEPTED 30 September 2022
PUBLISHED 28 October 2022

CITATION
Feng Y, Wu C, Huang X, Huang X, Peng L and Guo R (2022) Case report: Successful management of *Parvimonas micra* pneumonia mimicking hematogenous *Staphylococcus aureus* pneumonia. *Front. Med.* 9:1017074. doi: 10.3389/fmed.2022.1017074

# Case report: Successful management of *Parvimonas micra* pneumonia mimicking hematogenous *Staphylococcus aureus* pneumonia

Yanmei Feng[1†], Chunxia Wu[1†], Xiaohui Huang[2], Xia Huang[3], Li Peng[1*‡] and Rui Guo[4*‡]

[1]Department of Respiratory and Critical Care Medicine, The First Affiliated Hospital of Chongqing Medical University, Chongqing, China, [2]Department of Respiratory and Critical Care Medicine, Liangping People's Hospital, Chongqing, China, [3]Department of Critical Care Medicine, Chongqing University Three Gorges Hospital, Chongqing, China, [4]Department of Critical Care Medicine, The First Affiliated Hospital of Chongqing Medical University, Chongqing, China

*Parvimonas micra* is an anaerobic Gram-positive coccus frequently found in the oral cavity and gastrointestinal tract, but rarely in the lung. Therefore, pneumonia caused by *P. micra* is also rare. Although there are some reports of *P. micra* related pneumonia due to aspiration or blood-borne infection with definite remote infection source, there are no reported cases of hematogenous *P. micra* pneumonia in healthy adults lacking a remote source of infection. Herein, we described the intact disease of *P. micra*-related pneumonia mimicking hematogenous *Staphylococcus aureus* pneumonia in terms of chest imagery and diagnosed *via* metagenomic next-generation sequencing (mNGS). Interestingly, there was no clear remote pathogenic source identified in the patient. Microbiome analysis revealed dysbiosis of the oral flora possibly related to poor oral hygiene and a long history of smoking. The patient was treated with moxifloxacin for 3 months. Ultimately, computed tomography (CT) of the chest showed total resolution of the lung lesion. Clinicians need to update the etiology of community-acquired pneumonia. When antibiotic therapy is not effective, pathogen examination becomes very important. New methods of pathogen detection such as mNGS should be employed to this end. For the treatment of *P. micra* pneumonia, no standardized course of treatment was reported. Imaging absorption of lung infections may provide a more objective guidance for the duration of antibiotics in *P. micra* pneumonia.

KEYWORDS

***P. micra* pneumonia, dysbiosis, oral flora, poor oral hygiene, new etiology**

## Introduction

*Parvimonas micra*, previously known as *Peptostreptococcus micros* and *Micromonas micros*, is commonly found on human skin, in oral cavity, and among gastrointestinal flora (1). It is an anaerobic Gram-positive coccus with a diameter of 0.3–0.7 μm. This opportunistic pathogen is frequently isolated from infected root canals of teeth with chronic apical periodontitis, whereas remote infections are rare (2). A few sporadic cases of remote infection in patients with underlying diseases or a recent oral operation have been reported (3–6).

Because it is anaerobic, *P. micra* is not a dominant bacterium in aerobic environments, including the lung. Although there are some reports of *P. micra* pneumonia due to aspiration, hematogenous *P. micra* pneumonia is rare (7–9). Moreover, to the best of our knowledge, there are no reports of *P. micra*-related pneumonia induced by bloodstream infection without a definitive, remote pathogenic source.

The gold standard method of diagnosing *P. micra* infection is microbiological examination. However, it is difficult to detect using traditional cultural methods (10). Recently developed non-culture methods, such as metagenomic next-generation sequencing (mNGS), provide an alternative for the identification of unknown pathogens (11). As a new tool, mNGS is any of several high-throughput sequencing methods whereby billions of nucleic acid fragments can be simultaneously and independently sequenced. It can be used to precisely and rapidly identify potential pathogens regardless of pathogen type (bacterium, virus, fungus, parasite, and so on) (12). The mNGS is a promising method for diagnosing sophisticated infections, especially severe pneumonias require stay in the intensive care units (13, 14).

Herein, we describe *P. micra* pneumonia mimicking hematogenous *Staphylococcus aureus* pneumonia in terms of chest imagery and diagnosed *via* mNGS in pleural effusion. Interestingly, there was no definitive, remote pathogenic source identified in the patient. A cautious approach to diagnosis is necessary for rare cases such as this to avoid misdiagnosis, and clinical knowledge of *P. micra*-related pneumonia should be updated.

## Case presentation

A 74-year-old man was admitted to the Department of Respiratory and Critical Care Medicine of the First Affiliated Hospital of Chongqing Medical University on 25 March 2022 with a complaint of dry cough, fever, and intermittent chest pain for 17 days and shortness of breath after activity for 4 days. He denied night sweats and weight loss. There was no history of hemoptysis, recent contact with tuberculosis or irritant gas, or any other underlying health conditions, except for 20-year smoking history. When the symptoms first occurred, the patient underwent a series of computed tomography (CT) scans. At that time, he was treated with amoxicillin clavulanate potassium for 4 days and with levofloxacin for 6 days (**Figure 1**). His chest pain was significantly relieved and his temperature returned to normal. However, the patient continued to cough intermittently and experience shortness of breath after activity. As shown in **Figure 2**, consecutive CT images showed an increasing number of nodules and exudative inflammatory lesions with a newly emerged pleural effusion. Physical examination indicated normal vital signs (Body temperature: 36.2°C, Pulse rate: 70/min, Respiratory rate: 20/min, Blood pressure: 146/74 mmHg) but asymmetric breath sounds without rales or wheezing. Blood gas analysis indicated a Pondus Hydrogenii (PH) of 7.48, a Partial Pressure of Carbon Dioxide ($PCO_2$) of 37 mmHg, Oxygen Permeance ($PO_2$) of 73 mmHg, Bicarbonate ($HCO_3^-$) of 27.6 mmol/L, and oxygen saturation ($SO_2$) of 96%. His leukocyte levels were normal, but his erythrocyte sedimentation rate was elevated, at 61 mm/h.

According to his clinical symptoms and the dynamic changes observed in chest CT, we highly suspected an infectious lung disease. Because of the non-specific clinical manifestations, pathogenetic examination was very important for this patient. Therefore, we collected microbiological samples and performed routine bacteria culture. The GeneXpert MTB/RIF assay and mNGS were performed on 29 March 2022, 4 days after admission, in an attempt to identify pathogenic bacteria. Meanwhile, his antibiotic treatment was switched to moxifloxacin to better fight against Gram-positive bacteria and covered the antibacterial spectrum of anaerobic bacteria. As shown in **Table 1**, the laboratory tests, such as Galactomannan Antigen Testing (GM), β-D-glucan fungal antigen test (G test), and tests for cryptococcal pod antigen, were negative; however, the patient was positive for mycoplasma antibody (IgM). The pleural effusion was exudate consisting of 44% leukocyte. Samples of it were sent for routine bacteria culture and were analyzed using the GeneXpert MTB/RIF assay and mNGS. BALF samples were also subjected to routine bacteria culture and GeneXpert MTB/RIF assay. All samples returned negative in all of the tests except mNGS, which identified four specific reads of *P. micra* with 9% relative abundance from pleural effusion samples.

To search for the source of infection, enhanced CT of the oropharyngeal and abdomen as well as cardiac ultrasound were conducted. A medical history inquiring about toothache, periodontitis, and oral invasive operations was conducted, and the patient denied underlying oral diseases. No abscesses were detected in any CT image, and cardiac ultrasound revealed a lack of bacterial emboli. However, an examination of the oral cavity indicated that most tooth crowns of this patient were missing, while the roots remained. Oropharyngeal CT also suggested multiple root remnants with partial alveolar bone resorption. Further inquiries revealed that the patient wore dentures for an extended period of time; these were cleaned and soaked

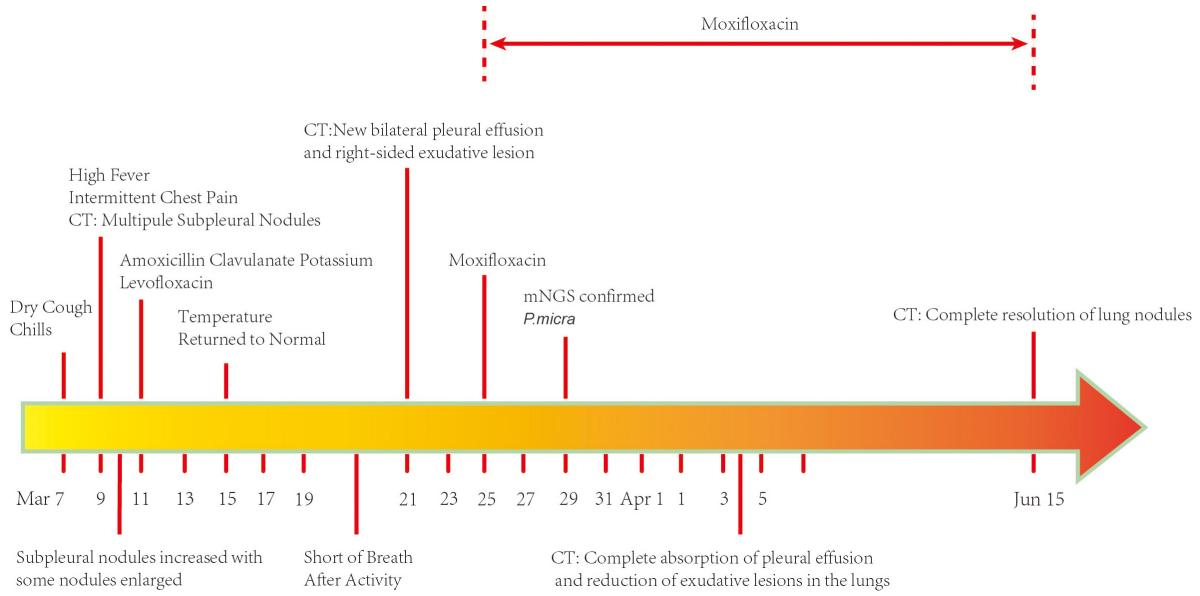


FIGURE 1
Timeline of the clinical course and duration of treatment.

in normal tap water that was not changed every day. Based on the poor oral hygiene and colonization of the oral cavity with *P. micra*, we intended to conduct mNGS to analyze oral and lung pathogens. However, because of the high cost of mNGS, we had to analyze the oral and lung microbiome by 16s rRNA gene sequencing. Interestingly, the results identified *Parvimonas* not only in the oral cavity but also in the BALF (**Figure 3**). Compared to the oral flora of healthy men (15), the patient's α diversity of the oral cavity was significantly reduced (**Figure 3**). Based on these factors, we speculated that the oral cavity could have been the potential infection source. Moxifloxacin treatment was continued. Fortunately, a follow-up chest CT on 4 April 2022 showed complete absorption of pleural fluid and significant resolution of the exudative lesions (**Figure 2**). Given that the adjusted treatment was effective, moxifloxacin was continued for 3 more months. Finally, a chest CT on 15 June 2022 showed almost total resolution of the lung lesion (**Figure 2**).

## Discussion

*Parvimonas micra* is part of the normal microbiome of the oral cavity, gastrointestinal tract, and skin. However, it can be a pathogen in patients with impaired immune function or with underlying disease. Cases of *P. micra* infection of the hip joint, pericardium, cervix, liver, and brain have been reported (4, 16–18). However, because of the aerobic environment of the lung, this pathogen is not common in the lung and it rarely causes pneumonia. Tsyshi et al. (19) reported a case of hematogenous lung abscess caused by *P. micra* in an 85-year-old male with diabetes. In that case, remote sites of infection were detected: apical periodontitis and an infratemporal fossa abscess.

Here, we report a case of *P. micra* pneumonia mimicking hematogenous *Staphylococcus aureus* pneumonia in terms of chest imagery without a definitive remote site of infection. There was no direct evidence of blood-borne infection, but we still highly suspected hematogenous infection based on the chest imagery. According to microbiome analyses of the oral cavity and lung by 16s rRNA gene sequencing, the patient's poor oral hygiene was suspected to be related to the infection. However, as mentioned above, *P. micra* is a normal component of the oral and intestinal flora in healthy people. The patient in our case denied any underlying disease, except for a long history of heavy smoking. It has been reported that smoking tobacco disrupts immune homeostasis, resulting in a variety of illnesses (20). It also affects oral microbiota composition (21). The level of *P. micra* and other bacteria in the oral cavity is higher in smokers than in non-smokers (8). We also noted poor hygiene with suspected periodontitis and decreased α diversity in the oral microbiome of our patient, accompanied by similar copies of *P. micra* between oral wash and BALF samples. Therefore, we speculate that our patient's *P. micra* pneumonia may have been induced by dysbiosis of his oral microflora and tobacco smoking.

Common hematogenous lung abscesses always present with high fever, cough with or without sputum, and multiple small subpleural nodules with dynamic change in CT scans. According to a previous systematic review (22), the common

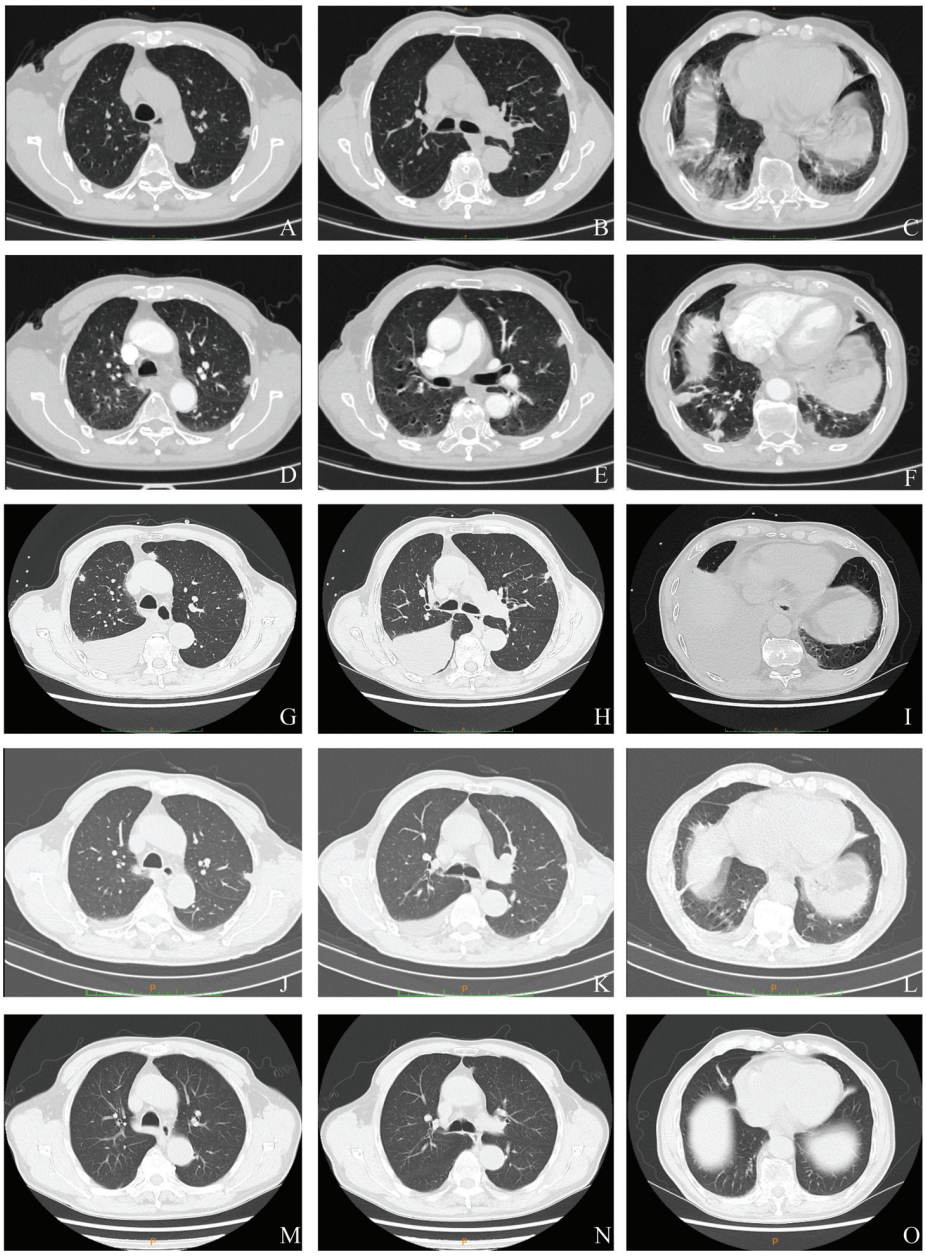


FIGURE 2
Serial chest computed tomography (CT) scans of the patient with *Parvimonas micra* pneumonia. **(A–C)** The initial CT scan on 9 March 2022 (2 days after symptom onset) shows subpleural nodules in both lungs, some nodules with ground glass appearance, and a few exudative inflammatory lesions in both lower lungs. **(D–F)** A CT on the next day (10 March 2022) showed more nodules and exudative lesions in both lungs and some enlarged nodules. **(G–I)** A follow-up scan (21 March 2022) after treatment with amoxicillin clavulanate potassium and levofloxacin showed multiple subpleural nodules with newly emerged bilateral pleural effusion and an exudative lesion in the right lung. **(J–L)** Another CT (4 April 2022) showed complete absorption of the pleural effusion and a reduced exudative lesion. **(M–O)** Another CT after moxifloxacin treatment for 3 months (15 June 2022) exhibited an almost normal chest image.

pathogens of hematogenous lung abscesses are methicillin-sensitive *Staphylococcus aureus* (MSSA) and methicillin-resistant *Staphylococcus aureus* (MRSA). Isolation of *P. micra* as the causative pathogen of a hematogenous lung abscess is rare. Little is known about the clinical characteristics of *P. micra* hematogenous lung infections. In our case, the patient showed the much similar manifestations to hematogenous lung infection. Because there are no known specific symptoms of hematogenous *P. micra* pneumonia, it was extremely critical to conduct a microbiological examination. Unfortunately, however, it is difficult to detect this microbe using conventional culture methods. Hence, we used the mNGS technique, which

TABLE 1 Laboratory tests for clinical pathogen identification.

| | Normal range | Result |
|---|---|---|
| **Blood** | | |
| Total lymphocyte count | 1,752–2,708/μL | 1,159/μL |
| CD4 + T | 561–1,137/μL | 460/μL |
| CD8 + T | 464–754/μL | 368/μL |
| B lymphocyte | 180–324/μL | 156/μL |
| Native killer cells | 175–567/μL | 116/μL |
| CD4 + /CD8 + | 0.89–2.01 | 1.25 |
| Tuberculosis antibody | Negative | Negative |
| GM test | <0.5 | 0.09 |
| Cryptococcal capsular antigen | Negative | Negative |
| Antinuclear antibody spectrum | Negative | Negative |
| ANCA | Negative | Negative |
| Anti-*legionella pneumophila* serum type I antibody IgM | Negative | Negative |
| Anti-*chlamydia pneumoniae* antibody IgM | Negative | Negative |
| Anti-*rickettsia Q fever* IgM antibody | Negative | Negative |
| Anti-*chlamydia pneumoniae* antibody IgM | Negative | Negative |
| Anti-*adenovirus* antibody IgM | Negative | Negative |
| Anti-*respiratory syncytial virus* antibody IgM | negative | Negative |
| IgM antibody against *influenza A virus* | Negative | Negative |
| Anti-*influenza B virus* IgM antibody | Negative | Negative |
| *Mycoplasma pneumoniae* antibody IgM | Negative | Positive |
| **BALF** | | |
| Bacterial smear | Negative | Negative |
| Fungal smear | Negative | Negative |
| Bacterial culture | Negative | Negative |
| Fungal culture | Negative | Negative |
| Smear of *Mycobacterium tuberculosis* | Negative | Negative |
| Tubercle bacillus culture | Negative | Negative |
| **Pleural Effusion** | | |
| Number of nucleated cells | $(0–8) \times 10^6$/L | $3,677 \times 10^6$/L |
| Ratio of multinucleated cells | | 44% |
| Ratio of monocytes | | 56% |
| Smear of *Mycobacterium tuberculosis* | Negative | Negative |
| Culture of pleural effusion | Negative | Negative |
| GeneXpert MTB/RIF assay | Negative | Negative |
| Tubercle bacillus culture | Negative | Negative |
| mNGS | | *P. micra* (4 copies with 9% relative abundance) |

has a wide detection range and does not need to specify the suspected causative microorganism in advance. In addition, comparing to conventional culture methods, the results are obtained very quickly (2–3 days *vs.* 5–7 days for conventional methods) and the positive rate of identified pathogens is much higher (95 *vs.* 54%) (23).

*Mycoplasma pneumoniae* IgM is an early antibody that appears after infection, and it usually appears only after 4–5 days and lasts 1–3 months or more. A positive IgM for *Mycoplasma pneumoniae* may indicate current infection with *Mycoplasma pneumoniae* or it may not, as some patients may show prolonged IgM seropositivity caused by prior *Mycoplasma pneumoniae* infection (24). So, in our case, the patient was thought to be a false positive *Mycoplasma pneumoniae* IgM and diagnosed with *P. micra* detection in pleural effusion with mNGS in our case. Normal pleural effusion fluid is sterile, and it can be identified as pathogenic if bacteria are detected in it. Therefore, we confirmed that *P. micra* was the pathogen causing the pulmonary infection in our patient rather than *Mycoplasma pneumoniae*.

Although *P. micra* is typically susceptible to antibiotics such as penicillin, clindamycin, metronidazole, and imipenem, drug-resistant strains may also exist (9, 25). In this case, amoxicillin

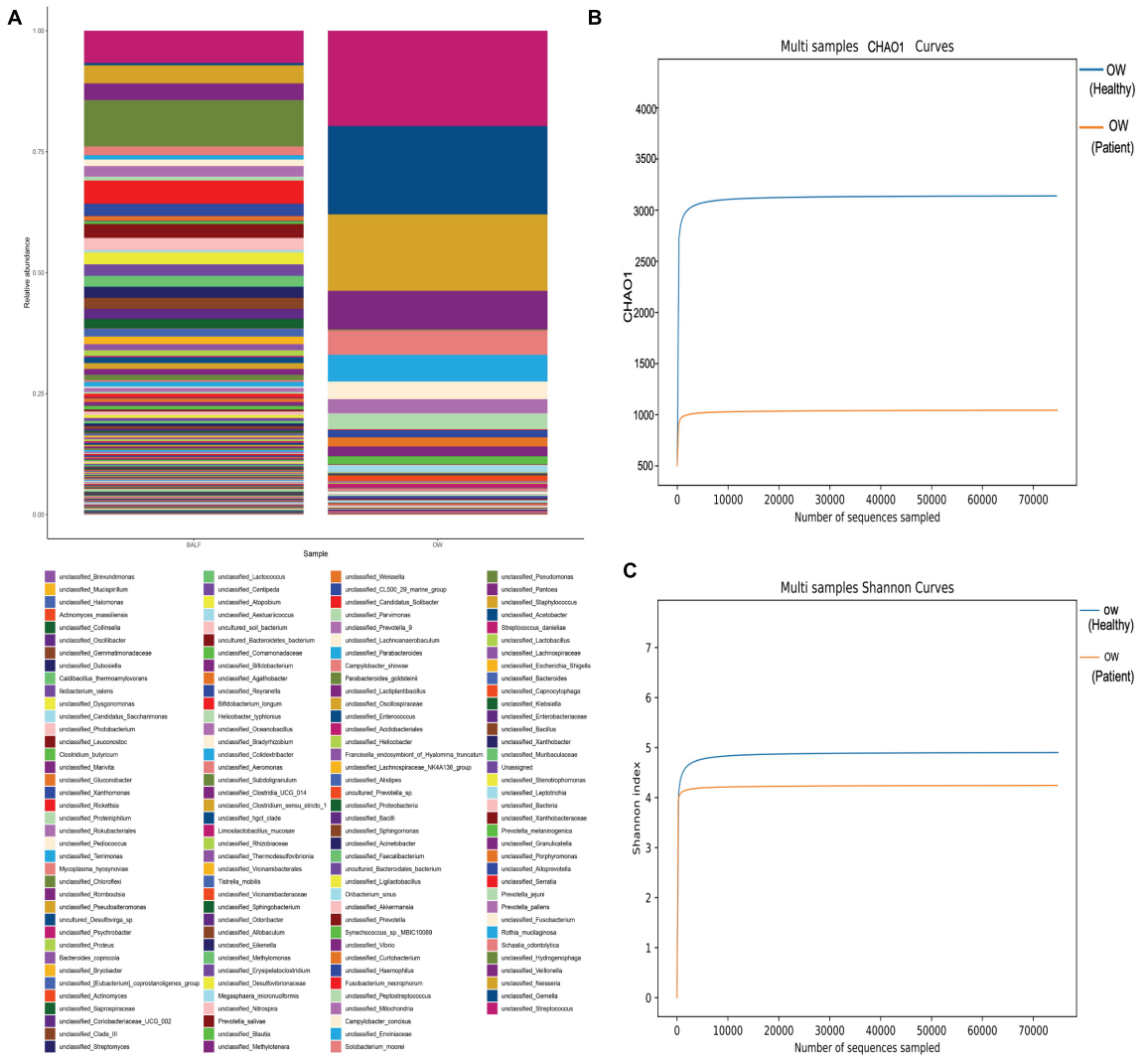


FIGURE 3
Comparison of the oral and lung microbiome (heatmap). **(A)** No significant differences were found in *P. micra* between oral wash and BALF samples (0.11% in BALF *vs*. 0.13% in oral wash). **(B,C)** The α diversity of the oral microbiome comparing the patient to a healthy man. Both the Chao1 and Shannon indexes were lower in the patient (Chao1: 986 *vs*. 3,079, Shannon index: 4.244 *vs*. 4.829).

clavulanate potassium and levofloxacin were administered successively. Unfortunately, the clinical symptoms of the patient remained poorly controlled and the lesions in the lung became exacerbated. So we highly suspected that the patient suffered from drug-resistant strains, even *P. micra* was theoretical sensitivity to penicillin (26). Hence, if possible, we recommend acquiring drug sensitivity test along with the pathogenic cultures or drug-resistant gene test, which may provide us with the necessary information to develop precise treatments.

The previous studies have suggested that the durations of antibiotic therapy for *P. micra* pneumonia are highly variable (8) and there is little evidence of hematogenous *P. micra* pneumonia. Watanabe et al. (7) reported a case of *P. micra*-related hematogenous lung abscess in which chest CT showed that the lung lesions resolved after 1 month of antibiotic treatment with ampicillin sulbactam. Ubukata et al. (19) reported a similar case where antibiotics were continuously administered for 3 months. Similarly, we administered moxifloxacin for 3 months in our patient. Considering the large variation in antibiotic duration to treat *P. micra* pneumonia, we recommend using lung imaging instead to guide the antibiotic regimen.

There were some limitations to this study. Due to the usage of antibiotics prior to admission and the relatively high cost of mNGS in the clinical setting, blood samples were not used for mNGS tests. In addition, the patient's oral and pulmonary flora were not analyzed after treatment, and thus any differences pre- and post-treatment with moxifloxacin could not be determined.

## Conclusion

In summary, we report a case of *P. micra* pneumonia in a patient without any apparent underlying diseases and no remote site of infection. Clinicians need to update the etiology of community-acquired pneumonia, especially in smoking patients with poor oral hygiene. When antibiotic therapy is ineffective, early initiation of mNGS is critical for the rapid screening of rare pathogens such as *P. micra*. If possible, we recommend choosing a reasonable antibiotic based on drug sensitivity tests of *P. micra* to avoid possible drug resistance. Finally, lung infection absorption as determined *via* imaging may provide more objective guidance of treatment than the duration of antibiotic treatment.

## Ethics statement

Written informed consent was obtained from the individual(s) for the publication of any potentially identifiable images or data included in this article.

## Author contributions

CW, XHH, and XH were involved in the patient's clinical treatment. YF and LP contributed to the diagnosis. RG analyzed the pathological and CT images. YF integrated all information and wrote the manuscript. LP and RG provided critical guidance and revisions for YF throughout the writing process. All authors contributed to the article and approved the submitted version.

## Funding

This work was supported by the Basic Research and Frontier Exploration Project of Chongqing Yuzhong District Science & Technology Committee (under Grant No: 20180139) and Medical Talents Program of Chongqing for Young and Middle-aged.

## Acknowledgments

We thank the patient for providing permission to share his information.

## Conflict of interest

The authors declare that the research was conducted in the absence of any commercial or financial relationships that could be construed as a potential conflict of interest.

## Publisher's note



## References

1. Ryan PM, Shin CP. Native joint infections caused by *Parvimonas micra*. *Anaerobe.* (2021) 71:102412. doi: 10.1016/j.anaerobe.2021.102412

2. Marinković J, Marković T, Brkić S, Radunović M, Soldatović I, Ćirić A, et al. Microbiological analysis of primary infected root canals with symptomatic and asymptomatic apical periodontitis of young permanent teeth. *Balk J Dent Med.* (2020) 24:170–7.

3. Watanabe T, Hara Y, Yoshimi Y, Fujita Y, Yokoe M, Noguchi Y. Clinical characteristics of bloodstream infection by *Parvimonas micra*: retrospective case series and literature review. *BMC Infect Dis.* (2020) 20:578. doi: 10.1186/s12879-020-05305-y

4. Cesta N, Foroghi Biland L, Neri B, Mossa M, Campogiani L, Caldara F, et al. Multiple hepatic and brain abscesses caused by *Parvimonas micra*: a case report and literature review. *Anaerobe.* (2021) 69:102366. doi: 10.1016/j.anaerobe.2021.102366

5. Randall D, Jee Y, Vanood A, Mayo D. Atypical presentation of periprosthetic joint infection after total knee arthroplasty due to *Parvimonas micra*. *Arthroplast Today.* (2020) 6:901–5. doi: 10.1016/j.artd.2020.09.021

6. Prieto R, Callejas-Diaz A, Hassan R, de Vargas AP, Lopez-Pajaro LF. *Parvimonas micra*: a potential causative pathogen to consider when diagnosing odontogenic brain abscesses. *Surg Neurol Int.* (2020) 11:140. doi: 10.25259/SNI_20_2020

7. Watanabe T, Yokoe M, Noguchi Y. Septic pulmonary embolism associated with periodontal disease: a case report and literature review. *BMC Infect Dis.* (2019) 19:74. doi: 10.1186/s12879-019-3710-3

8. Zhang Y, Song P, Zhang R, Yao Y, Shen L, Ma Q, et al. Clinical characteristics of chronic lung abscess associated with *Parvimonas micra* diagnosed using metagenomic next-generation sequencing. *Infect Drug Resist.* (2021) 14:1191–8. doi: 10.2147/IDR.S304569

9. Miyazaki M, Asaka T, Takemoto M, Nakano T. Severe sepsis caused by *Parvimonas micra* identified using 16S ribosomal RNA gene sequencing following patient death. *IDCases.* (2020) 19:e00687. doi: 10.1016/j.idcr.2019.e00687

10. Yu Q, Sun L, Xu Z, Fan L, Du Y. Severe pneumonia caused by *Parvimonas micra*: a case report. *BMC Infect Dis.* (2021) 21:364. doi: 10.1186/s12879-021-06058-y

11. Chiu CY, Miller SA. Clinical metagenomics. *Nat Rev Genet.* (2019) 20:341–55. doi: 10.1038/s41576-019-0113-7

12. Schlaberg R, Chiu CY, Miller S, Procop GW, Weinstock G, Professional Practice Committee and Committee on Laboratory Practices of the American Society for Microbiology, et al. Validation of metagenomic next-generation sequencing tests for Universal Pathogen Detection. *Arch Pathol Lab Med.* (2017) 141:776–86. doi: 10.5858/arpa.2016-0539-RA

13. Langelier C, Kalantar KL, Moazed F, Wilson MR, Crawford ED, Deiss T, et al. Integrating host response and unbiased microbe detection for lower respiratory

tract infection diagnosis in critically ill adults. *Proc Natl Acad Sci U.S.A.* (2018) 115:E12353–62. doi: 10.1073/pnas.1809700115

14. Long Y, Zhang Y, Gong Y, Sun R, Su L, Lin X, et al. Diagnosis of sepsis with cell-free DNA by next-generation sequencing technology in ICU patients. *Arch Med Res.* (2016) 47:365–71. doi: 10.1016/j.arcmed.2016.08.004

15. Chen B, Wang Z, Wang J, Su X, Yang J, Zhang Q, et al. The oral microbiome profile and biomarker in Chinese type 2 diabetes mellitus patients. *Endocrine.* (2020) 68:564–72. doi: 10.1007/s12020-020-02269-6

16. Ryan PM, Morrey BF. *Parvimonas micra* causing native hip joint septic arthritis. *Proc Bayl Univ Med Cent.* (2021) 34:486–8. doi: 10.1080/08998280.2021.1906827

17. Morinaga H, Kato K, Hisagi M, Tanaka H. Purulent pericarditis-induced intracardiac perforation and infective endocarditis due to *Parvimonas micra*: a case report. *Eur Heart J Case Rep.* (2021) 5:ytaa528. doi: 10.1093/ehjcr/ytaa528

18. Fujiwara E, Tsuda T, Wada K, Waki S, Hanada Y, Nishimura H. A rare case of cervical abscess caused by *Parvimonas micra*. *SAGE Open Med Case Rep.* (2021) 9:2050313X211024505. doi: 10.1177/2050313X211024505

19. Ubukata S, Jingu D, Yajima T, Shoji M, Takahashi H. A case of septic pulmonary embolism due to *Peptostreptococcus* micros with multiple infection of the head and neck. *Kansenshogaku Zasshi.* (2013) 87:761–6. doi: 10.11150/kansenshogakuzasshi.87.761

20. Jiang C, Chen Q, Xie M. Smoking increases the risk of infectious diseases: a narrative review. *Tob Induc Dis.* (2020) 18:60. doi: 10.18332/tid/123845

21. Lee YH, Chung SW, Auh QS, Hong SJ, Lee YA, Jung J, et al. Progress in oral microbiome related to oral and systemic diseases: an update. *Diagnostics.* (2021) 11:1283. doi: 10.3390/diagnostics11071283

22. Ye R, Zhao L, Wang C, Wu X, Yan H. Clinical characteristics of septic pulmonary embolism in adults: a systematic review. *Respir Med.* (2014) 108:1–8. doi: 10.1016/j.rmed.2013.10.012

23. Qian YY, Wang HY, Zhou Y, Zhang HC, Zhu YM, Zhou X, et al. Improving pulmonary infection diagnosis with metagenomic next generation sequencing. *Front Cell Infect Microbiol.* (2020) 10:567615. doi: 10.3389/fcimb.2020.567615

24. Jeon HE, Kang HM, Yang EA, Han HY, Han SB, Rhim JW, et al. Early confirmation of *Mycoplasma pneumoniae* infection by two short-term serologic IgM examination. *Diagnostics.* (2021) 11:353. doi: 10.3390/diagnostics11020353

25. Rams TE, Sautter JD, van Winkelhoff AJ. Antibiotic resistance of human periodontal pathogen *Parvimonas micra* over 10 years. *Antibiotics.* (2020) 9:709. doi: 10.3390/antibiotics9100709

26. Kim EY, Baek YH, Jung DS, Woo KS. Concomitant liver and brain abscesses caused by *Parvimonas Micra*. *Korean J Gastroenterol.* (2019) 73:230–4. doi: 10.4166/kjg.2019.73.4.230

frontiers | Frontiers in Public Health

TYPE Brief Research Report
PUBLISHED 26 January 2023
DOI 10.3389/fpubh.2023.1098965



OPEN ACCESS

EDITED BY
Hui Chen,
Brigham and Women's Hospital and Harvard Medical School, United States

REVIEWED BY
Elke Bergmann-Leitner,
Walter Reed Army Institute of Research, United States
Weihao Zheng,
University of California, San Francisco, United States

*CORRESPONDENCE
Elisa Maiques
✉ emaiques@uchceu.es
Consuelo Rubio-Guerri
✉ consuelo.rubio@uchceu.es
Giuseppa Purpari
✉ giuseppa.purpari@izssicilia.it

†These authors have contributed equally to this work

SPECIALTY SECTION
This article was submitted to Infectious Diseases: Epidemiology and Prevention, a section of the journal Frontiers in Public Health

RECEIVED 15 November 2022
ACCEPTED 06 January 2023
PUBLISHED 26 January 2023

CITATION
Padilla-Blanco M, Gucciardi F, Rubio V, Lastra A, Lorenzo T, Ballester B, González-Pastor A, Veses V, Macaluso G, Sheth CC, Pascual-Ortiz M, Maiques E, Rubio-Guerri C, Purpari G and Guercio A (2023) A SARS-CoV-2 full genome sequence of the B.1.1 lineage sheds light on viral evolution in Sicily in late 2020. *Front. Public Health* 11:1098965. doi: 10.3389/fpubh.2023.1098965



# A SARS-CoV-2 full genome sequence of the B.1.1 lineage sheds light on viral evolution in Sicily in late 2020

Miguel Padilla-Blanco[1†], Francesca Gucciardi[2†], Vicente Rubio[3], Antonio Lastra[2], Teresa Lorenzo[4], Beatriz Ballester[4], Andrea González-Pastor[5], Veronica Veses[4], Giusi Macaluso[2], Chirag C. Sheth[5], Marina Pascual-Ortiz[4], Elisa Maiques[4*], Consuelo Rubio-Guerri[1*], Giuseppa Purpari[2*] and Annalisa Guercio[2]

[1]Departamento de Farmacia, Facultad de Ciencias de la Salud, Universidad Cardenal Herrera-CEU (UCH-CEU), CEU Universities, Valencia, Spain, [2]Istituto Zooprofilattico Sperimentale della Sicilia "A. Mirri", Palermo, Italy, [3]Department of Genomics and Proteomics, Instituto de Biomedicina de Valencia del Consejo Superior de Investigaciones Científicas (IBV-CSIC) and Centre for Biomedical Network Research on Rare Diseases of the Instituto de Salud Carlos III (CIBERER-ISCIII), CEU Universities, Valencia, Spain, [4]Departamento de Ciencias Biomédicas, Facultad de Ciencias de la Salud, Universidad Cardenal Herrera-CEU, CEU Universities, Valencia, Spain, [5]Departamento de Medicina, Facultad de Ciencias de la Salud, Universidad Cardenal Herrera-CEU, CEU Universities, Valencia, Spain

To investigate the influence of geographic constrains to mobility on SARS-CoV-2 circulation before the advent of vaccination, we recently characterized the occurrence in Sicily of viral lineages in the second pandemic wave (September to December 2020). Our data revealed wide prevalence of the then widespread through Europe B.1.177 variant, although some viral samples could not be classified with the limited Sanger sequencing tools used. A particularly interesting sample could not be fitted to a major variant then circulating in Europe and has been subjected here to full genome sequencing in an attempt to clarify its origin, lineage and relations with the seven full genome sequences deposited for that period in Sicily, hoping to provide clues on viral evolution. The obtained genome is unique (not present in databases). It hosts 20 single-base substitutions relative to the original Wuhan-Hu-1 sequence, 8 of them synonymous and the other 12 encoding 11 amino acid substitutions, all of them already reported one by one. They include four highly prevalent substitutions, NSP12:P323L, S:D614G, and N:R203K/G204R; the much less prevalent S:G181V, ORF3a:G49V and N:R209I changes; and the very rare mutations NSP3:L761I, NSP6:S106F, NSP8:S41F and NSP14:Y447H. GISAID labeled this genome as B.1.1 lineage, a lineage that appeared early on in the pandemic. Phylogenetic analysis also confirmed this lineage diagnosis. Comparison with the seven genome sequences deposited in late 2020 from Sicily revealed branching leading to B.1.177 in one branch and to Alpha in the other branch, and suggested a local origin for the S:G118V mutation.

KEYWORDS

**SARS-CoV-2, B.1.1 variant, new sequence, virus monitorization, Sicily, COVID-19, novel SARS-CoV-2 genome sequence**

## Introduction

From the time of its emergence in late 2019 in China (1) and along the nearly 3 years of pandemic with a toll of >635 million cases and > 6.5 million deaths (2), the SARS-CoV-2 virus has evolved, accumulating mutations in its genome. This genome is a positive-sense single-stranded RNA (+ssRNA) that encodes four structural proteins (spike, S; envelope, E; matrix, M; and nucleocapsid, N), sixteen non-structural proteins (NSP1 to NSP16, all derived from the *ORF1ab* gene), and nine putative accessory factors (ORFs 3a, 3b, 6, 7a, 7b, 8, 9b, 9c,

and 10) (3) (see Figure 1 for a non-exhaustive scheme of the viral genome). Insertions, deletions, and particularly amino acid substitutions in the encoded proteins are the main actors of viral evolution, a process which is largely shaped by selection toward increased viral transmissibility, fitness and escape from antiviral challenges (antibodies and vaccines) (4). The D614G amino acid substitution in the S protein was one of the first changes that succeeded in being fixed in subsequent viral lineages since it increased viral transmissibility (5, 6) (reported up-to day in >13 million genome sequences deposited in GISAID, Figure 1). In the summer of 2020, the B.1.177 variant spreading from Spain incorporated another mutation, A222V, in the viral S protein, a change generally considered neutral (7), although such view might be challenged by the repeated events of independent re-emergence of this mutation (8). Variants B.1.160 and B.1.258 appeared approximately simultaneously with the B.1.177 variant and coexisted with it in some countries, (7, 9). They, respectively, hosted in the S protein the S477N and N439K substitutions (4), both of them mapping in the receptor binding domain (RBD) of the S protein, the part of S that mediates virus attachment to its cellular receptor (the angiotensing-converting enzyme 2, ACE2). Both mutations apparently enhanced slightly the affinity of the RBD for ACE2 (10), although these variants did not outperform B.1.177. Since then, and particularly after November 2020, new SARS-CoV-2 variants have appeared with significantly increased fitness relative to previous variants, not only in terms of transmissibility, but also in terms of evasion of neutralizing antibodies and vaccine-mediated immunity (11). Presently the World Health Organization (WHO) designates variants as Variants Being Monitored (VBMs), Variants of Interest (VOIs; presently none) or of Concern (VOCs, three in October 27, 2022, all from the Omicron lineage) for which there is either potentiality (VOIs) or clear evidence (VOCs) for increased transmissibility, severity or escape from diagnosis or from antibodies/vaccination; and, finally, Variants of High Consequence (VOHCs, presently none) which are of obligatory declaration and that are really those causing a severe and highly dangerous pandemic or highly epidemic situation [(12); and https://www.ecdc.europa.eu/en/covid-19/variants-concern].

As a part of the effort to monitor novel viral variants (13), we report here a unique variant identified by us in a retrospective study of samples collected in December 2020 in the island of Sicily (14). Among ∼60 samples analyzed, a sample revealed a novel variant that we feel merits report, as it adds substantial information in an insular area (Sicily) that hosts a relatively large population (∼5 million inhabitants) for which whole genome sequencing studies for the period of sample collection (September to December 2020) were extremely scarce (seven found in our search of GISAID: EPI_ISL_ values 2308744, 2308745, 2308746, 2308747, 2308749, 3274295, and 910332) despite the fact that >85,000 cases of COVID-19 had been diagnosed in the island by December 2020 (14). Monitoring of viral variants is an important task not only for tracing viral evolution, but also for health reasons that include the development of appropriate fast diagnostic tools and to anticipate possible vaccine evasion events in emerging variants. In addition to VOIs and VOCs, minority variants also are relevant, especially in terms of virus monitorization. In fact, some of the substitutions described for less prevalent variants have later on been reported in VOCs (13), some of them *via* independent events of re-emergence as observed for the A222V mutation in the S protein (8).

The unique SARS-CoV-2 genome sequence reported here was first identified by us by Sanger sequencing of limited regions of the genome, and then was fully confirmed as novel by next generation sequencing (NGS) of 99.7% of the viral genome. We found that the genomic sequence of this virus derives from a B.1.1 variant, but that it diverts from the canonical blueprint for this variant in an important number of changes. Thus, the viral genomic sequence reported here hosts 20 single-base substitutions (two on two adjacent bases of the same codon) resulting in 11 amino acid substitutions, of which only 4 are present in the canonical B.1.1 variant. Furthermore, the particular combination of genome sequence changes reported here has not been identified until now. Relations of the genomic sequence with the few sequences reported for that period in Sicily, and with other full genomic viral sequences are also reported here.

## Methods

### Sample procurement, processing and molecular techniques including Sanger sequencing of selected-regions, and whole-genome sequencing

The nasopharyngeal swab sample in which the present viral variant was found was procured in Palermo (Sicily, Italy) by the Virology Department of the Istituto Zooprofilattico Sperimentale della Sicilia "A. Mirri" (Palermo, Italy). This is a diagnostic center of SARS-CoV-2 and other emerging viruses that was routinely collecting nasopharyngeal swab samples for the detection of SARS-CoV-2. The collection date of our study's sample was December 4, 2020. The total RNA of our study's sample was positive for SARS-CoV-2 infection using a commercial real-time reverse transcription polymerase chain reaction assay (rRT-PCR) (14). It was sent, preserved in dry ice, for detailed molecular studies to the Health Sciences Faculty of UCH-CEU University (Valencia, Spain).

All steps involved in the molecular studies leading to Sanger sequencing of selected amplicons (Figure 1) have been reported previously by us (14). In short, following retrotranscription to cDNA, four qPCR assays were routinely carried out that provided a shortcut to typing the SARS-CoV-2 virus by using very limited automated Sanger sequencing of the four amplicons (bases 22160-22239 and 22728-23124 of the *S* gene, the longest of the two encoding part of the RBD; and bases 28871-28964 and 29558-29704 from the *N* and *ORF10* genes, respectively, Table 1). The amplicons were sequenced in a core gene sequencing facility (Príncipe Felipe Research Center of Valencia, Spain) using an ABI Prism 3730 sequencer, from Applied Biosystems (Foster City, CA, USA).

As the analysis of the sequences obtained in the Sanger approach using the Bioedit ver. 7.2.5 software (15) suggested a novel viral variant, we performed Next Generation Sequencing (NGS) of the entire viral genome by the approach described in detail in (16), in which Sequencing Multiplex SL (Valencia, Spain; a spinoff of the Health Research Institute of the Hospital Clínico de Valencia, INCLIVA) utilized Illumina NGS on cDNA retrotranscribed from the total RNA in our sample using random hexameric oligonucleotides and SuperScript IV reverse transcriptase (ThermoFisher). With this approach, 516,308 reads were obtained, and were submitted to the NCBI Sequence Read Archive (SRA) repository, under the BioProject accession number PRJNA900410. For analysis and reconstruction

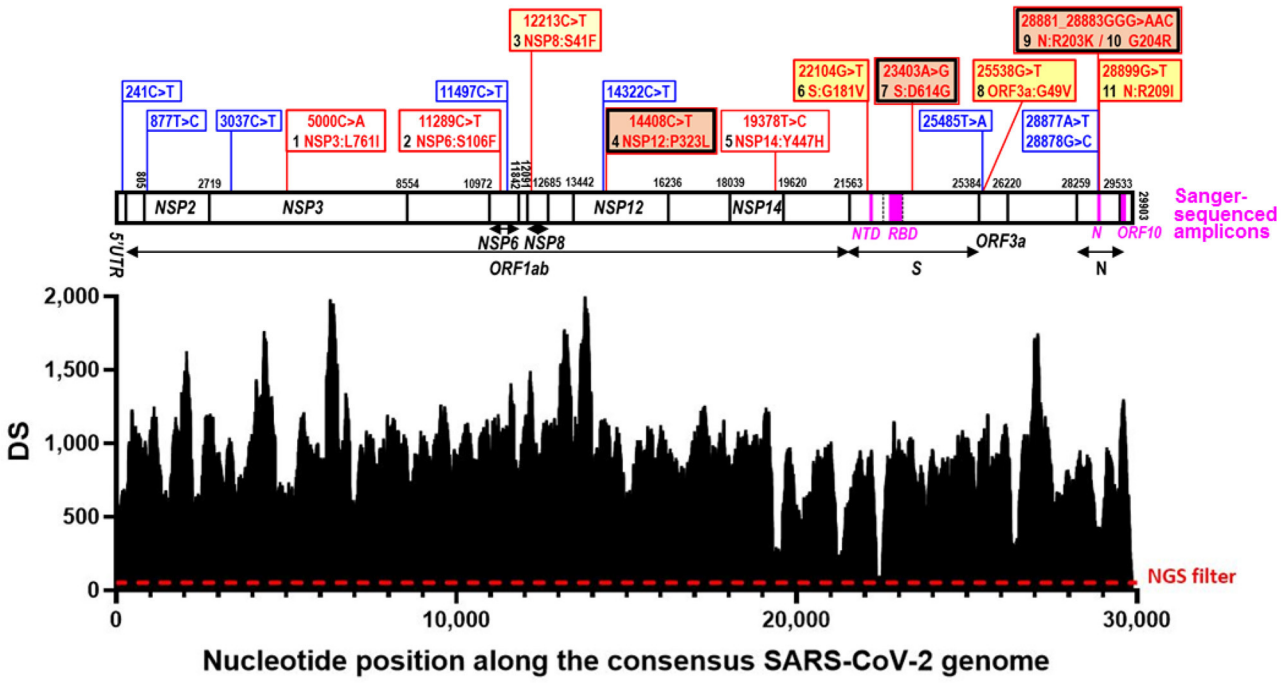


FIGURE 1
Deepness of sequencing (DS) along the viral genome and sequence variations identified. In the l*ower part,* SARS-CoV-2 genomic coverage obtained by next-generation sequencing (NGS). The horizontal axis corresponds to positions in the SARS-CoV-2 Wuhan-Hu-1 consensus genome sequence (GenBank ID: NC_045512.2) and the vertical one to the depth of the sequence (DS) at a given position. The dashed horizontal line marks the NGS filter (DS $\geq$ 50). *Above* this, aligned over the nucleotide positions, the viral genome is schematized as a horizontal bar, with identification of the genes hosting nucleotide substitutions in our reported genome. Gene boundaries are marked with vertical lines crossing the bar, giving their corresponding nucleotide position in the sequence. Gene names are inscribed into the bar or placed under it, with indication with horizontal short lines or double-pointed arrows, of their spans (including the one of *ORF1ab*, which is a polyprotein-encoding gene). The part of the *S* gene that encodes the Receptor Binding Domain (RBD) is marked within the genome bar using transversal broken lines to indicate its boundaries. The amplicons used in Sanger sequencing (Table 1) are marked as magenta-colored rectangles within the genome bar, with their abbreviated names given below in magenta. Blue and red vertical lines emerging up from the genome bar, respectively, mark synonymous and non-synonymous sequence variants, described in the corresponding banners (equally colored). For non-synonymous changes the banners inscribe the nucleotide change (nucleotide numbering is that for the complete genome) and the amino acid substitution (amino acid numbering is that for the sequence of the mature protein), also numbering in black the amino acid changes from 1 to 11 as they occur along the genome from 5′ to 3′. A double frame in black and red indicates that the amino acid change belongs to the canonical set for the B.1.1. lineage. The background color of the banner is orange for amino acid changes reported in millions of sequences, deep yellow for tens of thousands, light yellow for thousands, and white for smaller numbers. These numbers are given in Table 2.

of the whole genome sequence, the Galaxy platform (17) was used to carry out the bioinformatic analysis of the raw reads. Quality of reads was visualized using FASTQC and, using the Cutadapt software, reads with less than Q20 of quality and smaller size than 100 bp were removed, yielding 307,219 high quality sequences mapping to the SARS-CoV-2 consensus genome (Figure 1). These reads were aligned against the SARS-CoV-2 reference genome using the Burrows-Wheeler algorithm (BWA-MEM), obtaining the corresponding aligned file in BAM format, which was converted to the respective SAM binary file utilizing SAMtools. Finally, by the combination of SAMtools and BCFtools, we obtained a VCF file which contained not only the genomic positions which appeared mutated in our sample, but also the depth sequence (DS, number of times each genomic position was read by sequencing) of the vast majority of SARS-CoV-2 genomic positions. Positions which presented a DS higher than 50 and which were different to the consensus sequence in at least 75% of the reads that covered these positions were classified as mutated ones. Furthermore, the presence of these mutated positions was visualized using the Integrative Genomics Viewer (IGV) (18).

The final aligned sequence covered 99.7% of the entire viral genome, with only 90 positions of the 29,903 nucleotides of the whole reference viral genome (GenBank identifier NC_045512.2) not properly covered (positions 1–39 and 29,853–29,903) (Figure 1).

The obtained sequence was submitted to the GISAID database (19) (Accession ID: EPI_ISL_13157456). The sequence was used for BLASTN analysis (20) of GISAID and NCBI databases to test whether the obtained sequence had been reported previously. It was aligned with the consensus genome sequence and with the most relevant SARS-CoV-2 variants (including past and present VOCs). Following the alignment conducted with MAFFT aligner version 7 (21), aligned sequences were subjected to phylogenetic analysis using the MEGA11 software (22), as previously reported (16). In brief, distance matrices were calculated, and tree topology was inferred by the maximum likelihood method based on p-distances (bootstrap on 2,000 replicates, generated with a random seed). This process was

10.3389/fpubh.2023.1098965

TABLE 1 Nucleotide and amino acid substitutions found after Sanger sequencing of the four PCR-amplified viral genomic regions.

| qPCR reaction | Genomic target region/amplicon[a] | Nucleotide substitution[b] | Amino acid substitution[c] | GenBank accession number | Amino acid substitution searched for[c] | Known SARS-CoV-2 variants that could be detected |
|---|---|---|---|---|---|---|
| 1 | *S* (*NTD*)/22160-22239 | None found | None | OP618232 | S:A222V | B.1.177 |
| 2 | *N*/28871-28964 | 28877_28878 AG > TC | Synonymous | OP620391 | N:A220V | |
| | | 28881_28882 GG > AA | N:R203K | | | |
| | | 28883 G > C | N:G204R | | | |
| | | 28899 G > T | N:R209I | | | |
| 3 | *ORF10*/29558-29704 | None found | None | OP618233 | ORF10:V30L | |
| 4 | *S* (*RBD*)/22728-23124 | None found | None | OP618234 | S:N501Y | B.1.1.7 (Alpha) |
| | | | | | S:K417T<br>S:E484K<br>S:N501Y | P.1 (Gamma) |

The sequences obtained have been submitted to GenBank with the Accession Numbers given (column 5). The qPCR reactions were carried out to detect the changes causing the amino acid substitutions indicated in column 6 in order to identify the SARS-CoV-2 variants indicated in the last column.

[a]Figures refer to nucleotide positions in the whole genome reference sequence NC_0455.12.

[b]Substitution relative to the base in the consensus genome. As the sequencing was based on the genome retrotranscribed to DNA, thymine should correspond to uracil in the viral RNA genome.

[c]Amino acid positions are those for the encoded protein.

done, too, with the seven viral sequences from Sicily deposited in GISAID for the period of September to December of 2020.

## Results

As a shortcut to differentiate among major pre-existing variants, and particularly to identify B.1.177, a variant which was highly prevalent in Europe at the time of collection of this sample (7), we first PCR-amplified and Sanger-sequenced four genomic regions (Figure 1 horizontal bar; and Table 1). Analysis of three regions corresponding to the part of the *S* gene that encodes the N-terminal domain (NTD) of the S protein and two regions within the coding sequences of the *N* and *ORF10* genes (Table 1) did not uncover any characteristic B.1.177 substitutions, revealing instead in the *N* gene six nucleotide substitutions clustered in a group of two adjacent ones (affecting the same codon and constituting a synonymous change); in another group of three adjacent ones (affecting two successive codons, causing the two amino acids substitution R203K/G204R in the N protein) and a third isolated substitution also causing a non-synonymous change in the N protein (R209I). The R203K and G204R substitutions in the N protein are observed in the Alpha (B.1.1.7) and Gamma (P.1) variants, two variants that in December 2020 were increasing their prevalence and were of concern (9). For differentiation between Alpha and Gamma variants we used the fourth Sanger-sequenced amplicon. This amplicon encompasses a central region of the *S* gene that encodes a part of the receptor binding domain (RBD) of the S protein. Alpha and Gamma variants contain therein a unique combination of marker substitutions (Table 1) (9). To our surprise, we did not find in this amplicon any amino acid substitutions characteristic of these variants, failing to support the identification of our viral sample as belonging to the Alpha, Gamma or to the B.1.177 lineages. This strongly suggested that the virus in this sample represented a different, perhaps new variant, prompting us to use whole-genome sequencing by NGS to try to characterize it.

Of the 29,903 nucleotides of the complete reference sequence of the SARS-CoV-2 genome, our NGS approach generated high-quality sequence of appropriate deepness (see Methods) for nucleotides 40 to 29,853, corresponding to 99.7 % of the whole genome viral reference sequence (Figure 1). The sequence was assembled with appropriate bioinformatics tools (see Methods), identifying 20 base substitutions relative to the reference sequence, of which 12 were nonsynonymous substitutions (11 amino acid substitutions) and 8 were synonymous changes (Figure 1 and Table 2). Based on the SARS-CoV-2 variant classification of GISAID, the virus was automatically assigned by the GISAID server to the B.1.1 lineage, a European lineage traced back to the 4th of January of 2020 with 3 clear single nucleotide substitutions, 28881 G>A, 28882 G>A and 28883 G>C (23), all three present in our genomic sequence (Figure 1). The COV-LINEAGES organization webpage, visited on November 1, 2022 (23), gives 22,790 and 50,400 viral genomes designated and adscribed, respectively, to the B.1.1 lineage. Our sequence carries four of the five changes given in (23) as present in at least 75% of the sequences corresponding to the B.1.1 lineage: NSP12:P323L (equivalent to ORF1b:P314L; mapping in the NSP12 protein), S:D614G (S protein), and N:R203K and N:G204R (N protein) (Figure 1 and Table 2, banners with an inner black frame), only lacking the lineage marker mutation ORF8:S84L (ORF8 protein). The occurrence in our genomic sequence of four of the 5 marker sequence changes shared by 75% of the viral isolates ascribed to the B.1.1 lineage reinforce the adscription of our viral sample to that lineage. This adscription is supported, too, by the results of phylogenetic analysis that showed (Figure 2A) that our genome sequence clusters together with B.1.1 viral sequences (for simplicity, only one shown in Figure 2A).

In addition to the presence of four of the five "marker" mutations of the lineage, our genome sequence revealed seven additional non-synonymous sequence variations that are not characteristic of the B.1.1 lineage and that affect proteins NSP3, NSP6, NSP8, NSP14, S, ORF3a and N (abbreviated as mutations 1, 2, 3, 5, 6, 8, and 11, respectively; Figure 1 and Table 2). None of these amino acid changes was unreported, as shown by their occurrence in sequences

10.3389/fpubh.2023.1098965

TABLE 2 Base substitutions found by NGS of the viral genome, and corresponding amino acid substitutions, indicating the abundance and frequency of each amino acid change among the genome sequences deposited in the GISAID database on December 4, 2020 and, after the slash, on November 2, 2022.

| Base change[a] | Gene | Encoding mature protein | Amino acid substitution[b] | | | | ¿Change present in canonical B.1.1? |
|---|---|---|---|---|---|---|---|
| | | | No. | Change | Abundance in GISAID[c] | Frequency in GISAID (%)[c] | |
| 241 C > T | *5′ UTR* | – | – | – | NT | NT | NO |
| 877 T > C | *ORF1ab* | NSP2 | – | – | NT | NT | NO |
| 3037 C > T | | NSP3 | – | – | NT | NT | NO |
| 5000 C > A | | | 1 | NSP3:L761I | 19/1,196 | 0.003/0.009 | NO |
| 11289 C > T | | NSP6 | 2 | NSP6:S106F | 180/847 | 0.032/0.006 | NO |
| 11497 C > T | | | – | – | NT | NT | NO |
| 12213 C > T | | NSP8 | 3 | NSP:S41F | 208/3,111 | 0.037/0.023 | NO |
| 14322 C > T | | NSP12 | – | – | NT | NT | NO |
| 14408 C > T | | | 4 | NSP12:P323L | 0.5/13.3 ($\times 10^6$) | 93.21/97.25 | YES |
| 19378 T > C | | NSP14 | 5 | NSP14:Y447H | 15/556 | 0.003/0.004 | NO |
| 22104 G > T | *S* | S | 6 | S:G181V | 758/40,256 | 0.135/0.295 | NO |
| 23403 A > G | | | 7 | S:D614G | 0.5/13.3 ($\times 10^6$) | 93.96/99.19 | YES |
| 25485 T > A | *ORF3a* | ORF3a | – | – | NT | NT | NO |
| 25538 G > T | | | 8 | ORF3a:G49V | 229/38,469 | 0.041/0.283 | NO |
| 28877 A > T | *N* | N | – | – | NT | NT | NO |
| 28878 G > C[d] | | | – | – | NT | NT | NO |
| 28881 G > A[d] | | | 9 | N:R203K | 0.16/7.6 ($\times 10^6$) | 29.55/56.27 | YES |
| 28882 G > A[d] | | | | | | | |
| 28883 G > C[d] | | | 10 | N:G204R | 0.16/7.6 ($\times 10^6$) | 29.30/55.72 | YES |
| 28899 G > T[d] | | | 11 | N:R209I | 2,693/12,880 | 0.481/0.094 | NO |

[a]Nucleotide position, and substitution relative to the consensus SARS-CoV-2 Wuhan-Hu-1 genome (GenBank NC_045512.2). As the sequencing was based on the genome retrotranscribed to DNA, thymine should correspond to uracil in the viral RNA genome.
[b]Amino acid positions are those for the mature proteins.
[c]On December 4, 2020/November 2, 2022. NT, not tested.
[d]Detected by both Sanger sequencing of amplicons and by NGS of the whole genome.

previously deposited in the GISAID database (Table 2). All of them had already been reported by the date of collection of our sample in early December 2020 (Table 2), although two of them, 1 and 5 (affecting NSP3 and NSP14, respectively), had only been reported in very few sequences (<20 genomes) (Table 2). None of these two variants as well as the non-synonymous changes 2 (in NSP6) and 3 (in NSP8) has spread much, having been reported in <0.025% of the >13.6 million viral genomic sequences now deposited in GISAID. This low frequency does not support a substantial effect of these mutations on viral fitness. Variants 6, 8, and 11 (affecting S, ORF3a and N proteins, respectively; Figure 1, banners in deep yellow color) appear to have been somewhat more successful in spreading, as they have been found in, respectively, 40,256, 38,461, and 12,880 viral genomes deposited in GISAID. Only 11 genomic sequences deposited up to now in GISAID combine these three last sequence variants with the four highly prevalent sequence variants (sequence variants in orange and in deep yellow in Figure 1, giving the combination of variants, 4, 6, 7, 8, 9, 10, and 11). This occurrence is lower (8 instances) when mutation 1 is added to the above set of non-synonymous substitutions. Addition of any other of the three remaining variants, 2, 3, or 5, reduces the number of sequences to 1, our own sequence, that thus, it is unique in the database. This last result agrees with our independent BLASTN analysis carried out with the entire databases of full genome sequences deposited in GISAID and GenBank, which failed to identify any sequence with the full set of non-synonymous mutations identified in our genomic sequence.

We also investigated by phylogenetic analysis (Figure 2B) the degree of closeness of this novel viral genome sequence with the other seven SARS-CoV-2 genomic sequences reported in the period of September to December of 2020. Two of these genomes (labeled 3 and 4 in Figure 2B) belong to the B.1 lineage and can be considered the stem from which all other sequences in this group of eight sequences have evolved. This diversification occurred in two separate branches (Figure 2B). One branch encompasses four viral isolates (sequences labeled 5, 6, 7, and 8 in Figure 2B), which belong to the B.1.177 and B.1.177.75 lineages. The other branch encompasses the viral genome reported here and the one labeled 1 in Figure 2B, respectively belonging to B.1.1 and B.1.1.7 (Alpha) lineages. This phylogenic tree, which is based on the alignment of the entire genome sequences, thus taking into consideration synonymous and non-synonymous sequence changes, is confirmed by just looking at the non-synonymous changes observed in these eight

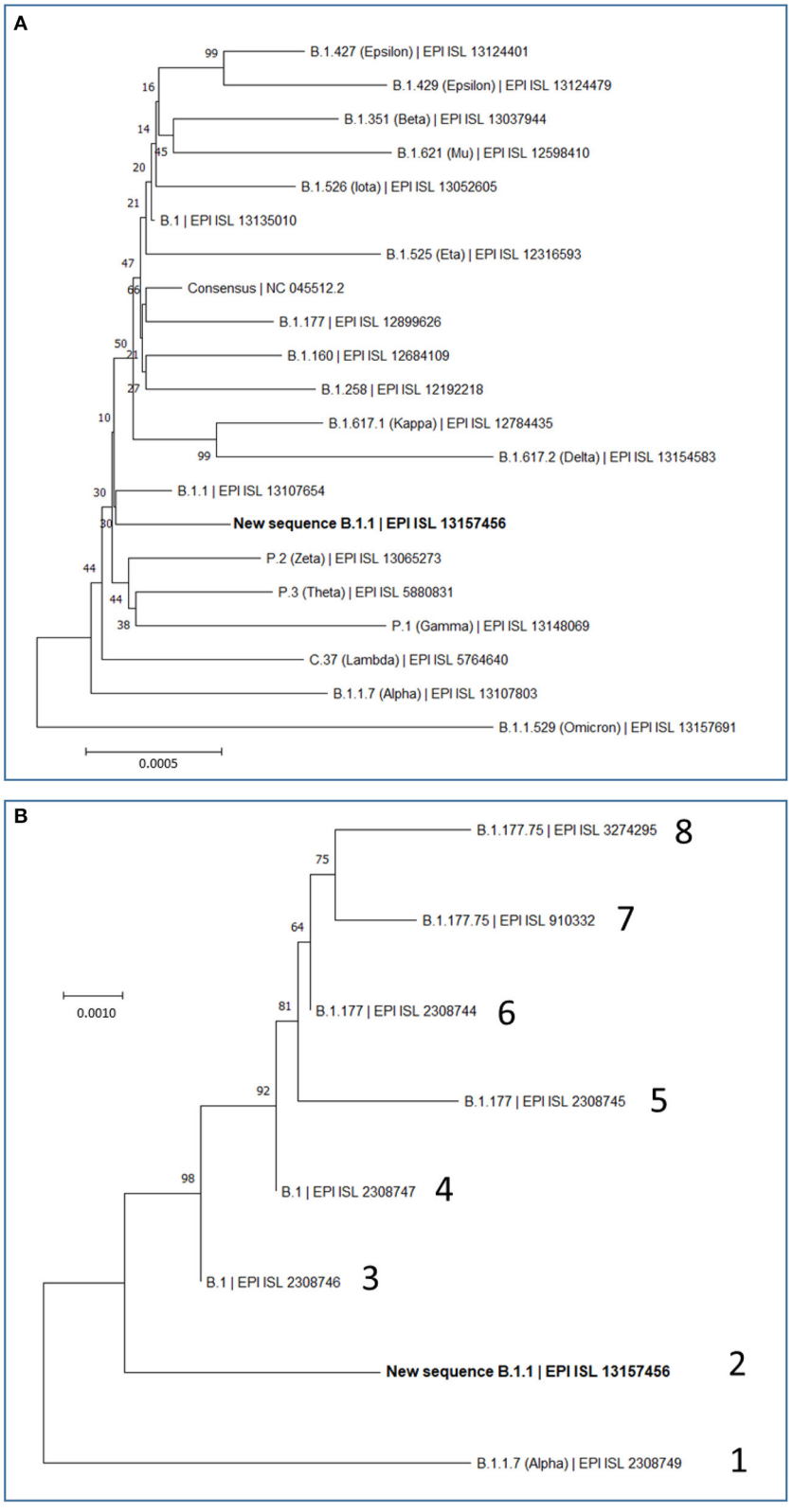


FIGURE 2
Maximum Likelihood Trees based on complete SARS-CoV-2 genomes. Evolutionary analyses were conducted in MEGA (see Methods), inferring the histories using the neighbor-joining method. Optimal trees are shown. The percentage of replicate trees in which the associated taxa clustered together is shown next to the branches. The scale bars measure phylogenetic distances as the indicated nucleotide substitutions per site. Optimal trees are shown. Trees are drawn to scale, with branch length in the same units as those of the evolutionary distance used to infer the phylogenetic tree. **(A)** Phylogenetic relations of our new B.1.1 sequence in the context of the most relevant SARS-CoV-2 variants, including variants which during the pandemic have been considered at least once as VOCs (Alpha, Beta, Gamma, Delta and Omicron) or VOIs (Epsilon, Mu, Iota, Eta, Kappa, Zeta, Theta, and Lambda), and also including the most prevalent variants (B.1, B.1.177, B.1.160, and B.1.258) that were circulating in Europe before the collection date of our study's sample.
*(Continued)*

FIGURE 2 (Continued)
This analysis involved 21 nucleotide sequences, with a total of 29,919 position in the final dataset. **(B)** Phylogenetic relations of our new B.1.1 sequence with the seven previously reported SARS-CoV-2 sequences from Sicily in the time spanning between September and December 2020. Sequence lineage and GISAID ID are given for each genome, giving it an arbitrary number (1–8). Our new B.1.1 sequence is highlighted in bold in **(A, B)**.

sequences (Supplementary Table 1). Only two amino acid changes, NSP12:P323L and S:D614G, are common to all eight sequences of Figure 2B. The top branch exhibits the S:A222V sequence that was very prevalent in Europe after the summer of 2020, having apparently spread from Spain, while the lower branch exhibits the characteristic N:R203K and N:G204R variants that emerged much earlier, in January 2020, in the B.1.1 lineage.

## Discussion

This study characterizes a novel SARS-CoV-2 variant that occurred in Sicily in the second wave of COVID-19, when the B.1.177 variant was the predominating lineage circulating through the island (14). Our novel variant has not been reported anywhere else, judged from its lack of deposit into the GISAID and GenBank databases, but it can be classified as belonging to lineage B.1.1. This last lineage had emerged very early on in the pandemic and incorporated the most successful [in terms of spreading (24)] combination of non-synonymous variants NSP12:P323L and S:D614G (Table 2). The mechanism of the effects of the NSP12 protein mutations P323L that led it to cosegregate with the S protein mutation D614G remain uncertain. NSP12 is the catalytic, major component of RNA-dependent RNA polymerase (RdRp) (25, 26), and the P323L substitution maps in the interaction domain of this polymerase (27). It is tempting to speculate that this mutation could favor the emergence of novel viral variants by impairing the 3′ to 5′ exonuclease proofreading activity of RdRp thus decreasing replication fidelity. This would agree with the observation of rapid generation of novel variants that occurred after the B.1 variant emerged and that accelerated later on (see the Introduction), although it is true that the appearance of novel variants must have also been favored by the increase of the number of infections occurring worldwide as COVID-19 crossed country boundaries and became a pandemic. In addition, this mutation may have helped the virus escape from antibodies raised in patients previously infected by the original Wuhan variant (28). This advantage should not be diminished by the fact that remdesivir, widely used in the treatment of severe COVID-19, appears to exhibit more affinity for the mutant form of RdRp than for the previous form of this enzyme not hosting this mutation (29), since only a minority of the infected population is treated with remdesivir (possibly <10% of the infected people).

In any case, our variant characterization and its comparison with the other seven viral specimens characterized in Sicily by having their whole genome sequenced in late 2020, help recreate a scenario in which two separating lineage branches were largely imported. Nevertheless, our viral isolate might attest some degree of local evolution toward the Alpha (B.1.1.7) lineage represented in one of the 8 sequenced genomes studied from late 2020 (Figure 2B). The uniqueness of the sequence reported here suggests some limited local evolution from the imported parental B.1.1 lineage. Whichever the level of local evolution, the main message of the observation of these 8 fully characterized Sicilian viral sequences is that variants roaming though continental Europe were also circulating in the island. This agrees with our previous conclusion based on the study of 54 viral samples obtained in Palermo (14), that isolation due to the insularity of Sicily was not an important factor, at least for the second-wave period of the pandemic, a period that did not show founder effects that could reveal the potential isolation due to insularity. Nevertheless, given the fact that S protein mutations are particularly prone to impact on virus fitness and on its escape from pre-existing antibodies (30), it is interesting that, of the two S protein amino acid variants observed in our viral genome, the G181V substitution has had modest but substantial success (Table 2) and appears to have a local origin. Thus, this mutation was found in the second half of year 2021 in 7 of 252 genotypes of the then dominant Delta lineage in the Italian mainland region of Calabria (31), which is the closest part of peninsular Italy to Sicily (from which it is separated only by the Messina straight) supporting the regional origin of this mutation. These facts render desirable the experimental investigation of the effects of this mutation on viral infectivity and sensitivity to antibodies.

Also interesting for its potential consequences is the G49V mutation in ORF3a, since G49 sits in the center of the hydrophobic cluster that seals the pore formed by the homodimer of this channel protein (Protein Databank entry 7KJR, https://www.rcsb.org/structure/7KJR) (32). ORF3a is emerging as a key element in the pathogenicity of COVID-19, mediating apoptotic and autophagy-related proinflammatory effects of the viral infection (33, 34) possibly by allowing $Ca^{2+}$influx into the cell, as this cation has been shown to be channeled across membranes by the ORF3a dimer (32). The ORF3a transmembrane pore is sealed at membrane level by a hydrophobic patch of residues that glues together its six (three per subunit) transmembrane helices. This patch centrally includes G49 (belonging to transmembrane helix 1). The replacement by valine of G49 in the G49V mutant might distort the 6-helix bundle of the dimer that constitutes the closed pore, possibly increasing the frequency of the opening and $Ca^{2+}$ passage, thus increasing disease severity by enhancing the proinflammatory and apoptotic potential of the virus. This possibility, and the modest but substantial success (Table 2) of this ORF3a variant, possibly justifies the experimental testing of the consequences of this amino acid substitution.

Of the other substitutions in our viral genome, the NSP12:P323L and S:D614G mutations are well-known for being epidemiologically very successful (24) but also for having been found more frequently in patients suffering severe COVID-19 than in those patients with milder COVID-19 (35). Similarly, the epidemiologically highly successful double substitution in the N protein R203K/G204R, has been reported to increase viral infectivity, fitness, and virulence and to promote a subgenomic RNA promoting recombination (36, 37). These effects of the N:R203K/G204R mutations might be further enhanced in the present virus by the coexistence of N:R209I, a drastic amino acid substitution just five amino acids downstream from the N:G204R mutation.

In contrast to the above-mentioned substitutions, amino acid changes 1, 2, 3, and 5 appear of little concern, given their very low representation in the mutational universe of SARS-CoV-2. In particular, the L761I substitution in NSP3 is chemically trivial and thus probably neutral, and the S106F substitution in NSP6, although chemically drastic, affects a site that may be tolerant to sequence variation since S106 sits in an extracellular loop of the NSP6 membrane protein (38) in a site of lesser conservation where it is flanked by large hydrophobic residues (LSGF; hydrophobic residues underlined; S in bold-type).

In conclusion, this study retrospectively characterizes a unique viral variant found in Sicily in late 2020 that belongs to the B.1.1 lineage but which also exhibits a relatively large constellation of amino acid substitutions additionally to lineage marker mutations. Our sequence exemplifies the convenience of continuous monitoring SARS-CoV-2 sequences to understand virus evolution. This provides much needed information for a period and location for which the circulating viral lineages were very scarcely explored. The comparison of this genome sequence with the few other whole genome sequences of SARS-CoV-2 obtained at the same location and time supports a dynamic interaction of the island with continental Italy and Europe, but does not exclude some contribution of founder effects, exemplified here in an S protein mutation found in significant but not majority ratios 6 months later in Calabria, just across the Messina straight.

## Data availability statement

The datasets presented in this study can be found in online repositories. The name of the repository and accession number can be found below: NCBI Sequence Read Archive; PRJNA900410.

## Ethics statement

The studies involving human participants were reviewed and approved by Ethics Committee of Cardenal Herrera CEU University, Valencia, Spain (no. CEI20/083 released on 10/09/2020), and it is in agreement with the Helsinki Declaration.

## Author contributions

VR, EM, CR-G, GP, and AG conceived the study. FG, AL, GM, GP, and AG performed molecular SARS-CoV-2 detection. MP-B, TL, BB, and AG-P did the molecular variant characterization and bioinformatic analysis. MP-B, VV, CS, and MP-O performed the phylogenetic analysis. MP-B and VR did the GISAID work. MP-B, BB, VR, EM, and CR-G analyzed the results. MP-B, FG, BB, VR, EM, CR-G, GP, and AG were responsible for writing the paper. All authors contributed to this task, making substantial intellectual contributions, and having read, corrected, and approved the manuscript.

## Funding

This research received external funding to CR-G from Conselleria de Innovación Universidades, Ciencia y Sociedad Digital: Subvenciones a Grupos de Investigación Emergentes (Ref, GV/2021/163); to VR from the Agencia Estatal de Investigación of the Spanish Government (Ref PID2020-120322RB-C21) and the European Commission-NextGeneration EU CSIC Global Health Platform, Spanish Ministry of Science and Innovation (Ref MCIN/AEI/10.13039/501100011033); and to the Istituto Zooprofilattico Sperimentale della Sicilia A. Mirri by the Project COVID-19: Traiettorie Evolutive di SARS-CoV-2 ed Indagine Sul Ruolo Degli Animali (IZS SI 03/20 RC), funded by the Italian Ministry of Health.

## Acknowledgments

We wish to express our gratitude to the sequencing services of Príncipe Felipe Research Center and Sequencing Multiplex SL (Valencia, Spain) for their magnificent professionalism, and to Nadine Gougeard (IBV-CSIC/CIBERER) for help with securing materials.

## Conflict of interest

The authors declare that the research was conducted in the absence of any commercial or financial relationships that could be construed as a potential conflict of interest.

## Publisher's note

All claims expressed in this article are solely those of the authors and do not necessarily represent those of their affiliated organizations, or those of the publisher, the editors and the reviewers. Any product that may be evaluated in this article, or claim that may be made by its manufacturer, is not guaranteed or endorsed by the publisher.

## Supplementary material

The Supplementary Material for this article can be found online at: https://www.frontiersin.org/articles/10.3389/fpubh.2023.1098965/full#supplementary-material

## References

1. Zhu N, Zhang D, Wang W, Li X, Yang B, Song J, et al. A novel coronavirus from patients with pneumonia in China, 2019. *N Engl J Med*. (2020) 382:722–33. doi: 10.1056/NEJMoa2001017

2. Coronavirus Resource Center. *Coronavirus COVID-19 Global Cases by the Center for Systems Science and Engineering (CSSE)*. Johns Hopkings Coronavirus Resource Center. Available online at: https://coronavirus.jhu.edu/map.html (accessed October 12, 2022).

3. Gordon DE, Jang GM, Bouhaddou M, Xu J, Obernier K, White KM, et al. A SARS-CoV-2 protein interaction map reveals targets for drug repurposing. *Nature*. (2020) 583:459–68. doi: 10.1038/s41586-020-2286-9

4. Mistry P, Barmania F, Mellet J, Peta K, Strydom A, Viljoen IM, et al. SARS-CoV-2 variants, vaccines, and host immunity. *Front Immunol*. (2022) 12:809244. doi: 10.3389/fimmu.2021.809244

5. Korber B, Fischer WM, Gnanakaran S, Yoon H, Theiler J, Abfalterer W, et al. Tracking changes in SARS-CoV-2 spike: evidence that D614G increases infectivity of the COVID-19 virus. *Cell*. (2020) 182:812–27. doi: 10.1016/j.cell.2020.06.043

6. Volz E, Hill V, McCrone JT, Price A, Jorgensen D, O'Toole Á, et al. Evaluating the effects of SARS-CoV-2 spike mutation D614G on transmissibility and pathogenicity. *Cell*. (2021) 184:64–75. doi: 10.1101/2020.07.31.20166082

7. Hodcroft EB, Zuber M, Nadeau S, Vaughan TG, Crawford KHD, Althaus C, et al. Spread of a SARS-CoV-2 variant through Europe in the summer of 2020. *Nature*. (2021) 595:707–12. doi: 10.1101/2020.10.25.20219063

8. Ginex T, Marco-Marín C, Wieczór M, Mata CP, Krieger J, Ruiz-Rodriguez P, et al. The structural role of SARS-CoV-2 genetic background in the emergence and success of spike mutations: the case of the spike A222V mutation. *PLoS Pathog*. (2022) 18:e1010631. doi: 10.1371/journal.ppat.1010631

9. *CoVariants*. Available online at: https://covariants.org/ (accessed October 12, 2022).

10. Chen J, Wang R, Wang M, Wei G-W. Mutations strengthened SARS-CoV-2 infectivity. *J Mol Biol*. (2020) 432:5212–26. doi: 10.1016/j.jmb.2020.07.009

11. Hirabara SM, Serdan TDA, Gorjao R, Masi LN, Pithon-Curi TC, Covas DT. SARS-CoV-2 variants: differences and potential of immune evasion. *Front Cell Infect Microbiol*. (2022) 11:781429. doi: 10.3389/fcimb.2021.781429

12. World Health Organization. *Tracking SARS-CoV-2 Variants*. Available online at: https://www.who.int/activities/tracking-SARS-CoV-2-variants (accessed October 12, 2022).

13. Smyth DS, Trujillo M, Gregory DA, Cheung K, Gao A, Graham M. Tracking cryptic SARS-CoV-2 lineages detected in NYC wastewater. *Nat Commun*. (2022) 13:635. doi: 10.1038/s41467-022-29573-1

14. Padilla-Blanco M, Gucciardi F, Guercio A, Rubio V, Princiotta A, Veses V, et al. Pilot investigation of SARS-CoV-2 variants in the island of Sicily prior to and in the second wave of the COVID-19 pandemic. *Front Microbiol*. (2022) 13:869559. doi: 10.3389/fmicb.2022.869559

15. Hall T. BioEdit: a user-friendly biological sequence alignment editor and analysis program for windows 95/98/NT. *Nucleic Acids Symp Ser*. (1999) 41:5–8.

16. Padilla-Blanco M, Vega S, Enjuanes L, Morey A, Lorenzo T, Marín C, et al. Detection of SARS-CoV-2 in a dog with hemorrhagic diarrhea. *BMC Vet Res*. (2022) 18:370. doi: 10.1186/s12917-022-03453-8

17. *Galaxy Platform*. Available online at: https://usegalaxy.org/ (accessed October 12, 2022).

18. Robinson JT, Thorvaldsdóttir H, Wenger AM, Zehir A, Mesirov JP. Variant review with the integrative genomics viewer. *Cancer Res*. (2017) 77:e31–4. doi: 10.1158/0008-5472.CAN-17-0337

19. *GISAID*. Available online at: https://gisaid.org/ (accessed October 12, 2020).

20. *BLASTN – NCBI*. Available online at: https://blast.ncbi.nlm.nih.gov/Blast.cgi (accessed October 12, 2022).

21. Katoh K, Misawa K, Kuma K, Miyata T. MAFFT: a novel method for rapid multiple sequence alignment based on fast Fourier transform. *Nucleic Acids Res*. (2022) 30:3059–66. doi: 10.1093/nar/gkf436

22. Tamura K, Stecher G, Kumar S. MEGA11: molecular evolutionary genetics analysis version 11. *Mol Biol Evol*. (2021) 38:3022–7. doi: 10.1093/molbev/msab120

23. *Cov-lineages – B.1.1 Variant*. Available online at: https://outbreak.info/situation-reports?pango=B.1.1 (accessed October 12, 2022).

24. Ilmjärv S, Abdul F, Acosta-Gutiérrez S, Estarellas C, Galdadas J, Casimir M, et al. Concurrent mutations in RNA-dependent RNA polymerase and spike protein emerged as the epidemiologically most successful SARS-CoV-2 variant. *Sci Rep*. (2022) 11:13705. doi: 10.1038/s41598-021-91662-w

25. Robson F, Khan KS, Le TK, Paris C, Demirbag S, Barfuss P, et al. Coronavirus RNA proofreading: molecular basis and therapeutic targeting. *Mol Cell*. (2020) 79:710–27. doi: 10.1016/j.molcel.2020.07.027

26. Pachetti M, Marini B, Benedetti F, Giudici F, Mauro E, Storici P, et al. Emerging SARS-CoV-2 mutation hot spots include a novel RNA-dependent-RNA polymerase variant. *J Transl Med*. (2020) 18:179. doi: 10.1186/s12967-020-02344-6

27. Hillen HS, Kokic G, Farnung L, Dienemann C, Tegunov D, Cramer P. Structure of replicating SARS-CoV-2 polymerase. *Nature*. (2020) 584:154–6. doi: 10.1038/s41586-020-2368-8

28. Gupta AM, Mandal S, Mandal S, Chakrabarti J. Immune escape facilitation by mutations of epitope residues in RdRp of SARS-CoV-2. *J Biomol Struct Dyn*. (2022) 1–11. doi: 10.1080/07391102.2022.2051746

29. Mohammad A, Al-Mulla F, Wei D-Q, Abubaker J. Remdesivir MD simulations suggest a more favourable binding to SARS-CoV-2 RNA dependent RNA polymerase mutant P323L than wild-type. *Biomolecules*. (2021) 11:919. doi: 10.3390/biom11070919

30. Xia X. Domains and functions of spike protein in SARS-CoV-2 in the context of vaccine design. *Viruses*. (2021) 13:109. doi: 10.3390/v13010109

31. De Marco C, Veneziano C, Massacci A, Pallocca M, Marascio N, Quirino A, et al. Dynamics of viral infection and evolution of SARS-CoV-2 variants in the Calabria area of Southern Italy. *Front Microbiol*. (2022) 13:934993. doi: 10.3389/fmicb.2022.934993

32. Kern DM, Sorum B, Mali SS, Hoel CM, Sridharan S, Remis JP, et al. Cryo-EM structure of SARS-CoV-2 ORF3a in lipid nanodiscs. *Nat Struct Mol Biol*. (2021) 28:573–82. doi: 10.1038/s41594-021-00619-0

33. Ren Y, Shu T, Wu D, Mu J, Wang C, Huang M, et al. The ORF3a protein of SARS-CoV-2 induces apoptosis in cells. *Cell Mol Immunol*. (2020) 17:881–3. doi: 10.1038/s41423-020-0485-9

34. Zhang X, Yang Z, Pan T, Long X, Sun Q, Wang PH, et al. SARS-CoV-2 ORF3a induces RETREG1/FAM134B-dependent reticulophagy and triggers sequential ER stress and inflammatory responses during SARS-CoV-2 infection. *Autophagy*. (2022) 18:2576–92. doi: 10.1080/15548627.2022.2039992

35. Biswas SK, Mudi SR. Spike protein D614G and RdRp P323L: the SARS-CoV-2 mutations associated with severity of COVID-19. *Genomics Inform*. (2020) 18:e44. doi: 10.5808/GI.2020.18.4.e44

36. Wu H, Xing N, Meng K, Fu B, Xu W, Dong P, et al. Nucleocapsid mutations R203K/G204R increase the infectivity, fitness, and virulence of SARS-CoV-2. *Cell Host Microbe*. (2021) 29:1788–801. doi: 10.1016/j.chom.2021.11.005

37. Leary S, Gaudieri S, Parker MD, Chopra A, Jamer I, Pakala S, et al. Generation of a novel SARS-CoV2 sub-genomic RNA due to the R203K/G204R variant in nucleocapsid: homologous recombination has potential to change SARS-CoV-2 at both protein and RNA level. *Pathog Immun*. (2021) 6:27–49. doi: 10.20411/pai.v6i2.460

38. Baliji S, Cammer SA, Sobral B, Baker SC. Detection of nonstructural protein 6 in murine coronavirus-infected cells and analysis of the transmembrane topology by using bioinformatics and molecular approaches. *J Virol*. (2009) 83:6957–62. doi: 10.1128/JVI.00254-09

frontiers | Frontiers in Medicine

TYPE Original Research
PUBLISHED 02 March 2023
DOI 10.3389/fmed.2023.1031455



OPEN ACCESS

EDITED BY
Xinyu Feng,
Chinese Center for Disease Control and Prevention, China

REVIEWED BY
Juan Diego Maya,
University of Chile,
Chile
Lúcia Maria Da Cunha Galvão,
Federal University of Rio Grande do Norte,
Brazil
Diana Carolina Hernández Castro,
Rosario University,
Colombia

*CORRESPONDENCE
Fred Luciano Neves Santos
✉ fred.santos@fiocruz.br

SPECIALTY SECTION
This article was submitted to Infectious Diseases: Pathogenesis and Therapy, a section of the journal Frontiers in Medicine

RECEIVED 30 August 2022
ACCEPTED 10 February 2023
PUBLISHED 02 March 2023

CITATION
Iturra JAD, Leony LM, Medeiros FAC, Souza Filho JAd, Siriano LdR, Tavares SBdN, Luquetti AO, Belo VS, Sousa ASd and Santos FLN (2023) A multicenter comparative study of the performance of four rapid immunochromatographic tests for the detection of anti-*Trypanosoma cruzi* antibodies in Brazil.
*Front. Med.* 10:1031455.
doi: 10.3389/fmed.2023.1031455



# A multicenter comparative study of the performance of four rapid immunochromatographic tests for the detection of anti-*Trypanosoma cruzi* antibodies in Brazil

Jacqueline Araújo Domingos Iturra[1], Leonardo Maia Leony[2], Fernanda Alvarenga Cardoso Medeiros[1], Job Alves de Souza Filho[1], Liliane da Rocha Siriano[3], Suelene Brito do Nascimento Tavares[3], Alejandro Ostermayer Luquetti[3], Vinícius Silva Belo[4], Andréa Silvestre de Sousa[5,6] and Fred Luciano Neves Santos[2,6]*

[1]Parasitic Diseases Service, Ezequiel Dias Foundation (FUNED), Belo Horizonte, Minas Gerais, Brazil, [2]Advanced Public Health Laboratory, Gonçalo Moniz Institute, Oswaldo Cruz Foundation (FIOCRUZ-BA), Salvador, Bahia, Brazil, [3]Chagas Disease Study Center (NEDoC), University Hospital, Federal University of Goiás (UFG), Goiânia, Goiás, Brazil, [4]Department of Health Sciences, Federal University of São João Del-Rei (UFSJ), Divinópolis, Minas Gerais, Brazil, [5]Evandro Chagas National Institute of Infectious Diseases, Oswaldo Cruz Foundation (FIOCRUZ-RJ), Rio de Janeiro, Brazil, [6]Integrated Translational Program in Chagas Disease from FIOCRUZ (Fio-Chagas), Oswaldo Cruz Foundation (FIOCRUZ-RJ), Rio de Janeiro, Brazil

Diagnosis of *Trypanosoma cruzi* (*T. cruzi*) infection in the chronic phase of Chagas disease (CD) is performed by serologic testing. Conventional tests are currently used with very good results but require time, laboratory infrastructure, and expertise. Rapid diagnostic tests (RDTs) are an alternative as the results are immediate and do not require specialized knowledge, making them suitable for epidemiologic studies and promising as a screening tool. Nevertheless, few studies conducted comparative evaluations of RDTs to validate the results and assess their performance. In this study, we analyzed four trades of rapid tests (OnSite Chagas Ab Combo Rapid Test-United States, SD Bioline Chagas AB-United States, WL Check Chagas-Argentina, and TR Chagas Bio-Manguinhos-Brazil) using a panel of 190 samples, including sera from 111 infected individuals, most of whom had low *T. cruzi* antibody levels. An additional 59 samples from uninfected individuals and 20 sera from individuals with other diseases, mainly visceral leishmaniasis, were included. All tests were performed by three independent laboratories in a blinded manner. Results showed differences in sensitivity from 92.8 to 100%, specificity from 78.5 to 92.4%, and accuracy from 90.5 to 95.3% among the four assays. The results presented here show that all four RDTs have high overall diagnostic ability. However, WL Check Chagas and TR Chagas Bio-Manguinhos were considered most suitable for use in screening studies due to their high sensitivity combined with good performance. Although these two RDTs have high sensitivity, a positive result should be confirmed with other tests to confirm or rule out reactivity/positivity, especially considering possible cross-reactivity with individuals with leishmaniasis or toxoplasmosis.

KEYWORDS
Chagas disease, serology, rapid diagnostic tests, performance, screening

# 1. Introduction

Chagas disease (CD) is a life-threatening, neglected tropical disease caused by the hemoflagellate *Trypanosoma cruzi* (*T. cruzi*). This parasite is responsible for an average of 12,000 deaths per year, and it is estimated that between 6 and 7 million people are infected worldwide (1, 2). However, despite the high mortality and morbidity, only 7% of *T. cruzi* carriers in Latin America are diagnosed and only about 1% receive etiologic treatment (3). *T. cruzi* is responsible for the highest parasitic disease burden in 21 Latin American countries, with a high prevalence in the southern Cone (4), where it is transmitted to humans mainly through contact with contaminated feces or urine from bloodsucking triatomine insects, also known as kissing bugs. Other routes of infection include congenital transmission, oral ingestion of contaminated food or beverages, transfusion of blood or blood products, and organ donation. Increasing international migration flows to non-endemic regions have led to the spread of *T. cruzi* infection beyond the borders of Latin America and have become a global health problem (5–7).

Successful diagnosis of CD depends on the stage of the disease, as different approaches (*in vitro* diagnostic (IVD) techniques) are used for each phase: an initial acute phase and a lifelong chronic phase. In the acute phase, which lasts up to two/three months, parasitological or molecular biology-based methods are typically used, while indirect serological methods such as indirect hemagglutination (IHA), enzyme-linked immunosorbent assay (ELISA), indirect immunofluorescence (IIF), chemiluminescence (CLIA), and electrochemiluminescence immunoassay (ECLIA) are used in the lifelong chronic phase (8). Although serological tests currently have high diagnostic performance, they require complex, specialized infrastructure and qualified personnel to perform. Therefore, IVD serological tests can be a significant barrier to access to diagnosis. The development of point-of-care (POC) devices such as rapid diagnostic tests (RDTs) has highlighted a way to circumvent the need for specialized infrastructure and personnel. These devices are designed to be simple, convenient, and intuitive to use. They require no refrigeration, no specialized infrastructure, no trained personnel, and no further processing by the user to obtain a result. Therefore, POC tests can be used to screen CD affected individuals, especially those living in rural or remote areas with limited access to health care. A negative RDT result excludes the disease, while positive results should be forwarded for diagnostic confirmation with other serological tests to exclude or confirm CD as recommended by the World Health Organization (WHO) (9, 10). Particular attention should be paid to the sensitivity of RDTs used as screening tests. A test with higher sensitivity (100%) is advisable because low sensitivity of the first level of testing in a screening algorithm may lead to excessive false-negative results and exclude people from accurate diagnosis, thereby underestimating the number of infected individuals. This strategy may improve access to diagnosis and treatment. Recently, the Pan American Health Organization (PAHO) recommended the use of ELISA or RDT as the sole test for seroepidemiologic testing (11).

Regarding the inconsistent diagnostic performance when using serological tests in different settings, some differences have been reported in the literature with respect to the parasite and the seven discrete typing units (DTUs) recognized today (12–14). However, other reports have found similar results when using conventional serology with samples from Mexico (mainly lineage TcI) (15) and also when using a single RDT with sera from different countries with lineages TcI, II and V, the main DTUs from endemic regions (16). In this study, samples from one region (Brazil) were used.

Considering the predicaments herein set forth, we endeavored to perform a multicenter systematic evaluation of the diagnostic performance of RDT kits available in Brazil. This is the first study comparing the performance of RDTs in Brazil for the diagnosis of chronic Chagas disease.

# 2. Materials and methods

## 2.1. Selection of RDTs

All commercial RDTs registered with the Brazilian Health Regulatory Agency (ANVISA) were included in this study. A total of four RDTs from four different manufacturers were available: OnSite Chagas Ab Combo Rapid Test® (CTK Biotech, United States), SD Bioline Chagas AB® (Abbott, USA), WL Check Chagas® (Wiener lab., Rosário, Argentina), and TR Chagas Bio-Manguinhos® (Bio-Manguinhos, Fiocruz, Rio de Janeiro, Brazil). The RDTs were sent by the General Coordination of Public Health Laboratories (CGLAB, Ministry of Health, Brazil) to each participating reference laboratory *via* a commercial shipping service. Importantly, RDTs from each brand were from the same batch.

## 2.2. Participating reference laboratories

The study was conducted in three participating Brazilian reference laboratories: The Advanced Public Health Laboratory (LASP) at the Gonçalo Moniz Institute (FIOCRUZ) in Salvador, Bahia; the Parasitic Diseases Service of the Ezequiel Dias Foundation (FUNED) in Belo Horizonte, Minas Gerais; and the Chagas Disease Study Center (NEDoC) at the Federal University of Goiás (UFG) in Goiânia, Goiás. All three participating reference laboratories performed the four RDTs with the same sample set. All participating laboratories adhered to Good Laboratory Practice and sample reactivity was repeated using conventional serology after the serum samples were thawed in the laboratory that provided the samples.

## 2.3. Sample collection

With an expected error of 2%, sensitivity of 99%, specificity of 99.5%, and confidence interval of 95%, the minimum sample number

was 48 sera from negative individuals and 96 sera from *T. cruzi*-positive individuals. We included 59 sera from *T. cruzi*-negative and 111 sera from *T. cruzi*-positive individuals from the existing sera bank at NEDoC. The *T. cruzi*-positive samples were previously collected from individuals with the chronic phase of CD with known epidemiological and clinical data (usually heart disease and/or megacolon and/or megaesophagus). These infected and uninfected individuals were tested in the laboratory at the request of Goias State physicians to confirm or exclude the diagnosis. This sample group consisted predominantly of samples with low or moderate reactivity in the serological tests: titration of less than 1:640 in IIF and IHA; reactivity indices between 1.2 and 2.0 (low reactivity) and 2.1 to 3.0 (moderate reactivity) in conventional ELISA. In addition, positive sera for visceral leishmaniasis (VL; $n = 10$), mucocutaneous leishmaniasis (CL; $n = 6$), and toxoplasmosis (TOX; $n = 4$) from the FUNED serum bank were included to evaluate cross-reactivity. All samples were thawed at −20°C without additional preservatives and previously tested for *T. cruzi* infection: indirect immunofluorescence (IIF; Anti-human IgG conjugated to fluorescein, Biomerieux® Marcy L'Etoile), indirect hemagglutination (IHA; Chagatest HAI screening A-V®, Wiener lab, Rosario, Argentina), ELISA with crude antigens (Teste ELISA para Chagas III®, Grupo Bios, Santiago, Chile), recombinant ELISA (Chagatest ELISA, recombinant v.3.0®, Wiener lab, Rosario, Argentina), chemiluminescence microparticle immunoassay (CMIA; Architect Chagas, Abbott Laboratories, Abbott GmbH, Wiesbaden, Germany), enzyme-linked immunosorbent assay (ELISA) with lysate/recombinant antigens (Gold ELISA Chagas®, REM Industry and Commerce Ltd., São Paulo, Brazil). Samples were aliquoted and coded so that members of the participating reference laboratory teams had no knowledge of their reactivity. Serum aliquots stored in dry ice were shipped by CGLAB to each participating reference laboratory using a commercial shipping service. The serological results for each serum using each of the serological techniques are shown in a Supplementary Table S1.

## 2.4. Immunochromatographic assays

RDTs were performed according to the technical instructions of the respective manufacturer. In each participating reference laboratory, the same sera were evaluated for all four RDTs. The results were read by two independent observers from each participating institution. In cases of doubt or disagreement, a third observer was consulted and the tests were repeated if consensus could not be reached. Final results were sent to the serum bank supervisor, who was the only person who knew the serological profile of the samples. A test was considered invalid if the control line was missing. After completion of the laboratory analysis, a consensus result between the three participating reference laboratories was compared with the serological profile of the samples and the performance of each RDT was determined.

## 2.5. Usability assessment

The criterion of ease of use in performing RDTs was quantified and compared. At the end of the study, the technical staff responsible for conducting the tests for the study were asked to complete a usability questionnaire for each RDT. This questionnaire was adapted from a conventional format used in several similar studies led by WHO/Foundation for Innovative New Diagnostics (FIND)/Médecins Sans Frontières (MSF)/Epicenter in 2001 (17, 18) and also in another international study on RDTs (19). The questionnaire was used to distinguish and evaluate the general characteristics of the tests and to assess the perception of the technical staff regarding the ease of use in performing each test. The questionnaires included information on the number of invalid tests, shelf life, storage temperature, amount of blood/serum/plasma required, number of steps and time required to perform the test, stability of results, additional material required, ease of opening the package, ease of performing the test, ease of identifying reagents, quality of instructions for use, and cost. Each item of the questionnaire was assigned an individual score, with a higher score indicating a more positive response. A total of 26 items could be evaluated.

## 2.6. Statistical analysis

To obtain a robust assessment of the performance of each kit, statistical tools were used by calculating the following diagnostic test parameters: Sensitivity (the probability of a test being positive in the presence of infection), Specificity (the probability of a test being negative in the absence of infection), Accuracy (the ability of a test to discriminate between target disease and health status), and Predictive Values (20, 21) using a dichotomous approach ($2 \times 2$ contingency table). Confidence intervals (CI) were determined at a 95% confidence level (95% CI), and the absence of overlapping 95% CI bars was used to infer statistical significance (22). Positive and negative predictive values were estimated for different prevalence scenarios. The chance of false-positive versus true-positive and false-negative versus true-negative results were calculated for the following prevalence values of chronic Chagas disease: 0.1, 1, 5, and 10%. The strength of agreement between the results of the RDTs and the serological profile of the samples was assessed using the Cohen's *kappa* coefficient ($\kappa$) and interpreted as follows: poor ($\kappa = 0$), slight ($0 < \kappa \leq 0.20$), fair ($0.21 < \kappa \leq 0.40$), moderate ($0.41 < \kappa \leq 0.60$), substantial ($0.61 < \kappa \leq 0.80$), and almost perfect ($0.81 < \kappa \leq 1.0$) agreement (23). Performance parameters were obtained using MedCalc for Windows v. 20.190 (MedCalc Software, Ostend, Belgium), whereas graphs were generated using GraphPad Prism 9 graphing software (San Diego, CA, United States). A study flowchart (Figure 1) and checklist were prepared according to STARD guidelines (24).

# 3. Results

A total of 190 serum samples were tested with four IgG *T. cruzi* RDTs (Supplementary Table S1). IgG survey in serum samples from 111 *T. cruzi*-positive samples showed variable values of sensitivity, ranging from 92.8% for OnSite Chagas Ab Combo Rapid Test, 95.5% for SD Bioline Chagas AB, and 97.3% for WL Check Chagas to 100% for TR Chagas Bio-Manguinhos (Table 1). For *T. cruzi*-negative samples, the highest value of specificity was obtained with WL Check Chagas (92.4%). A lower value was observed for SD Bioline Chagas AB, OnSite Chagas Ab Combo Rapid Test, and TR Chagas

10.3389/fmed.2023.1031455

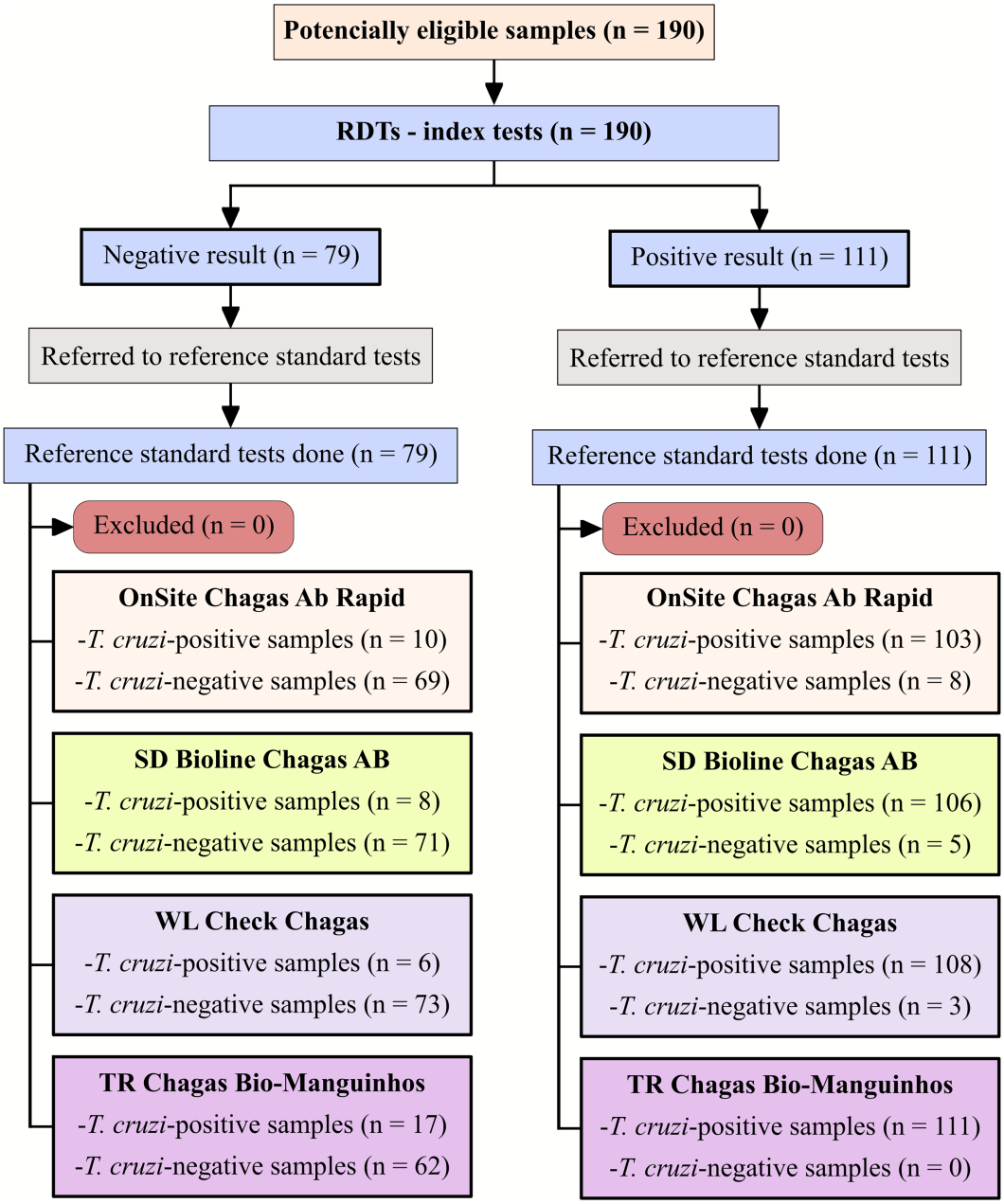


FIGURE 1
Flowchart depicting study design in accordance with the Standards for Reporting of Diagnostic Accuracy Studies (STARD) guidelines.

TABLE 1 Diagnostic performance and strength of agreement of four rapid diagnostic tests for the detection of *Trypanosoma cruzi* IgG.

| Performance parameters | OnSite Chagas Ab combo rapid test | WL check Chagas | SD Bioline Chagas | TR Chagas Bio-Manguinhos |
|---|---|---|---|---|
| SEN % (95%CI) | 92.8 (86.3–96.8) | 97.3 (92.3–99.4) | 95.5 (89.8–98.5) | 100 (96.7–100) |
| SPE % (95%CI) | 87.3 (78.0–93.8) | 92.4 (84.2–97.2) | 89.9 (81.0–95.5) | 78.5 (68.2–86.1) |
| ACC % (95%CI) | 90.5 (85.5–93.9) | 95.3 (91.2–97.5) | 93.2 (88.6–96.0) | 91.1 (86.1–94.3) |
| *k* (95% CI) | 0.80 (0.72–0.89) | 0.90 (0.84–0.96) | 0.86 (0.78–0.93) | 0.81 (0.72–0.90) |

SEN, sensitivity; SPE, specificity; ACC, accuracy; *k*, Cohen's Kappa coefficient; CI, confidence interval.

Bio-Manguinhos, which had specificity values of 89.9, 87.3, and 78.5%, respectively. Accuracy reached the highest value when samples were tested with WL Check Chagas (95.3%). A lower value was observed for SD Bioline Chagas AB (93.2%), TR Chagas Bio-Manguinhos (91.1%) and OnSite Chagas Ab Combo Rapid Test (90.5%).

Qualitative evaluation of the results using Cohen's *Kappa* method showed substantial agreement between the OnSite Chagas Ab Combo Rapid Test and the reference tests. For all other RDTs, qualitative evaluation of the results showed almost perfect agreement with the reference tests. Considering the 95% CI overlap, sensitivity, specificity, accuracy, and Cohen's *Kappa* index showed no differences among the four RDTs (Table 1).

The positive and negative predictive values were also estimated. Because the true prevalence of chronic CD varies from region to region, we used a hypothetical prevalence range to evaluate different scenarios. Figure 2 summarizes the association between the predictive values and the hypothetical prevalence scenarios. Decreasing prevalence resulted in low positive predictive values for all RDTs. Regarding the ratio of false-positive/negative to true-positive/negative, hypothetical prevalence values were used to represent most scenarios in which testing is performed. The chance of false-negative results relative to true-negative results was low for all tests and prevalence values (Table 2). On the other hand, the chance of false-positive results was predominantly high for any true-positive result, especially for low prevalence values (0.1 and 1%).

Regarding usability assessment, all RDTs were found to have the same storage conditions (room temperature $\leq 30°C$), require the same biological sample (whole blood, plasma, or serum), and results are stable for up to 30 min. Invalid tests were reported for <0.5% of RDTs performed. For all four RDTs, ease of performance, ease of opening the package, and interpretation of results were described as "very easy." The quality of the RDT instructions was described as "very good" for all RDTs. Some differences in the amounts of blood or serum/plasma required were noted for all four tests: OnSite Chagas Ab Combo Rapid Test and WL Check Chagas require 40 µl of blood, TR Chagas Bio-Manguinhos requires 10 µl, while SD Bioline Chagas AB requires 100 µl, the largest amount among them. None of the RTD assays require a device to read the results, so they can be used in field studies. OnSite Chagas Ab Combo Rapid Test, WL Check Chagas, SD Bioline Chagas AB and TR Chagas Bio-Manguinhos are one-step assays. As shown in Figure 3, TR Chagas Bio-Manguinhos and OnSite Chagas Ab Combo Rapid Test scored the highest (= 26), followed by SD Bioline Chagas AB and WL Check Chagas (score = 25).

## 4. Discussion

RDTs represent an interesting strategy for screening at-risk populations for acquisition of CD in low-resource and high-risk settings in endemic countries. WHO has set global targets and milestones for 2030 to eliminate transmission of *T. cruzi* through four modes of transmission (vectorial, transfusion, transplantation, and congenital) and achieve 75% coverage of the target population with antiparasitic treatment in 15 endemic countries in Latin America (25). This is an ambitious goal, as only 7% of *T. cruzi* carriers have been diagnosed and about 1% receive etiologic treatment (3). Thus, improving access to and demand for effective diagnosis, treatment, and care for CD is critical to controlling CD. Unfortunately, access to CD diagnostics remains one of the main barriers to control of this disease, as diagnosis in the chronic phase depends on laboratory infrastructure and qualified personnel. *In vitro* diagnostic tests at the point of care, such as RDTs, offer a promising strategy to address the gap in access to diagnosis that exists in many limited and isolated communities in endemic areas. However, similar to the enzyme-linked immunosorbent assay (ELISA), the performance of POC-IVD

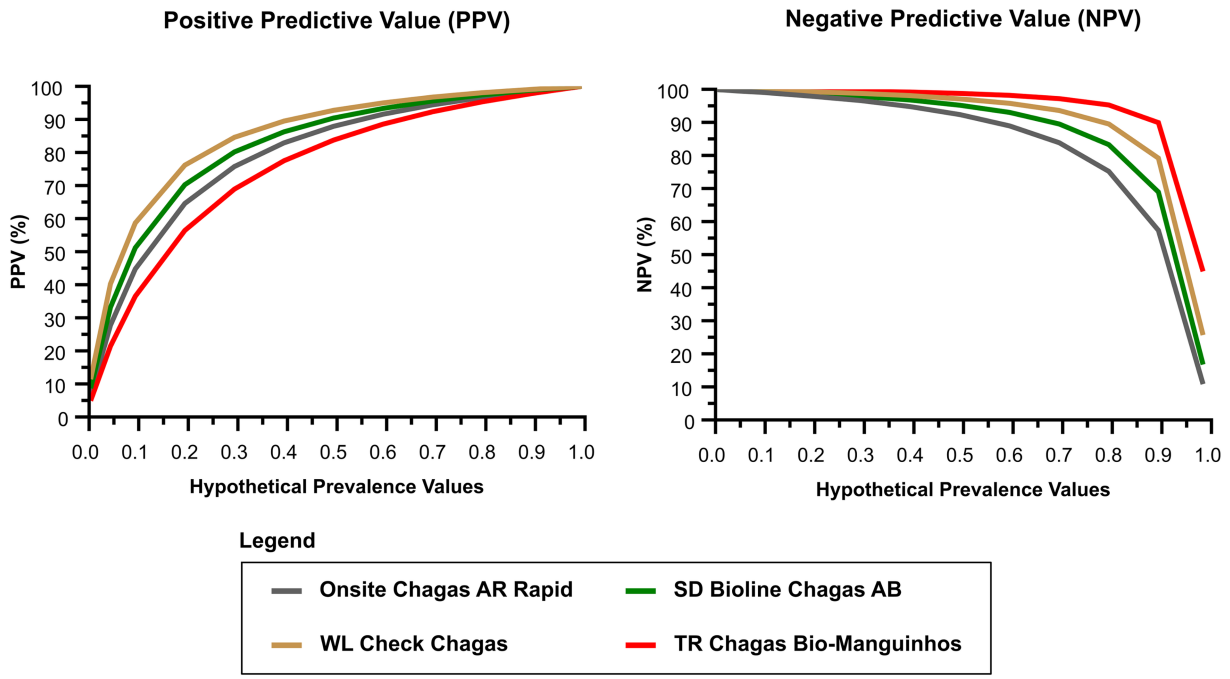


FIGURE 2
Positive and negative predictive estimates for different prevalence scenarios of chronic Chagas disease. NPV, negative predictive value; PPV, positive predictive value.

10.3389/fmed.2023.1031455

TABLE 2 Chance of false positive in relation to true positives and of false negatives in relation to true negatives for different prevalence values of chronic Chagas disease.

| Prevalence | OnSite Chagas Ab Combo rapid test | WL check Chagas | SD Bioline Chagas | TR Chagas Bio-Manguinhos |
|---|---|---|---|---|
| | False positives: true positives | | | |
| 0.1% | 136.4 | 78.3 | 105.1 | 214.8 |
| 1% | 13.5 | 7.7 | 10.5 | 21.3 |
| 5% | 2.6 | 1.5 | 2.0 | 4.1 |
| 10% | 1.2 | 0.7 | 0.9 | 1.9 |
| *False negative: true negatives* | | | | |
| 0.1% | <0.001 | <0.001 | <0.001 | NS |
| 1% | <0.001 | <0.001 | <0.001 | NS |
| 5% | 0.004 | 0.002 | 0.003 | NS |
| 10% | 0.009 | 0.003 | 0.006 | NS |

devices depends on the antigen preparation used, which warrants a systematic evaluation of their diagnostic performance (13). In this article, we evaluated the performance of four RTDs in the diagnosis of CD using samples from different Brazilian endemic areas.

In a comparative evaluation of 11 commercially available RDTs conducted by several national reference laboratories worldwide using a diverse panel of 474 samples, OnSite Chagas Ab Combo Rapid Test achieved a sensitivity of 90.1% and a specificity of 91%. In the same study, SD Chagas Ab Rapid showed a sensitivity of 90.7% and a specificity of 94% (19). Interestingly, WL Check Chagas showed a sensitivity of 88.7% and a specificity of 97%. Except for the sensitivity of WL Check Chagas, the sensitivity and specificity values of the other RDTs in the present study were within the 95% CI (19). According to the manufacturer, the sensitivity of WL Check Chagas was evaluated using four commercial serological panels with a total of 62 positive sera, and 61/62 (~98%) samples were correctly identified. However, the manufacturer reports a lower sensitivity (93.9%; 95% CI 91.1–96.6%) when the test was evaluated using a panel of 326 samples characterized by ELISA and IHA. Considering the confidence interval, both evaluations were consistent with the sensitivity observed in the present study (97.3%; 95% CI 92.3–99.4%). Similar sensitivity values were observed when serum samples were used during a WL Check Chagas field study (95.7%), although sensitivity was lower when the test examined whole blood (87.3%) (26). Accordingly, the manufacturer reported lower sensitivity (91.5%) when this RDT analyzed whole blood rather than plasma/serum. A possible interpretation for these differences in sensitivity is that different batches were used and the possibility exists that manufacturers changed the composition and proportions of the different antigens originally used after the results of the first reported studies (19) with lower sensitivity eight years ago. Information on which *T. cruzi* antigens were used in WL Check Chagas, SD Chagas Ab Rapid, and OnSite Chagas Ab Combo Rapid Test was not disclosed by the manufacturers.

In the present study, TR Chagas Bio-Manguinhos, using two recombinant *T. cruzi*-chimeric antigens deposited in different lines (27), correctly identified all positive samples and achieved a sensitivity of 100% (95% CI 96.7–100%) and a specificity of 78.5 (95% CI 68.2–86.1). This test is the most recent addition to the repertoire of available POC tests for CD, so there is a lack of independent studies evaluating its diagnostic performance. However, there are numerous studies evaluating the performance of these antigens in other IVD systems (27–35) and mammalian hosts (36–38). In a study of 280 CD-positive samples, IBMP-8.1 antigen showed a sensitivity of 98.9% (95% CI 96.9–99.6%) when used in an ELISA format and 98.6% (95% CI 96.4–99.4%) in a liquid microarray system, while IBMP-8.4 showed a sensitivity of 99.6% (95% CI 98–99.9%) in ELISA and 98.9% (95% CI 96.9–99.6%) in a microarray system (39). Similar results were obtained in a phase II study in Brazil (40), and the antigens maintained their performance in other studies in Argentina (41) and Spain (30). Moreover, no cross-reactions with visceral and mucocutaneous leishmaniasis were observed with IBMP-8.4 under ELISA or liquid microarray systems, while IBMP-8.1 in liquid microarray did not cross-react with visceral leishmaniasis, but cross-reactions for mucocutaneous leishmaniasis were observed in an IBMP-8.1 ELISA (0.7%) (32). Interestingly, the structural stability of IBMP chimeric antigens over time, pH and temperature variations, and in buffer systems was investigated. The structure and diagnostic performance were maintained under adverse conditions, suggesting a robust design (32). This robustness favors use in POC assays, as these devices must withstand harsh environments and be reliable enough to be easily used, interpreted, and stored.

The usability evaluation showed that no invalid result was obtained when *T. cruzi*-positive and negative samples were tested with all four RTDs. In terms of storage temperature, shelf life in months, stability of results, ease of reagent identification, ease of package opening, ease of performance, and quality of instructions, all four RTDs achieved similar results. OnSite Chagas Ab Combo Rapid Test, WL Check Chagas, and TR Chagas Bio-Manguinhos require volumes of up to 40 µl of whole blood, whereas SD Bioline Chagas AB requires 100 µl, a volume that is difficult to obtain by digital puncture, making this test unusable for epidemiological studies and as a screening tool. No RDT requires equipment to read results, making it feasible to use in the field. In addition, no assessed assay requires more than two steps to perform. For the WL Check Chagas, the test took more than 20 min to perform. WL Check Chagas and SD Bioline Chagas AB were the most complex tests (score = 25), while the highest score was achieved by TR Chagas Bio-Manguinhos and OnSite Chagas Ab Combo Rapid Test (score = 26). Of the four assays evaluated, the WL Check Chagas and TR Chagas Bio-Manguinhos were considered the

10.3389/fmed.2023.1031455

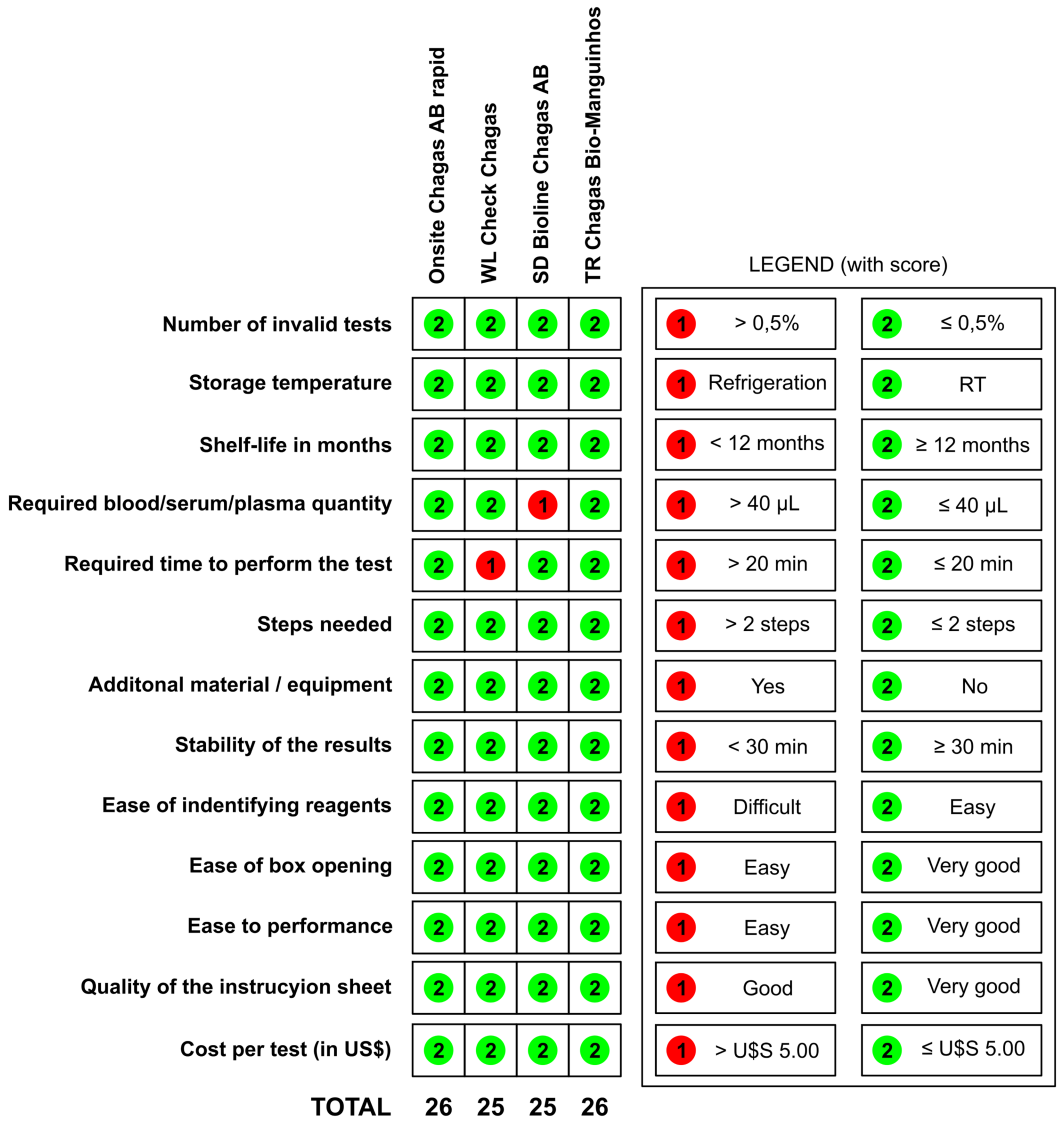


FIGURE 3
Validity and inter-reader reliability of four rapid diagnostic tests for the detection of IgG anti-*Trypanosoma cruzi*. RT (room temperature).

most suitable for use in screening studies because they are reliable and highly sensitive for the diagnosis of CD. According to the instructions of all four kits evaluated, the test result is independent of the type of biological sample used for the immunoassay, whether blood, serum, or plasma.

The main limitation of this study was the restriction on the use of samples with low or moderate reactivity in the serological tests (titration of less than 1:640 for IIF and IHA; reactivity indices between 1.2 and 2.0 (low reactivity) and 2.1 to 3.0 (moderate reactivity) for conventional ELISA). The selection of samples with low or moderate reactivity may lead to a decrease in the sensitivity values of the evaluated RDTs, which may not correspond to their use in a real population. However, the predominance of samples with these characteristics was propositaly intended to detect infected individuals with low titers, as in conventional serology, and to avoid the possible loss of infected individuals. Another limitation concerns the lack of band intensity analysis. This would be particularly important to verify the intensity of false-positive bands. However, visual analysis revealed bands of varying intensity for false-positive lines. Despite a consistent detection pattern of the control lines, we observed that false-positive results exhibited whitish spots over the antigen reaction area, while others showed bright to almost faint colors as a positive sign of detection. The presence of these whitish spots or faint bands over the antigen reaction area led to an increase in the number of false-positive results in low CD prevalence scenarios. Indeed, at prevalence values of 0.1 and 1%, the chance of false-positive results was predominantly high for each true-positive result, whereas false-negative results were low relative to true-negative results for all tests and all prevalence values.

The results presented here show that all four RDTs have high overall diagnostic ability. We believe that the antigenic variability of *T. cruzi* did not affect the performance evaluation of the RDTs, since we used only Brazilian samples. Indeed, sera from individuals infected

in Mexico (a region with TcI) have shown similar reactivity on conventional serology (15). Also, previous studies using other RDT (Chagas Stat-Pak), that was not included in this study because it does not have a current registration with ANVISA, performed with sera from different countries showed no differences in terms of different DTU (Tc I-II-V) in different regions of Latin America (16). Due to the overlap of 95% CI values, no differences were observed between the results for sensitivity, specificity, and accuracy. The high sensitivity values ensure that most (if not all) positive individuals are correctly diagnosed and referred to medical care. In the absence of laboratory facilities, the increased use of these rapid tests, which are reliable, cheap, and simple enough to be used by non-laboratory personnel, should contribute significantly to the effective control of CD and improve diagnosis and treatment, especially in remote and rural areas in endemic countries.

## Data availability statement

The original contributions presented in the study are included in the article/Supplementary material, further inquiries can be directed to the corresponding author.

## Ethics statement

The studies involving human participants were reviewed and approved by Institutional Review Board (IRB) for Human Research of the Gonçalo Moniz Institute (CAAE 67809417.0.0000.0040), the Ezequiel Dias Foundation (CAAE 21538619.4.2002.9507), and the Federal University of Goiás (CAAE 21538619.4.2001.5078). The ethics committee waived the requirement of written informed consent for participation.

## Author contributions

AL and FS designed the experimental procedure. JI, LL, FM, JF, and LS performed the RDT assays. VB and FS performed the statistical analysis. LL and FS wrote the article. JI, FM, JF, LS, ST, AL, VB, and AS helped to write the article. JI, LL, FM, JF, LS, ST, and FS performed data collection, analysis, and interpretation. AL provided the biological samples. FS prepared the illustrations and supervised the work. JI, AL, and FS provided the laboratory space. AS and FS obtained funding for this study. All authors contributed to the article and approved the submitted version.

## Funding

This research was supported by the Coordination for the Improvement of Higher Education Personnel in Brazil (CAPES; Finance Code 001 award to LL and FS). FS is a research grantee of the National Council for Scientific and Technological Development-Brazil (CNPq; grant number 309263/2020–4). The funders had no influence on the study design, data collection and analysis, decision to publish, or preparation of the manuscript.

## Acknowledgments

We thank Debbie Vermeij for assistance in revising the manuscript in English and proofreading. We also thank the Oswaldo Cruz Foundation (Fiocruz) for providing the commercial tests and the General Coordination of Public Health Laboratories (CGLAB, Ministry of Health, Brazil) for sending the commercial kits for each participating reference laboratory.

## Conflict of interest

AS and FS are employees of FIOCRUZ and one of the RDTs was produced by a subsidiary of FIOCRUZ (Bio-Manguinhos), but they are not involved in the production of this kit (TR Chagas Bio-Manguinhos).

The remaining authors declare that the research was conducted in the absence of any commercial or financial relationships that could be construed as a potential conflict of interest.

## Publisher's note

All claims expressed in this article are solely those of the authors and do not necessarily represent those of their affiliated organizations, or those of the publisher, the editors and the reviewers. Any product that may be evaluated in this article, or claim that may be made by its manufacturer, is not guaranteed or endorsed by the publisher.

## Supplementary material

The Supplementary material for this article can be found online at: https://www.frontiersin.org/articles/10.3389/fmed.2023.1031455/full#supplementary-material

## References

1. WHO. Chagas disease in Latin America: an epidemiological update based on 2010 estimates. *Wkly Epidemiol Rec*. (2015) 90:33–43.

2. Lee, BY, Bacon, KM, Bottazzi, ME, and Hotez, PJ. Global economic burden of Chagas disease: a computational simulation model. *Lancet Infect Dis*. (2013) 13:342–8. doi: 10.1016/S1473-3099(13)70002-1

3. Chaves, GC, Abi-Saab Arrieche, M, Rode, J, Mechali, D, Reis, PO, Alves, RV, et al. Estimating demand for anti-Chagas drugs: a contribution for access in Latin America. *Rev Panam Salud Publica*. (2017) 41:e45. doi: 10.26633/RPSP.2017.45

4. Pérez-Molina, JA, and Molina, I. Chagas disease. *Lancet*. (2018) 391:82–94. doi: 10.1016/S0140-6736(17)31612-4

5. Strasen, J, Williams, T, Ertl, G, Zoller, T, Stich, A, and Ritter, O. Epidemiology of Chagas disease in Europe: many calculations, little knowledge. *Clin Res Cardiol*. (2014) 103:1–10. doi: 10.1007/s00392-013-0613-y

6. Bern, C, and Montgomery, SP. An estimate of the burden of Chagas disease in the United States. *Clin Infect Dis*. (2009) 49:e52–4. doi: 10.1086/605091

7. Schmunis, GA, and Yadon, ZE. Chagas disease: a Latin American health problem becoming a world health problem. *Acta Trop*. (2010) 115:14–21. doi: 10.1016/j.actatropica.2009.11.003

8. Rassi, A, Rassi, A, and Marin-Neto, JA. Chagas disease. *Lancet*. (2010) 375:1388–402. doi: 10.1016/S0140-6736(10)60061-X

9. World Health Organization. *WHO Consultation on International Biological Reference Preparations for Chagas Diagnostic Tests*. Geneva: World Health Organization (2007). https://www.who.int/bloodproducts/ref_materials/WHO_Report_1st_Chagas_BRP_consultation_7-2007_final.pdf

10. World Health Organization. *Control of Chagas Disease. Second Report of the WHO Expert Committee*. Geneva, Switzerland: World Health Organization (2002). Available at: https://apps.who.int/iris/handle/10665/42443

11. PAHO. *Guidelines for the Diagnosis and Treatment of Chagas Disease*. Washington DC: Pan American Health Organization. (2019). Available at: https://iris.paho.org/bitstream/handle/10665.2/49653/9789275120439_eng.pdf?sequence=6&isAllowed=y

12. Zingales, B. *Trypanosoma cruzi* genetic diversity: something new for something known about Chagas disease manifestations, serodiagnosis and drug sensitivity. *Acta Trop*. (2018) 184:38–52. doi: 10.1016/j.actatropica.2017.09.017

13. Truyens, C, Dumonteil, E, Alger, J, Cafferata, ML, Ciganda, A, Gibbons, L, et al. Geographic variations in test reactivity for the serological diagnosis of *Trypanosoma cruzi* infection. *J Clin Microbiol*. (2021) 59:e0106221. doi: 10.1128/JCM.01062-21

14. Santos, FLN, Souza, WV, Barros, MS, Nakazawa, M, Krieger, MA, and Gomes, YM. Chronic Chagas disease diagnosis: a comparative performance of commercial enzyme immunoassay tests. *Am J Trop Med Hyg*. (2016) 94:1034–9. doi: 10.4269/ajtmh.15-0820

15. Luquetti, AO, Espinoza, B, Martínez, I, Hernández-Becerril, N, Ponce, C, Ponce, E, et al. Performance levels of four Latin American laboratories for the serodiagnosis of Chagas disease in Mexican sera samples. *Mem Inst Oswaldo Cruz*. (2009) 104:797–800. doi: 10.1590/S0074-02762009000500023

16. Luquetti, AO, Ponce, C, Ponce, E, Esfandiari, J, Schijman, A, Revollo, S, et al. Chagas' disease diagnosis: a multicentric evaluation of Chagas stat-Pak, a rapid immunochromatographic assay with recombinant proteins of *Trypanosoma cruzi*. *Diagn Microbiol Infect Dis*. (2003) 46:265–71. doi: 10.1016/s0732-8893(03)00051-8

17. Guthmann, JP, Ruiz, A, Priotto, G, Kiguli, J, Bonte, L, and Legros, D. Validity, reliability and ease of use in the field of five rapid tests for the diagnosis of *Plasmodium falciparum* malaria in Uganda. *Trans R Soc Trop Med Hyg*. (2002) 96:254–7. doi: 10.1016/S0035-9203(02)90091-X

18. Roddy, P, Goiri, J, Flevaud, L, Palma, PP, Morote, S, Lima, N, et al. Field evaluation of a rapid immunochromatographic assay for detection of *Trypanosoma cruzi* infection by use of whole blood. *J Clin Microbiol*. (2008) 46:2022–7. doi: 10.1128/JCM.02303-07

19. Sánchez-Camargo, CL, Albajar-Viñas, P, Wilkins, PP, Nieto, J, Leiby, DA, Paris, L, et al. Comparative evaluation of 11 commercialized rapid diagnostic tests for detecting *Trypanosoma cruzi* antibodies in serum banks in areas of endemicity and nonendemicity. *J Clin Microbiol*. (2014) 52:2506–12. doi: 10.1128/JCM.00144-14

20. Akobeng, AK. Understanding diagnostic tests 2: likelihood ratios, pre-and post-test probabilities and their use in clinical practice. *Acta Paediatr Int J Paediatr*. (2007) 96:487–91. doi: 10.1111/j.1651-2227.2006.00179.x

21. Ouchchane, L, Rabilloud, M, and Boire, J-Y. Sensibilité, spécificité et valeurs prédictives In: R Beuscart, J Bénichou, P Roy and C Quantin, editors. *Évaluation des Méthodes D'analyse Appliquées Aux Sciences de la Vie et de la Santé–Biostatistique*. Paris, France: Omniscience (2009). 49–78.

22. Payton, ME, Greenstone, MH, and Schenker, N. Overlapping confidence intervals or standard error intervals: what do they mean in terms of statistical significance? *J Insect Sci*. (2003) 3:34. doi: 10.1093/jis/3.1.34

23. Landis, JR, and Koch, GG. The measurement of observer agreement for categorical data. *Biometrics*. (1977) 33:159–74. doi: 10.2307/2529310

24. Cohen, JF, Korevaar, DA, Altman, DG, Bruns, DE, Gatsonis, CA, Hooft, L, et al. STARD 2015 guidelines for reporting diagnostic accuracy studies: explanation and elaboration. *BMJ Open*. (2016) 6:e012799. doi: 10.1136/bmjopen-2016-012799

25. WHO. *Ending the Neglect to Attain the Sustainable Development Goals: A Road Map for Neglected Tropical Diseases 2021-2030*. (2020) Available at: https://www.who.int/publications/i/item/WHO-UCN-NTD-%0A2020.01 (Accessed September 15, 2021).

26. Mendicino, D, Stafuza, M, Colussi, C, Del, BM, Streiger, M, and Moretti, E. Diagnostic reliability of an immunochromatographic test for Chagas disease screening at a primary health care Centre in a rural endemic area. *Mem Inst Oswaldo Cruz*. (2014) 109:984–8. doi: 10.1590/0074-0276140153

27. Silva, ED, Silva, ÂAO, Santos, EF, Leony, LM, Freitas, NEM, Daltro, RT, et al. Development of a new lateral flow assay based on IBMP-8.1 and IBMP-8.4 chimeric antigens to diagnose Chagas disease. *Biomed Res Int*. (2020) 2020:1803515. doi: 10.1155/2020/1803515

28. Santos, FLN, Campos, ACP, Amorim, LDAF, Silva, ED, Zanchin, NIT, Celedon, PAF, et al. Highly accurate chimeric proteins for the serological diagnosis of chronic Chagas disease: a latent class analysis. *Am J Trop Med Hyg*. (2018) 99:1174–9. doi: 10.4269/ajtmh.17-0727

29. Cordeiro, TAR, Martins, HR, Franco, DL, Santos, FLN, Celedon, PAF, Cantuária, VL, et al. Impedimetric immunosensor for rapid and simultaneous detection of Chagas and visceral leishmaniasis for point of care diagnosis. *Biosens Bioelectron*. (2020) 169:112573. doi: 10.1016/j.bios.2020.112573

30. Dopico, E, Del-Rei, RP, Espinoza, B, Ubillos, I, Zanchin, NIT, Sulleiro, E, et al. Immune reactivity to *Trypanosoma cruzi* chimeric proteins for Chagas disease diagnosis in immigrants living in a non-endemic setting. *BMC Infect Dis*. (2019) 19:251. doi: 10.1186/s12879-019-3872-z

31. Santos, FLN, Celedon, PAF, Zanchin, NIT, Leitolis, A, Crestani, S, Foti, L, et al. Performance assessment of a *Trypanosoma cruzi* chimeric antigen in multiplex liquid microarray assays. *J Clin Microbiol*. (2017) 55:2934–45. doi: 10.1128/JCM.00851-17

32. Daltro, RT, Leony, LM, Freitas, NEM, Silva, ÂAO, Santos, EF, Del-Rei, RP, et al. Cross-reactivity using chimeric *Trypanosoma cruzi* antigens: diagnostic performance in settings co-endemic for Chagas disease and American cutaneous or visceral leishmaniasis. *J Clin Microbiol*. (2019) 57:e00762–19. doi: 10.1128/JCM.00762-19

33. Santos, EF, Silva, ÂAO, Freitas, NEM, Almeida, MCC, Araújo, FLV, Celedon, PAF, et al. Performance of chimeric *Trypanosoma cruzi* antigens in serological screening for Chagas disease in blood banks. *Front Med*. (2022) 9:852864. doi: 10.3389/fmed.2022.852864

34. Celedon, PAF, Leony, LM, Oliveira, UD, Freitas, NEM, Silva, ÂAO, Daltro, RT, et al. Stability assessment of four chimeric proteins for human Chagas disease immunodiagnosis. *Biosensors*. (2021) 11:289. doi: 10.3390/bios11080289

35. Freitas, NEM, Santos, EF, Leony, LM, Silva, ÂAO, Daltro, RT, Medrado, LCV, et al. Double-antigen sandwich ELISA based on chimeric antigens for detection of antibodies to *Trypanosoma cruzi* in human sera. *PLoS Neglected Trop Dis*. (2022) 16:e0010290. doi: 10.1371/journal.pntd.0010290

36. Leony, LM, Freitas, NEM, Del-Rei, RP, Carneiro, CM, Reis, AB, Jansen, AM, et al. Performance of recombinant chimeric proteins in the serological diagnosis of *Trypanosoma cruzi* infection in dogs. *PLoS Negl Trop Dis*. (2019) 13:e0007545. doi: 10.1371/journal.pntd.0007545

37. Santos, F, Magalhães-Junior, JT, Carneiro, IO, Santos, FLN, Silva, ÂAO, Silva, JMC, Novais, et al. Eco-epidemiology of vectorial *Trypanosoma cruzi* transmission in a region of Northeast Brazil. *Acta Trop*. (2022) 225:106184. doi: 10.1016/j.actatropica.2021.106184

38. Costa, TF, Rocha, AVV, Miranda, LM, Lima, LFS, Santos, FLN, Silva, ÂAO, et al. Seroprevalence and detection of *Trypanosoma cruzi* in dogs living in a non-endemic area for Chagas disease in the legal Amazon region. *Brazil Vet Parasitol Reg Stud Rep*. (2021) 26:100648. doi: 10.1016/j.vprsr.2021.100648

39. Santos, FLN, Celedon, PAF, Zanchin, NIT, Brasil, TAC, Foti, L, Souza, WV, et al. Performance assessment of four chimeric *Trypanosoma cruzi* antigens based on antigen-antibody detection for diagnosis of chronic Chagas disease. *PLoS One*. (2016) 11:e0161100. doi: 10.1371/journal.pone.0161100

40. Santos, FLN, Celedon, PA, Zanchin, NI, Souza, WV, Silva, ED, Foti, L, et al. Accuracy of chimeric proteins in the serological diagnosis of chronic Chagas disease–a phase II study. *PLoS Negl Trop Dis*. (2017) 11:e0005433. doi: 10.1371/journal.pntd.0005433

41. Del-Rei, RP, Leony, LM, Celedon, PAF, Zanchin, NIT, Reis, MG, Gomes, YM, et al. Detection of anti-*Trypanosoma cruzi* antibodies by chimeric antigens in chronic Chagas disease-individuals from endemic South American countries. *PLoS One*. (2019) 14:e0215623. doi: 10.1371/journal.pone.0215623

# Frontiers in Public Health

**Explores and addresses today's fast-moving healthcare challenges**

One of the most cited journals in its field, which promotes discussion around inter-sectoral public health challenges spanning health promotion to climate change, transportation, environmental change and even species diversity.

---

## Discover the latest Research Topics

See more →

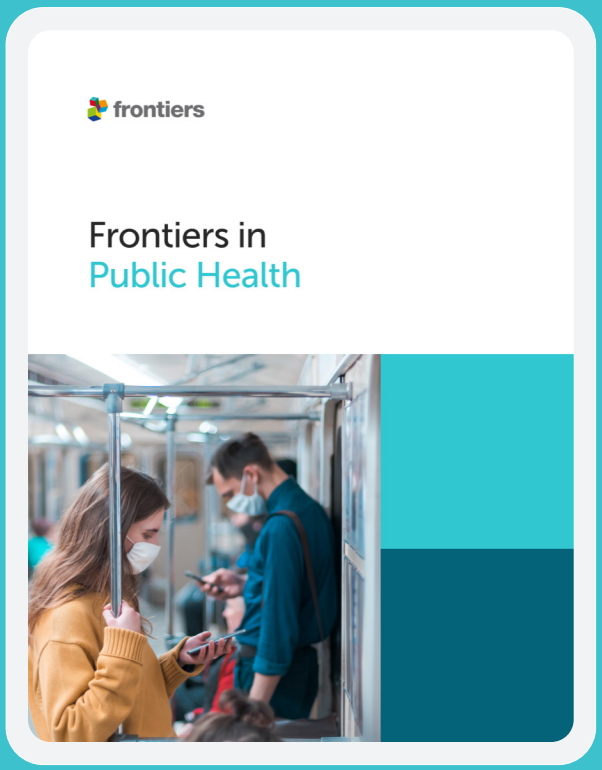


**Frontiers**

Avenue du Tribunal-Fédéral 34
1005 Lausanne, Switzerland
frontiersin.org

**Contact us**

+41 (0)21 510 17 00
frontiersin.org/about/contact